University of Southampton

Faculty of Engineering and Physical Sciences

School of Engineering

Data Technologies for Lower Limb Orthosis Design and Assessment

DOI: https://doi.org/10.5258/SOTON/T0047

by

Emily Sarah Kelly

ORCID ID 0000-0001-5776-6857

Thesis for the degree of Doctor of Philosophy

February 2023

University of Southampton

Abstract

Faculty of Engineering and Physical Sciences

School of Engineering

Doctor of Philosophy

Data Technologies for Lower Limb Orthosis Design and Assessment

by Emily Sarah Kelly

Lower limb orthoses, such as ankle foot orthoses (AFOs) or foot orthoses (FOs), can reduce pain, manage deformity and improve mobility for individuals with a range of musculoskeletal and neurological conditions. However, bioengineering research into orthosis design has been limited, with little consideration of how devices affect interfacing skin and soft tissues. Regarding FOs, plantar pressure metrics have been considered, but how they relate to the underlying tissues is unclear. Additionally, their effectiveness for people living with foot deformities, e.g. people with rheumatoid arthritis (RA), is not well understood. Thus, improved understanding of how tissues interact with orthoses, in terms of the mechanical and thermal boundary and tissue damage risk, is needed. This would be key to ensuring devices are effective and designed to meet user needs.

This research aimed to assess how lower limb orthosis design parameters affect soft tissue health and variation between individuals. A multi-modal approach was taken, combining experimental testing of AFOs and computational modelling of AFOs and FOs. *In vivo* pilot testing with five healthy participants examined plantar pressure metrics and microclimate with two AFO designs and two sock materials, during stationary standing and gait. The AFO with a more compliant material caused lower peak interface pressures and pressure gradients. Greater elevations in temperature and humidity occurred where the AFOs were more encompassing. Cotton socks controlled temperature better but humidity was higher than with bamboo socks.

Simplified forefoot computational models were developed to assess orthosis design parameters in two scenarios: five healthy individuals wearing AFOs, and 13 individuals with RA wearing FOs. Plantar pressures and shear strains were assessed for the effects on superficial and deep soft tissues, respectively. As with the experimental testing, softer interface materials resulted in lower interface pressures for both AFOs (-30 to -49%) and FOs (EVA vs Poron materials mean: -1.9 to -2.2%, $p<0.05$), but shear strain generally increased or was unchanged (AFOs: -4.4 to 4.3%; FOs mean: 3.3-5.3%, $p<0.01$). Total contact FOs reduced all pressure and strain metrics compared to flat FOs. An AFO undersized across its width produced similar pressure and strain predictions to a normally-fitted AFO, likely due to the specific conditions modelled. Inter-participant variability was high across all test conditions, and was often more prominent than intra-participant differences observed across designs. While design-related trends were generally consistent between all participants, there were exceptions. For the RA computational study, correlations were assessed between model predictions and clinical and morphological data, to determine whether the models could distinguish between condition presentations and severity, and thus determine individual FO requirements. BMI and first metatarsal head (MH1) curvature correlated with pressure and shear strain model predictions (BMI: $0.600<r<0.652$, $p<0.05$; MH1 curvature: $0.529<r<0.574$, $0.040<p<0.063$), but scores relating to pain and intermetatarsal bursitis did not. Relationships between model predictions and either tissue depth under MH1 or sesamoid bone offset could not be established, due to the small sample size and MR dataset limitations.

These studies represent novel methods to assess AFO and FO design, including the first FE modelling of a population with RA and comparison with clinical data. Important considerations for future orthosis research and clinical application have also been highlighted, such as differences in superficial plantar pressure and deeper shear strains trends, and high inter-participant variability. Future model development, to consider dynamic gait or other vulnerable foot regions, could further aid orthosis assessment. By optimising orthosis design, devices may be tailored to improve effectiveness and user comfort, and reduce tissue damage risk.

Table of Contents

Table of Tables

Table of Tables

Table of Figures

List of Accompanying Materials

This thesis is accompanied by the following raw data:

Emily Kelly (2023) Data Technologies for Lower Limb Orthosis Design and Assessment. [https://doi.org/10.5258/SOTON/D2203]

Research Thesis: Declaration of Authorship

Print name: Emily Sarah Kelly

Title of thesis: Data Technologies for Lower Limb Orthosis Design and Assessment

I declare that this thesis and the work presented in it are my own and has been generated by me as the result of my own original research.

I confirm that:

1. This work was done wholly or mainly while in candidature for a research degree at this University;
2. Where any part of this thesis has previously been submitted for a degree or any other qualification at this University or any other institution, this has been clearly stated;
3. Where I have consulted the published work of others, this is always clearly attributed;
4. Where I have quoted from the work of others, the source is always given. With the exception of such quotations, this thesis is entirely my own work;
5. I have acknowledged all main sources of help;
6. Where the thesis is based on work done by myself jointly with others, I have made clear exactly what was done by others and what I have contributed myself;
7. Parts of this work have been published as:

Kelly, E.S. et al., *Effects of Ankle-Foot Orthosis Design on the Pressure and Microclimate Between the Device and Limb*. Prosthetics and Orthotics International Vol. 45. p. 148, Paper presented at International Society for Prosthetics and Orthotics (ISPO) 18th World Congress 2021. [1]

Kelly, E.S. et al., *Predicting Forefoot-Orthosis Interactions in Rheumatoid Arthritis using Computational Modelling*. Frontiers in Bioengineering and Biotechnology. 2021; **9:**803725. [2]

Signature: ..... Date: 09/02/2023

Acknowledgements

I'd like to thank everyone who has played a part in the undertaking of my PhD, your support has made this possible.

Firstly, thanks to my supervisory team. To Prof. Catherine Bowen, for your clinical perspective, which has improved this thesis considerably. To Dr Peter Worsley, for your aid in setting up participant testing and guidance throughout. And to Dr Alex Dickinson, thank you for your consistent encouragement and support. I couldn't have asked for a better supervisory team and I have benefited greatly from all of your insights.

Thanks also to Dr Martin Warner for the use of and aid in the Health Sciences lab, and to Dr Andy Chipperfield for letting me borrow his treadmill for my testing. To Dr Neil O'Brien and everyone at Southampton General Hospital who was involved in preparing and pre-processing the MR data. And to Dr Lindsey Cherry and Dr Beth Keenan who collected the original MR and clinical data upon which much of this thesis was based. Thank you for letting me use your data, and for both of your help and support in my research.

To my fellow PhD students, thank you for your support and advice both in and out of the office. To my friends Rebecca, Cat, Vanessa, and Vivienne for all the much-needed deep and not so deep conversations. To Emma, Deag and David for the ongoing adventures and always giving me something fun to look forward to. And finally, thank you to my family, especially my sister Zoë, for your endless belief and encouragement which kept me going throughout.

Funding for this project was provided by the University of Southampton's EPSRC Doctoral Training Programme (ref EP/R513325/1).

Abbreviations

AFO.....Ankle Foot Orthosis

BMI.....Body Mass Index

CI .....Confidence Interval

CoF .....Coefficient of Friction

CSD-OPUS.....Client Satisfaction with Device subsection of the Orthotics and Prosthetics User Survey

CT .....Computed Tomography

DTI.....Deep Tissue Injury

ES AFO.....AFO Extra Strong (from Ortho Europe)

EVA.....Ethylene Vinyl Acetate

FE.....Finite Element

FEA .....Finite Element Analysis

FO.....Foot Orthosis

GRF.....Ground Reaction Force

ICRC.....International Committee of the Red Cross

IL-1α .....Interleukin-1 alpha

IL-1RA.....Interleukin-1 receptor antagonist

IQR.....Interquartile Range

LFIS-IF .....Leeds Foot Impact Scale – Impairment and Footwear subsection

LFIS-AP.....Leeds Foot Impact Scale – Activity Limitation and Participation Restriction subsection

MH.....Metatarsal Head, e.g. MH1 is 1st metatarsal head

MR(I) .....Magnetic Resonance (Imaging)

MTP joint.....Metatarsophalangeal joint

PG.....Pressure Gradient

PP .....Peak Pressure

Abbreviations

PPG ..... Peak Pressure Gradient

PPP ..... Peak Plantar Pressure

PPT ..... Pressure Pain Threshold

PTI ..... Pressure-time Integral

RA..... Rheumatoid Arthritis

RH ..... Relative Humidity

RQ{1,2,3}..... Research Question with 1, 2 or 3 specified

TEWL..... Transepidermal water loss

TR/TE..... Repetition time/Echo time

Chapter 1 Introduction

Orthoses are external devices that are used to alter aspects of the musculoskeletal system and the way it functions, for example to manage deformity, improve mobility or reduce pain. The reported number of people worldwide who require prosthetic or orthotic devices varies considerably from 35-100 million, based on estimates of 0.5-1.5% of the global population [3, 4]. The International Committee of the Red Cross (ICRC) found that there were four times more orthotics than prosthetics users across their centres worldwide [5], though it has also been suggested that the ratio of orthotic to prosthetic users is as high as 10:1 in the USA [6]. This would indicate that there could be anywhere from 28-80 million people worldwide requiring an orthosis. In 2015, it was estimated that there were 2 million orthosis users in England, a number that has likely increased due to greater prevalence of conditions such as diabetes, and improved neonatal and paediatric care leading to increased survival of children with disabilities [7]. Orthotics has often been dubbed a “Cinderella service”, frequently overlooked by both health services and research, despite the large number of people requiring orthoses. Although orthosis users outnumber prosthesis users considerably, the opposite is true of literature regarding both the services and device design [8]. As such, there is much that is not yet understood about the way orthoses interact with the body, and the comparative effectiveness of different designs. Improving the devices would not only aid the users but could also reduce the time and money spent by the health services.

There are different types of lower limb orthoses including foot orthoses (FOs), orthotic footwear, ankle-foot orthoses (AFOs), and knee-ankle-foot orthoses (KAFOs). A review of the Scottish Orthotics services in 2005 indicated that 89% of orthotist time was spent on lower limb orthoses, with the remaining 11% assigned to devices such as upper limb and spinal orthoses [9]. This distribution of time was also reflected by the American Board for Certification in Orthotics, Prosthetics and Pedorthics (ABC) [10], who went a step further to identify that out of all the orthotic devices, the most time was spent on AFO provision (18.2%). Despite their widespread use, there is a lack of complete demographic data identifying the number of orthosis users – many services do not record whether appointments are for providing a new orthosis or for other reasons. Additionally, there are multiple pathways in healthcare providers around the world for the prescription of an orthosis, with podiatrists, physiotherapists and occupational therapists playing a role. Despite this, from what data there is available, it is clear there are a significant number of orthosis users, predominantly using devices in the distal lower limb(s).

Wearing an orthosis can improve a person's quality of life and provide cost-saving benefits by supporting the physical and social health of the end user. The NHS estimated that for every £1 spent on orthotics services, £4 could be saved as a result of its provision [7]. This cost saving stems from reduced hospital stays, surgeries, and consultations to name a few. The improvement to independence and mobility enables people to work or go to school, increasing integration into society and reducing the requirement for social care. Currently, patients not receiving adequate orthotic care can cost the NHS around £390 million every year [7]. Comparatively, in 2015-2016 the reported annual cost of orthotic provision and services was £48.6 million, across the 55% of NHS trusts and health boards who had responded to a survey [11]. Similar findings have been identified in the US, where the Medicare payments of matched pairs of patients receiving lower limb orthoses were compared to those who did not, over an 18-month period. The analysis revealed significantly lower episode payments for those who received orthoses, compared to those who did not. This was estimated as a $2920 saving for the 2007-2010 period and $1939 for the 2011-2014 period [12]. The largest contributors to this were cost reductions in acute care hospitals and drug spending.

The benefits of having orthotic devices and services that satisfactorily meet requirements are clear. That orthotics is an area often overlooked by health services and research presents many issues, not only in patient access to orthotics services, but also with the technological development of the orthoses themselves. This results in many individuals being unsatisfied with their orthosis and an unmet need in healthcare research [13]. To understand orthotic requirements, first there must be an awareness of normal foot and ankle function and how the user's condition may have affected this.

1.1 Foot and Ankle Anatomy

The foot and ankle complex consists of 26 bones, in addition to the distal tibia and fibula, a total of 33 joints, 12 extrinsic muscles and numerous tendons and ligaments (Figure 1.1). This anatomy allows for motion of the foot in three planes whilst maintaining stability (Figure 1.2). In the sagittal plane, there is plantar- and dorsiflexion where the foot rotates either downwards away from, or upwards towards the shin. Inversion and eversion in the frontal plane involve the sole of the foot facing towards or away from the midline of the body. Finally, abduction and adduction in the transverse plane cause the forefoot to rotate towards or away from the midline [14]. These foot motions can be coupled into two broad categories: pronation, a combination of dorsiflexion, eversion and abduction; and supination, which consists of plantarflexion, inversion and adduction. Both of these types of movement are normal, and problems only arise if the movement is

excessive or if the foot's resting position is pronated or supinated due to deformities (e.g. pes planus or pes cavus).

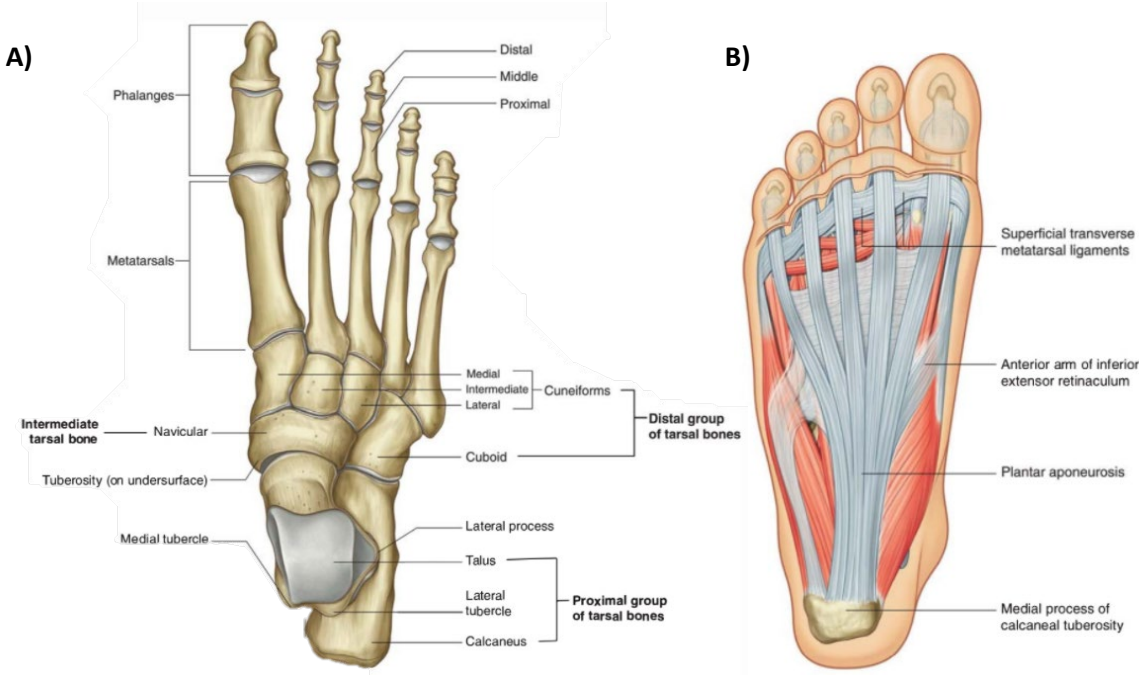

Figure 1.1: Anatomy of the right foot and ankle, **A)** Bony anatomy; **B)** Plantar aspect of the foot, indicating the plantar aponeurosis [15]

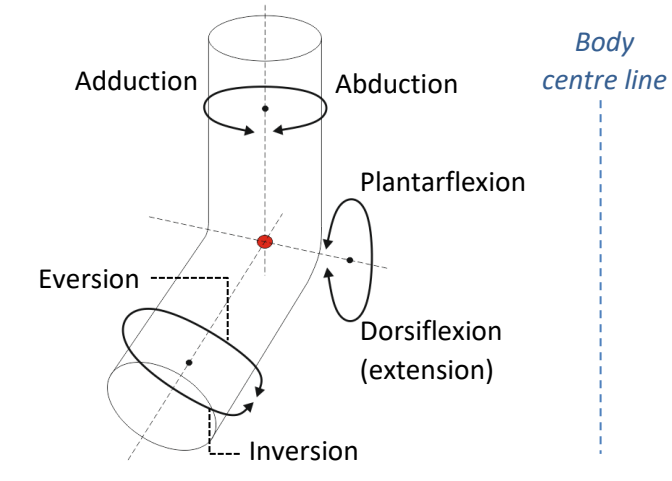

Figure 1.2: Simplified diagram of the right ankle and foot from an anterior view, detailing adduction/abduction, flexion/extension and inversion/eversion

The bone geometries, ligaments and muscles allow loads to be redistributed throughout the foot. During gait, both extrinsic and intrinsic muscles (originating proximal to and within the foot respectively) act to provide the different motions of the foot, with the intrinsic muscles primarily acting to stabilise the foot and enable toe movements [15]. The plantar aponeurosis also contributes to the stability of the foot and contracts to shorten the distance from heel to toe,

increasing the arch of the foot, and aiding propulsion during gait [16]. A fat pad stretches across the plantar surface of the foot, assisting load distribution and providing shock absorption [17]. In normal gait, the foot and ankle position changes from heel strike through to toe-off and the swing phase (Figure 1.3). The ankle begins with mild plantarflexion and inversion at heel strike before pivoting to bring the foot flat against the ground for mid-stance, where the foot is in eversion. The ankle then moves into dorsiflexion as the leg revolves forward around the ankle, and then returns to plantarflexion at toe-off. Finally, as the swing phase begins, the ankle moves into dorsiflexion to avoid the toes contacting the ground, which could cause tripping [14].

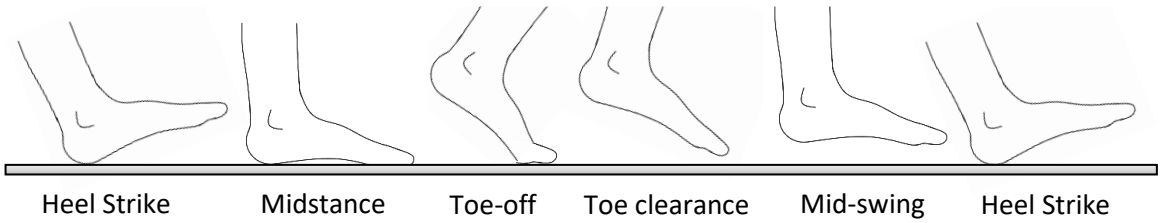

Figure 1.3: Stages of the gait cycle

The forefoot is a specific focus of this research, due to the pathologies that can occur there (see Section 1.2), and the importance of how orthoses interact with the tissues in this region (see Section 1.3.1). The main joints of the forefoot are the metatarsophalangeal (MTP) joints, where the metatarsal bones and phalanges meet (Figure 1.4A). Transverse ligaments run between the metatarsal heads providing stability to the joints, and various tendons attach so that the joints can provide flexion/extension and abduction/adduction [15] (Figure 1.4B). Two sesamoid bones are embedded in one such tendon beneath the 1st MTP. The sesamoids provide stability to the medial forefoot and play a key role in weight distribution during gait [18].

Generally, the forefoot follows the pronation/supination motions of normal gait described previously. In addition, the MTP joints are particularly active at the end of the stance phase, from heel-off to toe-off, when the MTP joints rotate as extension occurs, affecting the orientation of the metatarsal heads relative to the ground. The sesamoid bones also play a role in this time, aiding weight distribution and protecting the 1st MTP joint by distributing loads away from the metatarsal head. During stance, the sesamoids are proximal to the 1st MTP joint, but as the foot moves from midstance through to toe-off, and dorsiflexion occurs, the sesamoids shift distally to lie between the plantar aspect of the 1st metatarsal head (MH1) and the ground [18]. This highlights the dynamic nature in which the foot and ankle provide stability, mobility and weight transfer. From a young age, regularly loaded tissues are conditioned to become load tolerant [19, 20], however age and comorbidities can reduce this tissue tolerance making the skin and sub-

dermal tissue vulnerable to damage. This has implications for lower limb orthosis design in terms of protection of more vulnerable tissues.

A)

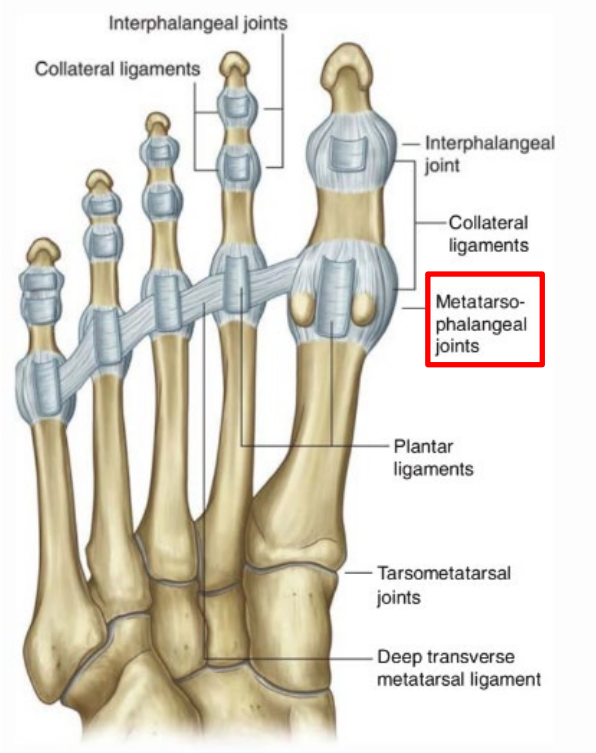

B)

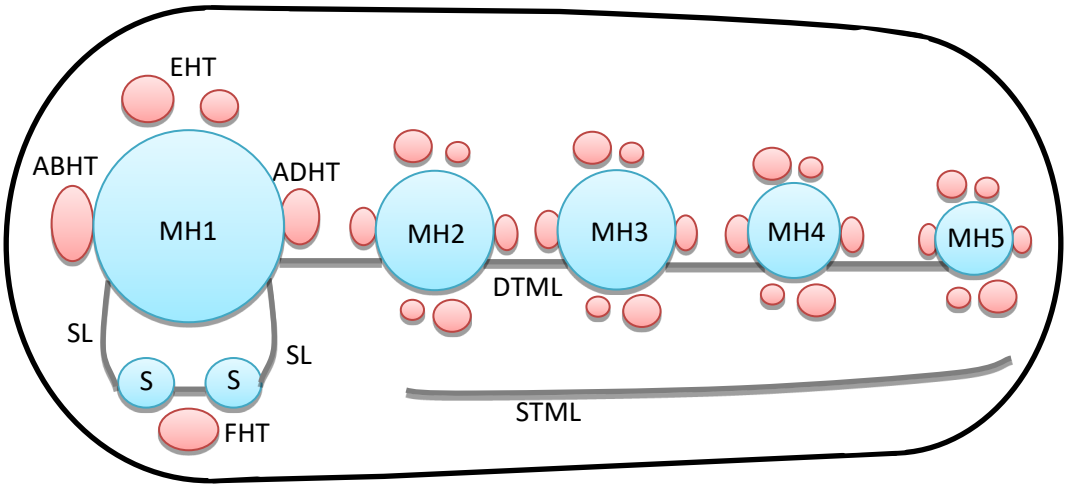

Key:

MH1-5 = 1-5th metatarsal heads
S = sesamoid bones
SL = sesamoid ligaments
DTML = deep transverse metatarsal ligament
STML = superficial transverse metatarsal ligament

FHT = flexor hallucis longis tendon
EHT = extensor hallucis longis/brevis tendons
ABHT = abductor hallucis tendon
ADHT = adductor hallucis tendon

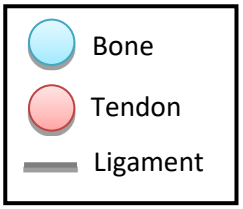

Figure 1.4: Anatomy of the forefoot, **A)** Plantar view of the forefoot joints, with the metatarsophalangeal joints highlighted in red box (adapted from [15]), **B)** Diagrammatic representation, with key anatomical features (adapted from [21, 22]). Note: MH2-5 also have equivalent flexor, extensor, abductor and adductor tendons.

1.2 Treatment of Foot Pathologies using Lower Limb Orthoses

Broadly, the purpose of lower limb orthoses can be corrective and/or accommodative, and the actions required vary with the user's pathology (Figure 1.5). Corrective orthoses, such as AFOs, provide support and stability to the user and may be used to improve alignment, prevent or reduce deformity, or affect biomechanics to improve motion. On the other hand, accommodative devices, such as FOs, focus on off-loading and protecting vulnerable regions or providing cushioning to improve comfort and reduce pain. As such, these two types of devices are used to treat very different foot/ankle pathologies.

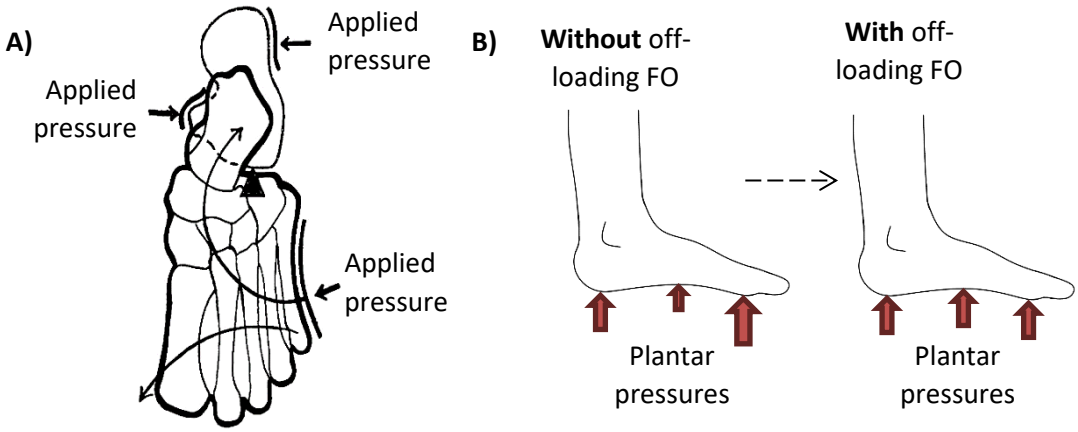

Figure 1.5: **A)** Example of 3-point corrective action applied by an AFO to improve medial-lateral foot alignment [23], **B)** Example of forefoot off-loading and pressure redistribution occurring with an accommodative FO.

1.2.1 Exemplar Conditions treated with AFOs

Neuromuscular or musculoskeletal conditions can impact the normal patterns of movement during gait, for example through muscle weakness or deformity leading to incorrect positioning of the foot. People with these conditions may benefit from the use of a corrective orthosis, such as an AFO, to improve mobility and foot positioning. For example, a cerebral vascular accident ('stroke') can lead to spastic equinus or equinovarus deformities, or foot drop, which result in the forefoot not lifting correctly during the swing phase of gait, limiting the foot's clearance. This can cause the toes to strike the ground first rather than the heel. AFOs have been shown to aid patients with such conditions by reducing excessive plantarflexion and positioning the ankle better at the point of initial ground contact [24]. This has the additional benefit of reducing fall risk of the individuals [25]. Another disease that may require treatment with an AFO is poliomyelitis, which alongside post-polio syndrome affects 12-20 million people worldwide and may lead to muscle weakness that impacts mobility [26].

Children may also use AFOs as a method of reducing the chances of deformity and increasing their ability to act independently [27]. One of the most prevalent indicating conditions is cerebral palsy, which occurs in 2-3 children per 1000 live births [28], and results in muscle spasticity in 75% of cases [29]. There are many other conditions that can also be treated using an AFO including multiple sclerosis [30], Charcot Marie Tooth disease [31], and myelomeningocele – a form of spina bifida [27]. These conditions can all cause muscle weakness, foot drop or paresis of the lower limb and so the use of an AFO can aid mobility and prevent falls.

1.2.2 Treatment of Rheumatoid Arthritis with FOs

Many neurological, musculoskeletal, or inflammatory conditions are treated with FOs, usually for off-loading purposes. This research focuses on rheumatoid arthritis (RA), where FOs are commonly prescribed as a cost-effective method of treating various foot problems. RA is an inflammatory disease, thought to affect between 0.5-1% of the population, and women more so than men [32]. The disease particularly affects a person's joints, though specific manifestations can vary between individuals. The forefoot can be especially affected by RA, with deformities frequently occurring at the MTP joints, alongside erosion and subluxation [33]. Hallux valgus is one of the more common deformities, and also causes the sesamoid bones to displace laterally [34]. Morphological changes may also occur in the surrounding soft tissues, with the plantar fat pad migrating away from under the metatarsal heads [35]. The MTP joints are then more vulnerable, with the shock absorption usually provided by the fat pad limited. People with RA also experience bursae inflammation or adventitial bursae formation due to high pressure and friction acting on the foot [36, 37] (Figure 1.6). These many changes can result in pain, increased plantar pressures, reduced foot function, and ulceration [33, 38]. Ulceration is most common at the dorsal aspect of the hammer toes and the plantar aspect of the metatarsal heads, with many of those ulcers recurring [39]. The skin can also be affected by the medication prescribed to treat RA, with side effects including skin atrophy and rashes [40]. Reduced keratinocyte proliferation, fibroblast size and collagen synthesis can result in the skin becoming thinner and more fragile, with inhibited wound healing [41].

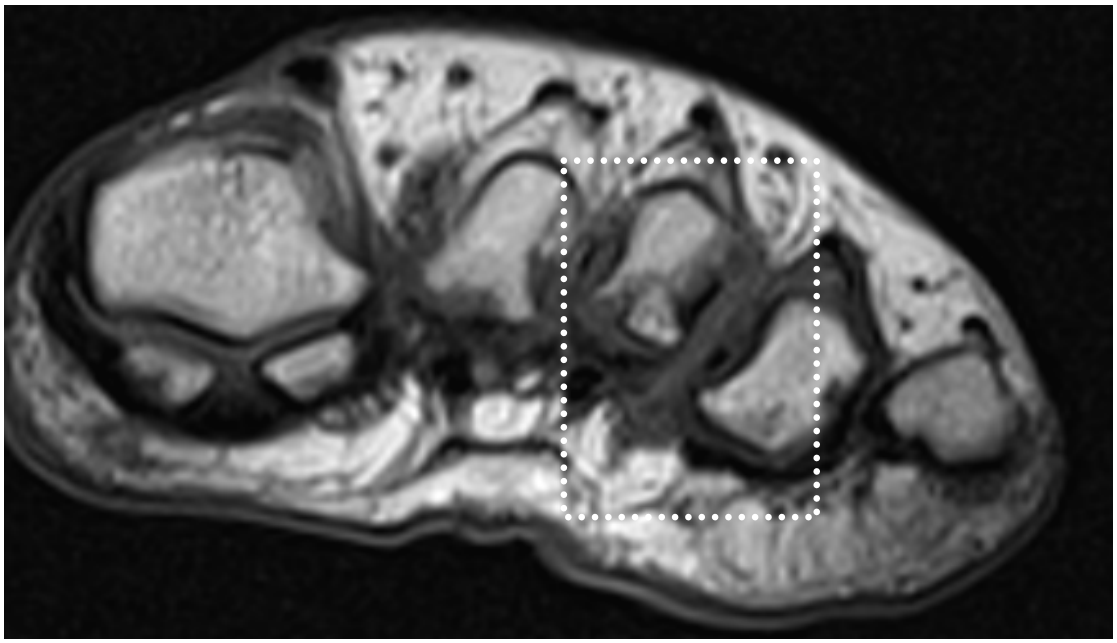

Figure 1.6: Coronal MR section of the metatarsal heads, with an intermetatarsal lesion due to rheumatoid arthritis identified (dark teardrop shape within dotted box) [21]

Both forefoot and rearfoot abnormalities in RA have an impact on a person's gait. Individuals tend to walk slower, with a reduced stride length and more flat-footed contact with the ground, due to the reduced range of motion of their affected joints [42]. Increased eversion of the foot and hyperextension of the MTP joints also occur, increasing the joints' vulnerability to loading [43]. The vulnerability is further exacerbated by the lateral offset of the sesamoid bones, which may no longer be in a position to provide optimal load distribution. These alterations often result in increased forefoot plantar pressures and shear forces, impacting tissue damage risk. However, some individuals have also been found to off-load painful regions of the foot, which may cause problems in adjacent regions [33, 44].

FOs may be prescribed to stabilise the foot and limit the adverse effects of the RA, by providing a cushioning material to replace the lost integrity of the soft tissue underneath and off-loading painful regions. However, while in some cases FOs have reduced pain and disability [45], there are limitations to their current effectiveness clinically which will be discussed further in the next section.

1.3 Lower Limb Orthosis Designs and their Current Limitations

Establishing normal foot anatomy and gait, and the pathological changes that can occur, provides an understanding of orthosis requirements. The type of orthosis prescribed – whether custom-made or off-the-shelf, the material used and the geometry – is dependent on the user's pathology

and needs. This applies both between individuals with different conditions and those with the same, as they will have differing presentations and condition severity.

1.3.1 AFOs

Material choice and geometry of AFOs generally varies with whether the devices are custom-made or off-the-shelf, with the latter typically only suitable for those with less severe conditions. Custom AFOs are generally manufactured from thermoplastics such as polypropylene, and the off-the-shelf devices made from plastic or carbon fibre. Cushioning may be added to pad regions of a custom AFO, but this tends to be on an ad-hoc basis with the material dependent on the clinician. Different designs that may be used include the posterior leaf spring, rigid, articulated, and anti-talus AFOs. Supra-malleolar devices are also available, which extend only to cover the malleoli of the ankle rather than continuing up the calf. Each device type has a different functionality and therefore indicators for patient use (Table 1.1). Off-the-shelf AFOs tend to be of the posterior leaf spring variety or similar. Softer AFOs are also available, made from lycra or silicone for example [46]. However, similarly to off-the-shelf devices, these are only suitable for some conditions.

Table 1.1: Examples of functionality and indicators for use of different AFO designs [24, 47-49].

AFO Design	**Image**	**Functionality**	**Indicators for Use**
Posterior leaf spring (ICRC [47])	Removed due to copyright	• Aids dorsiflexion, • Limited subtalar joint medio-lateral stabilisation.	• Muscle weakness in dorsiflexion only, • Little to no problems with muscle tone or mediolateral stability.
Rigid (ICRC [47])	Removed due to copyright	• Prevents ankle movements, • Stabilises medio-lateral movement of the subtalar joint, • Ad/abduction control.	• Moderate/severe foot deformity, • Hypertonicity, • Poor balance and stability, • Gait improvement desired.
Articulated (ICRC [47])	Removed due to copyright	• Free dorsiflexion, • Plantar flexion may be free or inhibited, • Stabilises medio-lateral movement of the subtalar joint.	• Muscle weakness in dorsiflexion only, • Dorsiflexion aid required for e.g. climbing stairs, • Gait improvement desired.

AFO Design	Image	Functionality	Indicators for Use
Anti-talus (ICRC [47])	Removed due to copyright	• Prevents ankle movements, particularly dorsiflexion, • Limited subtalar joint medio-lateral stabilisation.	• Correction required for subtalar pronation.
Supra-malleolar (Arizona AFO [50])	Removed due to copyright	• Allows dorsi- and plantarflexion, • Stabilises mediolateral movement.	• Mostly used in paediatric cases, • Pathologies such as flexible flatfoot (hyper-pronation, valgus).

While AFOs can provide many benefits, the negative aspects of wearing them can lead to users being unhappy with their device or preferring not to use it. As such, adherence (sometimes termed 'compliance') to device use becomes an important consideration. Alongside social factors, such as device aesthetics, some of the most common problems associated with AFO use are pain, inflammation and discomfort [31, 51-54]. These problems may occur particularly around bony prominences such as the navicular head, malleoli, and metatarsal heads where soft tissue protection is limited [27, 55]. Excessive sweating, and the potential associated skin problems, are also complaints of many AFO users [51, 53, 54, 56].

Some users will continue to wear their orthosis despite experiencing problems because the benefits provided outweigh the shortcomings. The rates of adherence with AFOs, and how adherence has been assessed, have varied throughout the literature, ranging from 54-89% in larger-cohort studies [54, 57-59]. The amount of AFO use prescribed, and thus what constitutes adherence, will depend on the user's condition, but the benefits of adhering to device use have been shown. For example, in the treatment of stroke, consistent use of an AFO over time can improve gait, mobility and participation compared to the immediate effects of the device [60]. Thus, the limitations of AFO designs must be addressed not only to reduce user pain and discomfort, but to ensure users wear their device as needed to prevent their condition worsening and reduce costs to health services.

1.3.2 FOs

Similarly to AFOs, FOs vary in material, geometry and whether custom or prefabricated. For RA, a combination of flat cushioning FOs, prefabricated (with generic foot contours) FOs, and custom-made FOs are prescribed (Figure 1.7), with the outer shell and cushioning materials varying in stiffness [61]. Other modifications to the FO geometry may be made to better protect specific regions, such as metatarsal domes or bars [62]. In the case of RA, the type of FO prescribed varies

with the individual's condition. For example, stiffer materials may be used to help prevent deformity and restrict over-pronation, but softer materials may be beneficial to those with rigid foot conditions [63]. However, prescription tendencies also vary between clinicians, as no single best practice has yet been established due to limited evidence of effectiveness of any one FO design. While some evidence of plantar pressure and pain reductions has been seen with certain orthoses over others, there has been no conclusive evidence found of improved foot function or gait parameters [62, 64]. There are other considerations in addition to clinical effectiveness. For example, while custom FOs have shown benefits over flat FOs [45], there may be limited difference in effect between custom and contoured prefabricated FOs [65]. Therefore, the extra expense and time delays associated with manufacture of a custom FO may not be worthwhile.

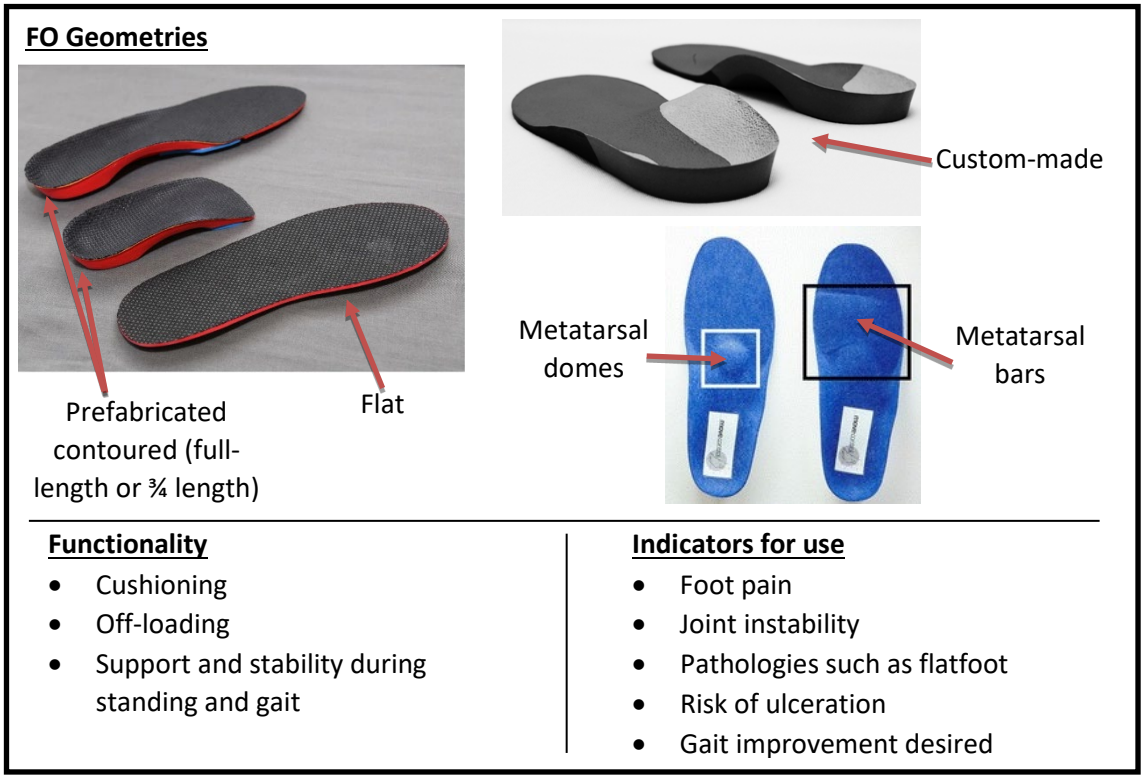

Figure 1.7: Examples of FO geometries, functionality, and indicators for use. Images from [66-68]

It should be noted that a limitation of many clinical and experimental studies assessing FO designs, is the focus on plantar pressure reduction to optimise the orthoses. This is particularly an issue in treating RA, where plantar pressure reductions have not always corresponded to improvements in condition. This will be discussed further in the literature review, Sections 2.1.1.1 and 2.2. An improved understanding of the effects of different FO designs is required, particularly on the internal soft tissue, to ensure they are effective at improving the individuals' quality of life.

1.4 Research Motivation and Overarching Aim

There is a common theme of orthosis design affecting a person's quality of life through the orthoses biomechanical and thermal interactions with the end user. These interactions have a direct effect on the soft tissue, and there are design-related limitations to current AFO and FO designs that could be improved through research. For AFOs, the tissue damage risk often stems from the device itself, having a rigid material contacting the limb for long periods of time resulting in increased pressure, shear and microclimate. Conversely, for FOs the tissue damage may be a result of the person's condition, which the orthosis may not fully alleviate when trying to offload and protect the vulnerable tissues.

This research aimed to address gaps in previous orthosis biomechanics studies, which for AFOs have primarily focussed on device functionality, namely their impact on gait or musculoskeletal function. Relatively little has been published on the devices' interaction with the underlying skin and soft tissues, or their effects on sweating or microclimate. Similarly, with regard to FOs, limited research has been carried out assessing their effect on deep soft tissues, particularly for people with RA. Computational studies that have compared FO designs have tended to only consider a single healthy individual.

Thus, the overarching aim of this research was to investigate how lower limb orthosis design parameters affect biomarkers related to the health of both superficial and deep soft tissues, and how those effects may vary between individuals who may have different requirements. A combined approach of experimental testing and computational modelling using previously collected MR data was utilised, and two scenarios were considered in this project:

1. The effect of AFO material and fit, using experimental and computational methods in a healthy group,
2. The effect of FO material, geometry, and shoe type using computational methods in a symptomatic group of people with RA.

By assessing two different orthosis types, the applicability of the computational methods to different devices, with varying degrees of foot and ankle interaction but commonality in the plantar region being of interest, could be observed.

The following chapter contains a review of relevant literature, assessing mechanisms of tissue damage and measurement methods, and previous computational modelling of AFOs, FOs and tissue damage. The review was used to determine suitable research questions and objectives, which are detailed at the end of Chapter 2.

Chapter 2 Literature Review

Risk of tissue damage is a key consideration in lower limb orthosis design. The purpose of the device may be to reduce damage, or the device may cause damage while fulfilling its intended function. To gain understanding of tissue damage risk, a literature review was performed to identify different tissue damage mechanisms and the various contributing factors. Following that, current tissue damage measurement techniques relevant to lower limb orthoses, experimental assessment of the different devices, and computational modelling of the lower limb for orthosis design were critiqued. The literature review was used to develop research questions, which are detailed along with the project objectives and novelty of the present work in Section 2.4.

2.1 Soft Tissue Damage

There are different mechanisms by which soft tissue damage can occur. These include damage due to direct cell deformation, ischaemia, reperfusion injury and lymphatic impairment [69]. Direct deformation damage may occur when the forces generate strain which is sufficiently high to cause damage within a short period of time, rupturing the cell cytoskeleton. However, lower forces may also cause damage if applied for a prolonged period. Ischaemia occurs when blood vessels are occluded, depriving the tissues of oxygen, resulting in anaerobic cell metabolic processes and eventually cell death [70]. This may be accompanied by lymphatic impairment, if lymph vessels are occluded by the loading, causing a build-up of toxins produced during metabolism. Injury may also be caused by reperfusion following a period of ischaemia, as the increase in blood flow to the tissues can result in cell damage [71]. This occurs through production of reactive oxygen species (ROS), imbalance of ions, triggering of inflammatory responses, and endothelial dysfunction [72].

The term pressure injury (PI), or pressure ulcer, is used to refer to tissue damage caused by applied pressures and/or shear forces. These injuries are often due to medical devices, such as orthoses, and classifications for the type and severity of PIs have been established (Figure 2.1). While it is most common for PIs to affect the superficial tissues first and then propagate towards the bone, in some cases deep tissue injury (DTI) can occur [73]. With DTI, damage begins in the deeper tissues, often beside the bone, and spreads towards the skin. As such, the presence of a DTI and the extent of the damage are harder to measure than with superficial injuries. Soft tissue injuries are particularly likely around bony prominences due to strain gradients, as the tissue compression against the bone is resolved into shear (deviatoric) strain [74]. Thus, where there is uniform strain in the tissue it is not necessarily indicative of tissue damage risk, even at high

magnitudes. Potentially damaging shear strains can also be generated in the superficial tissues, by external shear forces such as friction.

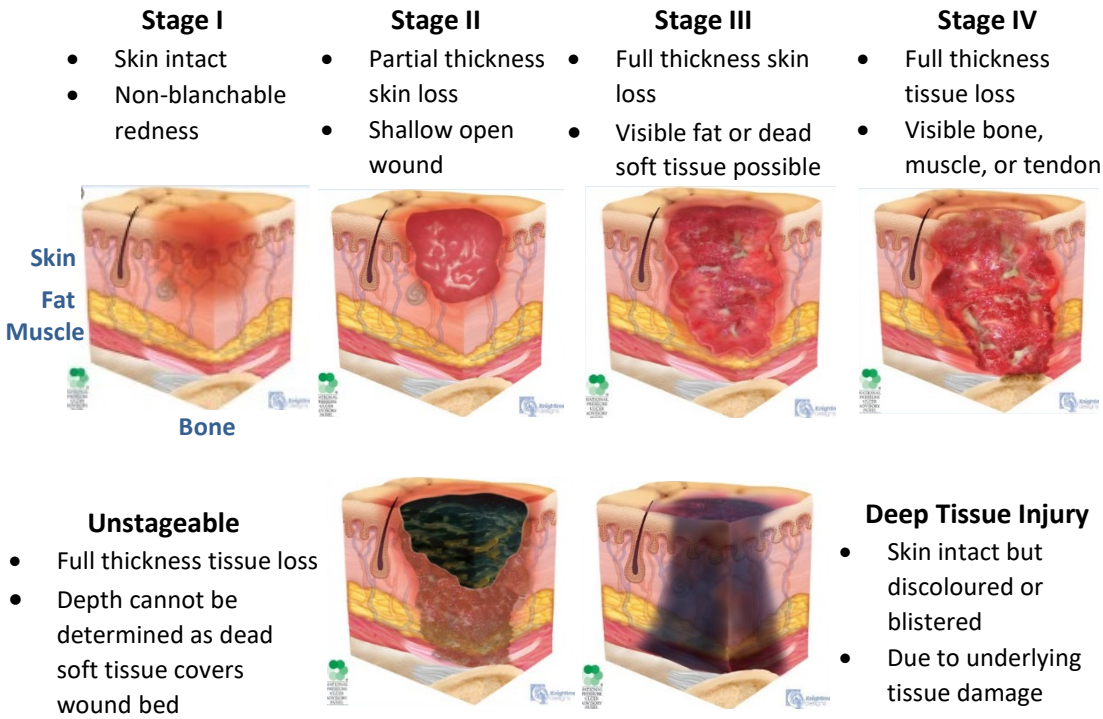

Figure 2.1: Classifications of pressure injuries that may occur due to medical devices [75]

2.1.1 Assessment of Tissue Damage and Tissue Damage Risk

There are various methods for assessing potential tissue damage due to loading (Table 2.1). The techniques to be used must be carefully chosen, as their suitability is dependent on the application. For example, choice of technique may depend on whether real-time responses are required, if the degree of damage is of interest, or if the technique can provide an early indicator that tissue damage may occur. Thus, an understanding of the feasibility and effectiveness of the different methods is beneficial. Ischaemia can be assessed by monitoring the microvascular response using transcutaneous gas tensions, indicated by a reduction in oxygen and subsequent increase in carbon dioxide [76]. Subepidermal moisture, elasticity and redness have been shown to detect whether skin was healthy or a pressure injury site, though could not determine the extent of the damage [77]. Transepidermal water loss (TEWL) has been found to increase in response to loading at regions including the heel, which is indicative of lost skin barrier integrity [78, 79].

The presence of certain biomarkers can indicate where loading is causing inflammation that could lead to tissue damage, prior to the damage occurring. Interleukin-1α (IL-1α) is an inflammatory cytokine that is released from viable corneocytes following mechanical deformation. Interleukin-1

Receptor Antagonist (IL-1RA) then acts competitively to inhibit the IL-1α [80]. The biomarkers can be measured non-invasively by taking a skin sebum sample using absorbent tape, and this method has been used previously to assess risk of tissue damage at the interface between the skin and a medical device [81, 82]. The ratio of IL-1α to IL-1RA can also show whether a controlled and balanced inflammatory response has occurred [83, 84]. Other cytokines have also been trialled as indicators of tissue damage, however the results were either not as clear or consistent as using IL-1α and IL-1RA or only showed a response after tissue damage was already occurring [82].

Imaging techniques can also be used to assess tissue damage. Magnetic resonance imaging (MRI) can be used to investigate musculoskeletal damage due to loading, which has been carried out previously through indentation testing of animal models [85, 86]. MRI has also been used to monitor oedema and muscle atrophy in residual limbs following transtibial amputation [87]. With regards to device-related tissue damage risk, imaging data can show risk in the form of deformations occurring, as used in comparisons of support surfaces [88, 89]. Similar methods could be carried out for lower limb devices, provided relevant loading conditions could be applied and the device was MR compatible. This may require use of an upright MR machine, or a device to apply loads during the scan [90]. Imaging data may also be used to provide anatomy for the assessment of device-related tissue damage risk through computational modelling, which is discussed further in Section 2.2.

Table 2.1: Techniques for assessing tissue damage risk

Measurement Technique	**Tissue Damage Mechanism Measured**	**Effectiveness and Ease of Use**
Transcutaneous gas tension	Ischaemia	• Real-time • Sensors would affect pressure distributions on skin • Sensors must be heated to above physiological conditions to be effective [91]
Transepidermal Water Loss (TEWL)	Skin barrier damage due to loading	• Not real-time, non-invasive • Early indicator of skin damage • Potentially dependent on location due to varying skin structure, but shown to be effective at the heel [78]
Colorimetric assessment of redness/erythema	Skin blood perfusion increases due to onset of tissue damage	• Not real-time, non-invasive • May not indicate degree of damage

Measurement Technique	Tissue Damage Mechanism Measured	Effectiveness and Ease of Use
Sub-epidermal moisture	Local oedema, inflammation	• Not real-time, non-invasive • Can identify oedema prior to skin damage occurring, in ulcer formation [92] • May not indicate degree of damage
MRI	Dependent on use – can indicate deformation, structural damage, morphological changes due to e.g. oedema	• Non-invasive • Tissue composition can be observed • May not be feasible due to machine access and expense
Biomarkers	Inflammation due to applied pressures and shear	• Effectiveness dependent on which cytokines assessed • Potentially not specific as react to various stimuli, e.g. chemical insults • Easy, non-invasive procedure • Not real-time (may be applied after an intervention) • Analysis time-consuming

2.1.1.1 Plantar Pressure Metrics

With regards to tissue damage in the foot, plantar pressures are often measured to examine the effectiveness of lower limb orthoses and footwear in alleviating pain and reducing the risk of tissue damage. In-shoe pressure sensors, such as the F-scan system (Tekscan, USA) or the Pedar system (Novel GmbH, Germany) provide a method of determining the pressure acting directly on the limb. The F-scan system provides a higher spatial resolution and thinner sensing insole. However, it does not conform as well to the foot due to the material used, which has high in-plane stiffness which can result in wrinkles in the sensor (Table 2.2). Hsiao et al. [93] analysed both sensing systems and showed that the F-scan system calibration technique and the age of the Pedar sensor influenced the sensor performance. Woodburn and Helliwell [94] found that the F-scan sensors displayed hysteresis of up to 21%. However, this maximum hysteresis was observed at an input pressure of 1200kPa, well above the maximum pressure Tekscan report of 862kPa and so the sensor may have been saturated. At lower input pressures, the hysteresis was lower, particularly during loading. It should also be noted that Woodburn and Helliwell's study was carried out over 20 years ago, and so the hysteresis measured may not reflect the current F-scan system which has been improved since then. However, while more recent studies have assessed different F-scan sensor characteristics, none were found that reported the hysteresis.

Table 2.2: Performance characteristics of the F-scan (Tekscan) and Pedar (Novel) systems

System Characteristic	F-scan	Pedar
Insole Thickness (mm)	0.18	1.9
Pressure Range (kPa)	483 or 862 (minimums not reported)	15-600 or 30-1200
Spatial Resolution	3.9 sensors per cm^2: up to 954 per insole	85 – 99 sensors per insole
Conformity	Poor conformity	Highly conforming, elastic material
Hysteresis	<21% [94]	<7% [95]
Time-dependent change [93]	<4.5%	4.4%
Sensing Technology	Resistive	Capacitive
Wireless Option	Yes	Yes

These systems have been used in various studies including assessing the risk of diabetic ulcers when using different insoles [96, 97], and evaluating footwear choices to reduce pain associated with gout [98] or arthritis [99]. In-shoe sensors have also been used to compare the effect of different AFO designs on peak plantar pressures and distributions [100-102]. In many of these studies, the plantar pressure data is divided into key regions of the foot, and the peak pressures for those regions compared between different interventions. However, by only looking at a single point of peak pressure, most of the spatial pressure data is lost, and so the results may not be indicative of the overall effect on the soft tissue and would not show whether gradients were present. Some studies [97-99] have also considered the pressure-time integral (PTI) as a method of including the temporal aspect of applied pressure during the gait cycle. This provides the benefit of showing how long high pressures are applied for, but again gives no spatial data. One study investigating prosthetic socket comfort examined the differences in socket pressure distributions, as well as peak pressures and temporal pressure data [103]. By analysing the pressure distributions, the researchers could indicate regions where pressure gradients and shear stress may have been higher. As shear loads have been found to influence tissue damage [104], analysing pressure distributions and gradients could provide a better indicator of tissue damage risk than just examining the peak pressures (discussed further in Section 2.3.4).

In the case of rheumatoid arthritis (RA) specifically, various experimental studies have assessed peak plantar pressures and PTIs to determine their relationship to other condition related factors such as pain and disability. However, while RA has generally been found to cause increased peak pressures in the forefoot [33, 44, 105], there has been mixed evidence on how well plantar pressure measurements represent the condition of the underlying soft tissue. PTIs have been shown to have a significant correlation with forefoot joint damage and pain, but peak pressures only correlated with joint damage at the 1^{st} and 4^{th} metatarsal heads and not at all with pain [38].

Others have found that both peak pressure and PTI were related to forefoot deformities at the metatarsophalangeal joints and toes but that neither was associated with pain or swelling [106]. When considering ultrasound-detectable pathologies, such as bursae, the location of peak pressures within the forefoot negatively correlated to pathology location [33]. This may have been due to individuals adopting compensatory gait changes to offload affected regions of the foot, and highlights a key limitation of only targeting peak pressures with interventions.

Plantar pressure pain thresholds (PPTs) for individuals with RA have also been examined to provide context for how pain relief may be achieved through FO use [107]. It was found that RA caused lower PPTs than a control group, indicating pain was felt at lower pressures. These lower PPTs may be due to manifestations of RA (see Section 1.2.2) increasing the vulnerability of the joints and tissues, thus reducing the applied pressure needed to cause pain. Additionally, the PPT for the RA group was more uniform across the sole of the foot, rather than being higher in load-bearing regions (e.g. under the metatarsal heads) as occurs in healthy individuals. This has implications for FO design for people with RA, as the lower PPTs must be considered if pain relief is targeted through pressure reductions. However, as mentioned previously, there are varied findings on the relationship between plantar pressures and pain for those with RA. As such, there may be more suitable metrics to assess pain relief with FOs.

2.1.2 Tissue Damage Thresholds and Factors affecting Tissue Damage Risk

Pressure or strain thresholds for tissue damage risk are an important consideration for assessing different orthosis designs. As it has been established that loading can be more damaging when sustained rather than only applied for a short period, a sigmoid curve was developed to indicate thresholds for predicting soft tissue injury. The curve accounted for both the magnitude and duration of pressure or tissue deformation [108]. This model indicated that in short time periods (<1h), muscle tissue can tolerate relative deformations of up to 75-80% whereas over longer periods the tolerance threshold reduces to 50% (Figure 2.2). Establishing thresholds for tissue damage risk allows more targeted interventions for those more at risk. However, tissue damage is a complex process with many potential mechanisms, and there are a number of influencing factors that were not considered in the sigmoid curve model, such as shear loading [104]. Shear strains in the soft tissue exceeding 50-60% have been found to cause direct deformation damage in rats [109]. However, this threshold would not account for other forms of damage, as ischaemia can occur at much lower loading magnitudes over a prolonged time.

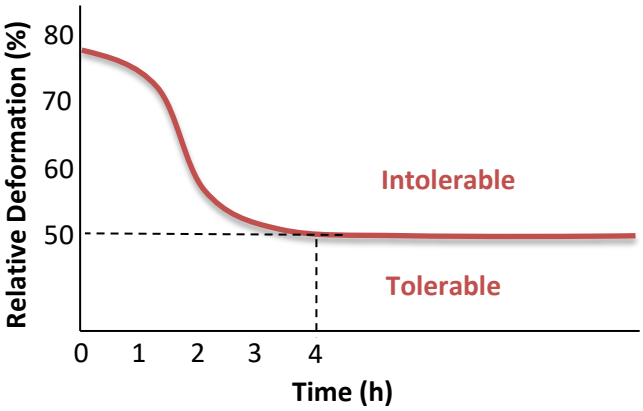

Figure 2.2: Sigmoid curve tissue damage model, adapted from [108]

The tissues' tolerance to loading also impacts how much load can be applied before damage occurs. This may be due to tissue structure varying at different locations or an individual having lower tolerance due to comorbidities, nutritional factors or sensory perception [74, 110]. For example, in RA the loss of plantar fat pad integrity and skin atrophy due to medication reduce the tissue's tolerance. Tissue can also adapt to loading over time to reduce the damage risk, for instance through callus formation due to repetitive stresses acting on the tissue, particularly at bony prominences and deformities. To protect the tissue, the keratin layer of the epidermis thickens thus increasing the tissue's tolerance to the loading [111]. However, this may also have negative implications if the presence of the callus results in increased pressures applied to the region due to a tighter fit with footwear for example [112]. Coleman et al. [113] developed a framework detailing the different factors that can contribute to tissue damage risk, separating the factors into loading conditions (i.e. extrinsic) and an individual's tolerance to the loading (intrinsic), (Figure 2.3). Microclimate has also been found to affect the likelihood of tissue damage, with temperature and humidity playing a role in tissue tolerance to loading [114].

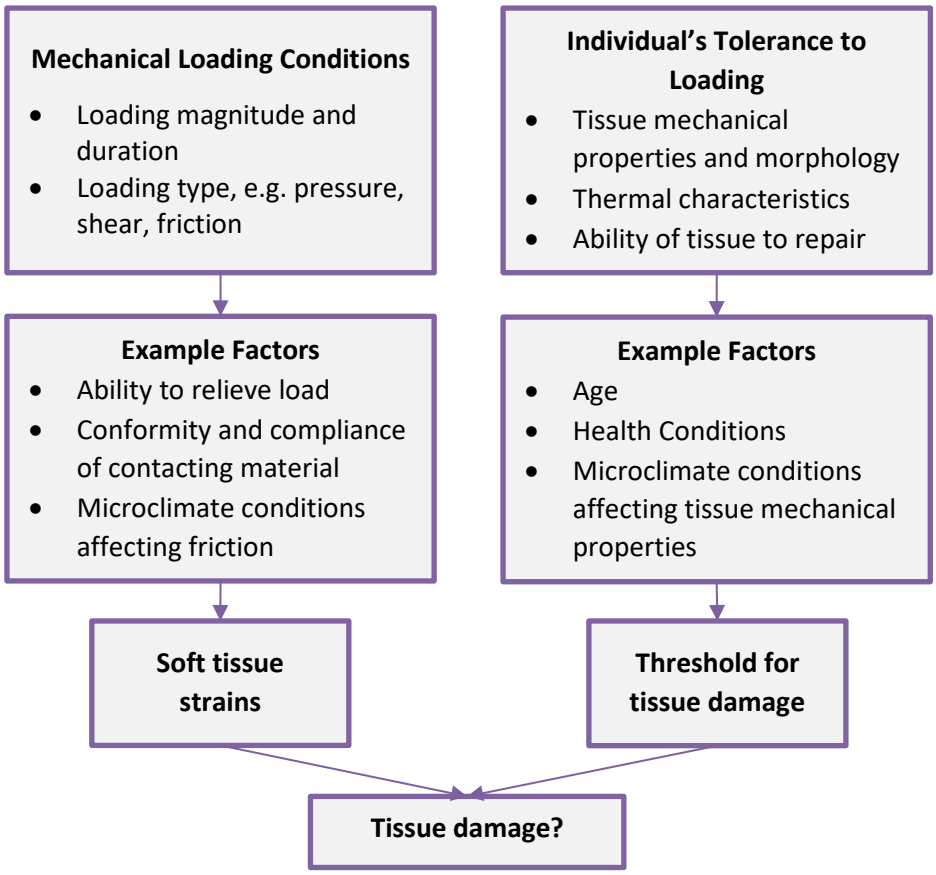

Figure 2.3: Schematic of the risk factors contributing to tissue damage, adapted from [113-116]

2.1.3 Effects of Microclimate of Tissue Damage Risk

The term microclimate relates to the humidity, temperature and air flow in a specific region. The microclimate next to the skin has been found to influence the occurrence of tissue damage. There are two factors that contribute to humidity on the skin – sweating and TEWL. Sweating is an active thermoregulatory process designed to cool the body, while TEWL is the passive diffusion of water out through the skin and into the environment [114]. Elevated moisture causes the skin to be more susceptible to damage. When the microclimate next to the skin changes, the stratum corneum – the skin's outermost layer – is affected first after which the effects propagate to deeper layers. In the case of relative humidity (RH) next to the skin increasing, the stratum corneum absorbs the fluid and skin hydration increases. This results in cell swelling and plasticization, reducing the skin's stiffness and shear strength [117]. It also increases the permeability of the skin, which makes it more prone to bacterial infection and irritant absorption [118].

Temperature has also been shown to have an effect on skin hydration, as increased temperature makes the skin more permeable to water, increasing TEWL [119]. As mentioned in Section 2.1.1, TEWL has also been found to increase under sustained periods of loading due to a compromised

skin barrier [79]. If the liquid cannot evaporate, TEWL and sweating will lead to moisture build-up on the skin. The stratum corneum can quickly recover and return to normal functionality and strength through evaporation of the moisture following removal of its source. However, if the skin surface is occluded by an impermeable orthosis, the heat and moisture are then trapped and build up on the skin, exacerbating the microclimate challenge.

Contact with another material also presents issues relating to friction and the resulting shear stresses, particularly as the coefficient of friction (CoF) can change with the skin's microclimate. There are two competing mechanisms when moisture is present at the skin – adhesion and lubrication. It is generally accepted that as the skin's topography is affected by increased hydration, there is greater contact area with the contacting surface and so adhesion – the main contributor to friction between a material and the skin – increases. As such, the CoF between hospital fabrics and the skin increases when the fabrics are wetted [120, 121]. The combination of increased friction and reduced mechanical strength of the skin increases the risk of skin delamination (blistering) [122].

Conversely, Ramirez et al. [123] found that the CoF between polypropylene and the skin reduced in the presence of artificial sweat. The difference in findings to the previously mentioned studies may have been due to the differing methods used to ascertain the CoF. Magnitude of contact pressure has been identified as a factor that can affect the CoF [104], and a higher pressure was applied in Ramirez et al.'s study. Additionally, Ramirez et al. tested rigid polypropylene, a more occlusive material than hospital fabrics, potentially allowing sufficient build-up of moisture for lubrication. Many AFOs are made from polypropylene or a similarly impermeable polymer. Although that might suggest similarity in friction conditions to Ramirez et al.'s study, they tested polypropylene directly against the skin. Generally, a sock is worn under an AFO, which would likely absorb moisture accumulating at the limb-orthosis interface. Thus, the CoF may increase with increasing hydration as was the case with hospital fabrics in contact with the skin. However, these studies all assessed the forearm or porcine skin, which will vary in structure and material properties to foot or ankle skin, potentially impacting friction. Additionally, highly dynamic loading is present during gait with an orthosis, but its effect on friction at the limb/device interface has not been investigated.

Consideration of microclimate with relation to AFOs and other lower limb orthoses is particularly important, given the occlusive nature of the materials and the high density of active sweat glands in the feet [124]. Additionally, some neurological conditions that can be treated with AFOs, such as footdrop after a stroke or cerebral palsy, can result in an impaired thermoregulatory system, impacting heat and sweat production [125-127]. Anecdotal evidence from highly experienced

physiotherapists (Solent NHS Trust) suggests that sweating is indeed a problem for children wearing AFOs, with some developing athlete's foot due to the moist conditions at the skin-orthosis interface. Current clinical solutions include changing socks throughout the day and the use of prescription deodorant. Little to no research has investigated whether the use of different materials in AFO design could aid in managing the microclimate at the interface. However, research for other applications has shown the effectiveness of tailoring material properties to better control microclimate and so has been considered below.

Some studies have investigated changes in microclimate with footwear and sock materials, either using a sweating foot manikin [128], or with participants undergoing exercise [129, 130]. Research into protective footwear has suggested that the microclimate within footwear should ideally be 28 to 34°C at a relative humidity of 60 to 65% for optimal user comfort [131, 132]. Various methods of maintaining this microclimate have been assessed. The use of sweat absorbent pads within footwear, which can also have antibacterial properties, has been shown to reduce the relative humidity of the skin, with no change to the temperature [129]. Bogerd et al.'s manikin study [128] found that sock material (mixes of wool, polyamide, and polypropylene) did not significantly affect heat loss, but that it could significantly impact moisture retention. West et al. [130] found that the less air permeable of two different running shoes led to increased foot skin temperature and relative humidity, when tested in a climate controlled room during a 40 minute run. Increased air speeds by the skin are known to aid heat and moisture dissipation [114]. Thus, more permeable footwear may allow greater airflow through the shoe during ambulation, providing better control of the microclimate and potentially improving comfort and tissue damage risk.

Most research into microclimate management relates to support surfaces, such as mattresses or wheelchair cushions. Studies have assessed the effect of various materials on microclimate, including foams, rubber, gels, and water floatation pads [133-137]. In many cases, a material may not be efficient at managing both temperature and relative humidity – for example, foam may control relative humidity better than gel but does not dissipate heat as well [133, 135]. Differences have also been shown in the effects of mattress material on the heel compared to the sacrum, potentially due to differences in skin structure [137]. Similarly to footwear, increased airflow can reduce the potential negative impact of a mattress on relative humidity and skin hydration [137-139].

In both support surface and footwear studies, microclimate management was considered for contacting materials that are far less rigid than an AFO may be. A more comparable application for AFO use might be face masks used for ventilation, typically featuring rigid and occlusive

plastics in contact with the skin. Wearing a mask can increase the skin hydration and TEWL, but using a silicone foam dressing as an interface material between the mask and skin can markedly reduce the change in skin hydration [140]. However, interface material choice is key as a hydrogel interface dressing was found to perform worse at limiting skin hydration increases than the plastic mask alone.

To optimise microclimate, materials must provide a balance in controlling the temperature and humidity, as well as limiting change to the CoF between the limb and the material when wet. However, AFOs have additional considerations that were not of concern in the other listed applications. As previously mentioned, different sock and shoe materials can impact the microclimate of the foot during activity. While airflow usually aids in maintaining the desired microclimate conditions, when occlusive materials are used next to the skin this mechanism may be impeded, further exacerbating the conditions. Understanding more about how AFOs affect the microclimate at the skin and how that may relate to risk of tissue damage could inform material choices for both lining materials and the AFOs themselves.

2.2 Experimental Assessment of Lower Limb Orthoses

Both AFO and FO designs have been assessed previously using experimental methods, though significantly more studies have considered the effect of different FOs on the limb than AFOs. This is likely due to the differing purposes of the devices (see Section 1.2). AFOs provide biomechanical correction whereas FOs are usually designed to protect vulnerable soft tissues, and so the experimental research has reflected this.

Most studies assessing AFO designs experimentally are concerned with comparing the functionality of the devices themselves (e.g. stiffness and range of motion). These were summarised in a recent review [141], which highlighted that the majority of these studies utilised a test jig, usually with a surrogate limb though some involved a participant limb [142, 143]. With regards to examining the effects of AFO design on the wearer, physical functioning and gait characteristics, such as ankle kinematics or stance phase time, are often measured [100, 102, 144]. The effect of different passive and powered AFOs on the metabolic cost of the wearer has also been assessed [145]. In these studies, the focus was still on whether the designs provide the desired corrective/assistive action, with limited consideration given to the risk of discomfort and tissue damage caused by the devices. A few studies have potentially incorporated this through examination of peak pressures across different regions [100, 101, 146]. However, no other pressure metrics were assessed in these cases, and there is debate over whether peak pressures correspond to tissue damage risk [147].

Participant testing of different FO designs frequently compare joint kinematics and gait characteristics in a similar manner to the assessment of AFOs. Additionally, these studies often assess pain, patient satisfaction, and different plantar pressure metrics [62, 64]. However, studies assessing the effectiveness of FO designs for people with RA through plantar pressure measurements have had mixed findings. This echoes the lack of clarity on the relationship between plantar pressures and how the underlying tissues are affected for people with RA (see Section 2.1.1.1). One review identified weak evidence of pain and plantar pressure reductions when custom FOs were used [64]. Another review found softer material FOs more beneficial than semi-rigid FOs in significantly reducing PTIs, though there was no significant difference in peak pressures, pain or physical functioning [62]. Similarly, a more recent study assessing different FO geometries found that there was little difference in peak forefoot pressures between designs but that the pressure during midstance did vary [148]. Potential offloading behaviour must also be considered, as it has been found that using plantar pressure reductions to optimise FO design may only be beneficial for people who have elevated pressures at baseline [149]. In that same study, though optimising FOs through pressure measurements led to significant improvements to pain and physical functioning, there was no relationship between the plantar pressures and the changes in pain and physical functioning themselves.

These studies indicate that while pressure metrics, and particularly PTI, may be useful to some degree in assessing FO design, there are limitations to how well they may indicate soft tissue health. Particularly for people with RA, the relationships between plantar pressure metrics and the underlying soft tissue pathologies are not fully understood. Similarly, very little research has been carried out into how different AFO designs affect the soft tissues, with the only consideration of this being the assessment of peak pressures. Additional metrics must be considered in order to fully comprehend how the soft tissues are affected with orthosis use, and the associated risk of damage.

2.3 Computational Modelling

Computational modelling is a useful family of tools for examining the human body, and its interactions with medical devices. The technique allows estimations to be made that would be difficult or unethical to determine experimentally, as well as providing greater control over input parameters and potentially reducing the costs involved. It is important in any computational modelling to balance the degree of complexity required for accuracy in a given scenario with any simplifications that may aid in developing and solving the model. The modelling approach must consider the model's purpose; for example, simpler models may be acceptable if a research question requires comparative analysis between devices or interventions instead of absolute

predictions. Applications for these models have included informing surgical technique, increasing understanding of the effects of pathologies and their treatments, and identifying optimal designs of implants or orthoses [150-153].

2.3.1 Modelling of the Foot and Ankle

Modelling of the foot and ankle has been carried out for numerous purposes, with differences in models usually stemming from the complexity required by each application. The many joints and connections in the foot mean that changes to the biomechanics of one region are likely to affect adjacent regions. A review by Wang et al. [154] detailed many interventions, such as ankle arthrodesis, that have been addressed through computational modelling and which require an understanding of the interconnected nature of the foot on pressure and stress distributions.

Model complexity can vary considerably, according to the geometries used, loading and boundary conditions, tissue material models, and the interactions between different structures. Simplifications to geometries might include fusion of the bones, particularly in the forefoot, or whether tendons, muscles, or ligaments have been included as discrete structures or grouped. The boundary conditions may be dependent on how the foot is being modelled, whether in 2D or 3D, and how much of the foot is included. When the tibia and fibula are present, the proximal aspects of the bones can be constrained [155]. In partial foot models, bones may also be constrained but this may impact tissue stress distribution as the skeleton can displace due to ground reaction forces (GRFs). However, this displacement has been found to be only 0.2mm during static standing [156]. Forces applied by muscles may also be modelled, often determined through electromyography (EMG) or estimated using inverse dynamics, based on kinetic measures from force plates and motion capture. The muscle forces may be included or omitted depending on complexity required, though how accurate the estimated forces are is relatively unknown [154]. Conversely, forward dynamics can be used if the motion of the body is desired and only forces are known.

Another important aspect is the tissue properties assigned, particularly relating to soft tissue which is anisotropic and displays non-linear, viscoelastic responses to loading. Some models will simplify the soft tissue to be linear elastic. However, most will incorporate hyperelasticity to better represent in vivo conditions [155, 157, 158]. Patient specific models may use ultrasound indentation to determine the soft tissue properties for the individual [150]. This may be particularly relevant if a condition such as diabetes has affected the soft tissue, in terms of plantar tissue stiffness and thickness for example [159]. However, care must be taken using ultrasound indentation as if the deformation applied is too small, the full non-linear response of the tissue

may not be seen. If the modelling is dynamic, then considering the viscoelasticity of the soft tissue may also be important [160]. Finally, friction or slip that may occur between the foot and a contacting material or within the foot between tissues may also be included in the model [161].

2.3.2 Modelling of AFOs

Computational modelling of AFOs has been limited to date, with most modelling of lower limb orthoses involving FOs. A review article published in January 2019 identified eight studies that had covered finite element (FE) modelling of AFOs, and a further 10 that combined experimental testing with computational modelling [141]. The majority of these studies focussed on determining the stress and/or strain in the orthosis, while changing loading conditions or device stiffness, with the goal of investigating failure of the devices and fatigue life. Because of this, most did not include the user's limb in the model. Only three studies identified in the review modelled the foot-AFO interaction, undertaken by Chu et al. [155], Uning et al. [162], and Jamshidi et al. [157]. Since the review took place, another model that considered both AFO and limb was developed by Darwich et al. [163]. Maruyama et al. [164] also produced a dynamic model considering the interactions between the AFO and limb during gait. However, the full text was not available in English and so their findings could not be properly considered.

Chu et al. [155] produced a 3D model containing simplified bone geometry along with ligaments and a bulk soft tissue domain within an AFO (Figure 2.4). Modelling the limb allowed them to analyse the effects of changing foot posture in gait, to compare between normal and abnormal gait caused by pathologies that would require an AFO. The different types of gait were represented by changing the magnitude of force applied through the Achilles tendon, which can increase with foot drop. The GRF was applied to represent heel-strike or toe-off, and the location the load was applied to was varied to represent different foot positions during gait. However, there was no mention of their model being validated, and their focus was on the fatigue life of the AFO rather than the soft tissues' response to mechanical loading. While they identified that the stress distributions in the AFO were asymmetric during gait, nothing was reported on how this may have affected the stress/strain of the soft tissues. Another shortcoming of the model was that all the materials were modelled as linear elastic, including the soft tissue which was given a Young's modulus of 1.15MPa. As the study was carried out over 20 years ago, incorporating non-linearity into soft tissue models would potentially have increased the complexity beyond what was computationally practical at the time. The limitations surrounding the use of this soft tissue property in the model have been discussed further in Section 2.3.5.1, as the magnitude is considerably higher than more recent reported values for the Young's modulus of plantar soft tissue [159].

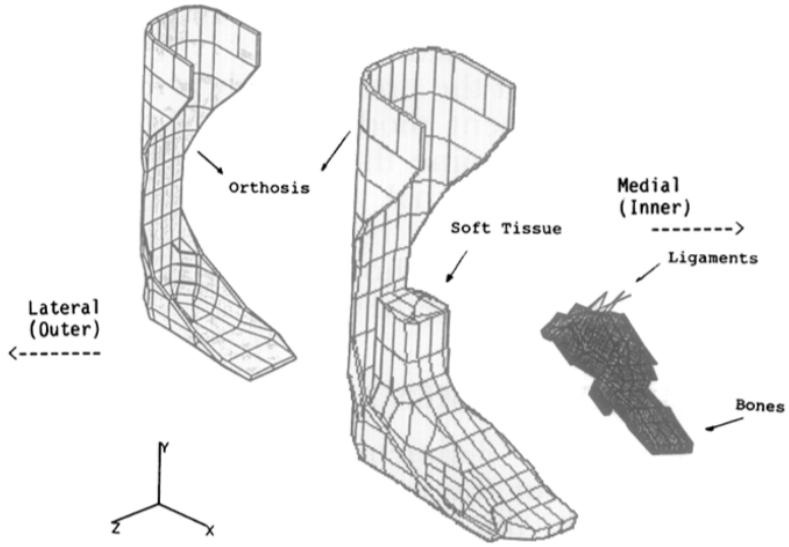

Figure 2.4: AFO model generated by Chu et al. [155]

Uning et al. [162] based their research on Chu et al.'s model using the same material properties, and thus the same limitations relating to soft tissue elasticity. However, they did also include the effects of friction between the orthosis and the foot – a key aspect when considering the effect of the orthosis on the soft tissues that Chu et al. had omitted. Uning et al.'s work was a preliminary study, and so while they intended to investigate loading at the foot-orthosis interface, no results were presented. Darwich et al. [163] also used Chu et al.'s model as the basis for their own, using the same material properties for the tissues, though the limb geometry was developed from computed tomography (CT) scans and so was more accurate. However, as they were more interested in the mechanical suitability of the AFO material and design, the impact that the AFO had on the limb, and soft tissue health biomarkers, was not considered.

Of the four studies, only Jamshidi et al. [157] investigated how an AFO affected the limb, producing a 3D model to determine how stress in the foot tissues were affected by the thickness and material of an insole within an AFO (Figure 2.5). Thus, the optimal material and thickness for maintaining normal gait while reducing tissue stresses could be determined. The foot model was based on MR images of a single individual and included all 26 bones as well as cartilage, ligaments, and tendons. It was not specified whether there were contact conditions in place at the joints. Both the soft tissue of the foot and the sole material were considered to be hyperelastic, described further in Section 2.3.5. Friction between the orthosis and the limb was also included. The AFO itself consisted of the sole plate, with additional insole and midsole attached, a hinged ankle joint and material encompassing the posterior calf. The sides of the foot and ankle region were not covered by the AFO. The study assessed the von Mises stress in

different foot regions caused by the orthosis configurations.

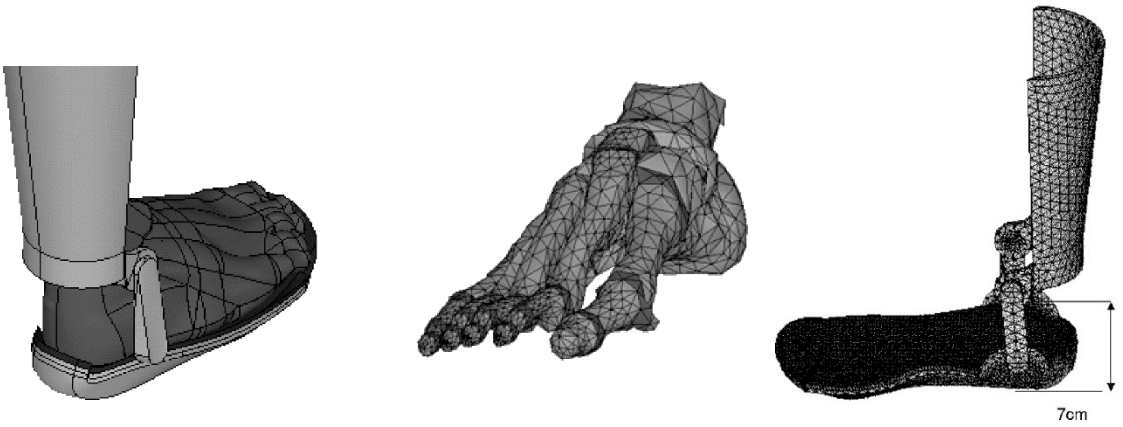

Figure 2.5: AFO model generated by Jamshidi et al. [157]

While not an AFO, recently Jena et al. [165] developed a model that investigated the effect of a spring-loaded polypropylene orthotic insert on deformation, plantar pressure and strain in the foot tissues (Figure 2.6). The foot geometry was constructed from CT data and the soft tissue modelled as hyperelastic, though all the model parts were bonded and so any effects of friction on the limb were not included. The loading was representative of gait mid-stance with single-leg contact, with a distributed load applied to the proximal cut surface of the bone, acting vertically down. The device was found to reduce the maximum strain in the tissue and redistribute the strain more evenly between the forefoot and the heel. However, as the load was applied vertically, it was acting at a different angle relative to the bone between the orthosis and control cases, which may have contributed to the differences in strain distributions.

Removed due to copyright

Figure 2.6: Models generated by Jena et al., with and without a rigid orthosis [165]

Though both socks and shoes are typically worn with AFOs, of these five studies, none included a sock or shoe upper and only Jena et al. included the shoe sole. Barefoot walking can lead to higher tissue stress and strain than when shod [166], likely due to the shoe sole providing shock absorption. There may be similar discrepancies between walking with an AFO while shod or

unshod, however this has not been verified. Studies which measured AFO-limb interface pressures used shod conditions with no comparison to wearing an AFO without a shoe [146]. Thus, it is unclear how plantar stresses would vary with the AFO directly contacting the ground in comparison to the AFO residing within a shoe. Additionally, while two of these studies evaluated tissue stress/strain, and so tissue damage risk, the focus was the plantar tissues. As such, no previous studies have investigated the soft tissue damage at bony prominences, where skin breakdown is known to occur.

2.3.3 Modelling of FOs

Computational models investigating different footwear and foot orthoses (FOs) have also been developed to evaluate risk of tissue damage. While there has been more research carried out in this area for FOs compared to AFOs, there are still gaps in the present literature. The general aim of FO modelling studies was to evaluate and compare the effectiveness of interventions, and the effect on tissue damage risk. However, many only considered plantar pressures and pressure relief, with few studies also assessing stresses and strains in the soft tissue [167, 168]. The focus of previous literature on plantar pressures is likely related to the focus that has been placed on evaluating FOs for the treatment of diabetes, where offloading pressures has proven effective. It may be that some findings from research into FO design for diabetes may also be applicable to the treatment of RA, in particular for those experiencing similarly elevated plantar pressures. However, due to the differing pathologies and the comparative lack of FO modelling research for RA specifically, whether some findings are translatable, and to what degree, has not been confirmed. Additionally, there is debate over the suitability of using interface pressure alone as an indicator of tissue damage risk, both in general and particularly in the case of RA (see Sections 2.1 and 2.3.4).

Models of FOs have assessed various design parameters including orthosis material stiffness, thickness, and geometry. They have also varied in configuration (Figure 2.7). Some have utilised 2D plane strain approximations, in either the sagittal or coronal plane [150, 158, 167]. However, there are limitations to this approach when assessing potential for tissue damage as the full spatial distribution of pressure or stress would not be viewable. 3D models have also been developed, which often also include the ligaments, cartilage and plantar fascia in addition to the bulk soft tissue group [168, 169]. Unlike the AFO models, the soft tissues in FO research have tended to be assigned hyperelastic constitutive models. The orthoses and shoe soles were also usually assumed to be hyperelastic, using Storakers' equation (discussed further in Section 2.3.5). However, a common limitation of the 3D models was that they generally only included the shoe sole and not the shoe upper [168-171], or did not include the shoe at all while assessing the FOs

[161, 172, 173]. Shoe uppers have been shown to influence soft tissue loading [167, 174, 175], and so excluding them would impact the model's ability to fully assess how the soft tissue was being affected.

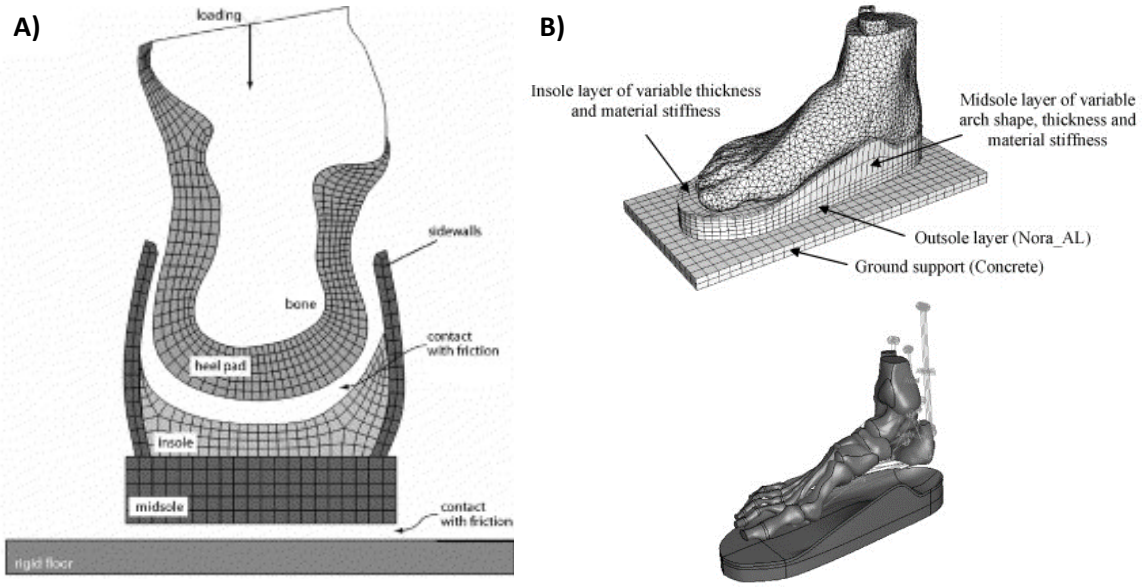

Figure 2.7: Examples of finite element (FE) models developed for FO design assessment. **A)** 2D model developed by Goske et al. [158]; **B)** 3D model developed by Cheung and Zhang [169]

Another limitation of modelling studies assessing FO design is that almost all only consider a single healthy individual. In only modelling one person, the results may be applicable to that individual, but will not necessarily apply to a wider population; that is, they are not generalised, or have low external validity. Additionally, various morphological changes occur due to conditions like RA (see Section 1.2.2), which affect the way that the tissues respond to applied loads. In only assessing healthy individuals, these changes would not be accounted for. There have been limited exceptions to this, with regards to modelling individuals or wider populations with pathology. Zhang et al. [172] assessed FO stiffness, wedge angle and arch height for an individual with post-traumatic midfoot arthritis, and Jafarzadeh et al. [173] optimised FO stiffness and shape for an individual with diabetes. Both studies utilised a 3D foot model that incorporated detailed bone geometry from CT data, ligaments and the plantar fascia. However, both studies modelled the orthosis as a linear elastic material, which would not fully represent its properties, and neither included a shoe in the model. Additionally, Jafarzadeh et al. focussed only on pressure reductions, as the focus was to reduce risk of ulceration in people with diabetes. Thus, the models were not used to assess any internal effects of the FO designs on soft tissue stresses or strains.

Telfer et al. [171] were the only researchers identified to assess FO design for a population, in this case of people with diabetes. The models were of the forefoot only and were highly

simplified, not including dorsal soft tissue or the shoe upper, and using geometric idealisation (cylinders and spheres of appropriate sizes, based on ultrasound measurements), to represent the metatarsals (Figure 2.8). The soft tissues were modelled using Ogden's hyperelastic equation and inter-metatarsal ligaments were included to stabilise and connect the bones. The simplifications allowed for faster computation so that the FOs could feasibly be adapted iteratively to suit each patient, but as would be expected, did limit the accuracy of the model predictions. The models underestimated experimentally measured in-shoe pressures, but did prove capable of producing optimised FOs that reduced forefoot pressures more than standard FOs. However, like other studies focussed on diabetes, only pressure reductions were assessed in the FO optimisation process. No computational study has been carried out to assess FO design for a population with RA, who could have different orthosis requirements to people with diabetes due to the differing pathology.

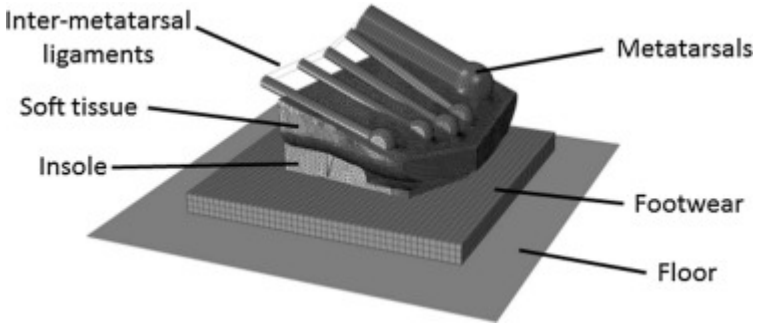

Figure 2.8: Example model developed by Telfer et al. [171] to optimise FO design for people with diabetes

2.3.4 Tissue Damage in Modelling

Modelling is often used as a method of predicting tissue damage risk, particularly for comparisons between different orthoses or medical devices. Generally however, these comparisons are done by comparing computational biomarkers such as peak pressures, stresses or pressure/stress distributions. Thus, there is little evaluation of whether those outcomes measures could result in tissue damage. As discussed in Section 2.1, there are different mechanisms of tissue damage including direct deformation, due to very high loading, and ischaemia, due to lengthy periods of lower loads. Different thresholds for tissue damage risk have been determined but none have considered all known mechanisms for tissue damage. The use of computational modelling means that internal tissue strains can be examined, with high strains known to correlate with areas of tissue damage [176]. Furthermore, internal shearing effects can be analysed – which are particularly prevalent near bony prominences and may lead to increased tissue damage risk [74]. The friction between soft tissue and a contacting material will also cause shear strains in the

superficial tissue, and so should be included if a model is assessing tissue damage risk. By using computational models to investigate how internal soft tissues are affected, regions at risk of tissue damage can be predicted, and this may be a better method than considering pressures applied to the skin alone.

Further considerations should also be made when trying to compare models to identify optimal device design. Comparing maximum values of internal strain means that results are influenced by localised peaks, due to differences in bone topography for example. As such, the results may not be reflective of the limb as a whole, and so would not provide a reliable comparison between interventions. To avoid such limitations, percentile values (e.g. 95th%) have been used as an indication of the stress or strain magnitudes reached in the tissues [177]. This provides a more robust method of assessment than using maximum values, as artefacts in the model predictions are excluded. Recent studies have also compared the volume of tissue in different strain ranges to see how much tissue may be at risk of damage due to high strains [109, 178]. This technique is not yet widely used, with many studies still only comparing peak stresses or strains, and some displaying contour plots as a comparison of distribution [167]. Determining the volume of tissue within a certain strain range provides quantitative results for a better method of comparison than describing plots qualitatively (Figure 2.9).

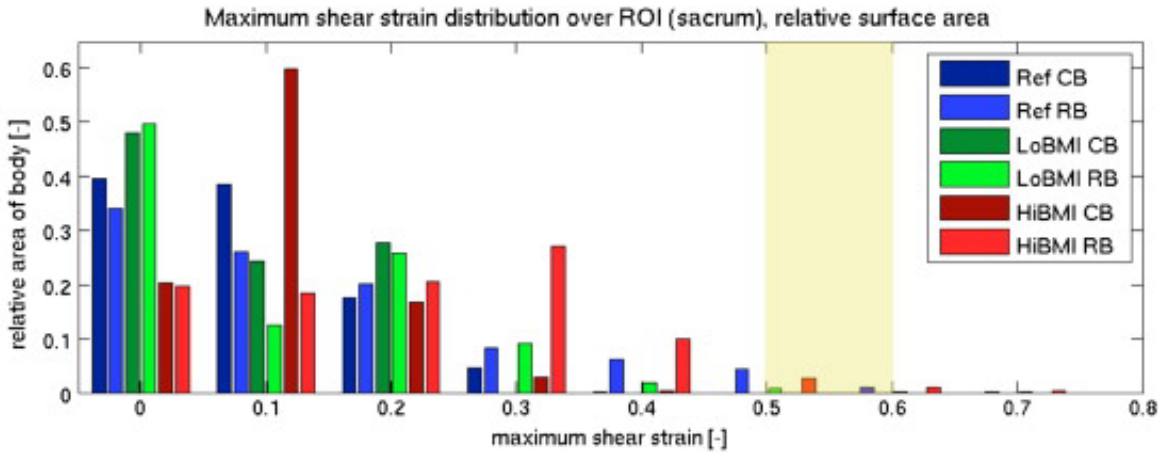

Figure 2.9: Example of assessing tissue damage risk by the area of tissue within each strain range, for 3 participants (Ref, Low BMI, High BMI) lying on 2 spine boards (CB, RB). The shaded area indicates the threshold for higher risk of tissue damage [109]

Another method that has potential for assessing tissue damage risk is to examine the pressure gradients at the skin interface. This has been previously used to assess pressure injury risk for wheelchairs and other forms of seating [179, 180]. Mueller et al. [181] proposed this method on the basis that a pressure gradient metric could represent shear effects as well as the normal load, and performed experimental testing to ascertain plantar pressures in the forefoot and rearfoot.

The rationale was that interface pressures do not necessarily cause tissue damage if they are uniform, but damage may be more likely if the pressure is uneven due to the shearing effects that may result in the soft tissues. Mueller et al.'s initial assessment only examined the correlation between peak plantar pressure (PPP) and peak pressure gradient (PPG), where PPG was calculated as the maximum difference between PPP and the pressure at an adjacent node, divided by the distance between nodes.

Follow-up studies did investigate how PPP and PPG correlated to the maximum shear stress in the soft tissue, though found that PPP had a stronger correlation than PPG [182, 183]. Despite this, their simulations showed that for a given value of PPP, the maximum shear stress increased with increasing PPG even when the overall magnitude of the load was reduced. It should be noted that there were several limitations to their studies. To calculate the shear stress in the soft tissue, they used functions which detailed the pressure applied to the plantar skin boundary and Laplace's equation to help determine the displacements occurring within the soft tissues. Hooke's Law was then used to convert the strains to stresses, which assumed the soft tissue to be linear elastic, isotropic and homogeneous. It also assumed that only small deformations were occurring, however the strain in the plantar tissue can increase significantly during gait which would breach this assumption. Additionally, only normal pressure applied to the tissue was used to calculate the underlying shear stresses, and so shear stresses applied to the skin were not considered. Finally, PPG was only calculated in the region immediately surrounding the peak pressure, and that value was used to represent half of the foot when comparing to the maximum tissue shear stress in the same region. Thus, a true spatial map of how interface pressure and pressure gradient related to shear stress in the soft tissue at a more localised level could not be seen. This study focussed only on plantar tissue, whereas high pressure gradients often occur near bony prominences. It is possible that the respective correlations between peak pressures or pressure gradients and tissue shear strain would be different near a bony prominence than in plantar tissue.

Despite the limitations of the previous studies, it is clear that pressure gradient metrics could provide additional information that would not be visible from examining peak pressures alone. Mueller et al. [181, 182] showed moderate to strong correlations between PPP and PPG, but though the metrics were related the strength of the correlations varied considerably between forefoot and rearfoot. Additionally, when comparing results between healthy and diabetic groups, the difference between groups was significant in the rearfoot for pressure gradient and shear stress but not for peak pressure [182]. Similarly, in seating research pressure gradient results at different seat tilt angles followed different trends than the peak pressure results [180]. As such, though much is still unknown about the relationships between peak pressure, pressure gradients

and shear stress in the soft tissues, the use of pressure gradients may aid the assessment of tissue health.

Another approach to modelling tissue damage is to examine vessel occlusion that could lead to ischaemia. Rohan et al. [184] modelled the effect of medical compression stockings on deep vein diameter, to determine how the vessel cross-section was affected by the external compression and internal muscle contractions in supine and standing positions. While the purpose of compression stockings is to limit blood pooling by restricting the vessel, the modelling principles used could also be applied to assessment of tissue damage risk due to vessel occlusion. In a study relating to pressure injury formation, Yamada et al. [185] showed the effects of vertical compression and tissue stiffness on a microvessel between a bony prominence in the sacrum and a mattress. The height of the microvessel and resistance to blood flow caused by the changing cross-section were examined to determine the effectiveness of using mattresses that aid pressure distribution. Microvessel modelling is an alternative method of assessing risk of ischaemia, rather than use of the sigmoid curve (see Section 2.1.2).

2.3.5 Model Inputs

2.3.5.1 Material Properties

Model inputs - such as material properties and CoF - have varied in literature. Bone, considered to be linearly elastic, has commonly been modelled with an elastic modulus of around 7.3GPa and a Poisson's ratio of 0.3 [151, 157, 186]. This elastic modulus is a balance of the properties of cortical (12-20GPa) and cancellous bone (0.25-0.53GPa) [187]. There is more variety in how soft tissue properties are modelled. Soft tissue can be modelled in bulk or separated into tissue layers, linear or hyperelasticity may be assigned to it, and it is often considered to be fully or nearly incompressible (Table 2.3).

Table 2.3: Exemplar soft tissue properties reported in literature

Tissue Type	Soft Tissue properties	Authors
Heel pad – from inverse finite element model and indentation testing	Ogden's hyperelastic: **Skin**: μ = 452kPa; α = 5.6 **Micro-layer**: μ = 95kPa; α = 4.9 **Macro-layer**: μ = 36kPa; α = 4.5	Ahanchian et al. [188]
Heel pad – indentation test and parametric assessment for skin	Ogden's hyperelastic: **Skin**: μ = 122kPa; α = 18 **Heel fat pad**: μ = 2.2kPa; α = 15.96	Gu et al. [189]

Tissue Type	Soft Tissue properties	Authors
Plantar – fat properties from cadaveric testing; skin stiffness adjusted parametrically	Ogden's hyperelastic: **Skin**: μ = 640kPa; α = 6.8 **Heel fat pad**: μ = 0.29kPa; α = 8.8	Spears et al. [167]
Heel pad – from ultrasound indentation	Ogden's hyperelastic: μ = 16.45kPa α = 6.82	Goske et al. [158]
Plantar under 2nd metatarsal head – from ultrasound indentation	Ogden's hyperelastic: μ = 37.5kPa α = 5.5	Chen et al. [168]
Plantar – from ultrasound indentation	Mooney Rivlin hyperelastic: C10 = 85.55kPa; C01 = -58.4kPa; C20 = 38.92kPa; C11 = 2.31kPa; C02 = 8.484kPa; D1 = 4.37x10^{-9}kPa^{-1}; D2 = 6.81x10^{-10}kPa^{-1} ν = 0.452	Jamshidi et al. [157]
Plantar – from ultrasound indentation	Linear Elastic: E= 150kPa ν = 0.45	Cheung et al. [151]
Not specified	Linear Elastic: E = 1150kPa ν = 0.49	Chu et al. [155]

The table provides several example soft tissue property sets used for computational modelling of the foot. Ogden's hyperelastic model was the most commonly used for modelling of the foot tissues, though the values used for each model parameter varied (Figure 2.10). The soft tissues were also often simplified to either a single bulk group or separated into fat and skin. Ahanchian et al. [188] separated the heel pad into layers for skin, a thinner micro-layer just under the skin, and a macro-layer between the micro-layer and calcaneus, identified on ultrasound images. Plantar skin is known to be stiffer than skin in other regions of the body, and so it would be important to ensure material properties were appropriately selected when modelling the foot and including a skin layer.

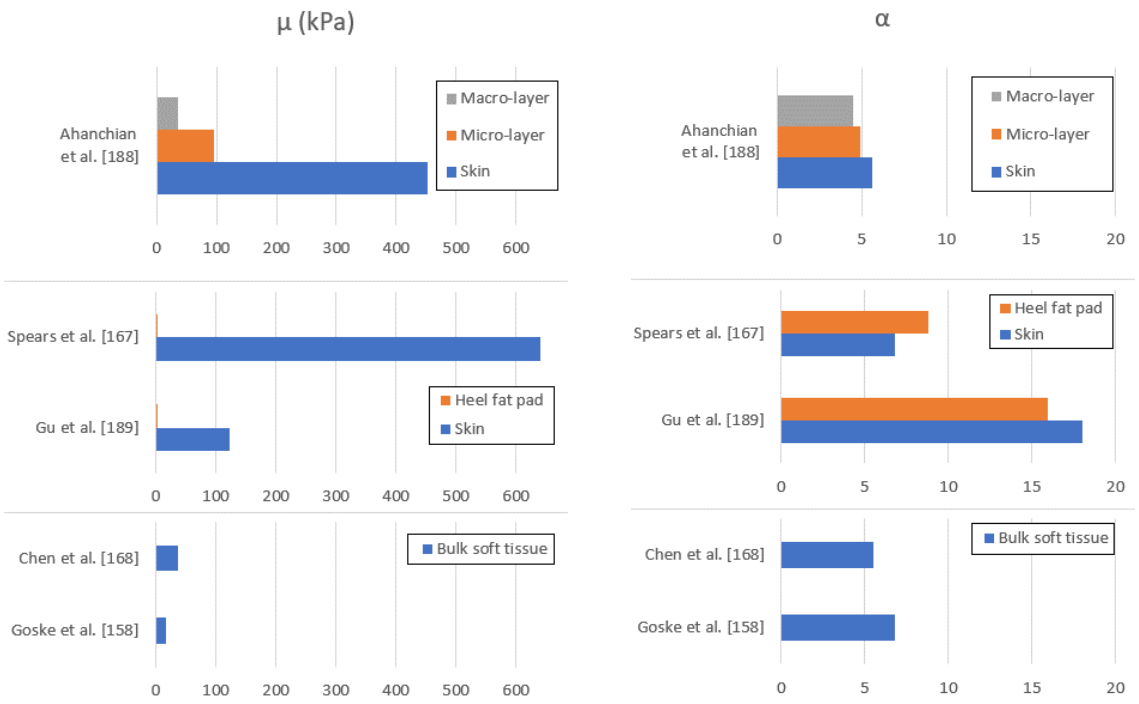

Figure 2.10: Range of values used for Ogden's Hyperelastic model parameters (μ and α) to represent the soft tissues of the foot, from the studies in Table 2.3

There was considerable difference in the Young's moduli used in the two linear elastic models reported. The modulus used by Chu et al. [155] in one of the few AFO modelling studies (see Section 2.3.2) was an order of magnitude greater than the value used by Cheung et al. [151], at 1150kPa (Chu et al.) *vs.* 115kPa (Cheung et al.). Cheung et al.'s value stemmed from ultrasound indentation of plantar soft tissue, which showed ranges of 43 to 118kPa depending on location and foot posture [159]. However, it is unclear what portion of the stress/strain response this represented, as only the moduli were reported rather than the full stress/strain behaviour, and the tissue was only indented to <10% of its initial thickness. This range of Young's moduli was considerably lower than the value assigned to the soft tissue by Chu et al., and it should be noted that tissue stiffness increases with increasing strain as would occur during gait. Though uncited, Chu et al. likely obtained the Young's modulus used for their model from a paper by Nakamura et al. [190], which reported that the Young's modulus of plantar soft tissue increased to 1150kPa at around 30% strain, though was significantly lower below 20% strain. Based on the results provided by the researchers, it is likely that this value was not actually the Young's modulus but the tangent modulus instead. While plantar soft tissue can reach and exceed 30% strain during gait, particularly at the heel, it may not reflect the overall behaviour of the soft tissue in the foot and the ankle [166, 191]. This emphasises the importance of applying non-linear or hyperelastic properties to soft tissue models.

AFOs have usually been modelled as linear elastic polypropylene, with elastic moduli reported as 1030MPa [155], 1175+/-100MPa [192], 1790MPa [165] and 2400MPa [193]. In actuality, the material has been found to behave non-linearly with the elastic modulus at 1390MPa at lower stresses before reducing as stresses exceed around 10MPa [194]. FO materials have different structures, stiffnesses and densities, which vary with the level of cushioning or support required of the orthosis. Many of these materials can also be used to pad an AFO to improve comfort and reduce tissue damage. Both FOs and shoe soles are often considered hyperelastic and compressible, with the behaviour modelled using Storaker's hyperelastic model or simplified to linear elasticity (Table 2.4. Table 2.5).

Table 2.4: Foot orthosis (FO) material properties reported in literature

Foot Orthosis Material (Brand)	**Material Model**	**Authors**
Closed-cell polyethylene foam with crosslinking (Plastazote, medium)	Storakers hyperelastic: μ_1 = 70kPa; μ_2 = -2kPa α_1 = 16.325; α_2 = -2.002 β_1 = -12.244; β_2 = 1.501	Chen et al. [170]
Closed-cell polyethylene foam with crosslinking (Plastazote, medium)	Storakers hyperelastic: μ = 198kPa α = 7.549 β = 0.169	Petre et al. [195]
Open-cell polyurethane foam (Poron Cushioning)	Storakers hyperelastic: μ = 620kPa α = 34.46 β = 0.040	Goske et al. [158]
Open-cell polyurethane foam (Poron Cushioning)	Storakers hyperelastic: μ = 144kPa α = 4.013 β = 0.057	Petre et al. [195]
Open-cell polyurethane foam (Poron Firm)	Storakers hyperelastic: μ = 229kPa α = 4.510 β = 0.010	Petre et al. [195]
Open-cell polyurethane foam (Poron, L24)	Storakers hyperelastic: μ_1 = 213kPa; μ_2 = -62.1kPa α_1 = 10.3; α_2 = -3.349 β_1 = 0.32; β_2 = 0.32	Cheung and Zhang [169]
Open-cell polyurethane foam (Poron, L32)	Storakers hyperelastic: μ_1 = -336.5kPa; μ_2 = 87.3kPa α_1 = 7.272; α_2 = -2.391 β_1 = 0.32; β_2 = 0.32	Cheung and Zhang [169]

Foot Orthosis Material (Brand)	Material Model	Authors
Open-polyurethane foam (PPT)	Storakers hyperelastic: μ = 78kPa α = 42.09 β = 0.054	Spears et al. [167]
Open-polyurethane foam (PPT)	Storakers hyperelastic: μ = 205kPa α = 4.167 β = 0.085	Petre et al. [195]
Open-polyurethane foam (PPT)	Storakers hyperelastic: μ_1 = 62kPa; μ_2 = -6kPa α_1 = 15; α_2 = -5 β_1 = -14.558; β_2 = 4.8529	Chen et al. [170]
Closed-cell EVA (Microcell Puff)	Storakers hyperelastic: μ = 1340kPa α = 28.14 β = 0.06	Goske et al. [158]
Closed-cell EVA (Microcell Puff)	Storakers hyperelastic: μ = 167kPa α = 22.882 β = -2.86	Chen et al. [170]
Closed-cell EVA (Microcell Puff)	Storakers hyperelastic: μ = 490kPa α = 7.24 β = 0.154	Petre et al. [195]
Closed-cell EVA (Microcell Puff Lite)	Storakers hyperelastic: μ = 1220kPa α = 48.29 β = 0.03	Goske et al. [158]
Closed-cell EVA (Microcell Puff Lite)	Storakers hyperelastic: μ = 265kPa α = 7.090 β = 0.114	Petre et al. [195]
Closed-cell EVA (Nora, SLW)	Storakers hyperelastic: μ_1 = 975.4kPa; μ_2 = -291.4kPa α_1 = 8.87; α_2 = -2.884 β_1 = 0.32; β_2 = 0.32	Cheung and Zhang [169]
Closed-cell EVA (Nora, SL)	Storakers hyperelastic: μ_1 = 1037kPa; μ_2 = 304.4kPa α_1 = 7.181; α_2 = -2.348 β_1 = 0.32; β_2 = 0.32	Cheung and Zhang [169]
Unspecified	Linear elastic: E = 1000 to 2500 kPa ν = unspecified	Zhang et al. [172]

Foot Orthosis Material (Brand)	Material Model	Authors
Unspecified	Linear elastic: E = 400 to 74000 kPa ν = 0.1	Jafarzadeh et al. [173]

Due to differences in naming convention of the FO materials in literature, it is often difficult to determine which variant of a brand has been used for modelling purposes. This, along with differences in material characterisation test used, led to variations in properties reported for similar materials. While most studies utilised uniaxial compression tests to develop the material models, Petre et al. [195] combined compression and shear strain testing to improve the accuracy of the models. Studies who used linear elastic properties for FO material often adjusted the stiffness to optimise the orthosis design, so the modelled FO did not necessarily correlate to a single specific material [172, 173].

Table 2.5: Shoe sole properties reported in literature

Authors	Material Model
Goske et al. [158]	Storakers hyperelastic: μ = 4240kPa α = 28.59 β = 0.0896
Spears et al. [167]	Storakers hyperelastic: μ = 153kPa α = 47.86 β = 0.061
Petre et al. [195]	Storakers hyperelastic: μ = 1588kPa α = 7.708 β = 0.292
Erdemir et al. [196]	Storakers hyperelastic: μ_1 = 2112kPa; μ_2 = -414.4kPa α_1 = 25; α_2 = 4.02 β_1 = 0.0365; β_2 = -0.437
Nakamura et al. [190]	Linear elastic: E= 800kPa ν = 0.22
Jena et al. [165]	Linear elastic: E = 3.85x10^{6}kPa ν = 0.4

2.3.5.2 Friction

In modelling a lower limb orthosis, there are two external interfaces where friction may occur – between the orthosis and the sock, and between the sock and the skin. Friction can also occur between tissues within the foot, but this was beyond the scope of the present research due to the additional model complexity and potential instability it may cause, and the focus on friction caused by the orthoses. The CoF at external interfaces may vary depending on humidity (see Section 2.1.3) or the magnitude of the applied force. Sanders et al. [197] found the CoF between the skin and a wool sock to increase with shear force, from 0.49 at 1N force to 0.66 at 4N. There has been some consideration of the CoF between different prosthetic and orthotic materials and socks (Table 2.6).

Table 2.6: CoF between prosthetic and orthotic materials and a dry sock

Material	Carlson [198] CoF	Sanders et al. [197] CoF
Spenco (silicone based neoprene)	N/A	0.69
Poron (open-cell polyurethane foam)	0.55	0.79
Medium Pelite (closed-cell polyethylene foam)	0.51	0.60
Firm Plastazote (closed-cell polyethylene foam with crosslinking)	N/A	0.64
Regular Plastazote (closed-cell polyethylene foam with crosslinking)	0.57	0.62
Nickelplast (closed-cell foam, ethylene vinyl acetate alloy)	N/A	0.71
PTFE Low friction interface	0.16	N/A
Polyethylene	0.30	N/A
CoPolyester	0.31	N/A
CoPoly (polypropylene with 5-10% polyethylene)	0.22	N/A
Calf Skin	0.49	N/A

Common cushioning materials such as Poron, Pelite and Plastazote, had CoF against a sock ranging from 0.51 to 0.79. The CoF between the sock and rigid AFO materials, such as polyethylene and the CoPoly, was much lower ranging between 0.22 and 0.31. This would suggest there would be more slip between a sock and the rigid AFO than there would be between the sock and any cushioning material or FO. Where comparisons were possible, Sanders et al. reported higher CoFs than Carlson, which may be due to differences in methods. It should also be noted that full descriptions of the materials in each study were not provided and so it is possible

that there were variations in the materials tested though given the same name. Additionally, the studies used different socks in the testing – Carlson used a cotton sock and Sanders et al. a wool sock, which would likely have differing surface properties thus affecting the load distribution and friction. The CoF may also have been influenced by pre-stretch, which neither study appears to have controlled.

The CoFs found for the sock-skin interface were higher than the values for the sock-AFO interface for the rigid materials but there was much overlap when compared against the CoF between a sock and cushioning material. This has implications for the friction and shear conditions, as slip is more likely at the lower CoF interface. If this slip is occurring between an AFO and sock, then it may reduce the shear loading acting on the soft tissues. Therefore, when applying padding to an AFO to increase comfort, the CoF at the two interfaces should be considered, in order to avoid the potentially damaging effects of shear loading.

2.3.5.3 Plantar Pressure Distributions

Plantar pressure measurements can provide insight into how ground reaction forces are distributed to different regions of the plantar foot, and as such can improve the accuracy of loading conditions applied to a model. There has been much research investigating plantar pressure distribution under various conditions, and either barefoot using pressure plates or shod using in-shoe pressure sensors. With regards to RA, many studies have assessed the pressure distributions between regions of the foot, for example the forefoot and rearfoot (Figure 2.11). As the forefoot can be particularly affected by RA (see Section 1.2.2), pressure distributions have also been assessed within the forefoot (Figure 2.12). However, the studies have varied in the breakdown of the forefoot regions, making it more difficult to collate and compare the load distributions.

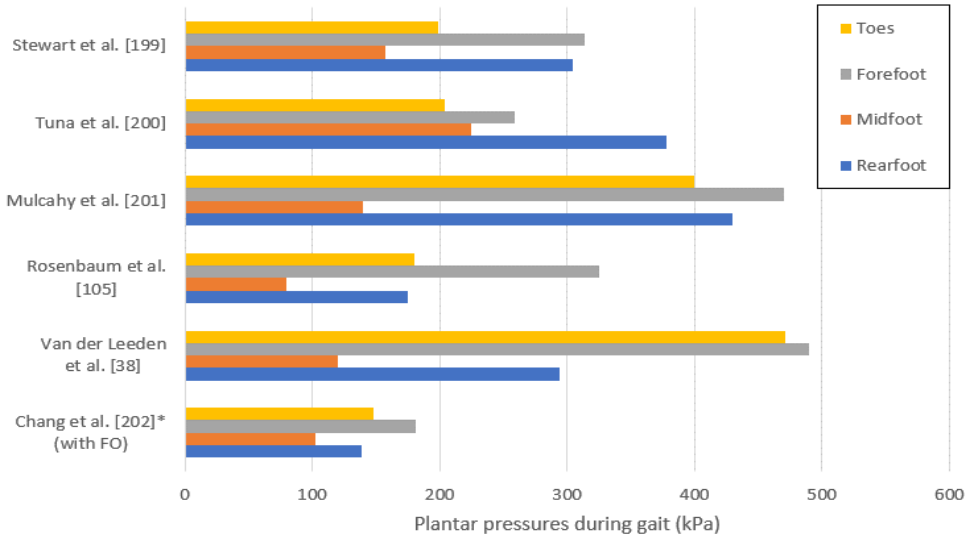

Figure 2.11: Plantar pressure distributions during gait for people with rheumatoid arthritis, identified from literature. *In-shoe pressures rather than barefoot.

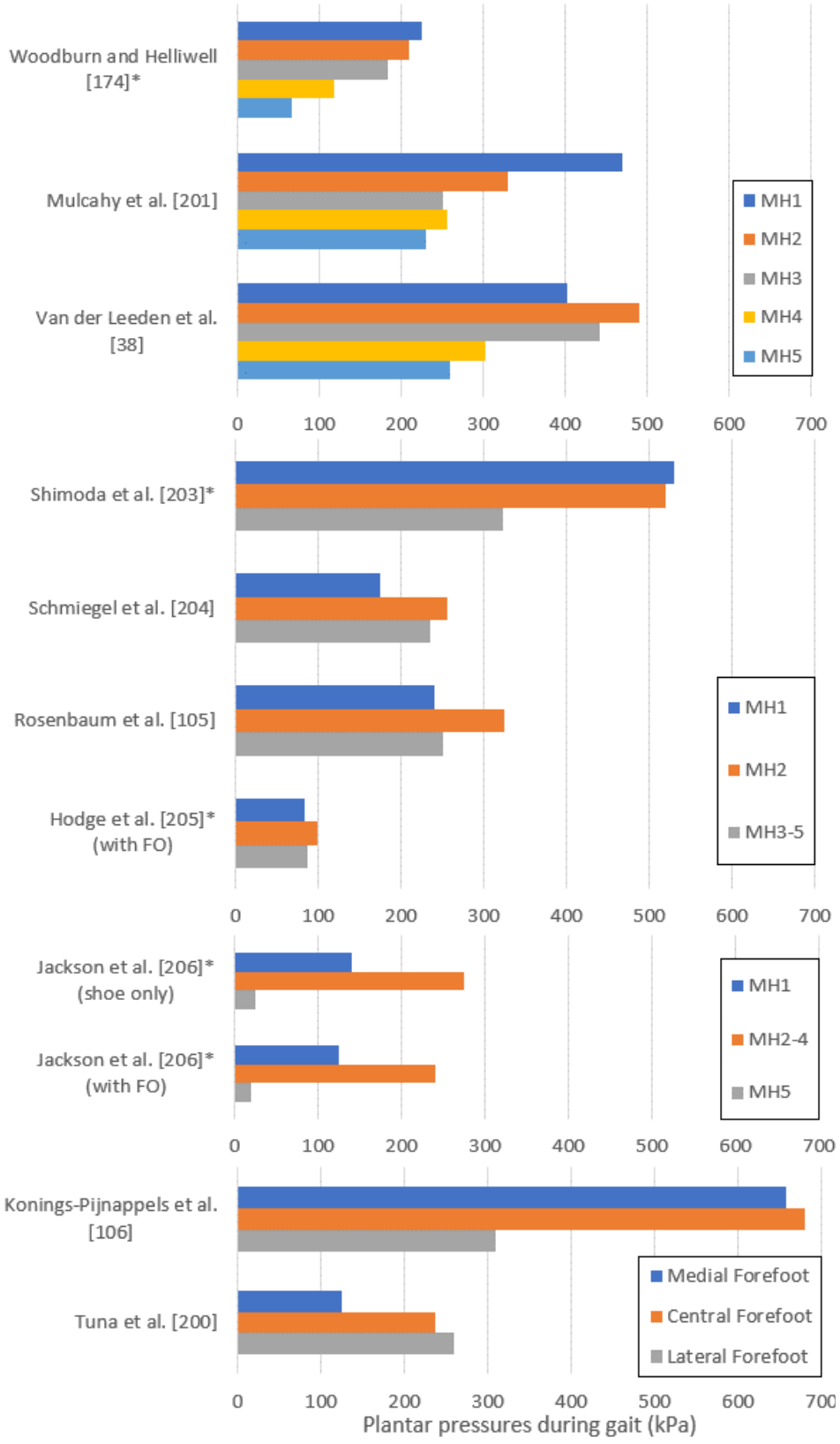

Figure 2.12: Forefoot plantar pressure distributions during gait for people with rheumatoid arthritis, identified from literature [38, 105, 106, 174, 200, 201, 203-206]. MHx = metatarsal head. Studies have been grouped by the forefoot locations assessed. *In-shoe pressures rather than barefoot.

From the six studies in Figure 2.11, the forefoot was most likely to experience the highest pressures, though in Tuna et al.'s study the rearfoot pressures were considerably higher [38, 105, 199-202]. These high forefoot pressures may be due to joint instabilities and deformities affecting gait patterns and pressure distributions [38]. Variation in average load distributions between studies was also observed in the forefoot. Three studies had peak pressures occurring under MH1 [174, 201, 203], and four under MH2 [38, 105, 204, 205]. Jackson et al., Konings-Pijnappels et al. and Tuna et al. showed peak pressures under MH2-4, the central forefoot and the lateral forefoot respectively [106, 200, 206]. This variation is likely due to a combination of differences in normal gait between individuals and off-loading of painful regions that may be occurring in some cases. The studies provide an indication of loading distributions that can be applied to computational models for individuals with RA. The majority of the studies measured the plantar pressures barefoot, and so the pressure distributions may differ from shod conditions. However, in the studies that measured in-shoe pressure, either with or without an FO, the pressure distributions were similar to the barefoot studies, though often at lower pressure magnitudes [174, 202, 203, 205, 206]. The lower pressures may be due to the shoe sole and orthosis, if present, providing a larger contact area, or reducing the resultant forces acting on the plantar surface of the foot.

There has been limited research into plantar pressure distributions with AFO use. Chung et al. [100] compared peak plantar pressures without an orthosis to those with a dynamic ankle orthosis. However, this device utilised two metal supports either side of the calf attached to the outer shoe and so did not feature a base plate in contact with sole of the foot. Nowak et al. [146] used the F-scan system to measure plantar pressures during gait, both at the interface between the foot and custom AFO and at the AFO/shoe interface. For the four healthy participants, average peak pressures in midstance were considerably higher at the AFO/shoe interface than the AFO/limb interface. Additionally, there were increased pressures distributed to the midfoot in comparison to pressure distributions without an AFO, likely due to the increased contact of the custom moulded AFO in that region. However, the calibration method for the pressure sensors was questionable, with all sensors calibrated to a single participant's weight rather than for each participant being tested. Calibration of the sensors to a specific individual is recommended by the manufacturers prior to use. Without a direct comparison between plantar pressures with and without and AFO using this method, the effect of an AFO on plantar pressures and distributions remains unclear.

Other model inputs to consider include the geometry of the limb and fit of the device. Limb geometry is often provided by scans of the individual, whether through 3D surface scanning or imaging techniques such as MRI or CT. Device fit is a particularly important factor with AFO use, where the orthosis may be applied to the limb with a tighter press-fit to correct deformities for

example. The fit of the orthosis may also vary with patient growth or changes in limb volume throughout the course of the day due to activity or oedema. Stick et al. [207] measured calf and ankle volume changes, based on circumferential changes, after 10 minutes of stationary standing and found that the calf volume increased by 2% and the ankle volume by 1%. Changes were also observed after 15 minutes of exercise – at an ambient temperature of 20°C, the volume decreased by around 1%, while at 36°C the volume increased by approximately 0.2%. This indicates how much the limb may change in a short time but does not provide a full picture of changes that could occur over longer periods. Krijnen et al. [208] found mean diurnal changes of lower leg volume to be an increase of 42-46ml (1.8%), however the range of changes varied from −434ml to +377ml. When comparing to values in other literature they found that leg volume could change by a mean of 4.8% during low activity periods of sitting over 8h. From this it is clear that limb changes can vary considerably on an individual basis, particularly with pathologies, which may need to be considered in lower limb orthosis design.

2.4 Summary, Research Questions and Objectives

The effect that an orthosis has on the soft tissue is an important consideration when assessing device designs. Whether this is the adverse effects of the orthosis itself, as is the case with an AFO, or due to the condition that an FO is attempting to alleviate, there is an associated risk of tissue damage. There are various mechanisms by which tissue damage can occur, and the likelihood is affected by factors such as microclimate, the type and duration of loading, pathological changes to the tissue and its tolerance to loading. Interface pressure measurements are often utilised as a method of assessing orthosis effectiveness and their effect on the underlying tissue. However, these pressures may not always correspond with how the tissue is being affected, particularly around bony prominences where pressures resolve into shear forces. This is also the case in the treatment of RA, where plantar pressures do not always correspond with forefoot pathologies, and there is mixed evidence of FO effectiveness.

This research focusses on two scenarios where gaps in current literature were identified. The first is considering the effect of AFOs on experimental and computational biomarkers related to tissue health. Wearing AFOs can lead to pain and discomfort, which may be exacerbated by heat and sweat accumulation at the limb-orthosis interface, and could result in tissue damage. However, research in this area has been limited in scope, with most studies examining impact on gait or fracture risk of the device itself, with limited evaluation of how AFOs affect the soft tissue. The second scenario is considering the effect of FOs on tissue health related biomarkers in the forefoot of people with RA. Computational modelling can provide improved understanding of how FOs interact with soft tissue internally. However, most modelling studies have assessed a single

healthy individual and to date, none have assessed FO design across a population of people with RA. Addressing these gaps in the current literature will pave the way for a more evidence-based approach to improving device design, to support patient and clinician reported experiences. This would enhance quality of life of the orthosis wearers, and also provide cost-savings benefits through improved adherence with device use and prevention of the individual's condition worsening.

To address the overarching aim of investigating the effects of orthosis design on tissue health, the following research questions and objectives were formed:

1. **How does AFO design affect the physical conditions between the device and skin interface?**
    - Through experimental testing, investigate the effects of AFO and sock design on the pressure and microclimate at the limb-orthosis interface, and provide input data for computational modelling
    - Through computational modelling, investigate the effect of AFO fit and interface material on pressure and shear strain in the forefoot
2. **To what extent can computational models of individuals with morphological changes in the forefoot distinguish between different aspects of RA disease?**
    - Develop computational forefoot models for a selection of individuals with RA
    - Compare model predictions indicative of tissue damage risk with relevant elements of clinical data and morphological measurements to determine whether the models can distinguish between the individuals' conditions
3. **To what extent can computational models provide knowledge to inform the design of safe and effective lower limb orthoses?**
    - Develop sets of computational models for healthy individuals to compare the effects of AFO fit and interface material on the soft tissue
    - Develop sets of computational forefoot models for individuals with RA to compare the effects of FO material and shape, and shoe type on the soft tissue
    - For each of the above cases, assess whether the models would be suitable to determine optimal orthosis design on an individual basis

2.4.1 Thesis Structure

The following chapters of the thesis will address the research questions and objectives as follows (Figure 2.13). Chapters 3 and 4 consider AFO design, through experimental testing and computational modelling respectively. Data from the experimental testing in Chapter 3 was used

to aid model development in the subsequent chapters. Chapter 5 covers the development of computational models of individuals with RA, comparing the model outcomes between individuals (see research question 2). Chapter 6 builds on the modelling work from Chapter 5 to assess different FO design parameters for the individuals with RA. Finally, Chapter 7 draws together the findings from each chapter to provide an overall discussion of the research carried out, the clinical implications, limitations, and potential future work.

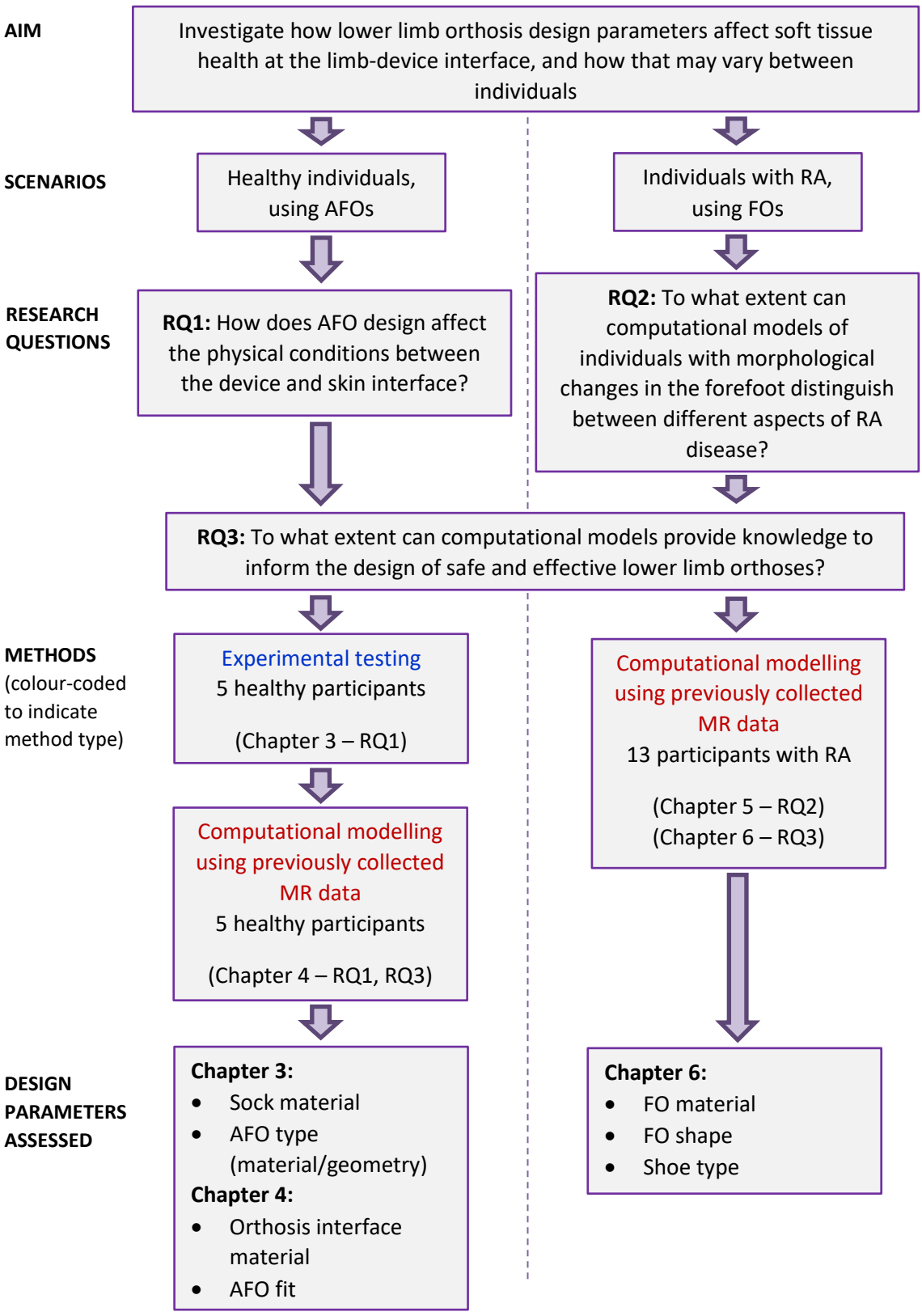

Figure 2.13: Flowchart detailing how the thesis chapters address the overarching aim and research questions

Chapter 3 Evaluation of AFO Design through Biophysical Measures

Wearing an AFO can result in pain and discomfort, particularly around bony prominences, likely due to the high pressures and shear forces applied by the device. The occlusive materials used for the devices also result in heat and sweat accumulation at the skin-device interface, which can exacerbate tissue damage risk. The literature review established that there is limited previous research considering how the devices affect soft tissue health, particularly with respect to microclimate. Pressure and microclimate at the AFO-skin interface, which are related to device comfort, are influenced by device materials and design. Material permeability and heat flux away from the skin may be optimised to minimise the build-up of elevated microclimate at the interface. As discussed in Section 2.1.3, research into how footwear and support surface materials affect microclimate has been carried out, but the same does not seem to have been considered for AFO materials. In this scenario both the AFO device and the material of the sock is of importance.

This pilot study aimed to investigate the effect of AFO and sock design on pressure, temperature and humidity at the limb-orthosis interface. A spatial map of pressure and microclimate was collected while AFOs of different designs and socks of different materials were worn during functional activities. As testing of this kind had not been previously performed, it was decided that a controlled evaluation would be carried out with healthy volunteers rather than AFO wearers to reduce risk. This also allowed for optimisation of the test protocol for future study, through identifying key parameters and anatomical locations.

This chapter addresses research question 1 through the following objectives:

RQ1: How does AFO design affect the physical boundary conditions between the device and skin interface?

- To investigate the effect of two different types of AFO and sock materials on pressure and microclimate at the limb-orthosis interface,
- To investigate the effect of AFO and sock type on participant perceived device satisfaction and comfort.

Parts of the work in this chapter were presented as a free paper entitled *"Effects of Ankle-Foot Orthosis Design on the Pressure and Microclimate between the Device and Limb"* at the International Society of Prosthetics and Orthotics (ISPO) 18th World Congress. [1]

3.1 Methods

3.1.1 Equipment

3.1.1.1 AFO and Sock Types

Two different off-the-shelf AFOs were chosen for the testing – the AFO Extra Strong and the Push AFO (Ortho Europe, UK) (Figure 3.1). Henceforth, these AFOs will be referred to as the ES AFO and the Push AFO, respectively. Off-the-shelf AFOs were used so that the healthy volunteers did not need to be fitted for custom AFOs, which would have required additional time and resources. Each AFO was available in small, medium and large sizes and the participants tried on the AFOs before the test sessions to determine which would fit best. These particular AFOs were chosen due to the differences in their design and materials (Table 3.1. Figure 3.1). The ES AFO was made from a rigid material which, unlike the Push AFO, was directly in contact with the limb and had a full-length foot plate. The straps of the Push AFO (apart from the dorsal strap) were elasticated, perhaps providing more compliance than the ES AFO, and attached at the calf rather than near the base of the heel.

Table 3.1: Characteristics of the ES and Push AFOs

Characteristic	ES AFO	Push AFO
Materials	Polypropylene Foam padding under calf strap	Glass fibre reinforced frame encapsulated by soft shell
Foot plate length	Full foot	¾ length
Attachment Mechanism	Velcro straps at calf and heel	Elasticated Velcro straps and additional straps across dorsal foot
Indications for use	Dorsiflexor weakness Light to moderate spastic equinus	Dorsiflexor weakness Ankle joint instability Light spasticity
Cost (at time of purchase)	£25.74 per unit	£195.69 per unit

Figure 3.1: Left – the AFO Extra Strong. Right – the Push AFO. Both AFOs acquired from Ortho Europe.

Two different sock materials were also tested. The material properties of different natural and synthetic fibres can influence the absorption and evaporation of sweat, as well as affect thermal comfort [209, 210]. Following discussion with clinicians on the types of socks recommended for AFO use, knee-high cotton (MySocks – 80% cotton, 17% polyamide, 3% elastane) and bamboo (Yomandamor – 70% bamboo fibre, 30% elastane) socks were chosen.

3.1.1.2 Sensors

F-scan in-shoe sensors (Tekscan, USA) were used to measure the plantar pressures. Both the F-scan system and the Pedar system (Novel GmbH, Germany) are commonly used for in-shoe plantar pressure measurements (see Section 2.1.1.1). However, the F-scan sensors have a higher spatial resolution, with up to 954 sensors per insole, and are more inobtrusive at 0.2mm thickness compared to the Pedar insoles 2mm thickness and up to 99 sensors per insole. Though the F-scan system is stiffer in-plane than the Pedar system, and so could crinkle if applied to curved surfaces, this was not a significant issue for this application. The pressure measurements were sampled at 50Hz, to accurately capture pressures throughout the gait cycle and to avoid aliasing. The majority of the frequency content of the gait cycle is below 10Hz [211].

Sensirion SHT75 sensors were used to measure temperature and humidity at the skin interface under the sock. Due to their size (5.1 x 19.5 x 3.1 mm plus connector), they were only used at key locations (Figure 3.2). This minimised the impact both on the measurements, due to the sensor connector potentially separating the contacting material from the skin, and on the participant. For example, they could not be used on the plantar surface as this would lead to discomfort from standing on the sensor. Less invasive K-type wire thermocouples were used to provide supplementary temperature measurements at more locations under the AFO. Three

thermocouples were placed on the control foot - at the lateral heel, 1st metatarsal head and calf. Care was taken to minimise rubbing of sensor wires under the AFO. The microclimate sensors were set to record at a frequency of 1Hz, which was sufficient to examine the changes over time. All the sensors used had suitable accuracy, resolution and range for the testing (Table 3.2), and streamed to a local laptop during the test sessions.

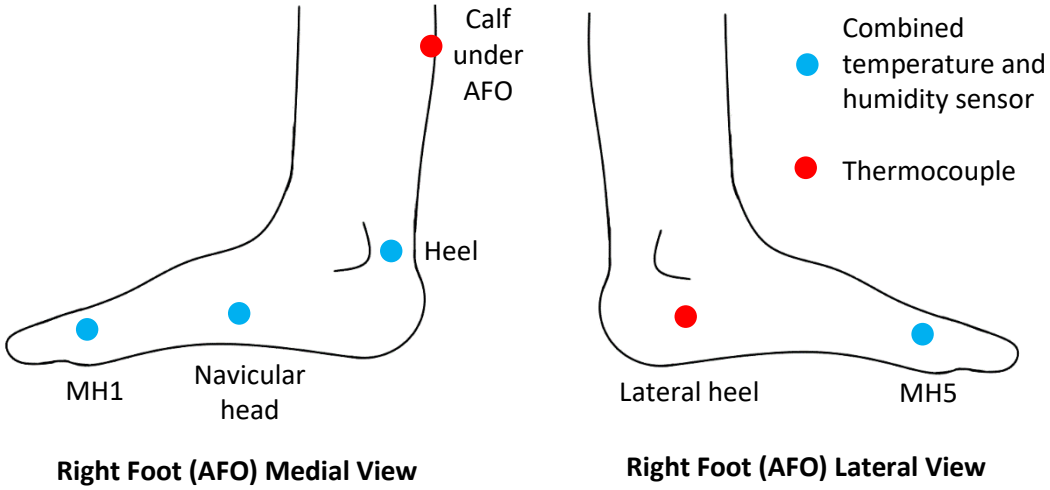

Figure 3.2: Temperature and humidity sensor locations on the AFO foot

Table 3.2: Sensor specifications

Sensor	Measures	Accuracy	Resolution	Sampling frequency	Range
F-scan [212]	Pressure	1.3-5.8% measurement error if calibrated properly [93]	Spatial: 3.9 per cm^2	Up to 750Hz	Up to 862kPa
Sensirion SHT75 [213]	Temperature Humidity (RH)	+/- 0.3°C +/-1.8 %RH	0.04°C 0.05 %RH	Max. of 1Hz to avoid self-heating	-40 to 123.8°C 0 to 100 %RH

The sensor wires were grouped together per leg and held in place using thigh bands to ensure that they did not present a tripping hazard while still allowing the full range of motion required for gait (Figure 3.3).

Figure 3.3: Example of a participant fitted with the ES AFO and temperature and humidity sensors, including the thigh bands ensuring the wires were not a tripping hazard.

3.1.2 Test Session Protocol

Five healthy volunteers were recruited for the study from the university population – a combination of males and females, all between the ages of 18-60 years old. The participant information sheet and protocol were discussed with each participant and informed consent was gained prior to the testing. Ethical approval for this study was granted by the University of Southampton (ERGO ID: 51969). The participants had to meet the following inclusion criteria:

- Aged between 18 and 60
- Able to walk for 15 minutes without stopping, twice with a 15 minute rest in between
- Able to stand still for 15 minutes unaided

Exclusion criteria included:

- Current skin condition in the lower leg and foot
- Compromised thermoregulatory system (for example: severe anhidrosis)
- Injury or disorder in the lower leg or foot that could cause pain while walking or wearing an AFO

A randomised cross-over trial was carried out, with two types of AFO and socks assessed in a random order and each participant testing all devices and socks. This allowed assessment of all independent factors whilst minimising the risk of bias due to participants becoming more accustomed to wearing the AFOs, or heat and sweat build-up throughout the test session. Each participant attended two 3h test sessions, with a different type of AFO worn in each session. The

two sessions were performed on different days to allow ample time for skin to recover. An appropriately sized AFO was chosen for each participant according to the manufacturer's guidelines. It was worn on the right foot, with the left foot providing a control without an AFO. The participants were asked to wear loose-fitting trousers or shorts so that the AFO could easily be worn underneath. Training shoes of an appropriate size were provided for the testing so that the same type of footwear was used for every participant (NDB Lightweight Cross-training running trainers). The AFO foot used a trainer one size larger than the control foot to account for the AFO. The bamboo and cotton knee-length socks were also provided – the bamboo socks were size 6-11 and the cotton socks were either size 4-7 or 8-11. As both socks were plain black, the participants were blinded to the type of sock in each test condition. The participants could not be blinded to the AFO type.

Each test session followed the same standardised protocol (Figure 3.4). The ambient temperature and humidity were recorded for two minutes immediately prior to the start of the test session. Baseline measurements for temperature and humidity of the skin were recorded for 1 minute prior to the sock being donned. Once the participant had been fitted with the AFO and trainers, the F-scan plantar pressure sensors were calibrated, using the F-scan software's Step Calibration method (F-scan Research v7.5, Tekscan, Massachusetts, USA). The calibration method involved the participant standing with all weight through one foot, and then shifting all weight to the other foot. This was then calibrated to the participant's weight.

This was followed by four test conditions with refractory periods between each condition. Temperature, humidity and pressure data were collected continuously throughout each test condition. During the standing test conditions, the participants stood for 15 minutes as stationary as possible and bearing their full weight as evenly as they could through both feet. For the gait conditions a treadmill was used, with the participants walking at a self-selected pace throughout the test sessions. The pace was then kept consistent for testing of both AFOs. The order of the test conditions was randomised to account for the effect of temperature and sweat accumulation throughout the session. Additionally, the socks were replaced between each test condition to minimise sweat accumulation, and were washed prior to use.

At the start of each recovery period, the participant filled out a questionnaire based on their experience from the previous test condition. An adapted version of the Client Satisfaction with Device module of the Orthotics Prosthetics User Survey (CSD-OPUS) was used [214], with questions relating to device affordability removed (Appendix A, p.161). The survey consisted of nine questions, with each scoring 1 to 4 depending on whether the participant had strongly agreed, agreed, disagreed, or strongly disagreed with the statement. Thus, the lowest possible

and optimal score was 9, and the highest possible score was 36. Comments could also be provided. The participants were monitored for skin damage between each test, through visual inspection.

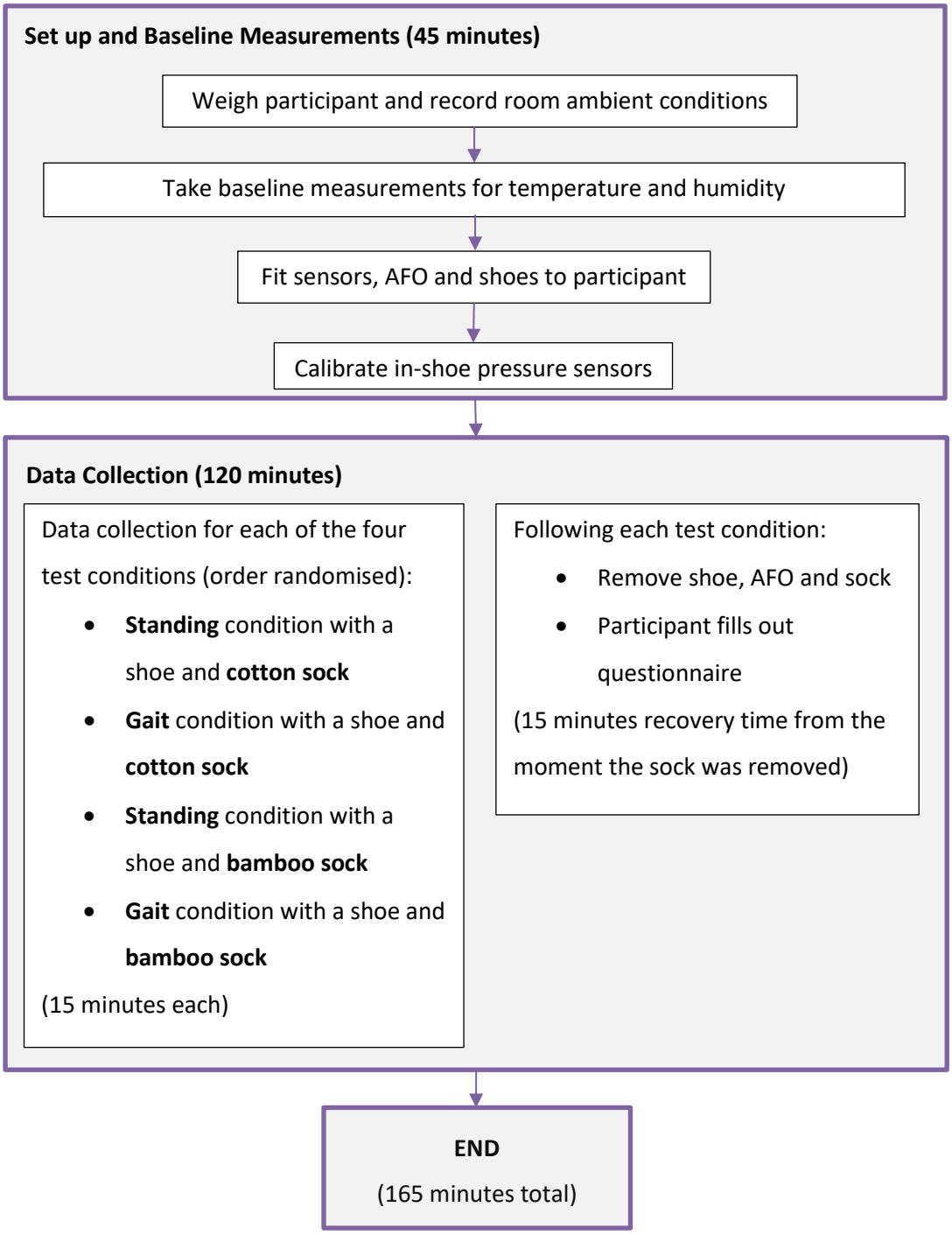

Figure 3.4: Session schematic

3.1.3 Data Analysis

Medians and interquartile ranges (IQR) were used to describe the results as the limited number of participants did not allow for determining the distribution of the data. Differences in trends between individuals (referred to as P1-P5) were also examined.

3.1.3.1 Pressure Measurements

Peak pressures, maximum pressure gradients, and pressure-time integrals (PTI) were assessed so that the magnitude, spatial and temporal aspects of plantar pressure could be examined, as all may impact tissue damage risk (see Section 2.1.1.1). This also allowed for comparison between the pressure gradient results and the other, more established, pressure metrics of peak pressure and PTI to determine whether the gradients provided additional information (see Section 2.3.4).

Initial analysis of the plantar pressure data gathered using the in-shoe F-scan sensors was carried out using the F-scan Research software. Prior to analysis, data for each test condition was inspected for any pressure spikes where one or two sensels (sensing elements) gave pressures considerably higher than any of the surrounding sensels and were present throughout the data for that condition. These were likely due to slight sensor crinkling, and were removed manually within the F-scan software. For the gait conditions, the frames were divided into maps of individual gait cycles, consisting of the maximum pressure that each sensel experienced during that gait cycle. A pressure map of the average gait cycle for the 15-minute test condition was then calculated. For the stationary conditions, the average plantar pressure distributions from the test conditions were found. These average stances for each test condition were then analysed further to determine the peak pressures and pressure gradients in different regions of interest of the foot (Figure 3.5). The foot was divided into the forefoot (excluding the toes) and rearfoot. It was then further partitioned to show the pressures under the 1st and 5th metatarsal heads, and the lateral, medial, and posterior heel. These sub-divisions were examined to see what pressures may have been caused by the proximity to the edge of the AFO. In the heel regions, the most lateral column of sensels was excluded from the analysis as contact between the AFO and the tab connecting the F-scan sensor with the data logger often led to high pressure spikes, which were considered experimental artefacts due to sensor crinkling.

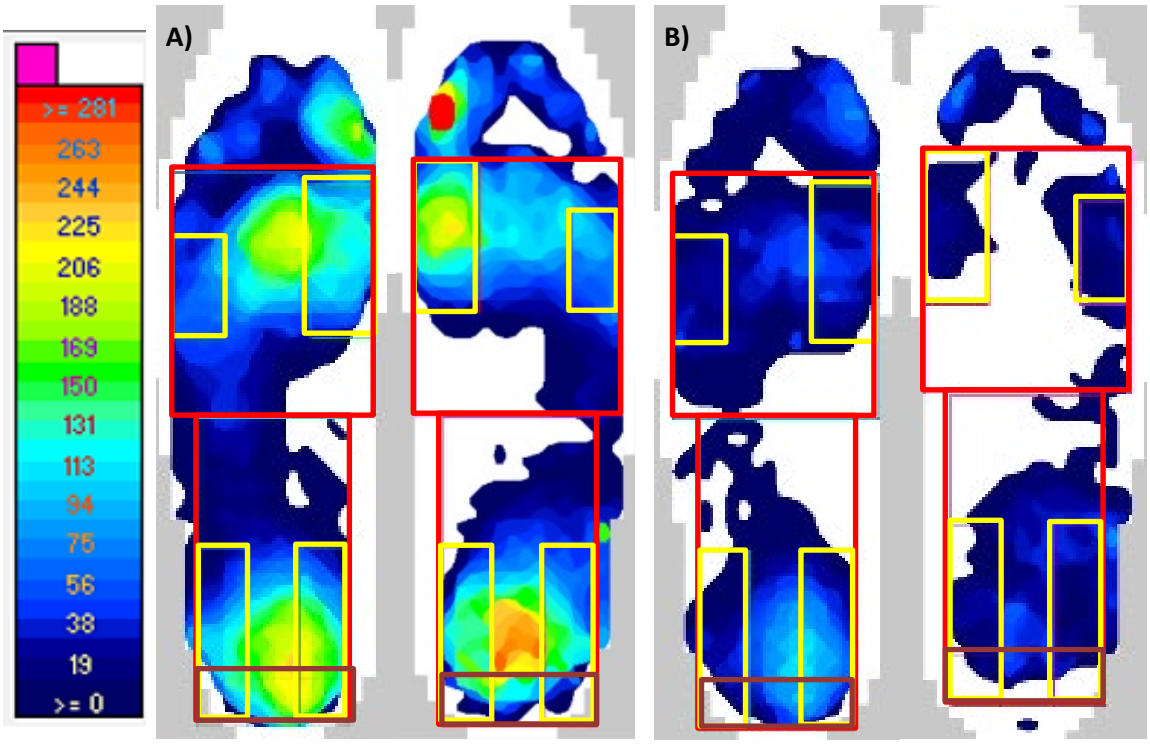

Figure 3.5: Examples of foot regions used, from P1 with ES AFO, bamboo sock: **A)** during gait, **B)** during stationary standing. Units: kPa.

The F-scan software calculated the peak pressure in different regions by averaging the peak pressures of four neighbouring sensels. To calculate the maximum pressure gradients in each region, code was developed in MATLAB (R2020b, MathWorks, Massachusetts, USA) to determine the differences in pressure between a sensel and all eight surrounding sensels before dividing each difference by the distance between the two sensels (Figure 3.6). The temporal aspect of the gait condition pressure data was also examined to see where the pressure remained higher for longer – which could indicate a higher risk of tissue damage. For each foot region, the pressure-time integral (PTI) was calculated using time as a percentage of the gait cycle to allow comparison between participants (Figure 3.7). Thus, PTI was only relevant to the gait test conditions and not the standing conditions.

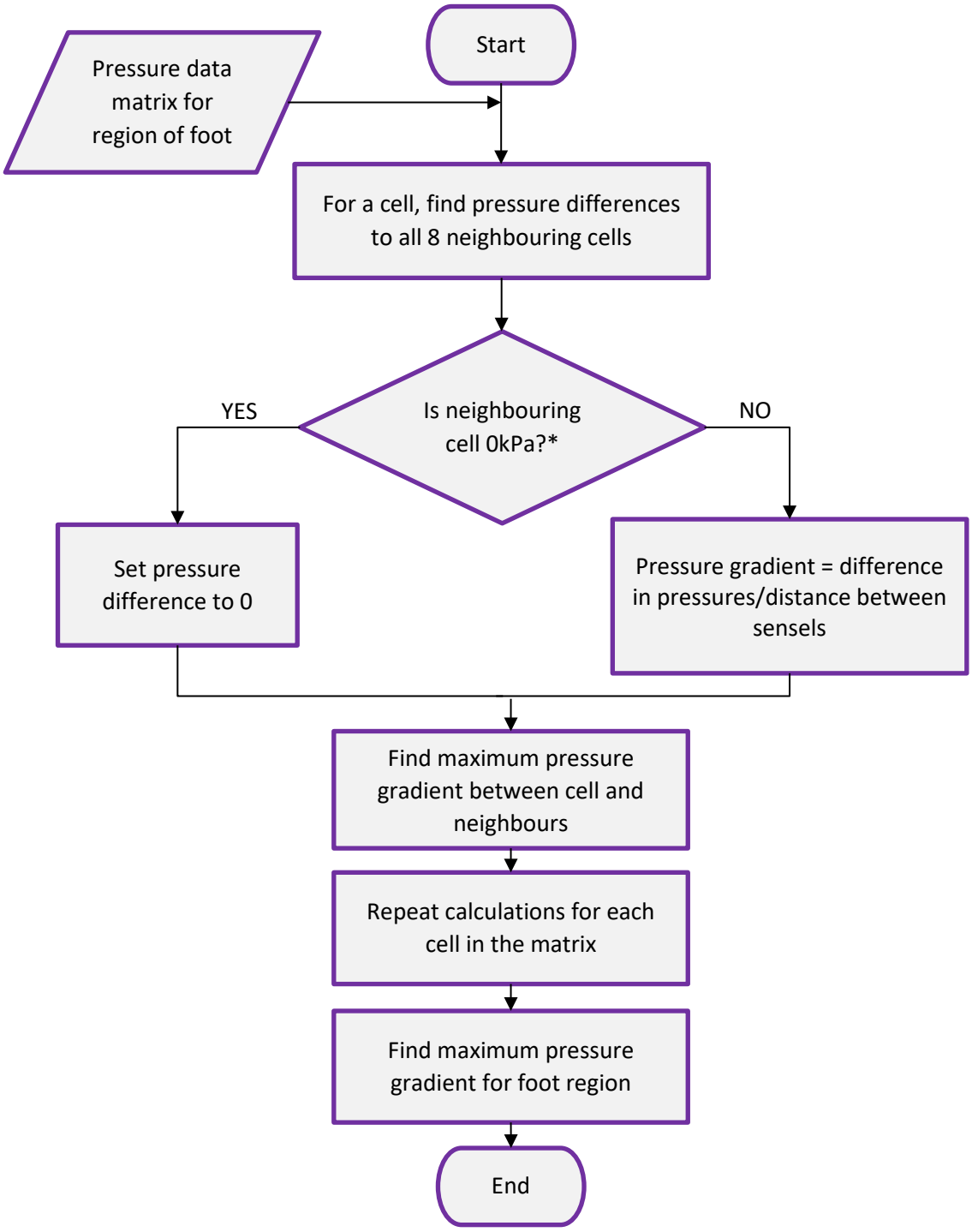

Figure 3.6: Flowchart of pressure gradient calculation code. Full code is given in Appendix B (p.162). *Neighbouring cells with 0 values may have been off the edge of the sensor and so may not have been indicative of there being no pressure applied there.

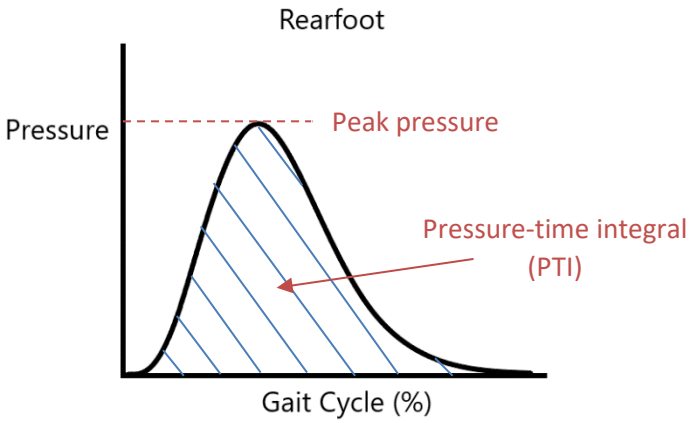

Figure 3.7: Example of pressures experienced in the rearfoot during gait, with pressure metrics indicated

A case study was carried out calculating the integral of the changing maximum pressure gradient throughout the gait cycle, similarly to the PTI calculation. This allowed both temporal and spatial data to be combined into one metric. Calculation of the change in pressure gradients throughout the average gait cycle could not be carried out in the F-scan software and could only be exported for an individual gait cycle. Thus, a sample gait cycle from Participant 1 was exported for both ES and Push AFOs, to compare the change in pressure gradient over time with the change in peak pressures.

3.1.3.2 Microclimate Measurements

The raw temperature and humidity data for each participant was analysed using MATLAB. Prior to analysis, a Hampel filter was applied to the Sensirion combined temperature and humidity sensor data to eliminate outliers due to measurement artefacts. For each sensor, the difference between the average baseline measurement and the average measurement from the final 10 seconds of the test conditions was calculated. Using the difference from the baseline allowed for comparison between participants and partially controlled for differences in ambient conditions that had translated to the baseline values. Temporal changes in the microclimate during the test conditions were also examined.

3.2 Results

The tables and figures in this section use short-hand for the different test conditions and some sensor locations:

- ES Bamboo – ES AFO with a Bamboo sock
- ES Cotton – ES AFO with a Cotton sock

- Push Bamboo – Push AFO with a Bamboo sock
- Push Cotton – Push AFO with a Cotton sock
- MH1 – First Metatarsal Head
- MH5 – Fifth Metatarsal Head

3.2.1 Pressure Results

The comparison between the AFO foot and control foot are shown for the peak pressures (Figure 3.8), maximum pressure gradient (Figure 3.9), and PTI (Figure 3.10) for the gait conditions. The overall trends between the ES AFO and Push AFO were also assessed. Comparisons of the broader forefoot and rearfoot regions have been focussed on, as the median trends between AFOs for the subregions of the forefoot and rearfoot (e.g. MH1 or lateral heel) generally reflected the trends of the overarching region. The exception to this was the PTI results in the rearfoot where the overarching region showed consistently higher PTIs for the ES AFO than the Push, but the lateral and medial heel showed more variable trends between AFOs. The AFO-control foot comparisons for the standing conditions and a full breakdown of the median and IQR results per foot region and test condition can be found in Appendix C (p.165).

3.2.1.1 Peak Pressures

During gait, the median peak pressures at all locations around the foot were higher for the ES AFO than for the Push AFO, with peaks of 352kPa (IQR: 212 – 407) and 268kPa (IQR: 196 – 275) respectively. This was generally the case with the standing test conditions as well, though for some conditions the peak pressures were very similar between AFOs (see Appendix C, pg. 167). When examining the differences between AFOs in individual participants, the ES AFO caused higher pressures than the Push AFO for P2 (432-875kPa *vs.* 196-354kPa), P3 (316-445kPa *vs.* 129-222kPa), P4 in the rearfoot (298-329kPa *vs.* 262-299kPa), P5 in the forefoot (303-352kPa *vs.* 269-279kPa). However, in other cases the pressures for the ES AFO were similar or lower than for the Push AFO: P1 (179-256kPa *vs.* 173-275kPa) P4 in the forefoot (208-212kPa *vs.* 222-233kPa), P5 in the rearfoot (162-170kPa *vs.* 266-268kPa). The variation in peak pressure results between participants was higher for the ES AFO than the Push AFO, particularly in the forefoot (Figure 3.8).

For the Push AFO, the control foot almost always experienced higher peak pressures than the AFO foot – the exception being P3 in the forefoot. For the ES AFO, the comparisons between the control and AFO feet were more mixed, with the AFO foot displaying lower peak pressures than the control foot for P2 in the cotton sock condition, P4, and P5 but not for the other participants. Sock type appeared to have little effect on peak pressures.

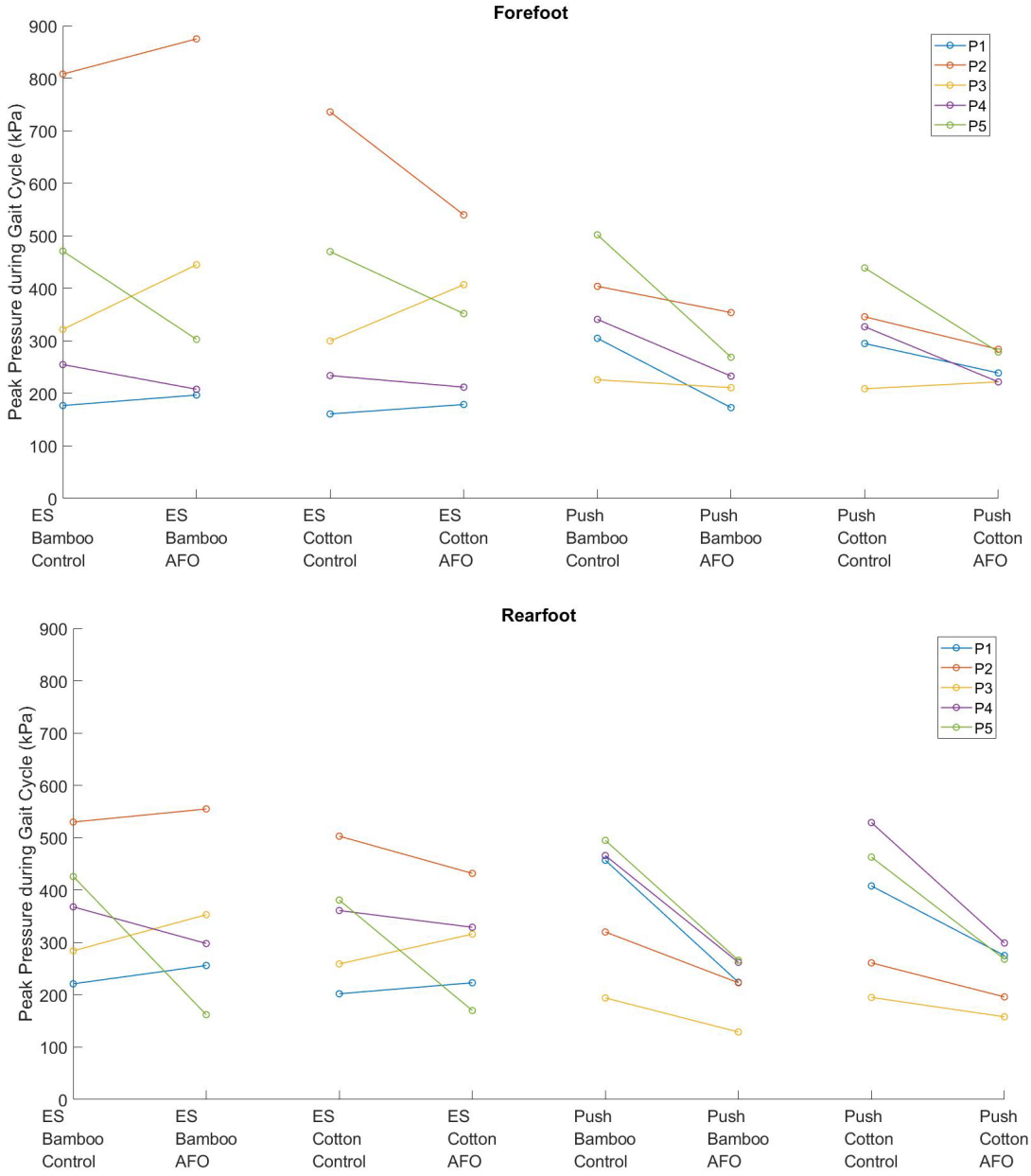

Figure 3.8: Comparison of the peak pressures in the forefoot and rearfoot during gait between the AFO foot and the control foot

3.2.1.2 Maximum Pressure Gradients

The maximum pressure gradients displayed similar trends to the peak pressures with the median values consistently higher for the ES AFO than the Push AFO. For example, in the rearfoot, the median PGs were 43.9kPa/mm (IQR: 41.9 – 50.0) and 63.3kPa/mm (IQR: 37.4 – 64.5) for the ES AFO, and 38.4kPa/mm (IQR: 38.2 – 38.4) and 35.1kPa/mm (IQR: 30.4 – 36.3) for the Push AFO (see Appendix C, pg. 165, for the full breakdown). There were also similarities in the individual participant responses, with greater variance in the ES AFO data than the Push AFO (Figure 3.9). Only P1 showed higher pressures gradients with the Push AFO than the ES, indicating a stronger

trend than was present for the peak pressures. Again, there was very little difference between the sock types.

Contrary to the peak pressure results, the AFO foot was more likely to experience higher pressure gradients than the control foot for both AFOs in the rearfoot. This occurred with all five participants for the ES AFO with control foot results ranging from 18.4-49.2kPa/mm and AFO foot results ranging from 27.3-91.0kPa/mm. In the forefoot, the responses were more mixed with 3/5 participants showing increases in pressure gradient with the ES AFO compared to the control foot. For the Push AFO, Participants 2 and 5 showed decreases compared to the control foot and Participants 3 and 4 consistently showed similar responses between feet (Figure 3.9).

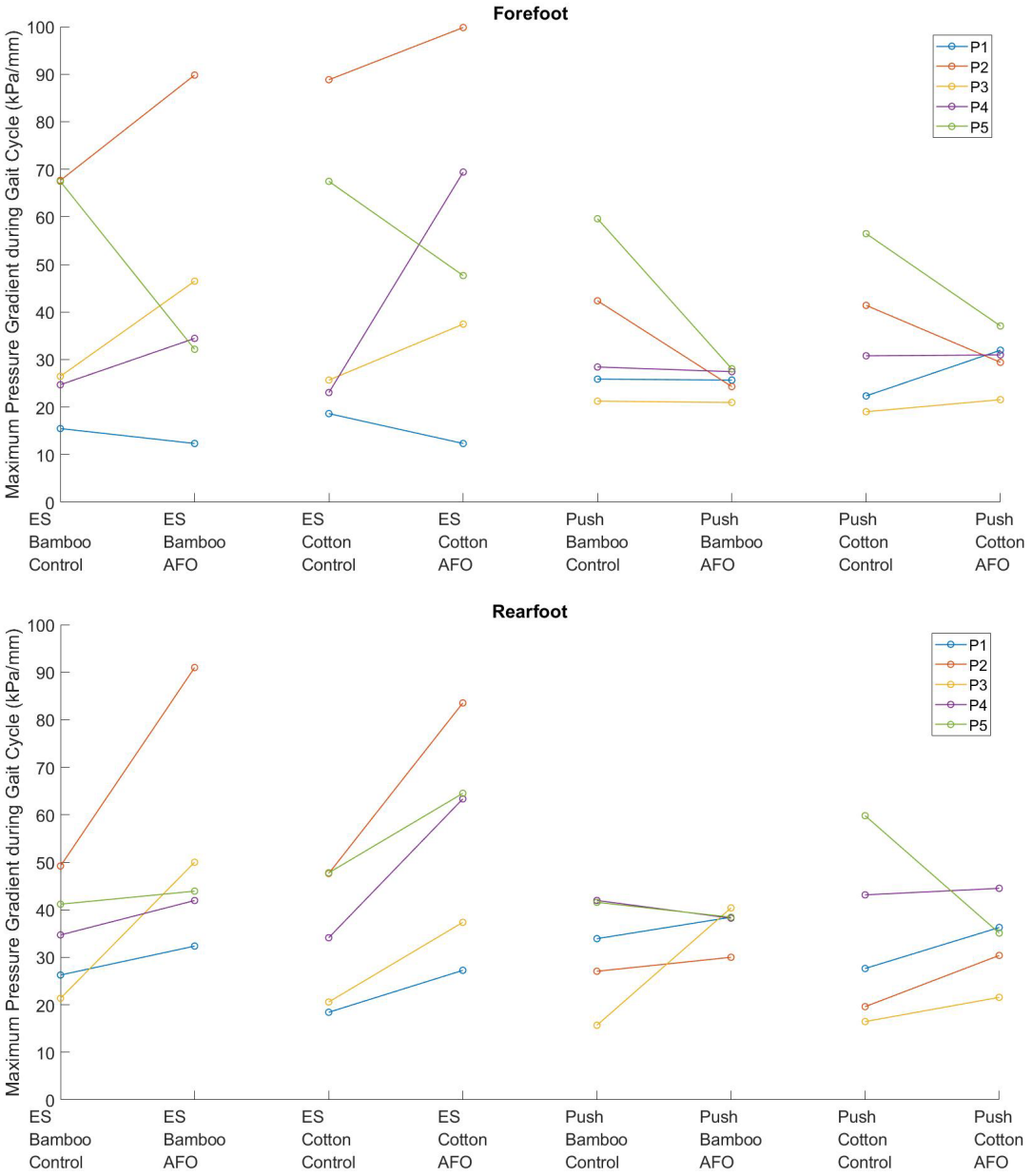

Figure 3.9: Comparison of the maximum pressure gradients in the forefoot and rearfoot during gait between the AFO foot and the control foot

3.2.1.3 Pressure-Time Integrals

Similar to the other pressure metrics, the PTIs (using time as a % of gait cycle) were generally higher for the ES AFO than the Push AFO, with median values ranging from 12237-14367 for the ES AFO and 10159-12074 for the Push AFO (see Appendix C). However, again this was not the case for all individuals with P1 and the P5 rearfoot data showing differing responses. The variance in the PTIs was generally smaller for the Push AFO than the ES AFO, particularly in the forefoot (Figure 3.10). As with the peak pressures, the Push AFO was observed to have lower PTI than the control foot, and this was much more pronounced in the rearfoot (Push AFO range: 7268-14742; Control foot range: 9300-24886). The only exception to this was the forefoot data for P3.

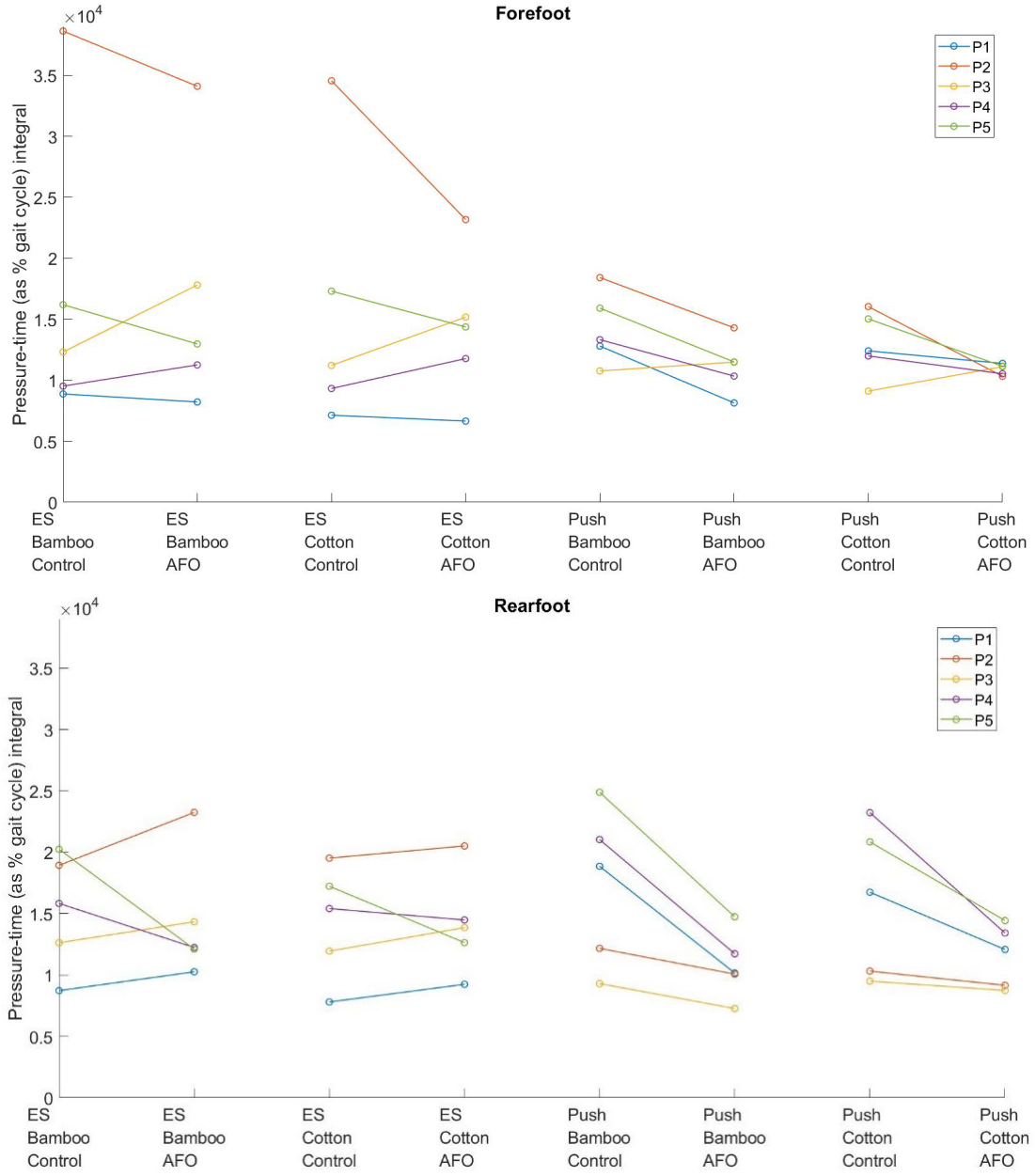

Figure 3.10: Comparison of forefoot and rearfoot pressure-time integrals during gait between the AFO foot and the control foot. Based on time as a percentage of the gait cycle.

3.2.1.4 Pressure Distributions

Across the participants, the peak pressures in the rearfoot tended to be in the centre of the heel, and in the forefoot were usually under the first or second metatarsal head. Example pressure distributions from Participant 3 are displayed for each AFO in gait (Figure 3.11) and standing test conditions (Figure 3.12). Note that different pressure scales were used for gait and standing.

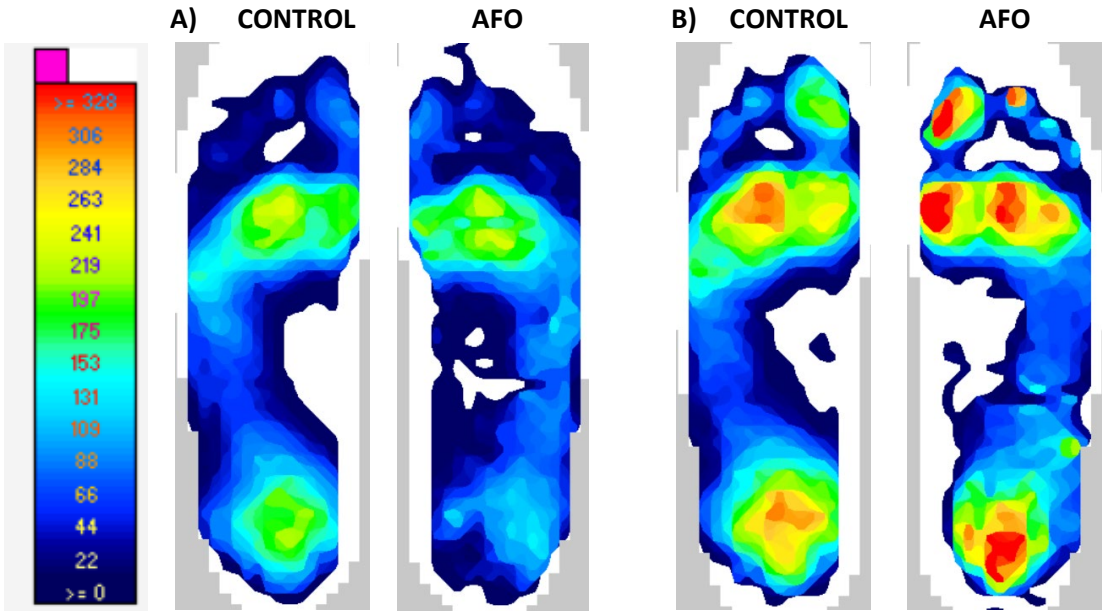

Figure 3.11: Pressure distributions for Participant 3, average stance during gait. **A)** With Push AFO. **B)** With ES AFO. Units: kPa.

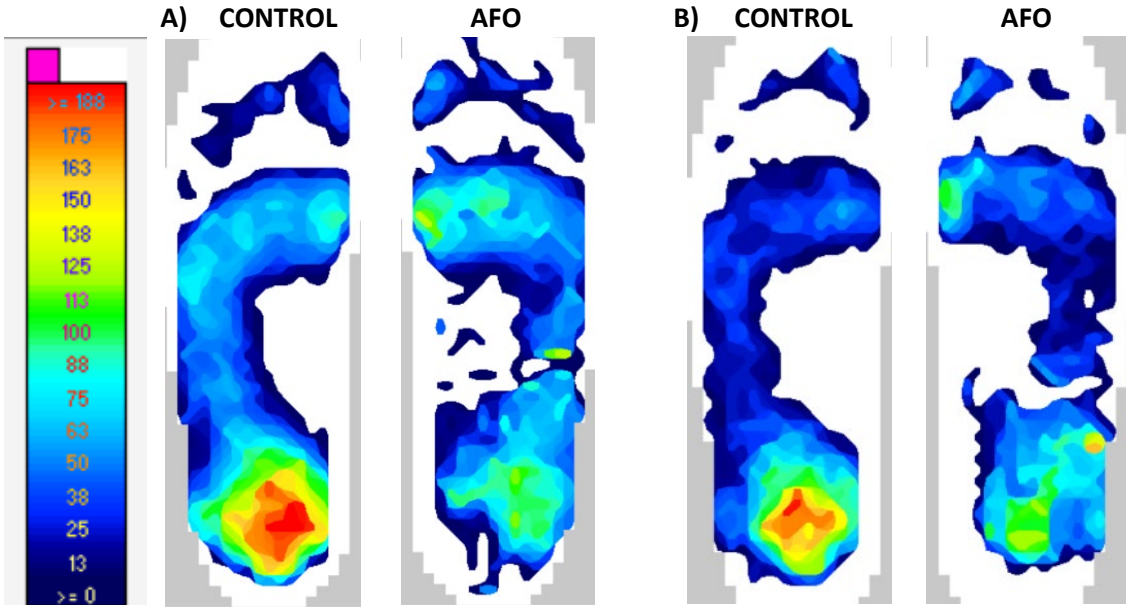

Figure 3.12: Pressure distributions for Participant 3, average stance during stationary standing. **A)** With Push AFO. **B)** With ES AFO. Units: kPa.

The exemplar pressure distributions from gait show the differences between AFO and control feet and between the two devices. The distributions clearly show the increased pressures with the ES AFO (Figure 3.11B) compared to the Push AFO (Figure 3.11A). This was also the case in the toe region, which was not included in the forefoot assessments in the previous figures. The differences between AFOs were not as noticeable in the standing data (Figure 3.12), though differences between the control and AFO feet were still present.

3.2.1.5 Case Study: Maximum Pressure Gradient Changes during Gait Cycle

An example gait cycle from Participant 1 was exported for both the ES and Push AFOs so that the change in pressure gradient over time could be compared to the change in peak pressure (Figure 3.13. Figure 3.14). Pressure-time integrals were calculated using both peak pressures and peak pressure gradients, for the full area under the curve and the area above 80% of the peak pressure (Table 3.3). The area above 80% of each pressure metric's curve was examined to show where the pressure was highest for longer, with 80% chosen as an arbitrary threshold that has been previously used in literature [103].

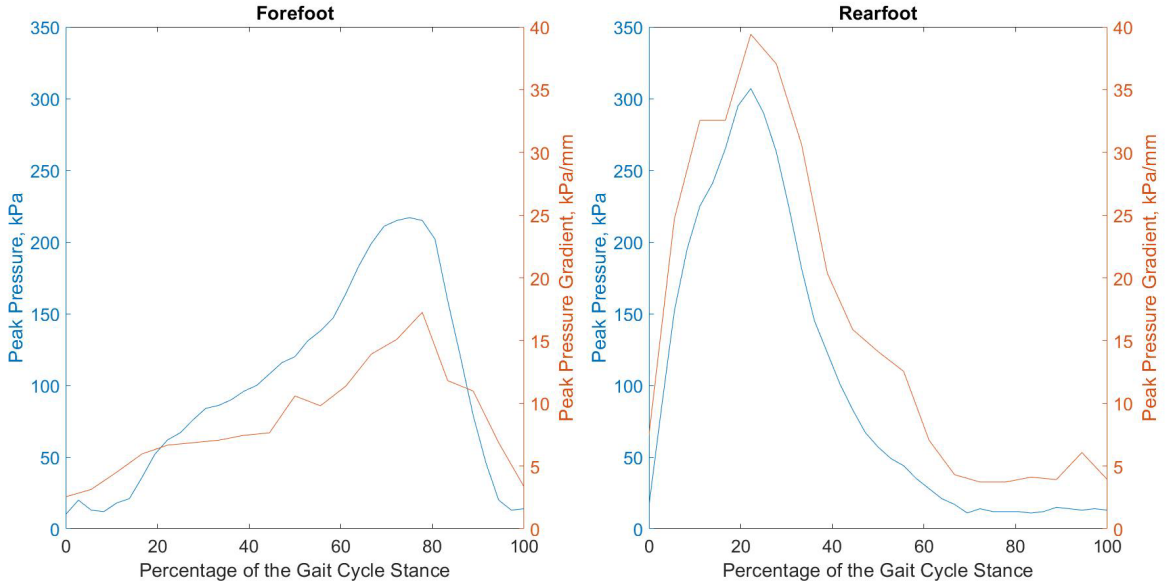

Figure 3.13: Peak pressures and pressure gradients over time during a sample gait cycle for the **ES AFO** – example from Participant 1, with a bamboo sock

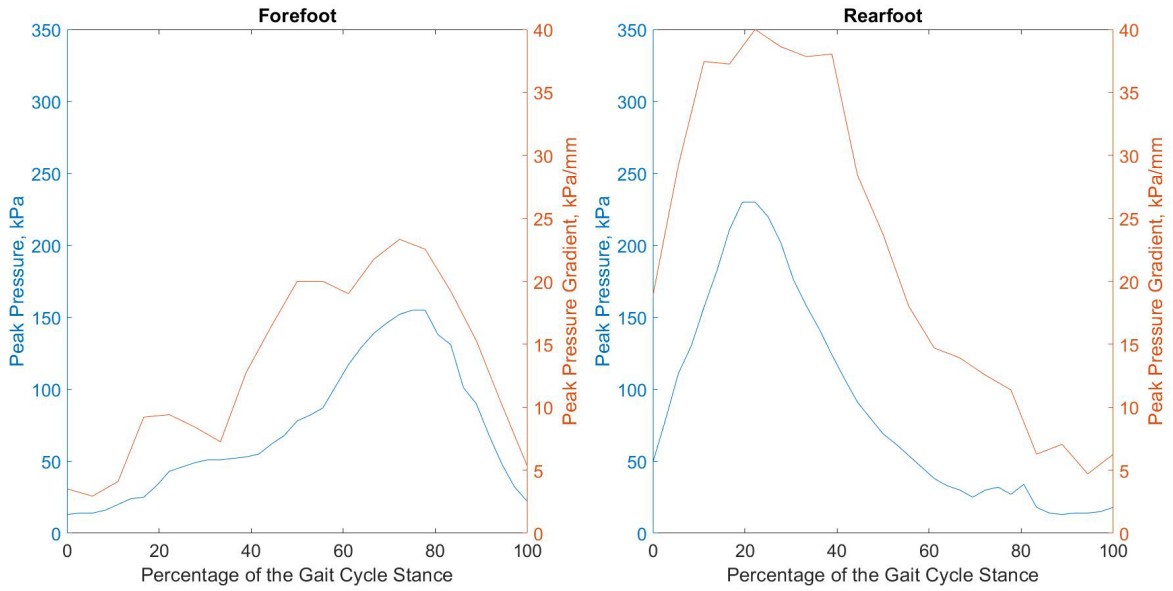

Figure 3.14: Peak pressures and pressure gradients over time during a sample gait cycle for the **Push AFO** – example from Participant 1, with a bamboo sock

Table 3.3: Integrals of peak pressure-time and peak pressure gradient as a percentage of the gait cycle for Participant 1

AFO Type	Foot Region	PTI for peak pressure	PTI for pressure gradient	PTI over 80% peak pressure	PTI over 80% peak pressure gradient
ES	Forefoot	10100	889	3470	170
ES	Rearfoot	10100	1660	3210	593
Push	Forefoot	7340	1370	2820	702
Push	Rearfoot	8980	2290	2460	1060

The changes in peak pressures and peak pressures gradients followed the same expected pattern of increasing in the rearfoot earlier in the gait cycle and increasing in the forefoot later in the gait cycle (Figure 3.13. Figure 3.14). However, there were differences in the comparison between AFOs. For the peak pressures, the PTI and PTI over 80% were consistently higher for the ES AFO compared to the Push AFO, but the opposite occurred for the pressure gradient PTIs (Table 3.3).

3.2.2 Temperature and Humidity Results

3.2.2.1 Combined Temperature and Humidity Sensors

The temperature and humidity results from the Sensirion combined sensors are displayed as differences from the baseline values for the gait conditions (Table 3.4. Figure 3.15. Figure 3.16).

Table 3.4: Change in temperature and relative humidity under AFO from baseline conditions, during gait displaying Median (IQR).

Foot Region	Test Condition	Temperature, change from baseline (°C)	Relative Humidity, change from baseline (%RH)
MH1	ES Bamboo	4.4 (1.7 – 6.7) *	3.0 (0.4 – 6.7) *
	ES Cotton	2.6 (0.5 – 3.0)	7.0 (0.7 – 8.6)
	Push Bamboo	3.1 (2.5 – 5.2)	-0.5 (-3.7 – 3.5)
	Push Cotton	1.8 (1.3 – 2.9) *	3.5 (2.0 – 9.6) *
MH5	ES Bamboo	3.6 (2.8 – 4.7)	3.7 (-0.2 – 4.5)
	ES Cotton	2.3 (1.9 – 4.3)	1.9 (-2.4 – 8.8)
	Push Bamboo	5.9 (5.0 – 6.5) *	-8.2 (-10.4 – 6.0) *
	Push Cotton	2.9 (2.9 – 4.0)	-3.8 (-5.0 – 1.4)
Navicular Head	ES Bamboo	4.6 (3.3 – 7.0) *	0.7 (-0.2 – 12.4) *
	ES Cotton	4.5 (3.6 – 4.9)	2.7 (0.4 – 15.6)
	Push Bamboo	8.3 (6.8 – 10.4) *	1.7 (-1.8 – 15.2) *
	Push Cotton	6.2 (2.8 – 7.0) *	4.0 (-3.3 – 7.3) *
Medial Heel	ES Bamboo	0.6 (0.1 – 0.7) *	-0.3 (-6.9 – 3.5) *
	ES Cotton	-0.9 (-1.4 – -0.1)	-0.4 (-4.6 – 2.6)
	Push Bamboo	1.2 (0.1 – 2.8) *	-3.3 (-7.0 – 6.4) *
	Push Cotton	0.8 (-0.2 – 2.0) *	-2.6 (-6.2 – 5.1) *

* Data from one participant failed to record or cut-off prior to end of the test condition.

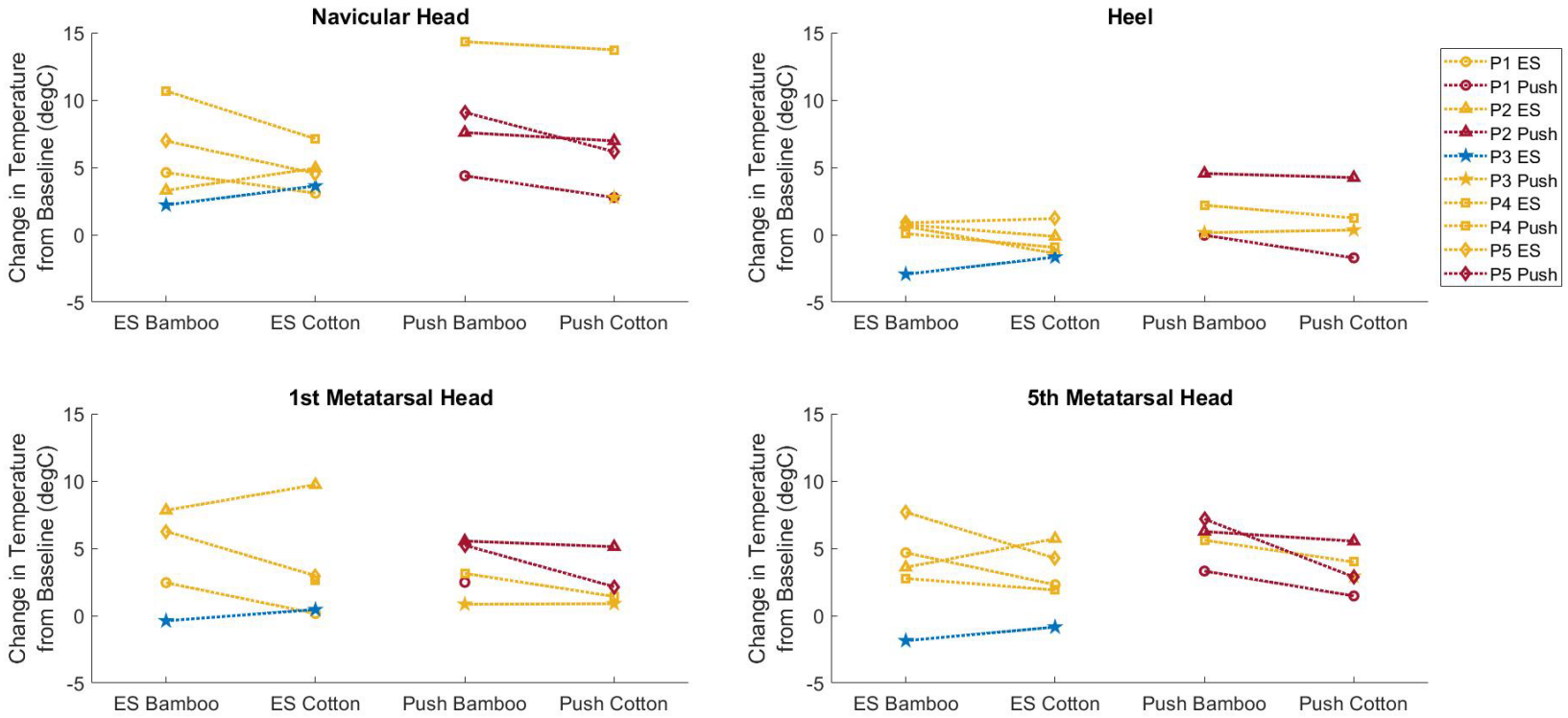

Figure 3.15: Temperature results for the gait test conditions, displaying individual participant's data as well as medians and ranges. Markers are colour coded to ambient temperature: Blue: <16°C, Yellow: 16-18°C, Red: 18-20°C

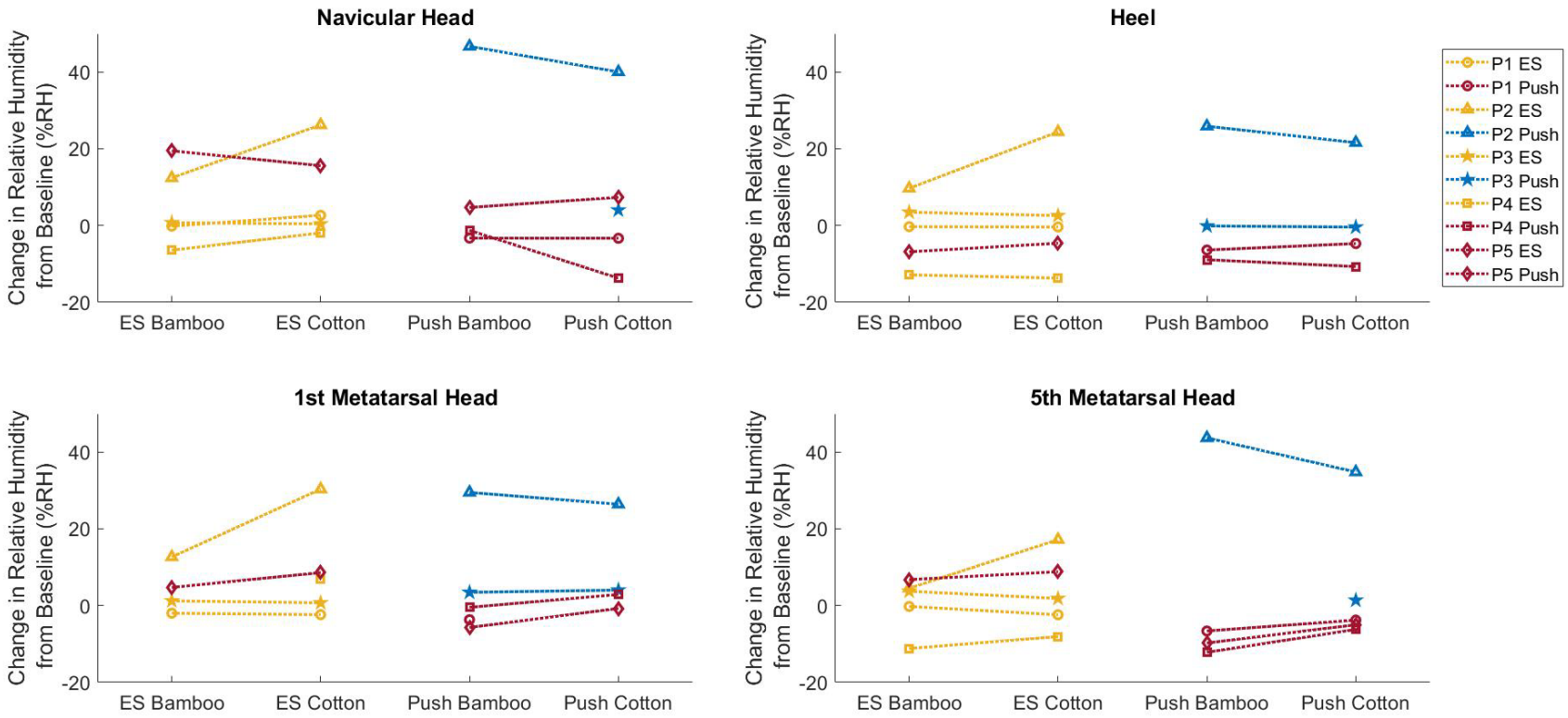

Figure 3.16: Relative humidity results for the gait test conditions, displaying individual participant's data as well as medians and ranges. Markers are colour coded to ambient humidity: Blue: 30-40%, Yellow: 40-50%, Red: 50-60%.

Generally, the temperature at each foot location increased from the baseline to the end of the gait test conditions (Figure 3.15). The navicular head location showed the greatest increase with median temperature changes from baseline ranging from 4.5 to 8.3°C. The heel location showed the lowest temperature changes compared to baseline, with median differences ranging from -0.9 to 1.2°C. At the navicular head, heel and fifth metatarsal head, the Push AFO caused a greater temperature increase than the ES AFO (Table 3.4). The variation in temperature results for the Push AFO was slightly greater than the ES AFO at the heel (-1.7 to 4.6°C *vs.* -2.9 to 1.2°C) and navicular head (2.8 to 14.3°C *vs.* 2.2 to 10.7°C) and slightly lower at the metatarsal heads (0.8 to 7.2°C *vs.* -1.9 to 9.7°C) (Figure 3.15). The change in temperature was consistently lower for the cotton sock than for the bamboo sock, which was most noticeable at the metatarsal heads. For example, at MH1 the median changes in temperature for the cotton and bamboo socks respectively were 2.6°C (11.9%) and 4.4°C (20.7%) for the ES AFO and 1.8°C (7.5%) and 3.1°C (12.3%) for the Push AFO (Table 3.4).

The relative humidity (RH) responses varied between participants and locations. Participant 2 displayed a far greater increase in RH throughout all test conditions than any other participant. This was particularly the case for the Push AFO, where the changes in RH ranged from 21.6 to 46.6%RH for P2 and -13.7 to 7.3%RH for the other participants (Figure 3.16). This difference was not present in the temperature results. Generally, the RH increased more for the ES AFO than the Push AFO at the metatarsal heads, with median changes of 1.9 to 7.0%RH and -8.2 to 3.5%RH for each AFO respectively. The Push AFO was more likely to cause a decrease in RH than an increase at the fifth metatarsal head (3/5 *vs.* 2/5 participants for Push and ES AFOs respectively). At the heel, the RH tended to show little change or a decrease, and the Push AFO caused a slightly greater median decrease than the ES AFO (bamboo sock: -3.3 *vs.* -0.3%RH; cotton sock: -2.6 *vs.* -0.4%RH). At the navicular head, the Push AFO caused a greater median increase in RH than the ES AFO (bamboo sock: 1.7 *vs.* 0.7%RH; cotton sock: 4.0 *vs.* 2.7%RH). Comparing the sock materials, wearing the cotton sock led to a consistently greater median increase in RH than the bamboo sock at the first metatarsal head and the navicular head (Table 3.4). At the heel and fifth metatarsal head, there were inconsistent median differences between the sock materials. However, assessing the participants individually, generally either 3/5 or 2-3/4 participants experienced greater increases in RH with the cotton sock compared to the bamboo sock (Figure 3.16). The exception to this was at the heel, where the results between socks where relatively similar (ranges: -13.7 to 24.4%RH *vs.* -12.9 to 25.9%RH for cotton and bamboo respectively).

The temperature results while standing followed similar trends to the gait results, though with smaller changes. The Push AFO caused greater median temperature increases than the ES AFO at the navicular head (3.0&3.2°C *vs.* 1.7&2.7°C), heel (0.7&1.5°C *vs.* -1.3&0.4°C), and fifth metatarsal

head (0.5&0.7°C *vs.* -1.0&0.0°C). The differences in RH between devices were minimal during the standing conditions (median differences: -0.4 to 1.5%RH *vs.* -5.4 to 1.3%RH for ES and Push respectively). It should be noted that where Participant 2 had far greater increases in RH than other participants in the gait conditions, they did not in the standing conditions.

In contrast to the gait conditions, the bamboo sock generally caused a greater increase in RH than the cotton sock during stationary standing, though the differences were quite small. For the ES AFO, the median RH changes ranged from 0.0 to 1.5%RH for the bamboo sock and -0.4 to 0.2%RH for the cotton sock. In the temperature results, the cotton sock led to slightly greater median temperature increases than the bamboo sock at the navicular head (2.7°C&3.2°C *vs.* 1.7°C&3.0°C) and heel (0.4°C &1.5°C *vs.* -1.3°C &0.7°C). Line graphs of the individual participant data and the full median and IQR data for the standing test conditions can be found in Appendix D (p.170).

3.2.2.2 Temperature Results for AFO *vs.* Control Foot

To further examine the effect of the AFOs on temperature, thermocouple data from the AFO and control foot were compared for the first metatarsal head, heel, and calf during gait (Table 3.5. Figure 3.17.). Similar results for the stationary standing conditions can be found in Appendix D, pg.172.

Table 3.5: Temperature change under AFO vs control foot during gait displaying median (IQR).

Foot Region	Test Condition	Temperature, change from baseline (°C) AFO foot	Temperature, change from baseline (°C) Control foot
MH1	ES Bamboo	4.4 (1.7 – 6.7)*	3.5 (3.3 – 4.1) *
	ES Cotton	2.6 (0.5 – 3.0)	2.6 (1.1 – 3.7)
	Push Bamboo	3.1 (2.5 – 5.2)	6.0 (3.5 – 6.9)
	Push Cotton	1.8 (1.3 – 2.9) *	3.0 (2.0 – 4.9) *
Lateral Heel	ES Bamboo	6.2 (6.0 – 7.8)	4.3 (3.6 – 7.3)
	ES Cotton	5.5 (4.5 – 6.2)	2.2 (2.1 – 2.5)
	Push Bamboo	6.2 (4.4 – 7.4)	3.5 (3.2 – 4.6)
	Push Cotton	5.5 (3.9 – 6.1)	2.4 (0.7 – 2.6)
Calf	ES Bamboo	3.4 (3.4 – 5.3)	2.4 (0.8 – 3.5)
	ES Cotton	4.5 (1.7 – 7.3)	0.2 (-0.2 – 1.5)
	Push Bamboo	6.9 (3.9 – 7.1)	5.1 (1.1 – 5.6)
	Push Cotton	6.8 (4.9 – 7.4)	1.8 (0.4 – 3.5)

* Data from one participant failed to record.

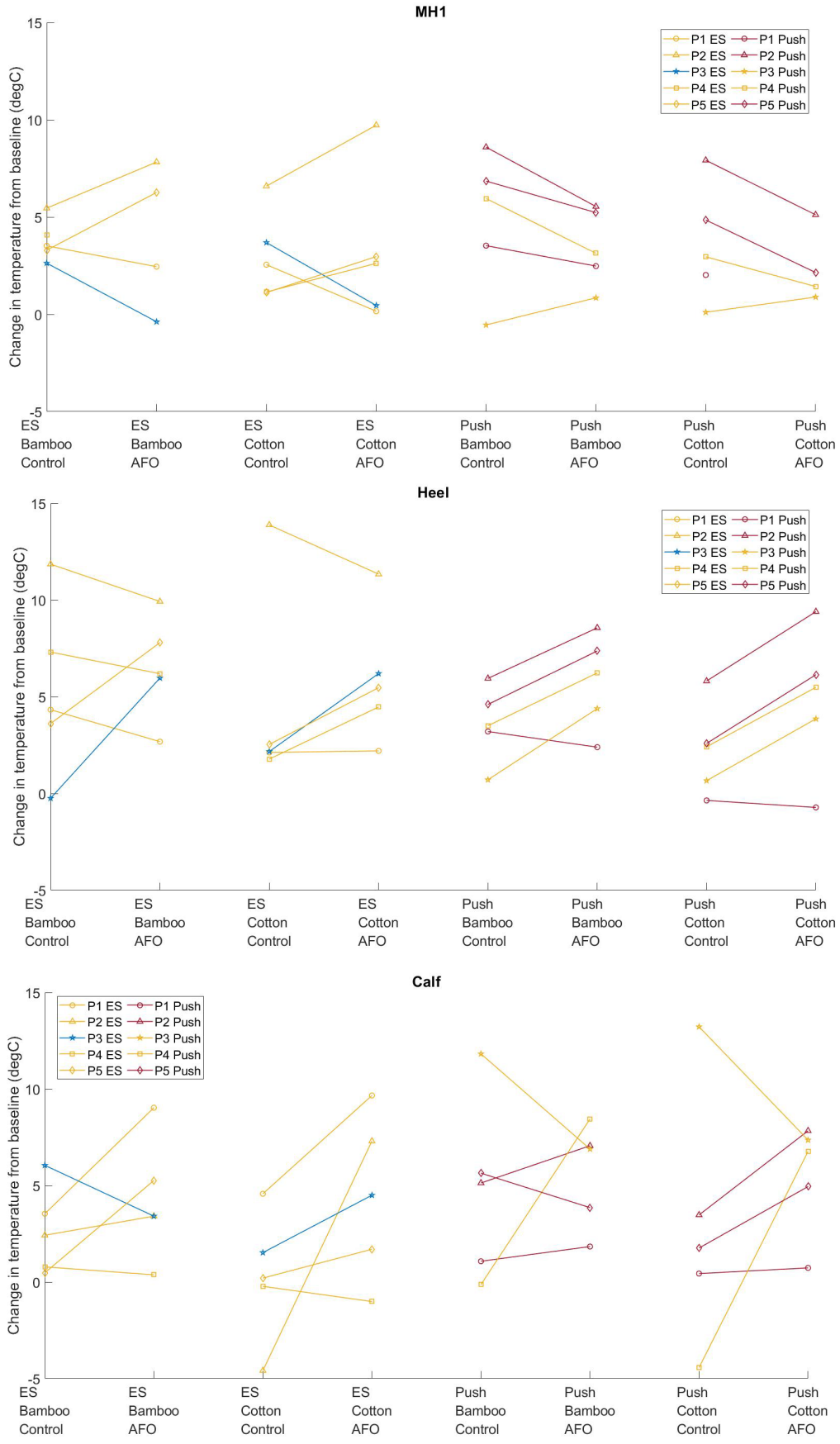

Figure 3.17: Comparison of temperature changes from baseline between the AFO foot and the control foot during gait. Colour coded to ambient temperature: Blue: <16°C, Yellow: 16-18°C, Red: 18-20°C.

The Push AFO caused an increase in temperature compared to the control foot at the heel in 4/5 participants during gait (range: -0.8 to 3.7°C). The Push AFO also caused a decrease in temperature at the metatarsal head in 3-4/5 participants when compared to the control foot (ranges: -3.1 to 1.4°C), with only Participant 3 consistently displaying an increase. The responses at the calf had less clear trends (ranges: -5.9 to 11.2°C). The ES AFO temperature results showed more variable responses than the Push AFO, but increased compared to the control foot in 3-4/5 participants at the calf (range: -2.6 to 11.9°C), 3/5 participants at the 1st metatarsal head (range: -3.2 to 3.1°C), and 2-4/5 participants at the heel (range: -2.5 to 6.2°C) (Figure 3.17).

The control foot temperature data showed the differences between the cotton and bamboo sock without the presence of the AFO. In the gait test conditions, the bamboo sock caused greater temperature increases than the cotton sock in 3-5/5 participants across the test conditions and locations (medians of 2.4 to 6.0°C *vs.* 0.2 to 3.0°C, Table 3.5). This was similar to the trend noticed previously with the combined temperature and humidity sensors (Table 3.4), and also to the thermocouple data for the AFO foot at the metatarsal head and heel (Table 3.5). However, at the calf the temperature increase on the AFO foot was often greater for the cotton sock than the bamboo sock.

3.2.2.3 Temporal Profile of Microclimate

The above microclimate results detailed the changes in relative humidity from baseline to the end of the test condition. Temporal changes in microclimate throughout the test conditions are also relevant. An example is provided for the navicular head location during gait with the ES AFO and bamboo sock, showing the relative humidity responses (Figure 3.18A) and corresponding temperatures (Figure 3.18B).

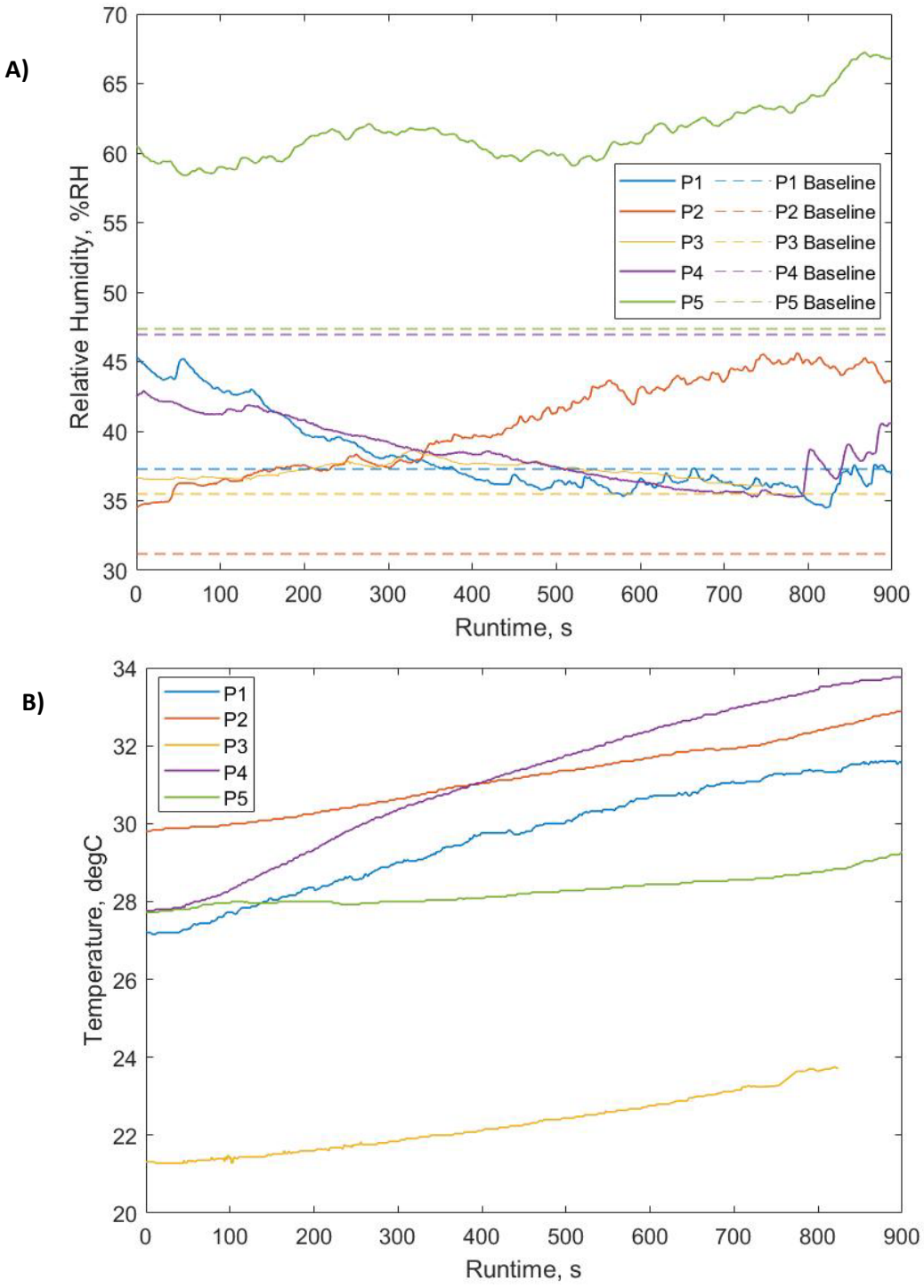

Figure 3.18: **A)** Relative humidity results at the navicular head during gait with the ES AFO and bamboo sock. Baseline values for each participant are also shown. **B)** Corresponding temperature results

The temperatures tended to increase consistently throughout the gait conditions. However, there were different relative humidity responses depending on the participant. The humidity responses could broadly be categorised into:

- General increase throughout test condition (Participants 2 and 5)
- Decrease in humidity before levelling off or increasing towards the end of the testing (Participants 1 and 4)

- Little change in humidity throughout test condition (Participant 3)

Each participant tended to show similar responses throughout the test sessions, though there was some variation. For example, at some foot locations (e.g. the heel) the humidity was more likely to decrease continuously to the end of the test condition.

3.2.3 Questionnaire Results

The CSD-OPUS survey consisted of nine questions, with each scoring 1 to 4 depending on whether the participant had strongly agreed, agreed, disagreed, or strongly disagreed with the statement. The overall scores (out of 36) and scores for some of the more relevant questions were averaged for the first 5 participants (Figure 3.19), with lower scores indicating higher satisfaction with the device. The questionnaire items deemed most relevant to tissue health were:

- My orthosis is comfortable through the test session
- My skin is free of abrasions and irritations
- My orthosis is pain free to wear

The median overall scores during gait were generally slightly higher, signifying lower satisfaction, for the ES AFO compared with the Push AFO (median scores of 19-20 *vs.* 18 respectively). However, this was not the case for all participants as both Participant 4 and Participant 5 showed slightly higher satisfaction with the ES AFO than the Push (scores of 9 *vs.* 10 and 20 *vs.* 21 respectively). Overall satisfaction was sometimes higher for the standing conditions compared to gait – this was the case for Participants 2 and 3 with the ES AFO, and Participants 1 and 5 for the Push AFO. There was considerable variation in overall scores between participants.

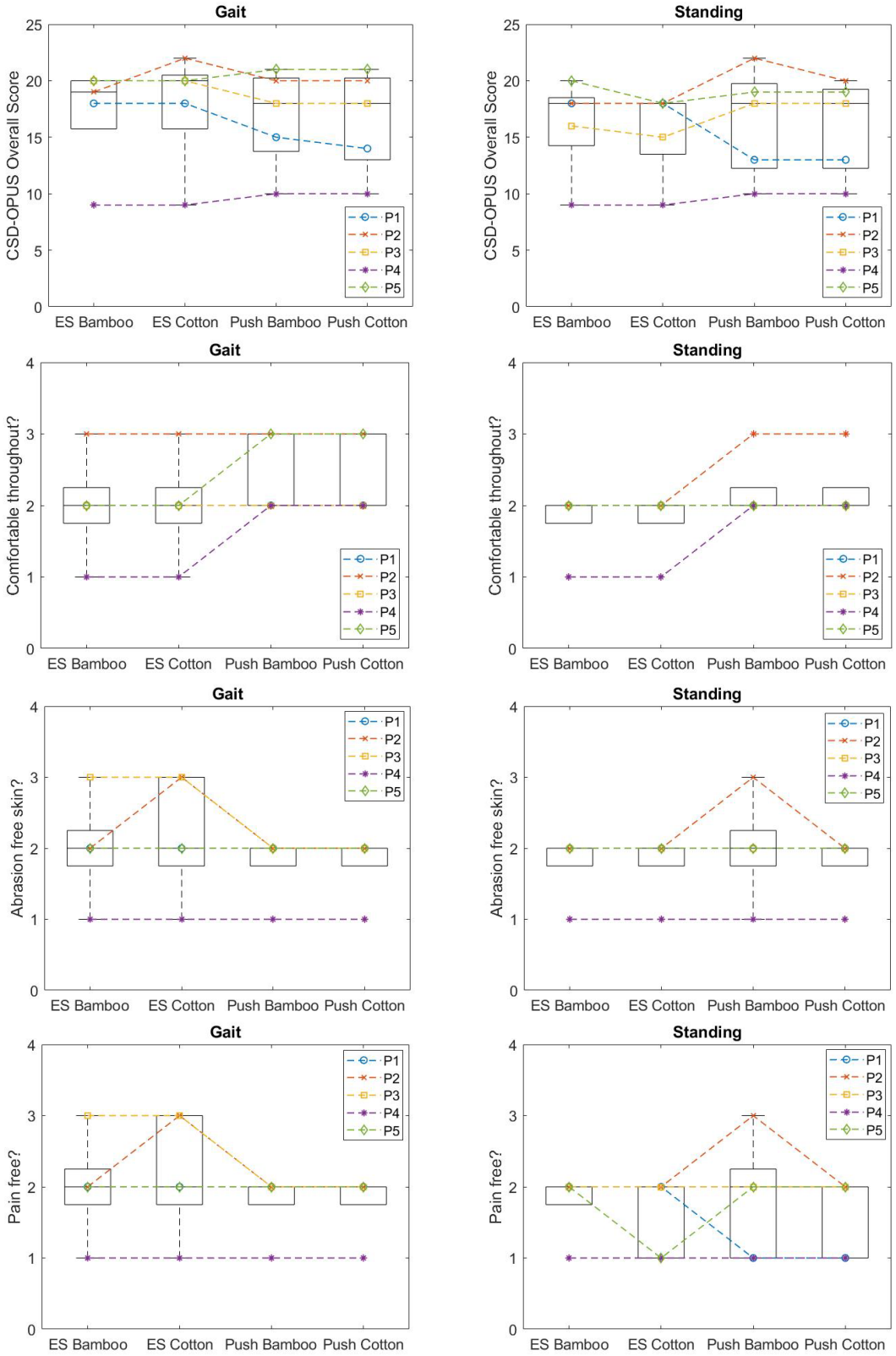

Figure 3.19: CSD-OPUS questionnaire results for gait and stationary standing conditions for the overall scores and questions relevant to tissue health

Though the individual questions highlighted each gave median responses of 2 (agreement with the positive statement), there were differences between test conditions observed in certain

participants. The standing conditions were more likely to be pain free than the gait conditions, and the Push AFO was less likely to be comfortable than the ES AFO. Participant 4 consistently found the ES AFO more comfortable to wear than the Push AFO (scores of 1 *vs.* 2). They also commented that they thought wearing the Push AFO all day would make their leg ache, maybe due to the straps connecting the foot plate to the calf region of the AFO. Participant 5 also found the ES AFO more comfortable to walk in than the Push AFO (scores of 2 *vs.* 3), and mentioned that the lack of full foot plate in the Push AFO may have meant they were using their toes more. Conversely, Participant 3 found the ES AFO gait conditions more painful and more likely to cause skin abrasion than using the Push AFO (scores of 3 *vs.* 2), though gave both AFOs the same rating for comfort. Participant 2 gave pain and skin abrasion scores of 2 to most test conditions, but ranked the gait condition with the ES AFO and cotton sock and the standing condition with the Push AFO and bamboo sock worse with scores of 3. The gait with cotton sock test condition was the second of the two walking conditions for that participant so it is possible they experienced more issues with the ES AFO over time. However, it is unclear why that particular standing condition was worse than others.

3.3 Discussion

The aims of this pilot study were to investigate the effects of AFO and sock materials on pressure and microclimate, and to evaluate different sensor locations and metrics for their effectiveness at assessing the devices. As there was a limited number of participants involved in this study, it is difficult to draw firm conclusions about the risk of tissue damage with the different AFO and sock materials. However, the trends that were present in the different outcome measures provide key information that may be used to develop future studies.

3.3.1 Pressure

The pressure metric results were compared to pressure distribution trends and magnitudes from literature, to determine whether the present results were reasonable. In this study, the median peak pressures during gait ranged from 233 to 355kPa in the forefoot and 224 to 457kPa in the rearfoot across the test conditions. The median maximum pressure gradients ranged from 25.7 to 47.6kPa/mm in the forefoot and 27.6 to 63.3kPa/mm in the rearfoot. Literature on plantar pressure data within AFOs is limited. Chung et al. [100] reported peak pressures of 205-223kPa and 173-198kPa in the forefoot and rearfoot respectively, lower than in the present study but the AFOs they were testing did not have base plates. Nowak et al. [146] recorded plantar pressure data inside a traditional moulded AFO, though found the peak pressures to be 159kPa in the forefoot and 102kPa in the rearfoot. Their results were far lower than those in the present study

but are also lower than many in-shoe pressure results for without an AFO. The discrepancy may have been due to Nowak et al.'s calibration of the F-scan sensors, which was not described in detail but was carried out according to only one of the participants' weights and prior to the sensor being trimmed and fitted to the AFO.

Lung et al. [215] tested in-shoe pressures in healthy individuals without an orthosis – with mean peak pressures of around 400kPa and 275kPa in the forefoot and rearfoot respectively. They also found the mean peak pressure gradients to be approximately 45kPa/mm in the forefoot and 25kPa/mm in the rearfoot. While not including an AFO, the results were relatively similar to the control foot results in the present study (Figure 3.9). Mueller et al. [182] also examined plantar pressure gradients, though in barefoot healthy individuals, and found mean PG results of 68kPa/mm and 7kPa/mm in the forefoot and rearfoot respectively. Most studies reporting PTI results for gait do not normalise their results to the gait cycle and thus comparisons could not be made. However, Laing et al. [103] did report PTI based on the gait cycle for pressures over 80% of the peak pressure in prosthetic sockets, which ranged from 994 to 3191. This was similar to the present case study examining PTIs over 80% in one participant, which ranged from 2460-3470 (Table 3.3), suggesting the results of this study were reasonable. The range of PTIs using the full pressure-time curve was understandably higher than this at 10159-18853, however no data could be found in literature to compare this to.

In the present study, the peak plantar pressures measured in the AFO foot were generally lower than the control foot, suggesting that the participants were shifting their weight away from the AFO foot while walking. This was corroborated by the PTI results, which were also lower in the AFO foot than the control particularly in the rearfoot, showing participants were moving through heel strike quicker on the AFO side. The effect was more noticeable for the Push AFO than the ES AFO. For the ES AFO, the PTI was often more balanced between the AFO and control feet indicating a more even gait. The shifting of weight away from the AFO may have been due to healthy participants not being accustomed to wearing an AFO, or the discomfort that it may have caused. Another potential explanation for why this occurred more frequently with the Push AFO lies in the AFO designs. During the testing, it was often difficult to don the shoe over the AFO, despite the larger shoe sizes used. This was particularly an issue with the ES AFO, where the Velcro ankle strap attached at the base of the device either side of the heel (Figure 3.3), and so the strap often caught and loosened as the shoe was donned. If this occurred, the shoe was removed and the strap re-tightened. However, it may have escaped notice in some cases, or the strap may have loosened during gait due to the insecure fixation method. Thus, the participants' gait may not have been as affected as it would be with the ankle held more firmly in place. The Push AFO had a far more secure dorsal strap, and so was potentially more effective at adapting the participants' gait.

Unlike the peak pressures and PTIs, the pressure gradients in the AFO foot were generally higher than in the control foot as the presence of the device caused pressure gradients even where the pressure magnitude was lower. The exception to this was at the forefoot with the Push AFO – where the ¾ length thin base plate did not tend to increase the pressure gradients. Generally, the ES AFO was more likely to cause higher pressure gradients when compared to the control foot, and particularly in the rearfoot (86% median increase for ES AFO from control *vs.* 27% increase for Push AFO). This was probably due to the design of the device with the rigid polypropylene contacting the skin, without the pressure of a softer interface layer which the Push AFO had. The higher pressure gradients experienced with the ES AFO may indicate increased risk of skin damage. Having gradients in the applied pressure can increase the likelihood of stress concentrations in the underlying skin and soft tissue, and may indicate where shear forces are present (see Section 2.3.4). Thus, pressure gradients may be the more useful pressure metric for this application as they account for any offloading occurring, and showed the differences between the devices clearly.

Due to the cyclic nature of gait, the peak pressure and pressure gradients would be relieved frequently, and so the maximum values may not directly translate to tissue damage risk. Thus, the PTI metric was used to compare the temporal aspect of the applied pressures due to each AFO. However, as PTI is calculated from peak pressures throughout gait, though it was considered for multiple foot region, it does not fully consider spatial pressure distribution. Thus, the case study was performed to determine whether changes in peak pressures over time (PTI) corresponded to changes in pressure gradients over time. Similar trends were seen in changes in pressures and pressure gradients over time (Figure 3.13. Figure 3.14), but there were differences when comparing the AFOs. This was particularly noticeable in the PTI over 80% of the peaks, where for the peak pressures the PTI over 80% was lower for the Push AFO than for the ES AFO, but the opposite occurred for the pressure gradient metric (Table 3.3). Thus, the pressure gradients may be higher for longer where the peak pressures are not, which may have implications for tissue damage risk. However, it should be noted that this was just a sample gait cycle from one participant, chosen from part way through the test condition, and not may not be fully representative of the average gait of each participant.

Also of note from the case study was that the pressures and pressure gradients never fell to zero between gait cycle stances, as there was always contact with the AFO (Figure 3.13). Although these maximum pressures would not be present across the full forefoot or rearfoot, it was likely these measurements were coming from the same specific area of the foot. Thus, in certain areas of the foot, full off-loading and pressure relief would not be experienced during the gait cycle.

The sock type appeared to have little impact on the pressure results, suggesting that any differences between sock design (e.g. material, thickness, fit to limb) did not affect the interface pressures. However, as only sock material was considered in this study, a more in-depth assessment of different sock parameters would be needed to confirm this.

There were some limitations to using the F-scan system with the AFOs. Although the in-shoe sensor was thin and conformed well to the foot, when placed within the AFO it could not always lie completely flat. This was particularly an issue with the ES AFO which had a rigid base plate, and led to the AFO foot pressure measurements being slightly more sporadic than the control foot or resulting in the occasional drop-out of a row of sensels. Generally, this was more of an issue in lower pressure regions such as the midfoot, and so the software's noise threshold of 3kPa may have also contributed to this effect. However, if the high stiffness of the AFO led to crinkles in the sensor and affected whether all the sensels were recording applied loads, this may have impacted the accuracy of the results.

Another potential limitation stemmed from the training shoes that were used in the testing. These were provided to the participants so that they would fit the AFOs and to ensure pressure results were not affected by differences in, for example, sole geometry between participants' personal shoes. However, there may have been differences in how well the provided shoes fit each participant potentially impacting gait, and thus pressure results. Nonetheless, it was likely that any negative impact on gait due to the training shoes was negligible compared to the impact of wearing an AFO for those unaccustomed to it.

3.3.2 Temperature and Humidity

While there has been little to no previous research carried out investigating microclimate with AFO use, data is available for other applications such as running shoes and insoles. West et al. [216] had participants sit for 10min and then run on a treadmill at 7.5km/h while wearing two different shoes. Though this was a faster speed than the present study, the presence of an AFO here may have counter-balanced this. Their mean foot skin temperature results after 15min on the treadmill were increases of around 6°C. This was relatively similar to the present study, where the temperature increases were 4.5-8.3°C at the navicular head, and 1.8-5.9°C at the metatarsal heads. West et al. also reported mean in-shoe RH increases of 17-26%RH, higher than this study where the maximum median RH increase was 7%RH. This discrepancy may have been due to the higher speed used by West et al., or differences in the ambient conditions which in their case were controlled to 23°C and 35%RH – generally hotter and less humid than the present study.

Gil-Calvo et al. [217] measured plantar temperatures using an infrared camera after a 10min warm-up jog followed by a 20min run for two different insoles and a control condition. Again,

their results were relatively similar to the present study, observing temperature increases of 6.2-7°C from immediately prior to immediately after running. Shimazaki et al. [218] looked at skin temperatures in different regions of the foot while wearing different shoes, but did not provide full results for this. However, exemplar data showed a 1.5°C increase after 15min of gait at 6km/h in a similar location to the heel sensor in the present study, where the temperature change was -0.9 to 1.2°C. Whilst these studies differed from the present one in the devices being assessed and the gait speeds, the similarities observed lend credibility to the results of this study.

As of yet, there are no formal criteria for what constitutes an ideal microclimate during AFO use. From the perspective of comfort, it has been suggested that temperature and relative humidity in footwear should not exceed 34°C and 65% respectively (see Section 2.1.3). How those thresholds might relate to tissue damage risk in this scenario is less clear, as no previous research has quantitively assessed microclimate during AFO use. Broadly, the results from this study were below the stated comfort thresholds. However, in a limited number of test conditions for some participants, the microclimate rose to maximum values of 36°C and 75%RH. It should also be considered that the test conditions were only 15 minutes long and the changes in microclimate may not have plateaued by that point. As such, for the purposes of this study, the AFOs and socks have been assessed on their ability to limit the change in microclimate on the basis that smaller changes would be less likely to result in discomfort and tissue damage.

The Push AFO tended to cause a greater increase in temperature and lower increase in relative humidity than the ES AFO. The main exception to this was at the navicular head where the Push AFO increased the relative humidity more than the ES AFO. This was likely related to device design, as the more occlusive material of the ES AFO may have inhibited moisture dissipation away from the skin. However, at the navicular head the Push AFO has additional straps which are not present on the ES AFO, potentially leading to the difference in trends at that location (Figure 3.20). The degree of coverage the AFO provides could also explain the temperature results. In the median results (Table 3.4), the Push AFO caused greater increases in temperature than the ES AFO at the navicular head, heel and fifth metatarsal head, regions where there is a higher degree of coverage with the Push AFO due to the straps. At the first metatarsal head, the ES AFO caused a greater increase in temperature than the Push. This region was well clear of straps on the Push AFO and the longer foot plate of the ES AFO may have had more of an influence into the temperatures. However, it should be noted that these trends between temperature change and AFO type were not the case for all participants (Figure 3.15). For the metatarsal heads in particular, this may have been influenced by the fit of the AFO to the individual impacting how close the device straps came to the sensor for the Push AFO. As would be expected, the standing

test conditions produced far lesser changes in microclimate than the gait conditions and in most cases there were limited discernible trends.

Figure 3.20: Coverage of AFOs compared to combined temperature/humidity sensor locations (indicated with red circles)

The cotton sock tended to lead to a greater increase in humidity but lower increase in temperature than the bamboo sock. Relative humidity tends to have more of an impact on tissue damage risk than temperature (see Section 2.1.3), suggesting that the bamboo sock could be more beneficial. This aligns with anecdotal evidence from physiotherapists (NHS Solent Trust), who recommend bamboo socks to AFO users to aid sweat-related issues. However, it should be noted that the two sock types were not identical outside of the material difference. As such, the differences in the results may also have been due to design factors such as sock thickness and tightness of the weave, which could affect heat flux and moisture absorption.

The ambient temperatures ranged from 12 to 19°C, though only one test session was below 16°C, and the ambient humidity ranged from 34 to 60%. The results presented were not normalised for these differing ambient conditions. The data could be standardised to set ambient conditions, however that would not account for physiological responses occurring due to the specific ambient conditions of the test sessions. For example, a lower ambient temperature could result in the humidity displaying little change from the baseline conditions due to the lack of thermoregulatory response. Simply standardising this to a higher ambient temperature would not cause the humidity response to show an increase due to the onset of sweating which would likely then occur. Controlling the ambient conditions during future testing may allow for easier comparison between device designs, but would not represent the full range of conditions experienced during everyday life. Alternatively, if more participants were tested, a cluster analysis could be performed to assess responses in high *vs.* low ambient temperature and humidity conditions.

The different responses of relative humidity over time observed between participants may have been partly due to differing ambient conditions (Figure 3.18). Thus, the ambient and baseline relative humidity and temperature were examined to determine whether ambient conditions may have had an effect on the response type (Table 3.6). The low ambient and baseline temperature for Participant 3 could explain why the humidity did not markedly change, as there may have been no need for a thermoregulatory response to produce sweat. However, the ambient and baseline conditions do not seem to provide an obvious reason for why Participants 1 and 4 displayed a different relative humidity response than Participants 2 and 5. Full ambient and baseline measurements can be found in Appendix E (p.172).

Table 3.6: Ambient and baseline microclimate conditions for the ES AFO, colour coded to show the lowest to highest conditions across the participants (ordered by ambient temperature).

Participant	RH Response (Figure 3.18A)	Ambient Temperature – ES AFO (°C)	Navicular Head Base Temperature – ES AFO (°C)	Ambient RH – ES AFO (%RH)	Navicular Head Base RH – ES AFO (%RH)
3	→	12.0	21.5	49.9	35.4
2	↗	16.2	29.6	40.8	31.2
1	↘↗	16.4	26.9	43.8	37.2
5	↗	17.0	22.2	51.9	47.4
4	↘↗	17.9	23.1	48.0	46.9
Key:	Lowest				Highest

There are other possible explanations for the different relative humidity responses between participants. Variability in the participants' thermoregulation would have affected the responses, particularly as the walking speed was self-selected and so the chosen speed may have affected some participants more than others. Another factor to consider is that airflow through the shoe would promote dissipation of heat and moisture (see Section 2.1.3). However, differences in the fit of the AFO and shoe may have allowed for variation in airflow between participants. Airflow during gait may also explain the initial decrease in humidity seen in some participants, particularly if the humidity had built up in the shoe prior to the test condition. Any increases in the humidity towards the end of the test condition could be due to increased sweat production that the airflow could not fully counteract. These factors may also have contributed to Participant 2's elevated RH results compared to the other participants, which weren't reflected in the temperature results.

Some issues arose during the testing, relating to the measurement of the temperature and humidity. For many of the gait test conditions, temperature and humidity data from the combined sensors were only available from four participants due to sensors disconnecting mid test

condition (Table 3.4). During initial testing, it was found that the Sensirion combined temperature and humidity sensors had a tendency to twist and/or disconnect from the connectors due to the shifting motion of the foot during gait. This was partially remedied after the first three participants by applying micropore tape over the sensor pins to reduce sensor movement and risk of disconnection. This also allowed for easier donning of the socks and improved the contact between the sensor and the skin. Applying tape over the pins, ensuring that it did not cover any of the sensing element, had little effect on the temperature and humidity being recorded by the sensors (Appendix F, p.177). Across four sensors, applying the tape affected the temperature by <0.25°C and the relative humidity by <1.7%RH. Despite this fix, the occurrence of the sensors disconnecting could not be eliminated entirely. This was likely very dependent on each participant's foot anatomy, the fit of the AFO, and the motion of the foot during gait.

Another potential issue was degree of contact between the sensor and the skin. The sensors were taped in such a way to conform to the skin as much as possible, but there may have been slight differences in the amount of contact across the different sensors and test sessions. This was not likely to have been an issue during the test conditions, as the sock aided in holding the sensors tight to the skin. However, the initial baseline measurements – taken prior to the sock being donned – may have been affected, and so too would the results calculated as a change from baseline. Unfortunately, this was unavoidable as the baseline measurements needed to be taken without the sock to observe the effect of the different sock materials. In the future, to account for both the contact and disconnection issues, it may be beneficial to determine a more robust sensor attachment method or utilise alternative sensors.

3.3.3 Questionnaire

As expected, there was higher satisfaction during stationary standing than during gait. There was a slight trend towards lower overall satisfaction scores during gait with the ES AFO compared to the Push AFO, which corresponded to generally higher peak pressures and pressure gradients. However, this was not the case for all participants, particularly when examining the individual question on device comfort where the Push AFO tended to perform worse (Figure 3.19). Generally, there was much clearer variation in the overall satisfaction scores between participants than between test conditions, and frequently the participants gave the same score across all test conditions. Where there were differences in satisfaction between test conditions, no participants' responses differed by more than 1 point on the scale for any given question. However, this sometimes meant that a participant 'agreed' with a questionnaire statement for one test condition but 'disagreed' for another, indicating a clear difference in sentiment. In many cases, differences of agreement *vs.* disagreement occurred between the standing and gait conditions, but for some (e.g. Participant 5's comfort with device) the differences were between AFOs.

There were potential reasons for the limited trends between test conditions. Firstly, only five participants were tested in this pilot study, making trends difficult to discern, particularly when using a 4-point scale with limited responses available. In a larger sample size, trends may have been more apparent, especially where they were beginning to emerge between devices. Secondly, the test conditions were only 15-minutes long each – a relatively short period of time compared to how long the devices would be worn by users. The questionnaire itself is perhaps more suitable for assessing longer-term device use. Indeed, the statement regarding comfort reads:

My orthosis is comfortable throughout the day.

The participants were informed to base their responses on how the device had felt during the 15-minute test condition. However, it is possible that the satisfaction with the AFOs would be different during long-term use compared to short-term. One participant even commented that if they had to wear the Push AFO all day, they thought it would make their leg ache. Not every participant left comments on the questionnaire but for those that did, the comments generally reflected the responses to the individual questionnaire statements. For example, indicating if one AFO felt less comfortable than the other – clearly showing that for some participants there were noticeable differences between devices.

The sensors and wires present under the AFO may have caused some degree of discomfort, potentially affecting the questionnaire results. While the placement of the sensors and wires aimed to minimise irritation and rubbing, it may still have affected some participants due to individual differences in anatomy, gait, and fit of the AFOs. Three of the five participants added written comments to the questionnaire relating to sensors or wires.

- Participant 1 commented that the Push AFO was slightly more painful during the second gait condition (using a cotton sock) than the first but that it may just have been due to the wires and it was only a minor difference
- Participant 2 commented that for some gait conditions the sensors caused slight irritation and mentioned the sensor at the navicular head in particular
- Participant 4 commented that they could feel the navicular head sensor slightly during gait with the ES AFO. However, this was not reflected in the questionnaire scores which indicated strong agreement with the comfort and satisfaction with the device.

There was not much that could be done to limit discomfort due to the sensors further – the number of the Sensirion combined temperature and humidity sensors used was already limited as they were bulkier than the thermocouples. The AFOs used here did not allow for embedding the sensors to reduce interference, but this should be considered for future testing.

3.4 Summary

The purpose of this testing was to assess how AFO design affected the boundary conditions between the device and the limb, with implications towards tissue damage risk. To this end, two different AFOs and two sock materials were tested for their effect on pressure and microclimate, and participant satisfaction with each device was assessed. The Push AFO, with a more conforming interface material, caused lower peak plantar pressures and pressure gradients than the ES AFO. These lower pressures also seemed to relate to higher satisfaction for some of the participants. Microclimate appeared to be dependent on device design, with the more enclosing Push AFO generally causing greater temperature increases, and a greater increase in RH at the navicular head. However, the ES AFO performed worse than the Push AFO at controlling the RH at the other foot locations, particularly in the forefoot, due to its full-foot plate and more occlusive material. The relative humidity responses over time varied considerably between participants, potentially due to the ambient conditions, participant physiology, walking speed and airflow through the shoe. The sock materials had little impact on the pressure results, but did affect microclimate, with the cotton sock limiting the change in temperature better but the bamboo sock performing better to control the relative humidity. As such, a bamboo sock may provide more benefits in terms of reducing the impact of sweat-related issues.

Testing of this kind had not been performed before, particularly regarding microclimate, and so the assessments of how AFO type and sock material affect pressure and microclimate provide novel contributions to the field. As such, this pilot study also aimed to identify key parameters for future studies. The trends observed in the standing test conditions were generally minimal, with no additional information that wasn't also observed in the gait conditions. Thus, in future the test protocol could be narrowed to only assess gait conditions. With regards to the pressure metrics, the pressure gradients provided clearer trends between AFOs than peak pressure or PTI and was not affected by potential off-loading of the AFO foot. As such, pressure gradients may be a more useful metric for assessing tissue damage risk for this application. Finally, the microclimate results showed the importance of choosing sensor locations based on both vulnerable regions, such as the navicular head, and coverage of the devices being tested. Ambient conditions were also a factor in the relative humidity results, so must be carefully considered. These findings have provided a basis that future testing may build upon, to further assess the effects of device design on the physical boundary conditions at the orthosis-limb interface.

Chapter 4 Evaluation of AFO Design through Computational Modelling

Chapter 3 investigated the effects of AFO designs on the limb through an experimental pilot study. The devices' effect on the limb superficial tissues was examined through measures such as plantar pressures. This provided greater understanding of both the similarities and variation in responses different individuals had to device design, and how future testing could best evaluate interface conditions and user satisfaction. Computational modelling can also provide key data to inform orthosis design, particularly regarding how loading generated by the devices may risk damaging the deeper soft tissues. Previous computational studies assessing AFO design have focussed on device functionality and mechanical failure, with very limited research investigating the effect on the limb (see Section 2.3.2). Additionally, no previous AFO modelling studies have assessed multiple people, which is vital given the variability that was observed between participants in Chapter 3. Improved understanding of how AFOs affect soft tissue health, through computational assessment of different design parameters, would allow designs to be optimised to reduce tissue damage risk and could improve the wearers' satisfaction and adherence.

The aim of this study was to assess the effects of AFO interface material and fit on soft tissue health using simplified forefoot models. The forefoot was chosen as a region of interest due to the bony prominences of the metatarsal heads, which can result in tissue damage with AFO use. There are a number of reasons why an AFO may be ill-fitting – an off-the-shelf device may not perfectly match the wearer's foot size, a child may outgrow their device, or the volume of the wearer's limb may fluctuate throughout the day (see Section 2.3.5, p.45). Having an ill-fitting device may result in discomfort and increased risk of tissue damage, if strain concentrations form. Whether the AFO is made solely from rigid polypropylene in contact with the limb, or if there is a soft conforming material at the interface may also affect load transfer, and therefore soft tissue health. The experimental testing in Chapter 3 showed that interface material may have influenced superficial plantar pressure measurements, and the computational modelling in this chapter aimed to ascertain whether similar trends would be observed in the deeper tissues.

This chapter addresses research questions 1 and 3 through the following objectives:

RQ1: How does AFO design affect the physical conditions between the device and skin interface?

- Develop simplified forefoot models of healthy individuals, including an AFO and footwear to assess the pressure and strain conditions in the limb

RQ3: To what extent can computational models provide knowledge to inform the design of safe and effective lower limb orthoses?

- Investigate the effect of interface material on soft tissue, through comparison of a standard polypropylene AFO to a polypropylene AFO padded with a cushioning material,
- Investigate the effect of AFO fit on the soft tissue, through comparison of a standard flat AFO to an undersized AFO.

4.1 Methods

A finite element analysis (FEA) study was performed using MR data that had been previously collected by Cardiff University Brain Research Imaging Centre (CUBRIC, Dr Bethany Keenan), to develop image-based computational models.

4.1.1 Participants

The MR data utilised in this study had been collected previously during a study at Cardiff University, involving both healthy individuals and those with Haglund's deformity, which affects the rearfoot. The participants had no other foot conditions, or history of surgery or broken bones in the foot. As the models in the present study were localised to the forefoot rather than the rearfoot, all participants were considered to be healthy for these purposes. Forefoot models were developed for 5 individuals (1 male, 4 female; age range: 25-50 years, see Appendix G p.179 for more details), who will be referred to as N1-5.

Ethical approval was granted for the original study by Cardiff University School of Psychology Ethics Committee (EC.18.03.13.5264). Secondary data analysis ethical approval for this study was granted by the University of Southampton (ERGO ID: 48710).

4.1.2 MR Segmentation

The MR data had been previously collected with a Dual Echo Steady State (DESS) sequence in the sagittal plane (repetition time/echo time (TR/TE): 13.48ms/4.79ms, resolution: 0.6x0.6x0.6mm). This was carried out using a 3T scanner (Magnetom Prisma, Siemens, Erlangen, Germany) with a foot/ankle and four-channel flex coil with the plantar forefoot rested against a flat support. The data were segmented using ScanIP (Simpleware ScanIP N-2018.03-SP2 Build 55, Synopsys, Mountain View, USA). Masks were created for the skin, underlying soft tissue and bone using greyscale thresholds (Figure 4.1A). Where the scans included the proximal phalanges, these were fused to the metatarsals (Figure 4.1B). The skin, soft tissue and bone masks were then smoothed using a recursive gaussian filter. A 2mm thick sock was generated by dilating the skin mask in-

plane. This was repeated to form a 5mm shoe upper, and a 15mm sole was then added to represent a simplified training shoe (Figure 4.1C-E). The footwear model also featured one of the four AFO configurations (further described in Section 4.1.3).

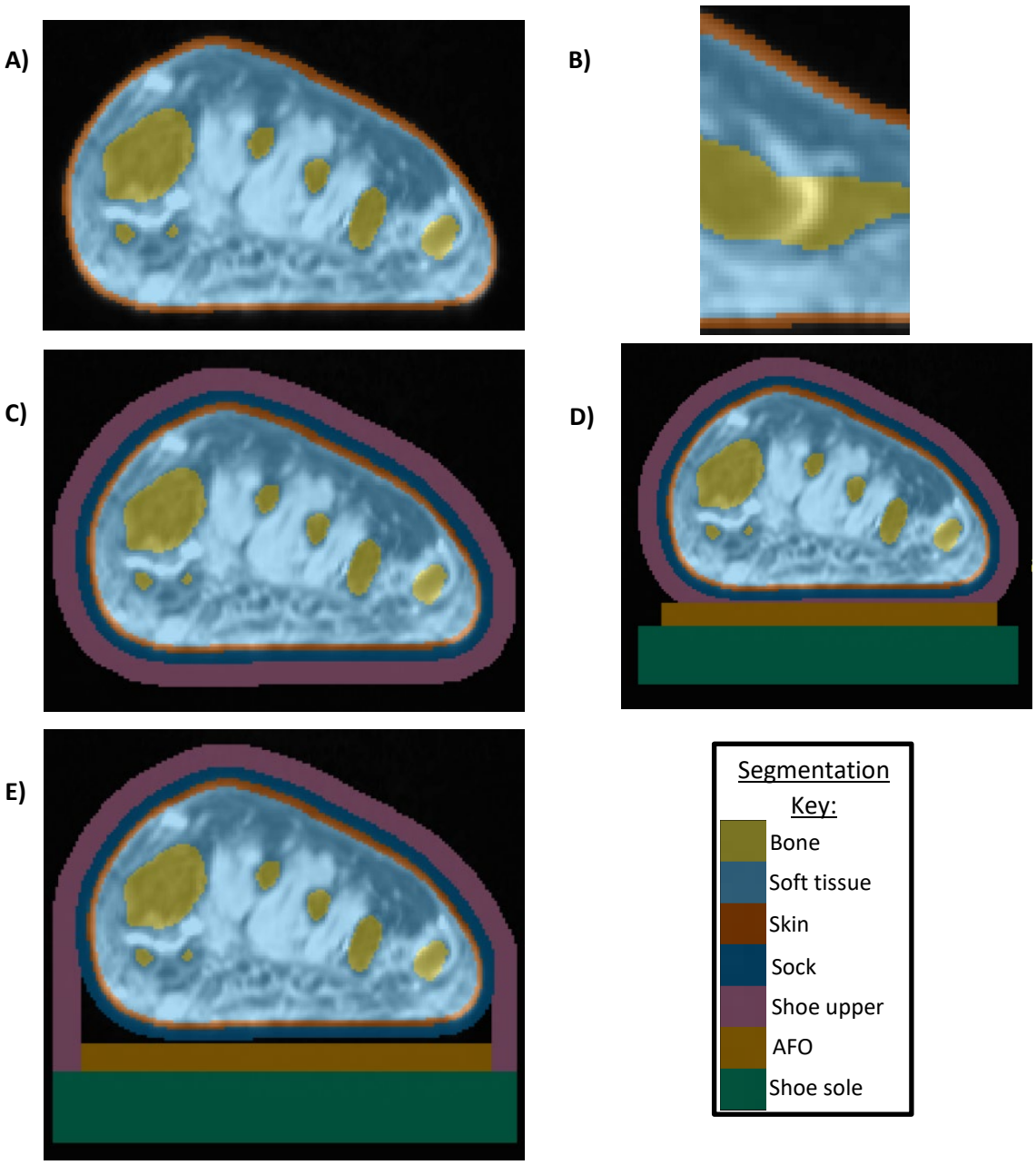

Figure 4.1: Segmentation process (exemplar images from N1), **A)** Segmentation of skin, underlying soft tissue, and bone using greyscale values; **B)** Fusion of metatarsophalangeal joints; **C)** Dilation of limb to create sock and shoe upper; **D)** Addition of shoe sole and AFO; **E)** Fully segmented forefoot, with shoe upper extended down to meet the sole and removed from inside shoe.

4.1.3 Finite Element (FE) Models

The segmented geometries for each participant were imported into COMSOL Multiphysics v.5.5 (COMSOL Inc., Stockholm, Sweden) for model development and FE analysis (Figure 4.2). Four models were generated for each participant, assessing different AFO configurations (Table 4.1. Figure 4.3).

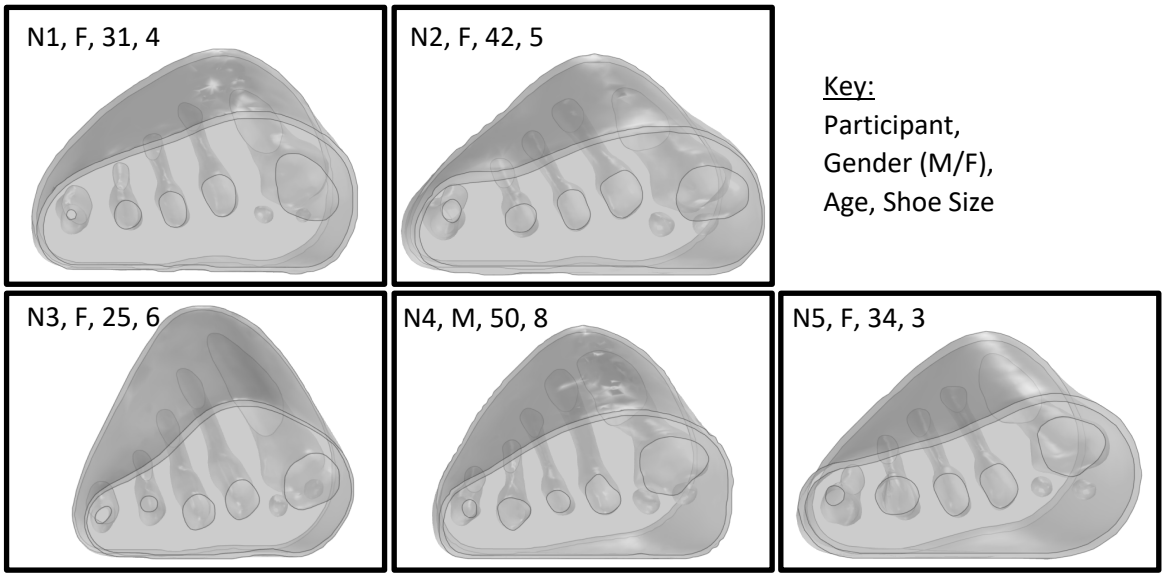

Figure 4.2: Modelled forefeet (skin, encapsulated bulk soft tissue, bones) of the participants, with gender and age indicated

Table 4.1: AFO configurations modelled for each participant

AFO Configuration	Description
Normal_PP	Flat AFO, 6mm polypropylene, spanning the full shoe width
Normal_C	Flat AFO, 4.5mm polypropylene + 1.5mm cushioning material (Poron), spanning the full shoe width
Undersize_PP	Flat AFO, 6mm polypropylene, undersized by 5% of full width on both sides of device
Undersize_C	Flat AFO, 4.5mm polypropylene + 1.5mm cushioning material (Poron), undersized by 5% of full width on both sides of device

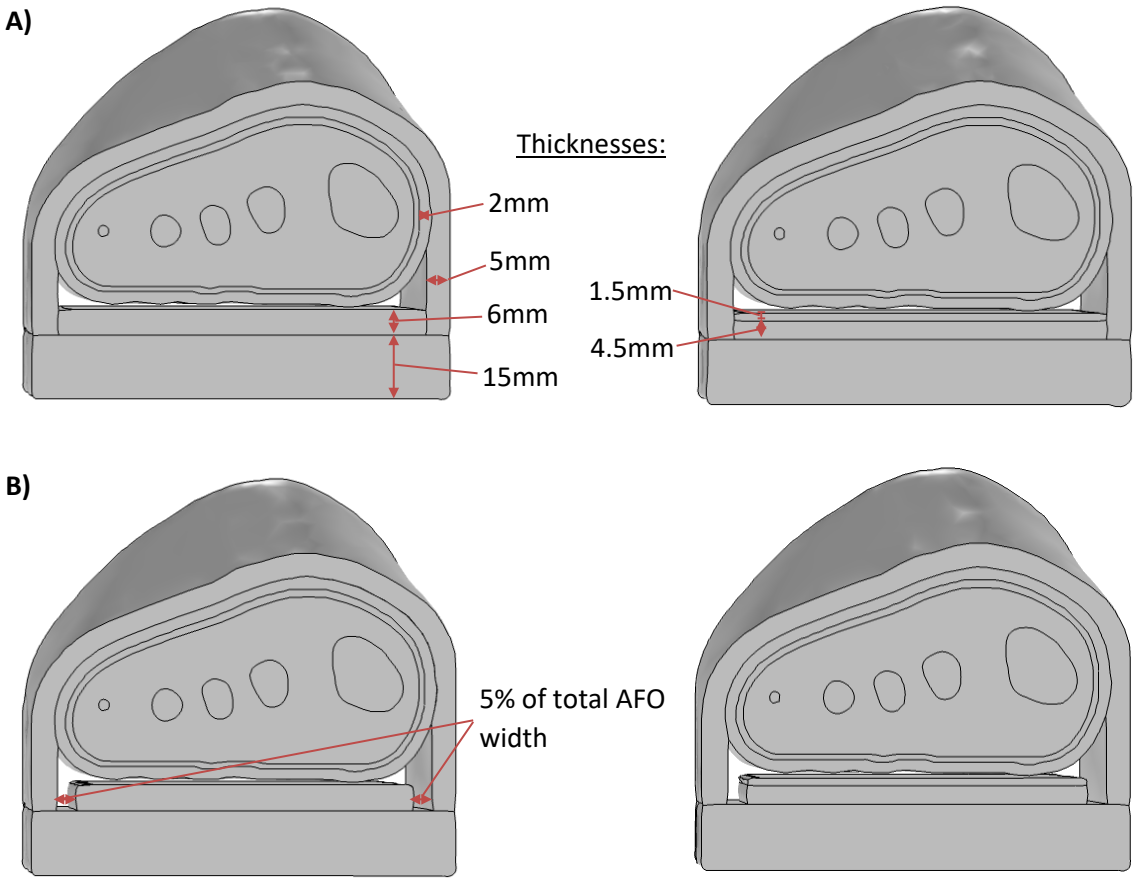

Figure 4.3: Example models (N1) developed for **A)** Normal_PP – 6mm polypropylene AFO (left) and Normal_C – 4.5mm polypropylene with 1.5mm cushioning (right); **B)** Undersize_PP – 6mm polypropylene AFO undersized by 5% (left) and Undersize_C – 4.5mm polypropylene with 1.5mm cushioning, undersized by 5% (right).

Each AFO configuration was flat and 6mm in total thickness – either 6mm of polypropylene, or 4.5mm of polypropylene with 1.5mm of Poron Cushioning for the models given a softer interface material. Poron is a polyurethane foam which may be used as a cushioning material with lower limb orthoses. The undersized AFO was created by removing 5% of the total width of the flat AFO from both sides of the device. This percentage was chosen based on measurements of the different sizes of ES AFO, which was an off-the-shelf polypropylene device used for the testing in Chapter 3. The 5% difference represented the worst-case undersized fit in the forefoot between the standard off-the-shelf sizes (see Appendix H, p.180).

Material properties of the shoe upper, AFO, sock and bone were assumed to be linear elastic (Table 4.2). The skin and soft tissue were modelled using a first order Ogden hyperelastic model for incompressible materials, using the following strain energy function W_s:

$$W_s = \frac{\mu}{\alpha}(\lambda_1{}^{\alpha} + \lambda_2{}^{\alpha} + \lambda_3{}^{\alpha} - 3) \quad \text{Eq4.1.}$$

The cushioning and shoe sole materials were modelled using Storakers model for highly compressible foam:

$$W_s = \frac{2\mu}{\alpha^2}(\lambda_1{}^{\alpha} + \lambda_2{}^{\alpha} + \lambda_3{}^{\alpha} - 3 + \frac{1}{\beta}(J_{el}{}^{-\alpha\beta} - 1)) \quad \text{Eq4.2.}$$

For both equations, μ represents the shear modulus, α the deviatoric exponent, β the volumetric exponent, J_{el} the elastic volume ratio, and λ_i the principal stretches in each direction.

Table 4.2: Material properties for linear elastic shoe sides, AFO, sock, bone and hyperelastic soft tissue, cushioning material, shoe sole

	Elastic	**Elastic**	**Hyper-elastic**	**Hyper-elastic**	**Hyper-elastic**	
Material	**Young's Modulus (MPa)**	**Poisson's Ratio**	**μ (kPa)**	**α**	**β**	**References**
Shoe upper	8.5	0.061	-	-	-	[219]
AFO	1030	0.43	-	-	-	[155]
Sock (cotton)	1.8	0.4	-	-	-	[220, 221]
Bone	7300	0.3	-	-	-	[161]
Skin	-	-	452	5.6	-	[188]
Soft Tissue (exc. skin)	-	-	36	4.5	-	[188]
Cushioning (Poron)	-	-	144	4.013	0.057	[195]
Shoe sole	-	-	1588	7.708	0.292	[195]

A fixed constraint was applied to all bone domains except the sesamoids, which were allowed to move as they are able to with the flexor hallucis brevis, in which they are embedded. The cut boundaries of the modelled foot section were assigned a fixed displacement perpendicular to the cutting plane (Figure 4.4). A friction model was applied to boundaries, between the sock and shoe upper with a static coefficient of friction (CoF) of 0.55, between the sock and purely polypropylene AFO, with a static CoF of 0.22, and a CoF of 0.55 between the sock and cushioning interface material in the relevant model configurations [198]. The orthosis, shoe sole and upper were bonded together, as were the bones, soft tissue and skin.

Vertical and medial components of the ground reaction force (GRF) were applied to the external boundary of the shoe sole in contact with the ground, to represent midstance of gait. The medial force was 5% of the participant's body weight [222]. The vertical force was also scaled, using the participant weight and comparative length of forefoot section:

$$GRF_{vertical}\ (N) = Participant\ Weight\ (kg)\ \times 9.81\ \times \frac{Forefoot\ section\ length}{Full\ foot\ length} \times 1.4 \quad \text{Eq4.3.}$$

The multiplier of 1.4 represented the relative load distributed to the forefoot during midstance compared with the rest of the foot. This single load value was adjusted across the forefoot's width, using multipliers of 1.05, 1.26, 1.06, 0.88 and 0.75 for the load under the first to fifth metatarsal heads, respectively (Figure 4.4). These distributions were determined using gait pressure data of healthy individuals, collected with F-scan in-shoe sensors (Tekscan, Massachusetts, USA) (see Appendix I, p.182 for more details).

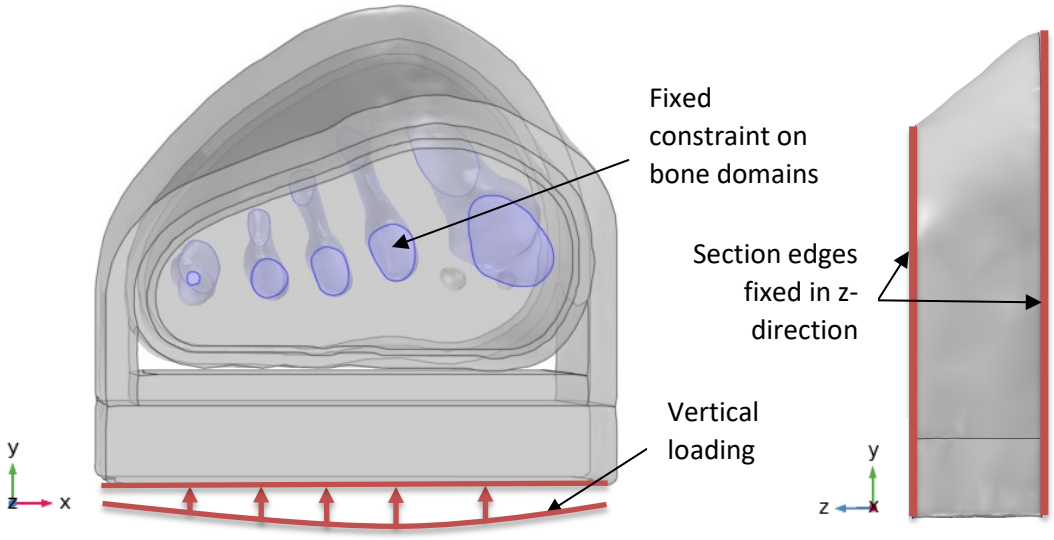

Figure 4.4: N1 model, indicating vertical loading and boundary conditions

A 2nd order tetrahedral mesh was used with local refinement in the thin skin and sock domains, and at the cushioning material/sock boundary where relevant (Table 4.3. Figure 4.5). Mesh convergence was assessed using N1 models. For the mesh used, results deviated from those obtained with the finest mesh by less than 3% for the 99thth% percentile shear strain, and by less than 6% for the 99thth% percentile pressure. Similarly, a sensitivity analysis was performed to ensure that the proximity of the forefoot section's cut edges to the region of interest would not affect the model results (Appendix J, p.184).

Table 4.3: Mesh input parameters. Note that region 3 was only relevant to the models with a cushioning material at the limb/AFO interface.

Mesh Input Parameter	Region 1: Sock, skin	Region 2: Soft tissue and bone	Region 3: Cushioning upper boundary	Region 4: AFO (inc. cushioning) and shoe sides	Region 5: Shoe sole
Maximum element size (mm)	1.51	3.6	0.9	5	5.5
Smallest element size allowed (mm)	1.51 – 1.51/3	3.6 – 3.6/3	0.9 – 0.9/3	5 – 5/3	5.5 – 5.5/3
Maximum element growth rate	1.3	1.3	1.3	1.3	1.3
Curvature factor	0.3	0.3	0.3	0.3	0.9
Resolution of narrow regions	1.2	1.2	1.2	1.2	0.4

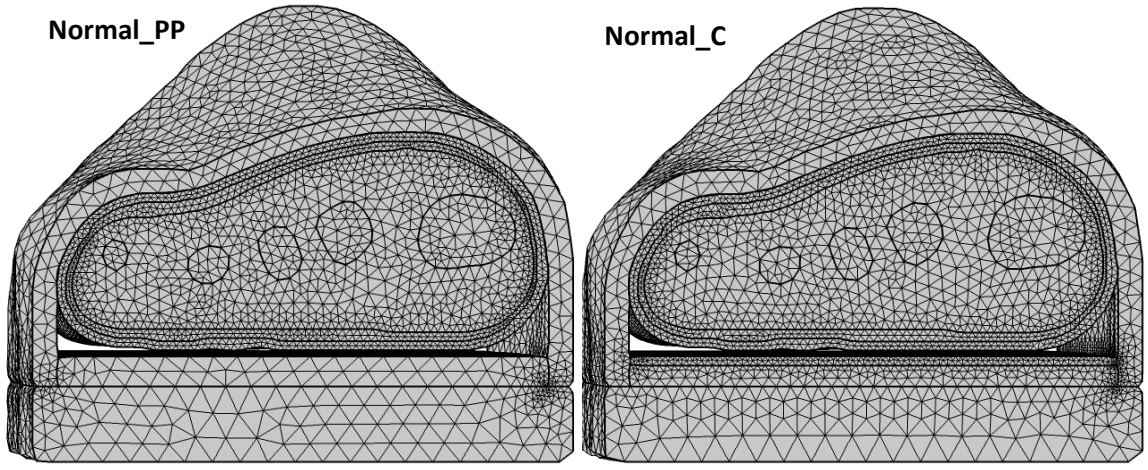

Figure 4.5: Exemplar meshes from N2 Normal_PP and Normal_C models

4.1.4 Data Analysis

Four parameters were used to provide indications of tissue damage risk, that had been used previously in literature [77, 223, 224]. Data from the models were processed in MATLAB to calculate the following:

1. 99^{th} percentile shear strain (calculated from Green-Lagrange strain tensor) in the soft tissues,
2. volume of tissue above 10% shear strain,
3. 99^{th} percentile plantar pressure,
4. maximum plantar pressure gradient.

These parameters were chosen to show the orthoses' effect on both the superficial (interface pressures) and deeper soft tissues (soft tissue strains), and to assess the potential relationship between pressure gradients and shear strains (see Section 2.3.4). As was discussed in the literature review, assessing the volume of soft tissue above a threshold strain can indicate how much tissue may be at higher risk of tissue damage.

The percentile calculations were based on soft tissue volume for shear strain and orthosis/limb interface area for plantar pressure. 99th% values were used rather than maxima so that outliers due to highly localised peaks were excluded, facilitating the model comparisons. The percentile value (99th) was chosen based on examination of the relevant histograms, so that the majority of the pressure or strain was included. For the pressure gradient calculations, the plantar pressure data was resampled to a 5x5mm resolution to reflect experimental F-scan sensor measurements. The pressure results along the cut edges of the forefoot sections were omitted from this resampling process as they were affected by the boundary conditions. The maximum pressure gradient was then found by calculating the pressure difference between each point and its neighbours, divided by the distance between points.

As the samples size was limited, statistical analyses could not be performed. Instead, the median and interquartile ranges (IQR) were compared between the different AFO configurations. Trends were also examined on an individual level across each participant.

4.2 Results

The median and IQR 99th% shear strain, volume of tissue over 10% strain, 99th% plantar pressure and maximum pressure gradient predictions for the five participants are presented for each of the four AFO configurations (Table 4.4). The model predictions for each of the five participants individually are also displayed (Figure 4.6).

The 99th% plantar pressure and maximum pressure gradient predictions followed similar trends, with the cushioned AFO producing lower results than the purely polypropylene AFO in all five participants. The reductions ranged from 49.5 to 83.9kPa (29.6 to 49.4%) and 5.5 to 14.4kPa/mm (27.6 to 54.6%) (Figure 4.6). There was comparatively little difference and no clear trends in the pressure metrics between the undersized and full-width AFOs, with differences ranging from -2.8 to 12.8kPa (-1.8 to 8.1%) and -6.3 to 2.7kPa/mm (-24.1 to 18.8%).

Table 4.4: Median (IQR) for the model predictions for each AFO configuration. Normal_X = full-width AFO; Undersize_X = AFO undersized at both edges; X_PP = polypropylene AFO; X_C = polypropylene AFO with cushioning layer

AFO Configuration	99th% shear strain in soft tissues, %	Volume of tissue of 10% shear strain, mm3	99th% plantar pressure, kPa	Max. plantar pressure gradient, kPa/mm
Normal_PP	18.5 (14.1 - 19.5)	6750 (2876 - 8275)	158.5 (157.3 - 161.6)	26.2 (25.9 - 26.4)
Normal_C	17.7 (13.7 - 19.5)	5221 (2675 - 7407)	105.1 (95.4 - 106.7)	12.8 (12.3 - 14.4)
Undersize_PP	19.3 (15.1 - 20.1)	7149 (3458 - 8765)	159.1 (158.8 - 170.1)	25.3 (25.1 - 25.3)
Undersize_C	18.8 (14.7 - 19.8)	5998 (2964 - 7623)	104.4 (97.7 - 107.5)	12.8 (12.6 - 14.4)

There was also minimal difference in the 99th% shear strain predictions, with differences ranging from -0.81 to 0.55% strain (-4.4 to 4.3%) comparing the cushioned to polypropylene AFOs and 0.24 to 1.12% strain (1.5 to 7.7%) comparing the undersized to full-width AFOs. However, though the magnitudes of the differences were minimal, there were trends present. 4/5 participants showed reduced strains with the cushioned AFOs and 5/5 participants showed higher strains with the undersized AFOs (Figure 4.6). These same trends were present in the results for volume of soft tissue over 10% shear strain, where the differences between AFO configurations were more noticeable in magnitude. Similarly to the pressure metrics, the differences in volume between the cushioned and polypropylene AFOs (-2386 to 101mm^3) were generally greater in magnitude than the differences between the undersized and full-width AFOs (134 to 1218mm^3). The exception to this was participant N2, who was the only participant who did not show reduced strains with the cushioned AFO.

The spatial distributions of shear strain and plantar pressures were similar between participants. The shear strains were elevated in the soft tissue surrounding the bones, particularly around the first metatarsal head and sesamoid bones (Figure 4.7). The plantar pressures were generally highest in the medial forefoot, under the first and/or second metatarsal heads (Figure 4.8). There were limited noticeable differences in shear strain distribution between AFO configurations, but the presence of the cushioning material noticeably affected the pressure distributions. For the models with polypropylene directly in contact with the limb (Figure 4.8A&C), the plantar pressures were affected considerably by the surface topography of the limb causing pressure gradients. Adding a cushioning layer to the interface increased the contact area between the limb and device, resulting in a more even pressure distribution (Figure 4.8B&D).

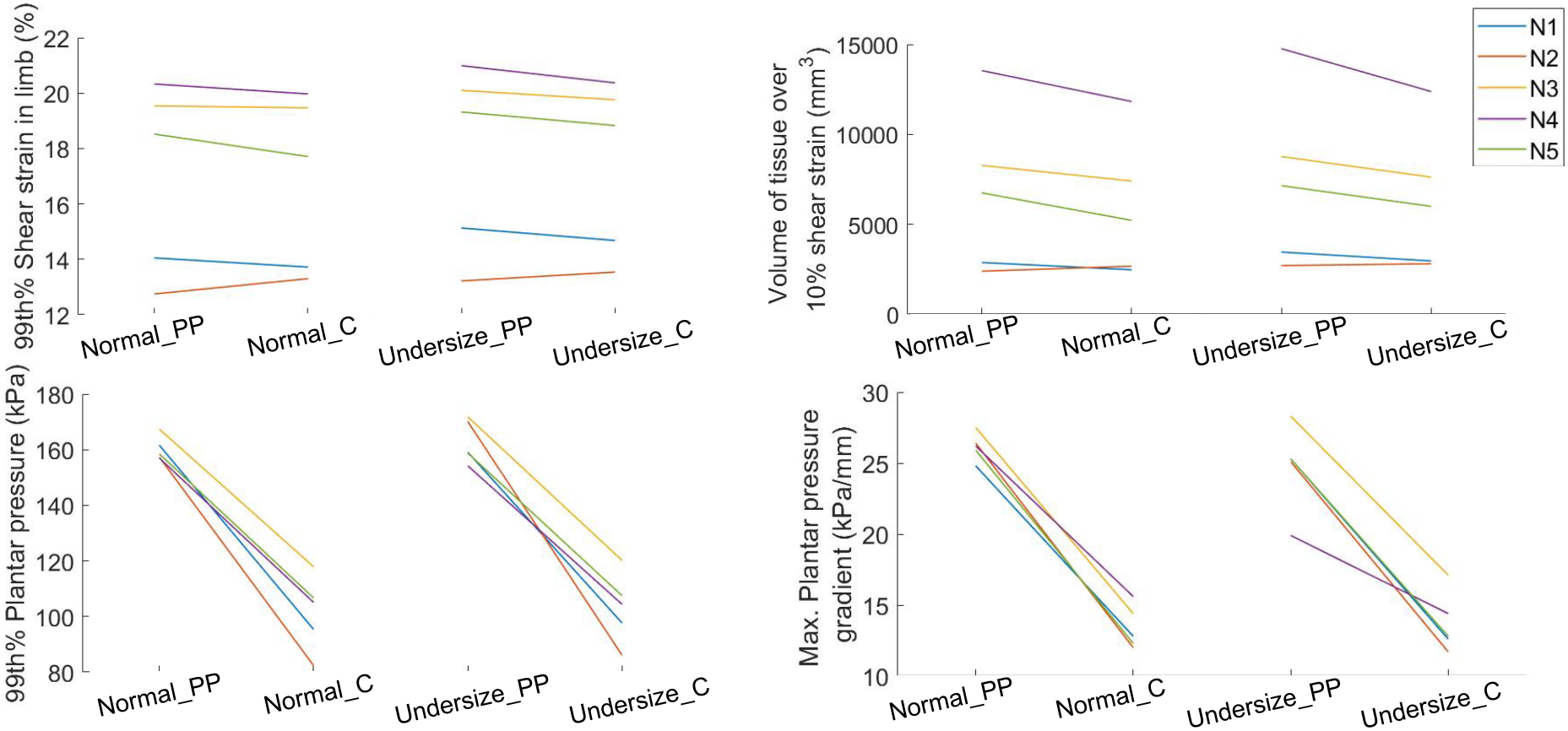

Figure 4.6: Strain and pressure model predictions for each participant across the four AFO configurations. Normal_X = full-width AFO; Undersize_X = AFO undersized at both edges; X_PP = polypropylene AFO; X_C = polypropylene AFO with cushioning layer.

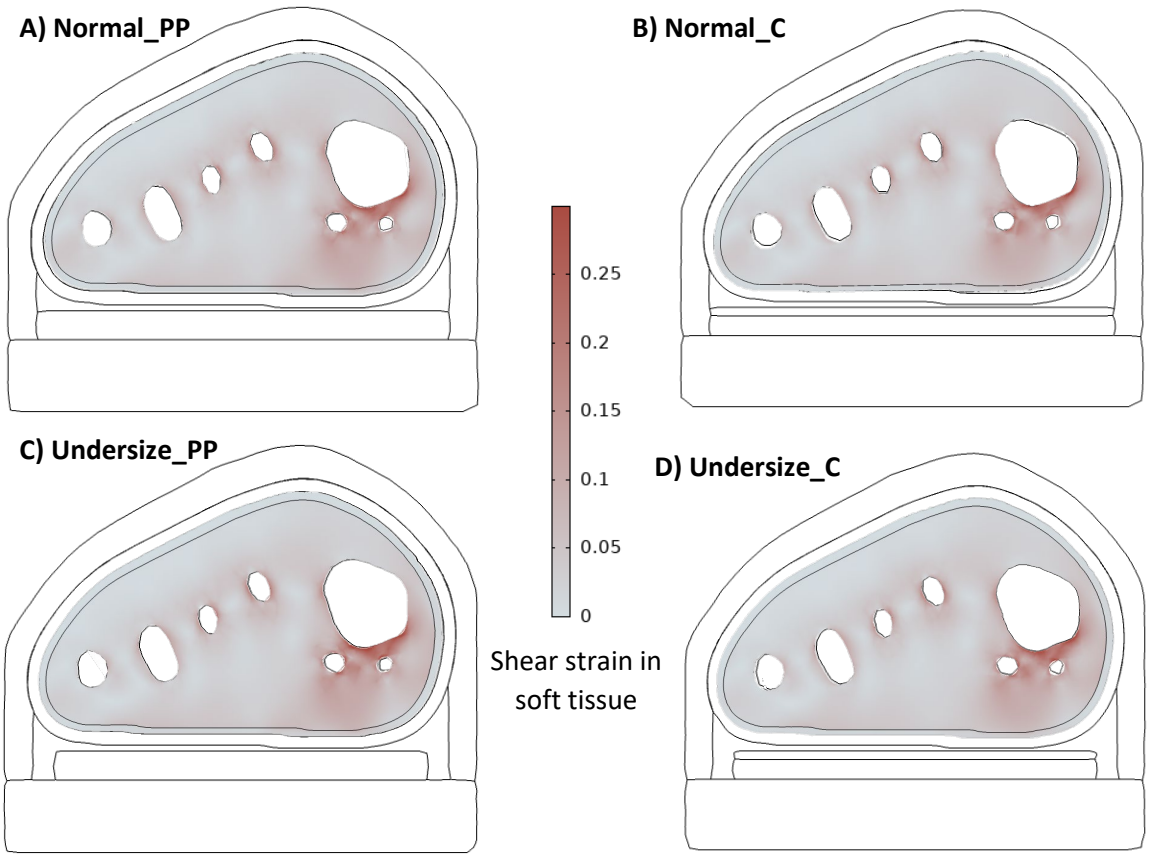

Figure 4.7: Example shear strain distributions (N1 models) of a cross-section through the sesamoid bones for **A)** Normal_PP; **B)** Normal_C; **C)** Undersize_PP; **D)** Undersize_C

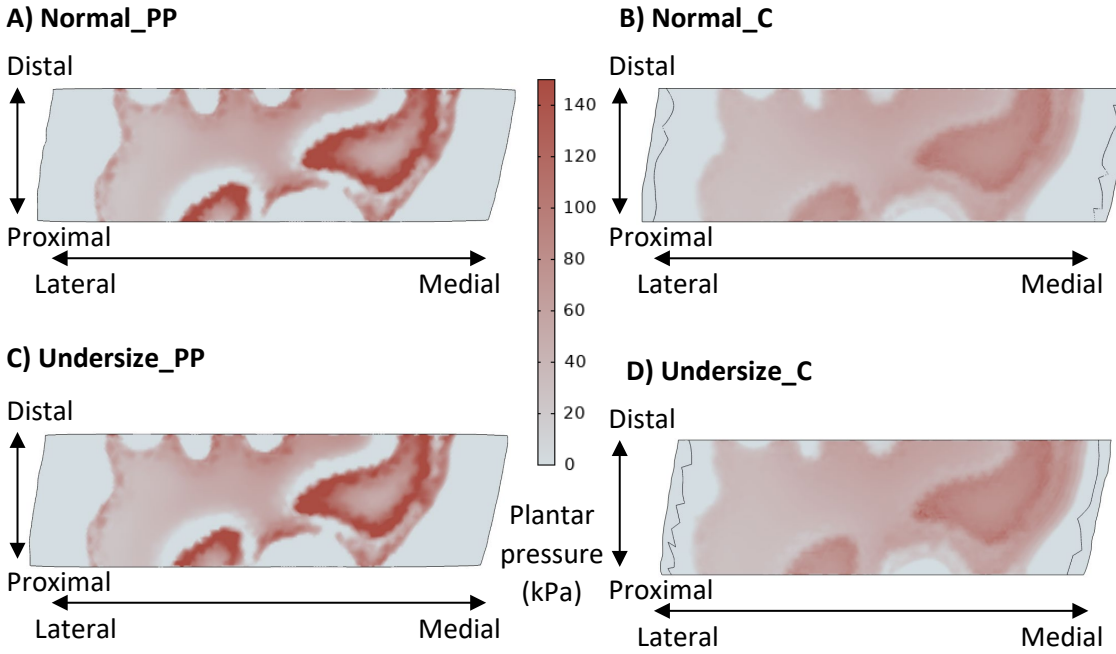

Figure 4.8: Example plantar pressure distributions (N1 models) for **A)** Normal_PP; **B)** Normal_C; **C)** Undersize_PP; **D)** Undersize_C

4.3 Discussion

This study aimed to investigate how AFO fit and interface material affected the soft tissues of the forefoot, and the subsequent risk of tissue damage across five healthy participants. The undersized AFO caused higher soft tissue shear strain than a full-width AFO for all participants, though the differences were minimal, and there were no discernible differences between the pressure or pressure gradient results. Applying a layer of cushioning material to the polypropylene AFO led to clear reductions in plantar pressures and pressure gradients. The cushioning also tended to reduce the shear strain in the tissue but again the differences were small, particularly for the 99th% shear strain. Inter-participant variability in the strain predictions was far greater than the differences present between any of the AFO configurations. This was not the case for the pressure and pressure gradient predictions, particularly comparing the variability to the differences between the AFOs with and without cushioning (Figure 4.6).

The study provides novel predictions of the deep tissue responses to wearing an AFO, and the models can be corroborated through comparison of the interface condition predictions to values obtained experimentally. The 99th% plantar pressures in this study ranged from 154-172kPa with the polypropylene AFO and 82-120kPa with an added cushioning layer. These ranges can be compared to midstance pressures from the experimental testing of AFOs detailed in Chapter 3 to assess validity of the models. The full midstance pressure and pressure gradient results from the experimental testing are detailed in Appendix K (p.186). The ES AFO that was tested in Chapter 3 was a polypropylene AFO similar in design to the AFOs modelled here without cushioning. The midstance peak plantar pressures in the forefoot ranged from 65-216kPa (median: 122kPa) across the five participants and two gait conditions with the ES AFO. With the Push AFO, which featured a layer of soft conforming material at the limb interface, the peak midstance pressures ranged from 78-121kPa (median: 105kPa) experimentally. Thus, the models followed similar trends to the experimental testing in that the presence of a softer cushioning layer at the limb-orthosis interface tended to reduce the plantar pressures. The magnitudes of the plantar pressures between the models and experimental data were also similar, though the variability between participants was greater in the experimental testing. In particular, the minimum value for the polypropylene AFO without cushioning (ES AFO) was much lower during experimental testing than the modelling equivalent. This may have been due to the simplifications made to the models. However, it should also be noted that the healthy volunteers in Chapter 3 were not the same healthy volunteers who were modelled in this chapter, and so differences could be due to differences in the participants involved in each study and the limited sample sizes.

The pressure gradient predictions from the models were also compared to the results of the experimental testing. The model pressure gradients ranged from 19.9-28.3kPa/mm with the polypropylene AFO, and 11.7-17.1kPa/mm with the added cushioning layer. Experimentally, the maximum pressure gradients during midstance with the polypropylene AFO (ES AFO) ranged from 7.1-65.1kPa/mm (median: 17.8kPa/mm) and for the cushioned AFO (Push AFO) ranged from 9.2-23.1kPa/mm (median: 16.9kPa/mm). As with the pressure comparisons, the ranges of pressure gradient measured experimentally were wider than for the model predictions but the magnitudes and trends were similar. Though direct pressure and pressure gradient comparisons could not be made due to the different participants, the similarities between the model predictions and experimental pressure and pressure gradient results provide an indication that the model results are indeed valid.

There is little previous literature that the present model predictions can be compared to. Only one previous experimental study was identified which tested the plantar pressures during gait with a relevant AFO device (see Section 2.3.5.3). Nowak et al. [146] utilised the F-scan system to measure pressures during gait throughout the AFO-limb interface in four healthy individuals. Though the material of the AFOs tested was not specified, they were custom moulded and as such it is likely the devices were made from polypropylene or a similar material which are commonly used [225]. They reported peak plantar pressures in the forefoot of 158.5±50kPa during midstance, occurring on the medial side of the foot. This lends further credibility to the model predictions presented here, which had a very similar median and locations of peak pressures.

There are also very few previous modelling studies for comparison, which have assessed how the limb is affected by an AFO, as noted in Section 2.3.2. Jamshidi et al. [157] developed a full foot model for an individual with drop foot, and varied the thickness and composition of an insole within an AFO. However, they only reported the von Mises stress in the foot, which was not examined in the present study as it was not considered appropriate for assessing soft tissues. Von Mises stress is a scalar value typically used as a failure criterion, which prevents the different stress components from being assessed. Their reported von Mises stresses at the plantar surface of the forefoot ranged from around 150-190kPa for the different orthosis configurations. While slightly higher than the plantar pressures with the equivalent AFO with cushioning layer in the present study, this could be explained by the difference in loading conditions. The loads applied in this study represented gait midstance, whereas Jamshidi et al. dynamically modelled the full gait cycle including toe-off which would likely result in higher forefoot pressures. The only other relevant previous study was carried out by Jena et al. [165], and examined a 10mm thick polypropylene orthosis insert (see Figure 2.6). Similarly to Jamshidi et al., only a single individual was modelled. They reported maximum plantar pressures with the orthosis of 320kPa and

maximum strains of 44.8%. As these were maximum values rather than percentile values, it is not surprising that they are higher than the predictions from the present study, where the 99th% shear strain in the soft tissues ranged from 12.8-21.0%. The discrepancies may also have been due to the fact that the maximum values Jena et al. reported appear to have occurred in the rearfoot rather than the forefoot. While the exact strain values in the forefoot were unclear from their plot, the plantar pressure distribution in the forefoot appeared to be much more in line with the results of the present study at around 100-200kPa.

Having established that the model predictions were within the expected ranges measured experimentally and in the literature, the effects of the AFO design parameters can be examined. When comparing AFO fit, the undersized AFO consistently caused higher shear strains and volume of soft tissue over 10% strain than the full-width device. However, the differences themselves were small, particularly for the 99th% strain where the differences were all less than 1.2% strain. The effect of device fit on the plantar pressure and pressure gradients was less clear. The undersized devices resulted in higher pressures in 3 to 4/5 participants, depending on the configuration, and higher pressure gradients in 2/5 participants compared to the full-width equivalents. Interface material, on the other hand, had considerable effect on the pressures and pressure gradients, with an added cushioning layer consistently reducing pressures (differences of 50-84kPa) and pressure gradients (differences of 5.5-14.4kPa). The shear strain variables also tended to decrease with the added cushioning (4/5 participants), but the differences were still small as a proportion of the shear strain magnitude (<0.9%). As such, while there were trends present in the shear strain results between the design parameters assessed, the difference may not be clinically relevant. However, this may only be applicable to the forefoot and specific AFO designs modelled here, particularly in the case of AFO fit. This has been discussed further later, and could also apply to the limited difference in pressure predictions between AFO fit.

If only considering the pressure metrics, the results of this study would suggest that interface material may be more important than device fit to protect the soft tissues. Indeed, the experimental results in Chapter 3 (see Section 3.2.1) also showed the importance of interface material in reducing plantar pressure metrics. However, though this may be the case for protecting the superficial tissues, the risk of damage to the deeper tissues – indicated by the shear strain results – did not appear to be altered by either design parameter. Given that the tissue strains were highest in the deeper tissues surrounding the bone, these deeper tissues may be more vulnerable than the superficial region. This may be particularly problematic as the presence and severity of deep tissue injuries (DTIs) are harder to determine clinically than superficial damage (see Section 2.1). Although lower strains may cause tissue damage if sustained, the higher strains in the deep tissues could cause damage in a much shorter period

[108]. Thus, if tailoring AFO design to better protect at risk deeper tissues, plantar pressures may not be as useful a metric to assess the designs by. Previous research in pressure injury prevention has also established the benefits of assessing strains in the deeper soft tissues rather than only considering interface pressures [147].

The high variability in shear strain predictions between participants is also a key takeaway of this study, particularly as inter-participant variability led to a greater effect than the differences between AFO design parameters. This high variability was likely due to the differing morphology and magnitudes of the applied loads between participants. This has implications for future modelling studies, particularly if assessing orthosis designs by comparisons to threshold values to assess tissue damage risk. While there have been previous modelling studies that have assessed lower limb orthosis design, whether AFOs or other devices, most have only modelled a single individual (see Section 2.3). If only assessing one individual, care must be taken when drawing conclusions about the tissue damage risk of different device designs, as there is insufficient information to distinguish the effect of the device design parameters from the individual's morphology. For example, if an individual who produces low model predictions is modelled (e.g. N2 in the present study), designs may appear universally safer for the soft tissues than if the individual produces high model predictions (e.g. N4). Thus, the importance of modelling multiple participants in studies of this nature is clear, to show a fuller picture of how soft tissues can be affected by device design. In a clinical context, this high variability may indicate a need for bespoke devices for people at higher risk of tissue damage, who may have differing requirements than those at lower risk.

In the present study, AFO fit did not seem to have much effect on the model predictions. This would provide justification for the standard size ranges used for off-the-shelf devices, through the assumption that fit is unlikely to affect tissue damage risk. However, while that may be true for the specific scenario modelled here, it may not translate to how the AFO interacts with the rest of the foot, for example. It was thought that an undersized AFO would lead to elevated strains due to the device edges interacting with the soft tissues. However, for the loads applied during the modelling, the undersized AFO edges did not contact the limb for any of the five participants (see Figure 4.8C&D for N1 example). It should also be noted that with the polypropylene AFO models (Undersize_PP), the plantar contact areas were lower than with the cushioned AFOs (Undersize_C) and so also further from the AFO edges. The lack of interaction between the AFO edges and the limb may have been because loads representative of midstance were used, rather than the maximum forefoot loads that would occur during gait at toe-off. Thus, the loads may not have been high enough to displace the AFO into the foot to cause contact at the edges, particularly as the load was applied as a parabola which decreased towards the edges of the foot.

Additionally, the modelled scenario was idealised in that the undersized AFO was positioned centrally within the shoe, rather than skewing to one side which would create a larger discrepancy in width on the other. These results may also have been affected by the use of a generic load distribution across the forefoot, which peaked under the 2nd metatarsal head. In reality, the load distribution varies between individuals which could result in increased interactions with the AFO edge than were seen here, depending on where the load is distributed to more heavily. Indeed, even between the five healthy participants from Chapter 3 whose gait was assessed to calculate the generic forefoot load distribution, the distributions varied considerably (see Appendix I, pg. 182). Thus, an undersized AFO may still present issues in the forefoot if the device were positioned differently or the user walked with a different gait pattern than was represented here. Furthermore, to fully assess how AFO-limb interactions would vary between people, personalised load distributions would need to be applied to the models. This was not possible for this study as the imaging data had been obtained previously, and no gait data was available for the modelled participants.

There are some limitations to the study that should be acknowledged. As the MR dataset contained individuals with Haglund's deformity in the heel, only the forefoot region could be modelled to represent non-pathological anatomy. While the metatarsal heads are a vulnerable region, which can experience tissue damage with AFO use, there are other vulnerable regions which need to be considered to fully evaluate different AFO designs. In particular, the navicular head and the malleoli regions are also at considerable risk of damage due to the bony prominences [27, 55]. Rearfoot section models developed using similar methods to the present study, with the required adjustments to loading and boundary conditions, would be useful for assessing the same design parameters. Additionally, in modelling the forefoot region alone, the AFO only directly contacted the plantar region of the foot, as is usually the case with the devices. In other foot regions, the AFO would be much more encompassing of the limb. Thus, the relationships observed between the AFO fit and interface material in the forefoot region, or lack thereof, may not apply elsewhere in the foot. For example, where an undersized AFO is more encompassing, it could lead to an increased press-fit of the device on the limb, increasing the pressures applied. This would be a particular issue near bony prominences, such as the malleoli or navicular head, if the device design did not allow for off-loading in those regions. Similarly, the addition of a cushioning interface material, which had little impact on tissue strains in this study, may have more effect at those bony prominences where there is no plantar fat pad between the AFO and bone to provide protection [27, 146].

The models utilised simplified foot anatomy including combining the soft tissue underlying the skin to one bulk group, fusion of the MTP joints, and fixation of the metatarsal bones. These

simplifications may have affected the results obtained from the models. However, the simplified anatomy was deemed appropriate for this study, as the purpose was comparison between models built using the same methods, rather than determination of absolute values. One model simplification that could be improved upon was that the same material properties of the soft tissue were assigned for each individual. In actuality, the material properties would vary depending on whether the tissues are affected by pathologies such as muscular dystrophy or multiple sclerosis, or different muscle to fat ratios of the underlying soft tissues. Previous sensitivity analyses of soft tissue material properties in foot modelling have shown that pressures and stresses can be affected considerably by the stiffness of the soft tissues [226, 227]. This was partially accounted for by the inclusion of a skin layer which is much stiffer than the underlying tissue, particularly in the plantar region. However, to accurately assess tissue damage risk with device design, an individual's tissue vulnerability would need to be accounted for through subject-specific soft tissue properties.

In general, future modelling of individuals who would wear AFOs, with pathological changes to foot tissues, would be required to assess device designs to build on this work with healthy individuals. It is possible that different results would emerge, particularly when it comes to the modelling of people with deformities, particular tissue vulnerabilities, or affected gait and so load distributions. Additionally, an important consideration for device design is that AFOs are used for corrective purposes and so often need to apply a certain level of pressure to the limb. While design device may be tailored to reduce tissue damage risk through the reduction of pressures or strains, this must be balanced with retaining the device functionality. Finally, as only a limited number of individuals were assessed in this study, firm conclusions about the effects of the two AFO design parameters cannot be drawn. To confirm the results from the study and the trends observed, further modelling would be required with a larger sample size and individuals with pathological changes to foot tissues. Despite this, as there is such limited previous research in this area, these findings add to the current state of knowledge in the field and could help inform future research.

4.4 Summary

There have been very few previous computational modelling studies assessing how an AFO may affect soft tissues. Of those, none have modelled more than one individual or have included the shoe in the assessment. This study considered orthosis design variables across five individuals and assessed both superficial and deep tissue loading conditions, and thus presents a novel approach to considering tissue health with AFO use. In this study, simplified forefoot models were used to assess the impact of AFO interface material and fit on metrics indicative of tissue health (research

question 1). The addition of a softer cushioning interface material reduced the plantar pressures and pressure gradients considerably but had little impact on the strain metrics. An undersized AFO caused minimal difference in plantar pressures or shear strain in the soft tissues compared to a full-width AFO, though the strains were consistently slightly higher for the undersized AFO.

Whether computational models could provide knowledge to inform device design (research question 3) was also addressed in this study, through the consideration of how effective these simplified models were at assessing AFO design parameters. While the present models could aid in device design, it is also clear from the results that modelling other vulnerable foot regions would be required to fully assess AFO design. Nonetheless, the results have highlighted key points of consideration for future device assessment:

- Firstly, the models indicated that even in healthy individuals the inter-participant variation in results may be high, particularly in the shear strain predictions, due to differing participant morphology and magnitude of applied load. Thus, it cannot be assumed that findings obtained from one individual would be relevant to others.
- Secondly, trends suggested that interface pressure metrics may not be indicative of the loading occurring in the deeper tissues, observed through the shear strain metrics.

Further research of different scenarios and with a larger, more clinically relevant sample would be required to ascertain whether the discrepancies between pressure and strain metrics are more generally applicable.

Chapter 5 Evaluation of the Effects of Rheumatoid Arthritis on the Forefoot through Computational Modelling and Clinical Assessment

As discussed in Section 1.2.2, foot orthoses (FOs) are commonly prescribed to those with rheumatoid arthritis (RA) to reduce pain and disability by off-loading regions of the foot. The condition can particularly affect the forefoot, with the metatarsophalangeal (MTP) joints and plantar fat pad being displaced. It can also result in bursa-like lesions forming between metatarsals or in the plantar region of the forefoot. A previous study at the University of Southampton (FeeTURA) assessed various aspects of RA, including presence of bursae and their relation to plantar pressures, through ultrasound and MR imaging data [21, 33]. Clinical data was also collected from the participants, including assessments such as the Leeds Foot Impact Scale which is split into two subsections for impairment and footwear (LFIS-IF) and activity participation (LFIS-AP). The more relevant of the two for this study is the LFIS-IF score as it covers pain experienced and as such may impact FO use.

This research has built upon the FeeTURA study to determine whether computational models developed from the MR data can predict the pain and soft tissue vulnerability experienced by the individuals with RA. The use of computational modelling provides benefits over previous experimental assessment of FOs for RA cohorts, in the easy examination of the internal effects of loading, something which has not been assessed before. Additional novelty stems from the assessment of FO effectiveness across a group of individuals with RA (see Chapter 6), rather than a single healthy individual as previous modelling studies have done. By developing models that predict regions of tissue vulnerability, and verifying whether this aligns with clinical data such as body mass index (BMI), LFIS-IF and presence of bursae, FOs could be designed that target off-loading of specific foot regions to provide personalised orthotic solutions. As the region of interest, the forefoot, was the same as for the previous chapter assessing AFO design, similar methods were used to develop the computational models used in this chapter which have a similar purpose regarding FOs.

This chapter addresses research question 2 through the following objectives:

RQ 2: To what extent can computational models of individuals with morphological changes in the forefoot distinguish between different aspects of RA disease?

1. Develop and run computational forefoot models for a selection of individuals with RA of varying severity and a healthy control,
2. Measure key morphological features that could affect comfort and tissue damage risk,
3. Compare the previously collected clinical data and morphological measurements with the model outputs indicative of tissue damage risk:
    a. For the individuals with RA *vs*. a healthy control,
    b. Between the individuals with RA and to assess which clinical or morphological factors have the most impact on tissue damage risk.

The work in this chapter has been published in Frontiers in Bioengineering and Biotechnology: *"Predicting Forefoot-Orthosis Interactions in Rheumatoid Arthritis using Computational Modelling"* [2].

5.1 Methods

This study involved secondary analysis of patient imaging and clinical outcome data sets from established studies (FeeTURA) [21] by image-based computational modelling.

5.1.1 Participants

MR and questionnaire data were obtained, which had been collected from participants with RA during FeeTURA [21], including assessments of condition severity through subjective means such as the Leeds Foot Impact Scale. The scale consists of two subsections: the impairment/footwear section (LFIS-IF) includes pain and footwear choices, while the second section covers activity limitation and participation restriction (LFIS-AP) [228]. Instances of bursae between and beneath the MTP joints were also recorded, along with joint erosion and synovial hypertrophy. Detailed methodology for how these parameters were determined was published previously by Cherry et al. [21]. Of the original 30 participants for whom MR data were available, 13 (aged 29-73, all female) were selected for the present study, purposively sampled to represent a range of LFIS-IF scores. These participants will henceforth be referred to as RA1-13. The purpose of this study was to assess the performance of the models across a range of condition presentations. As such, the selection of participants was not controlled in any other way, so that potentially influencing factors would not be excluded.

A healthy individual, with no known medical conditions or history of musculoskeletal injuries to the foot and ankle, was assessed for comparison (female, aged 31 years). MR data for this individual had been collected in a previous study at the Cardiff University Brain Research Imaging Centre (CUBRIC, Dr Bethany Keenan). Ethical approval was granted for the original studies by

Southampton and South West Hampshire Local Research Ethics Committee (NIHR ref. 24427) and Cardiff University School of Psychology Ethics Committee (EC.18.03.13.5264). Secondary data analysis ethical approval for this study was granted by the University of Southampton (ERGO ID: 48707 and 48710).

The participant selection and subsequent segmentation, measurement and FE modelling processes were completed by different researchers (Dr Alex Dickinson and Emily Kelly respectively) so that the study could be carried out blinded to the participants' reported condition severities. If substantial deformity was present, these were visible during the segmentation process and so could not be completely blinded. However, as the same procedure was followed for developing each participant model, this should have had minimal impact on the study results.

5.1.2 MR Segmentation and Morphological Measurements

MR data for the RA participants had been collected specifically for the FeeTURA study in 2010-2011. The MR sequencing is detailed in the FeeTURA study in full [21]. The T1-weighted spin echo sequence taken in the coronal plane was used for this study (repetition time/echo time (TR/TE): 656ms/15ms, slice thickness: 3mm, in-plane resolution: 0.52x0.52mm). MR data for the healthy volunteer had been collected with a Dual Echo Steady State (DESS) sequence in the sagittal plane (TR/TE: 13.48ms/4.79ms, resolution: 0.6x0.6x0.6mm). This was carried out using a 3T scanner (Magnetom Prisma, Siemens, Erlangen, Germany) with a foot/ankle and four-channel flex coil with the plantar forefoot rested against a flat support.

The MR data were segmented and prepared for modelling in ScanIP, using similar methods to those detailed in Chapter 4 (see Section 4.1.2). The RA participants' MR data had been collected using a standardized foot position, with the coronal slices perpendicular to the metatarsal parabola. However, as the data were not originally collected for modelling purposes, the images were not orientated within the coronal plane, in positions appropriate for gait. Thus, the data were rotated in the coronal plane using ScanIP to ensure all the forefoot sections were appropriately and similarly orientated, using the metatarsal heads as references. The greyscale threshold values used to create the skin, underlying soft tissue and bone were consistent across all participants except for the healthy volunteer, where the values were adapted to suit the different MR sequencing that had been used. The footwear model developed for this chapter represented a simplified leather shoe. This was given a 3mm thick upper and 6mm sole, allowing space for a total contact FO with a 3mm minimum depth (Figure 5.1A).

Morphological measurements were taken using ScanIP's linear measurement tool, to be used as potential indicators of condition severity (Figure 5.1B). The first metatarsal head (MH1) region

was investigated as a key bony prominence, potentially increasing the risk of damage to the surrounding tissue. Assessments were made regarding the sesamoid bone orientations, observing whether they were neutrally positioned under MH1 (normal position) or shifted laterally beyond MH1 (displaced position) (Figure 5.1C), and measuring the lateral distance from the medial edge of MH1 to the medial edge of the sesamoid. This measure was presented as a percentage of MH1 width. The depth of tissue under MH1 was measured to indicate tissue migration. Surface meshes of MH1 were exported to MATLAB (R2020b, MathWorks, Massachusetts, USA), to calculate the average principal curvature of the medial plantar quarter of MH1, using code sourced from MathWorks File Exchange [229, 230].

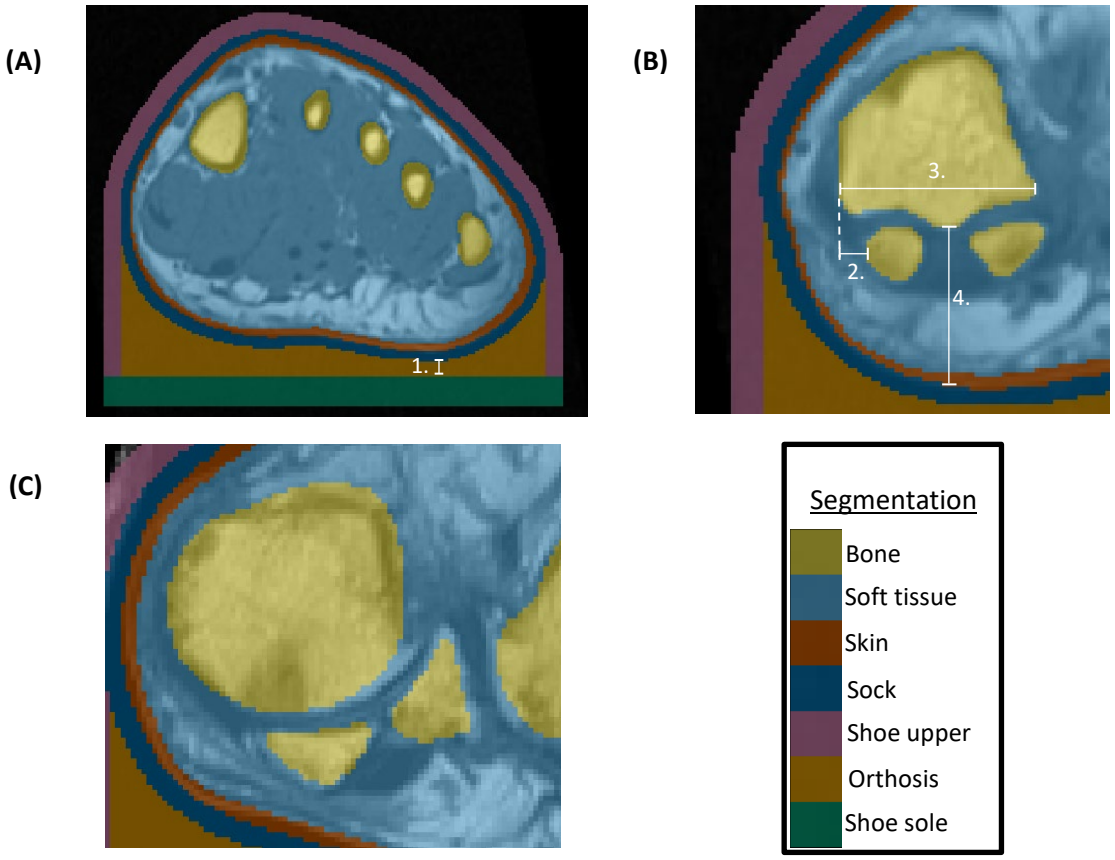

Figure 5.1: **A)** Segmentation of bones, skin, soft tissue from RA3 MRI, with addition of sock, shoe upper, orthosis, shoe sole, indicating minimum orthosis depth (1.); **B)** Morphological measurements for RA3 showing sesamoids in a normal position, with 2. Lateral distance from MH1 edge to sesamoid, 3. MH1 width, 4. Tissue depth under MH1 **C)** RA1 MRI showing example of sesamoids in a displaced position

5.1.3 Finite Element Model

The segmented geometries were imported into COMSOL for FE analysis, and again the models were developed using similar methods to those in Chapter 4 (see Section 4.1.3). The differences in

methods, mainly due to the change in the modelled orthosis and footwear, were as follows. The shoe upper was still considered linear elastic, but was assigned material properties relevant to a leather shoe (E=200MPa, v=0.3) [158]. The FO was assigned the hyperelastic material properties of Poron, which was used as a cushioning material in Chapter 4 (Table 4.2). All other material properties were consistent with the previous chapter.

The boundary and loading conditions were also applied as per Chapter 4, with friction applied to the boundaries between the sock and FO or shoe upper with static coefficients of 0.55 [198]. The load distributions, both within the forefoot and between the forefoot and other regions, had been calculated from healthy individuals. However, the distributions were deemed suitable for the participants with RA as well, as they agreed with values from literature (see Section 2.3.5.3). A summary of the differences between the models in the present chapter and the methods from the previous chapter has been provided (Table 5.1).

Table 5.1: Features of Chapter 5 segmentation and model development methods that differed from Chapter 4

Difference in Methods	**Description/Values**
Leather shoe dimensions	Shoe upper thickness – 3mm Shoe sole thickness – 6mm
Leather shoe upper material properties	Young's modulus – 200MPa Poisson's ratio – 0.3
Orthosis geometry	FO with minimum depth of 3mm
Orthosis material (Poron Cushioning)	Storakers Hyperelastic material properties: μ - 144kPa α – 4.013 β – 0.057
Friction at orthosis/sock boundary	CoF – 0.55

A 2nd order tetrahedral mesh was used with local refinement in the thin skin and sock domains, and at the orthosis/sock boundary (Table 5.2). Mesh convergence was assessed using RA1 models. For the mesh used, percentile shear strain and pressure results were within 2.5% of the finest mesh results (see Appendix J, p.184).

Table 5.2: Mesh input parameters

Mesh Input Parameter	Region 1: Sock, skin	Region 2: Soft tissue and bone	Region 3: FO upper boundary	Region 4: FO and shoe sides	Region 5: Shoe sole
Maximum element size (mm)	1.68	4	1	5	5.5
Smallest element size allowed (mm)	1.68 - 1.68/3	4 - 4/3	1 – 1/3	5 – 5/3	5.5 – 5.5/3
Maximum element growth rate	1.3	1.3	1.3	1.3	1.3
Curvature factor	0.3	0.3	0.3	0.3	0.9
Resolution of narrow regions	1.2	1.2	1.2	1.2	0.4

5.1.4 Data Analysis

As before, four parameters were extracted from the models to provide indications of tissue damage risk:

1. 99^{th} percentile shear strain (calculated from Green-Lagrange strain tensor) in the soft tissues,
2. volume of tissue above 10% shear strain,
3. 99^{th} percentile plantar pressure,
4. maximum plantar pressure gradient.

Further details of how these parameters were determined can be found in Section 4.1.4. Alongside these model predictions, clinical data for the participants were assessed including BMI, LFIS-IF scores, instances of bursae, erosion and synovial hypertrophy at the joints, and the MRI-based anatomical measures mentioned above. For some analyses, the BMI was grouped into normal BMI ($18.5 \leq BMI < 25 kg/m^2$) and high BMI ($BMI \geq 25 kg/m^2$).

SPSS Statistics (v.27, IBM Corp., Armonk, NY, USA) was used to carry out statistical analyses of the model results and participant data. Shapiro-Wilk normality tests were performed to determine whether parametric or non-parametric tests were appropriate. Disease duration, lateral sesamoid offset and volume of tissue over 10% shear strain were found to be non-parametric. The remaining FE model predictions, morphological measurements and clinical data were found to be parametric. Pearson correlation analyses were performed to determine the relationships between parametrically distributed variables, and where variables were skewed, Spearman's correlations were used.

5.2 Results

5.2.1 Demographic and Morphological Comparisons

All 13 RA participants selected for this secondary analysis had relatively established disease, of duration over 1yr and varying morphological presentations (Figure 5.2). Longer disease duration was correlated with sesamoid bones offset (r=0.698, p=0.008) (Figure 5.3A). The sesamoid offset also correlated with soft tissue depth under MH1 (r=-0.721, p=0.005). Longer disease duration did not correlate significantly with reduced soft tissue depth, potentially due to the confounding effects of foot size and BMI (Figure 5.3B). Despite this, longer disease duration was not necessarily associated with a worse clinical presentation (Figure 5.3C&D). For example, in participants with RA for over 10 years, there was an even split of people with low *vs.* moderate to high foot impairment (LFIS-IF threshold of 7 [231]). RA6 and RA10 had low LFIS-IF scores and instances of bursae, erosion and hypertrophy despite their longer disease durations and thus higher sesamoid offset and lower tissue depth under MH1. The opposite was observed for RA1 and RA8.

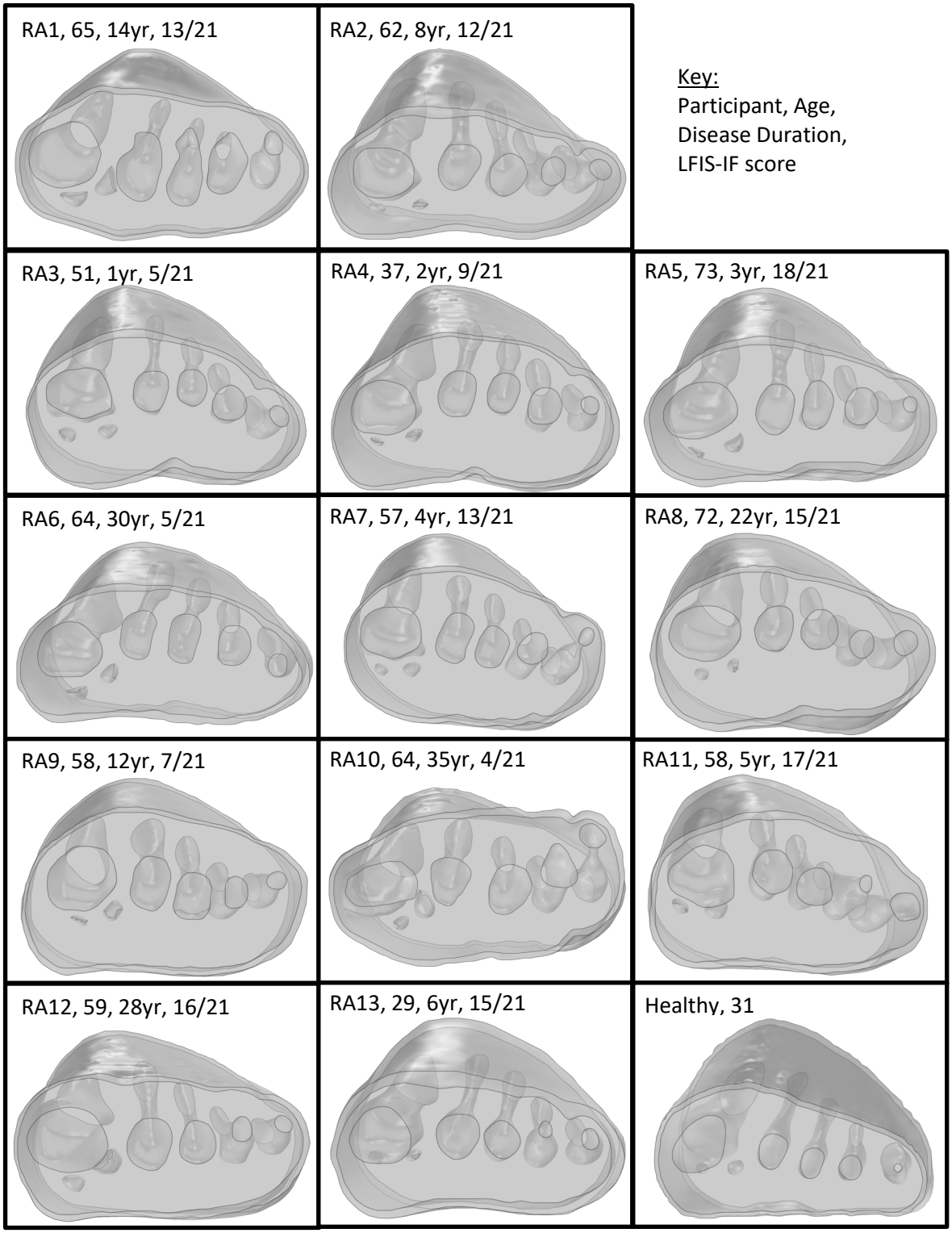

Figure 5.2: Modelled forefeet (skin, encapsulated bulk soft tissue, bones) of the 13 participants with RA and 1 healthy participant, with age and disease duration indicated.

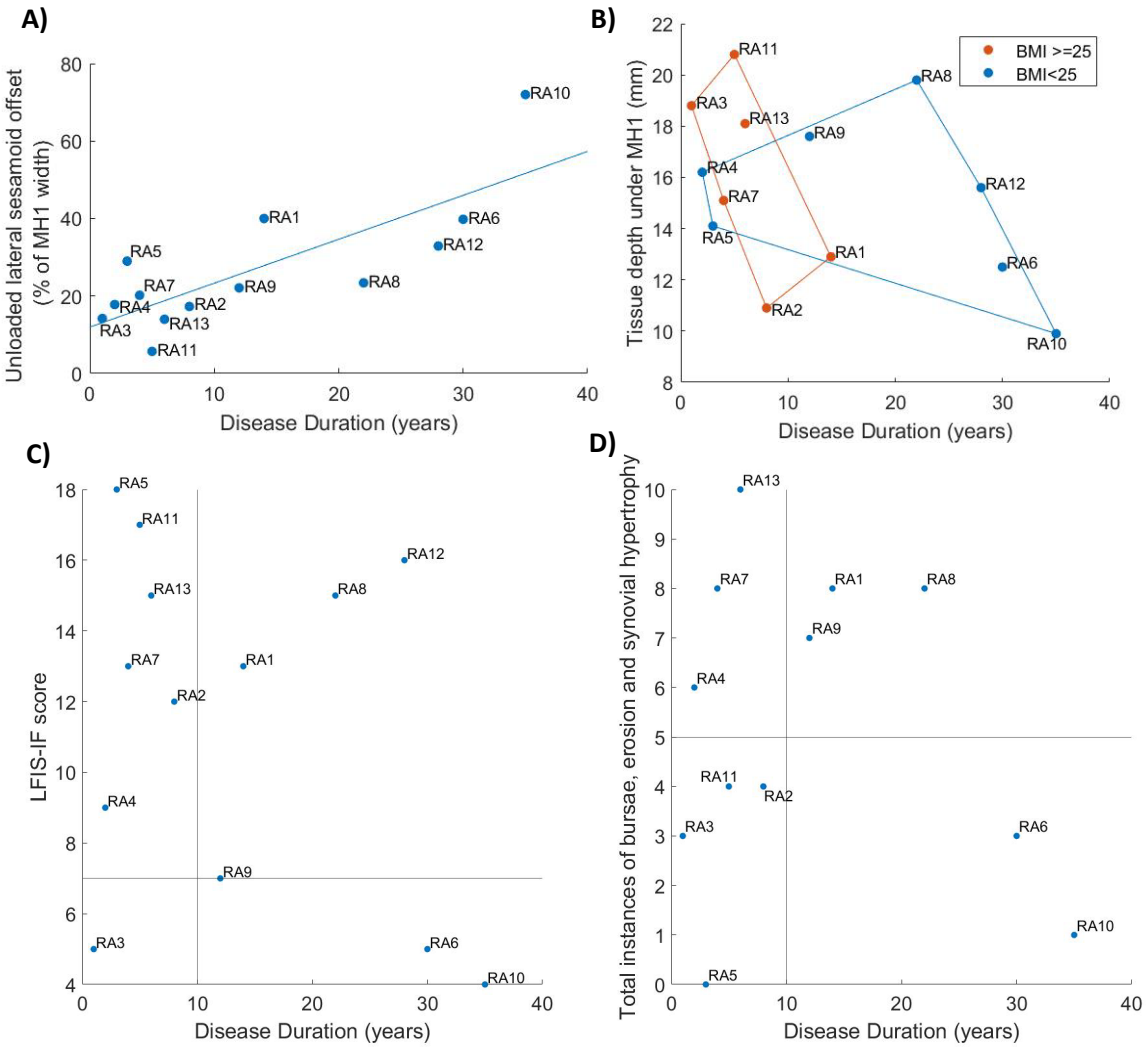

Figure 5.3: Correspondence of disease duration to: **A)** Lateral offset of the sesamoid bones; **B)** Tissue depth under MH1 with groupings for normal vs high BMI; **C)** LFIS-IF score with quadrants indicating short vs long duration and low vs moderate/high LFIS score; **D)** Instances of bursae, erosion and synovial hypertrophy at the MTP joints, with quadrants showing short vs long duration and low vs high instances. Note: data for RA12 was missing for instances of bursae, erosion and hypertrophy and so n=12.

5.2.2 RA and Healthy Control Comparisons

The healthy participant had a normal BMI and sesamoid bones in a neutral position, confirming their suitability as a control. The healthy participant's FE model predictions generally fell at the lower end of the RA models' range, either just within or below the interquartile range (IQR) (Table 5.3). The exception was the pressure gradient results where the healthy participant fell towards the upper end of the IQR. Note that n=12 for instances of bursae, erosion, and synovial hypertrophy, as data was unavailable for RA12.

Table 5.3: Median (IQR) results for the clinical data, morphological measurements and model predictions. The healthy participant rank indicates where they fell within the RA dataset, with 1 being lowest and 14 highest. X= denotes where rankings were tied.

	Measure	**RA participants (n=13)**	**Healthy participant (n=1)**	**Healthy participant (n=1)**
		Median (IQR)	**Median (IQR)**	**Rank (out of 14)**
Clinical Data	BMI	24.8 (22.3 – 28.4)	22.3	4=
	Disease duration (years)	8 (4 – 22)	NA	NA
	LFIS-IF (0-21)	13 (7 – 15)	NA	NA
	Instances of bursae (0-9), erosion (0-5), synovial hypertrophy (0-5)	5 (3 – 8)	NA	NA
Morphological Measurements	Depth of tissue under MH1 (mm)	15.6 (12.9 – 18.1)	16.7	9
	Unloaded lateral offset of sesamoid from MH1 edge (% of MH1 width)	22.1 (17.3 – 32.9)	14.4	2=
	Average principal curvature of MH1 (mm^{-1})	0.149 (0.128 – 0.163)	0.079	1
Model Predictions	99^{th}% shear strain in soft tissues (%)	13.7 (12.3 – 16.7)	12.3	5
	Volume of tissue over 10% shear strain (mm^3)	3214 (2359 – 6407)	1418	4
	99^{th}% plantar pressure (kPa)	62.9 (59.3 – 65.6)	55.6	4
	Maximum plantar pressure gradient (kPa/mm)	3.1 (2.6 – 3.4)	3.4	10

5.2.3 Model Outcomes across Participants with RA

Across all participants, the highest plantar pressures were located under the 1^{st} or 2^{nd} metatarsal heads (Figure 5.4). Peak shear strains were concentrated in the soft tissue around the bones, particularly the medial 1^{st} metatarsal head aspect and sesamoid bones.

The model predictions displayed differences between participants with RA for some parameters, with BMI and MH1 curvature appearing to have the greatest impact (Figure 5.5). The four participants with the highest BMIs all produced model predictions above the median values (RA3, RA7, RA11, RA13). There was no discernible trend in model results for the participants with the four lowest BMIs (RA5, RA6, RA8, RA9). Overall, there were strong significant correlations

between BMI and 99th% shear strain, volume of tissue over 10% shear strain, and 99th% plantar pressure ($0.600<r<0.652$, $p<0.05$) (Table 5.4).

Similarly, 3 of the 4 participants with lowest MH1 curvature (i.e. highest radius) accounted for 3 of the 4 lowest model predictions for strain and pressure gradient metrics (RA1, RA10, RA12). Those with the four highest curvatures also had 2-3 of the highest pressure and strain predictions, with a clear distinction between those with high curvature and high BMI (RA3, RA7) and high curvature but normal BMI (RA5, RA6). Overall, MH1 curvature was moderately correlated with borderline significance to all four model predictions ($0.529<r<0.574$, $0.040<p<0.063$). This was the only parameter to produce a significant correlation with the pressure gradients.

Sesamoid offset and tissue depth under MH1 also displayed moderate to strong correlations with the shear strain variables and to a lesser extent the 99th% plantar pressure ($-0.578<r<-0.758$, $p<0.05$ and $0.464<r<0.627$, $0.022<p<0.110$ respectively). This would suggest that higher pressure and strain results stemmed from reduced sesamoid offset and higher tissue depths, which would be associated with more normal anatomy. However, it should be noted that the four participants with the lowest sesamoid offsets (RA2, RA3, RA11, RA13) all had BMIs in the top five of the group, and those with the highest sesamoid offsets (RA1, RA6, RA10, RA12) all had either MH1 curvature or BMI within the lowest four of the group. Similar trends were found with the tissue depth variable.

Neither the LFIS-IF score or instances of bursae, erosion and synovial hypertrophy correlated with model predictions. Where there were potential trends for low or high rankings within the dataset, these could also be attributed to MH1 curvature and BMI. Full results for each participant, indicating the highest and lowest ranked participants for each variable can be found in Appendix L (p.188).

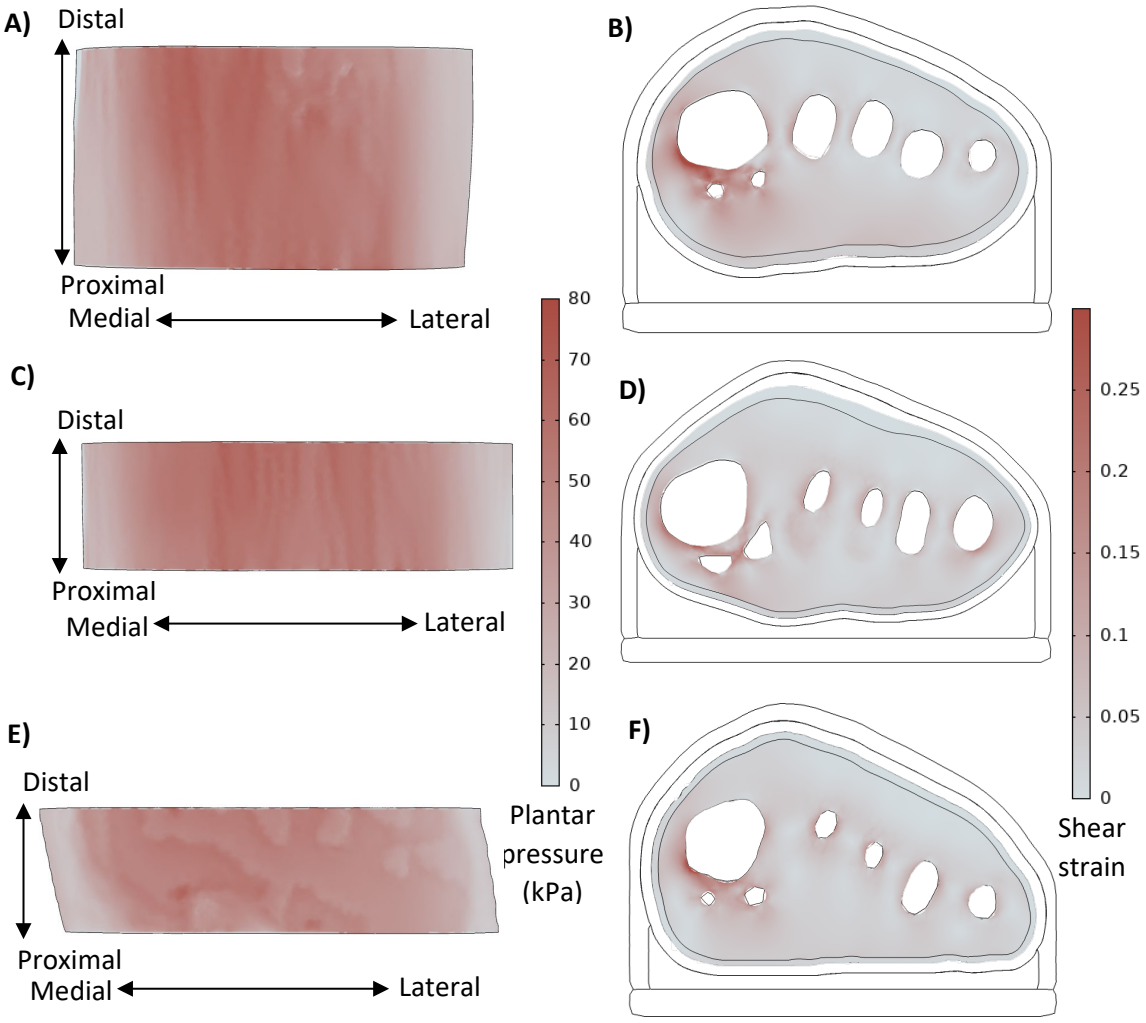

Figure 5.4: Plantar pressure and shear strain (taken from slice through sesamoid centre) distributions, for **A&B)** RA8 with sesamoids in neutral position, BMI=21.7, MH1 curvature = 0.144 mm^{-1}, and **C&D)** RA1 with displaced sesamoids, BMI=26.7, MH1 curvature = 0.112 mm^{-1}, and **E&F)** Healthy participant, BMI=22.3, MH1 curvature = 0.079mm^{-1}

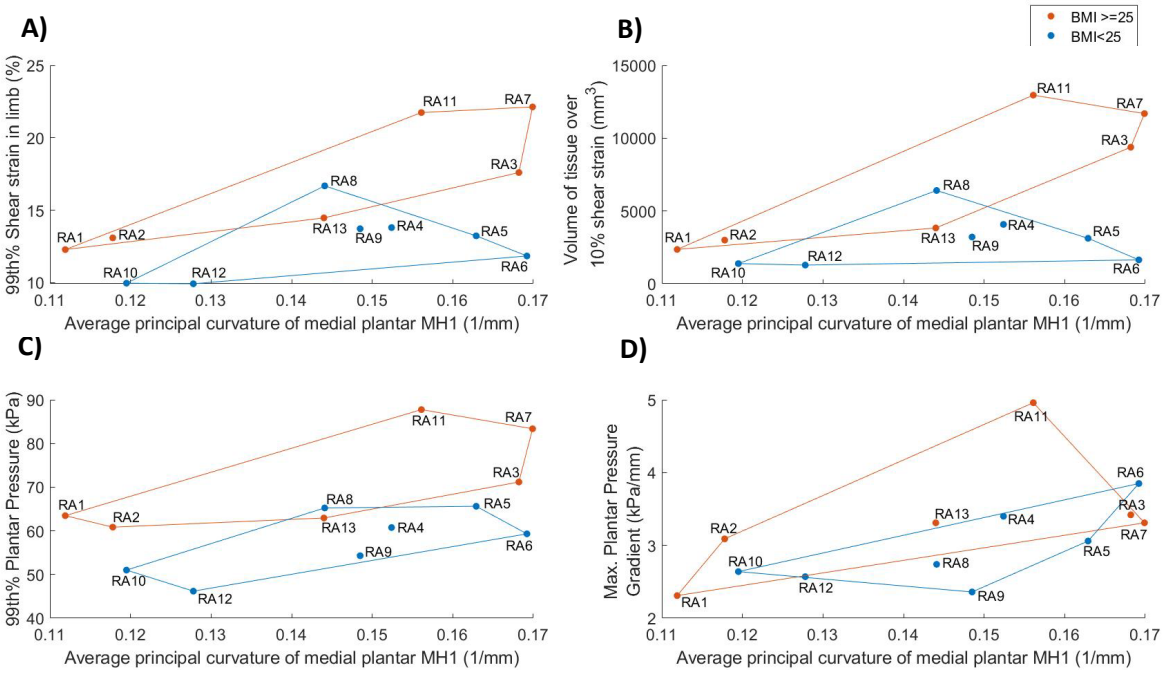

Figure 5.5: Average medial plantar MH1 curvature results, separated into normal vs high BMI groups, for: **A)** 99th% shear strain in the soft tissue; **B)** volume of tissue in the limb over 10% shear strain; **C)** 99th% plantar pressure; **D)** maximum plantar pressure gradient

Table 5.4: Correlations for model predictions with the clinical data and morphological measurements. Moderate to strong correlations (>0.4) are bolded. * indicates significant (p<0.05) correlation.

Variable 1	**Variable 2**	**Correlation (p value)**
99th% Shear strain in soft tissues	Instances of bursae, erosion, synovial hypertrophy	0.284 (0.372)
	Unloaded lateral offset of sesamoid	**-0.662 (0.014)***
	Tissue Depth under MH1	**0.623 (0.023)***
	LFIS-IF	0.271 (0.370)
	Disease Duration	**-0.601 (0.030)***
	Average principal curvature of MH1	**0.574 (0.040)***
	BMI	**0.600 (0.030)***
Volume of tissue over 10% shear strain	Instances of bursae, erosion, synovial hypertrophy	0.157 (0.627)
	Unloaded lateral offset of sesamoid	**-0.758 (0.003)***
	Tissue Depth under MH1	**0.627 (0.022)***
	LFIS-IF	0.222 (0.467)
	Disease Duration	**-0.709 (0.007)***
	Average principal curvature of MH1	0.543 (0.055)
	BMI	**0.652 (0.016)***

Variable 1	Variable 2	Correlation (*p* value)
99th% Plantar pressure	Instances of bursae, erosion, synovial hypertrophy	0.128 (0.691)
	Unloaded lateral offset of sesamoid	**-0.578 (0.038)***
	Tissue Depth under MH1	**0.464 (0.110)**
	LFIS-IF	0.323 (0.281)
	Disease Duration	**-0.621 (0.023)***
	Average principal curvature of MH1	**0.529 (0.063)**
	BMI	**0.644 (0.018)***
Max. plantar pressure gradient	Instances of bursae, erosion, synovial hypertrophy	-0.206 (0.520)
	Unloaded lateral offset of sesamoid	**-0.485 (0.093)**
	Tissue Depth under MH1	0.374 (0.208)
	LFIS-IF	0.126 (0.681)
	Disease Duration	-0.335 (0.264)
	Average principal curvature of MH1	**0.557 (0.048)***
	BMI	**0.452 (0.121)**

5.3 Discussion

The aim of this study was to determine whether simplified computational forefoot models would produce differing biomechanical predictions depending on condition severity in people with RA, e.g. LFIS-IF score and morphological measures, or other relevant factors such as BMI. These predictions were also compared to model predictions from a healthy individual to determine any differences. Models capable of producing different predictions between these individuals would allow for personalised FO design to improve treatment. The model predictions differed between the foot MR data for a healthy individual and the data for those with RA, as seen in the pressure and strain results (Table 5.3). Comparing to a single healthy individual does not confirm the models would distinguish between cohorts of healthy vs. RA, but the results do provide another point of comparison for condition severity. Within the RA group, higher BMIs corresponded to higher model predictions of soft tissue shear strain and plantar pressure, as did higher medial plantar MH1 curvature (indicating a less rounded, more sharply curved bone contour). The models could not distinguish between LFIS-IF score or instances of bursae, erosion and synovial hypertrophy. RA prevalence is significantly higher in women than men [232], and all participants in this study were female. However, this does mean the findings are only applicable to women with RA and may not apply to men with RA. The predicted pressure and strain varied considerably across the participants, emphasising the importance of evaluating multiple individuals. Previous

studies using single cases or healthy cohorts are unlikely to provide a robust assessment of interventions.

The plantar pressures predicted by the models (median: 63kPa, IQR: 59-66kPa) fell within the expected bounds of forefoot pressures during midstance in the presence of an FO. Experimental testing of in-shoe midstance pressures of five healthy participants recorded median peak forefoot pressures of 131kPa (IQR: 95-151kPa), see Appendix K (p.186) for details of the testing. Though higher than the pressure results in the present study, the experimental pressures were measured without an FO. FOs have been shown to reduce plantar pressures by 56% during stance [233], which would bring the experimental results far more in line with the model predictions. A recent study by Simonsen et al. [148] measured in-shoe plantar pressures for people with RA wearing orthoses, and found that at 50% of the stance phase, peak pressures ranged from approximately 17-54kPa, with a mean of around 29kPa with a custom FO. Previous studies of healthy individuals have found mean midstance forefoot pressures of approximately 70kPa [234] and 132kPa (s.d. 65kPa) [235], though these values were obtained barefoot which causes higher plantar pressures than when shod. Additionally, the shear strains in the present models were concentrated around the bones, with lower tissue strains elsewhere (Figure 5.4). These strain distributions are a well-established occurrence in the foot [236], and correspond to common sites of ulceration due to RA [39]. The models predicted results within the expected range, and produced trends based on participant clinical and morphological data. This is a promising sign that the models would be suitable for assessing FO and footwear choices across at least a female population, represented in the present study.

One of the clearest trends observed was the effect of BMI on pressure and shear strain predictions, with high BMI (≥25kg/m^2) posing more risks. The differences in model results between participants were not just due to the applied loading conditions, which were based on participant weight. Three participants (RA1, RA3, RA7) had identical weights and thus similar applied loads, but their BMIs differed as did the model results. Individuals with both RA and increased BMI experience increased pain, MTP joint swelling, activity limitation, and in-shoe pressures but little change to barefoot pressures [175]. Thus, restricting the foot within a shoe caused more issues for those with higher BMIs, who may already be adversely affected due to higher loads going through the foot [237]. Additionally, people with high BMI may have different requirements for an FO to provide the necessary shock absorption. The importance of including the shoe in modelling of this nature is clear, and the present approach could be adapted for future FO design research in different groups at high risk of soft tissue injury in the foot, because the models can assess the effects of varying morphology, disease presentation and footwear choice.

The curvature of the medial plantar MH1 was also related to the model predictions. Individuals with a more rounded MH1 tended to produce lower model results and vice versa. The highest shear strains were also observed in the tissue surrounding this region. This was likely due to a combination of the medially skewed loading, and compression of the tissue between the bony prominence and orthosis/shoe. This parameter is not currently considered during FO or footwear assessments, but could provide additional information for such a use, particularly in identifying individuals with higher bone curvatures who may require more protection.

MH1 curvature was the only parameter that significantly correlated with the model pressure gradient predictions. Again, this likely relates to it being a bony prominence, where pressure gradients are higher and indicative of shear strain [179, 181]. The lack of relationship between pressure gradients and other variables is understandable, particularly for BMI, given that the measure is not magnitude-based. Additionally, the FO may have reduced pressure gradients across all participants, including the healthy control, limiting differences between them.

Increased tissue depth under MH1 and reduced sesamoid offset were also connected to increased pressure and shear strain predictions. However, this may have been an indirect effect due to BMI and MH1 curvatures. The majority of participants with longer disease durations had normal BMIs, while most with shorter durations had high BMIs (Figure 5.3B). Sesamoid offset increased with duration, so trends observed for normally positioned sesamoid bones may have been due to high BMIs instead, through artefacts of the small population. Similar overlaps were found with high sesamoid offset and low MH1 curvature. It should also be noted that the participants with highly displaced sesamoid bones (RA1, RA6, RA10, RA12) did not necessarily have worse conditions according to LFIS-IF scores and instances of bursae, erosion and synovial hypertrophy (Figure 5.3C&D).

The strength of this study was the consideration of these inhomogeneities and variations within the study population. However, a few limitations should be acknowledged, which arise because the images used to develop the models were not originally collected for the purposes of simulation. First, the MR data used for the RA models had been collected in unloaded positions. Thus, the shape of the plantar foot varied considerably between participants, affecting the thickness of orthotic present in different forefoot regions, including where reduced tissue depth may have resulted in increased FO thickness (Figure 5.2). Given that FO thickness may influence pressure and strain [158, 168], inter-participant comparisons may have been affected by differing FO thicknesses due to the varying plantar profiles. These limitations in the dataset make it difficult to draw conclusions on the effect of sesamoid offset and tissue depth under MH1 in these models. Further work with imaging collected in a stance position but low, nominal loading, or a

larger sample size, would be required to ascertain if these two RA-related variables were truly identifiable in participants' model results. The small sample size in the present study may also have affected the other correlations, and so assessment of a larger cohort would confirm those results.

The models were not capable of distinguishing between participant's LFIS-IF scores or instances of bursae, erosion or synovial hypertrophy, though there are possible explanations. First, the LFIS-IF score is a subjective measure, based on each individual's perception of their experience and pain threshold. A clear example of this was RA5, who's LFIS-IF score was highest at 18 despite having no instances of bursae, erosion or synovial hypertrophy visible on ultrasound (Figure 5.3). Difficulty in linking subjective and objective measures is not uncommon. A previous review into sitting discomfort found that the only objective measure that appeared to be significantly correlated to reduced discomfort was a more uniform pressure distribution [238]. There was no clear evidence that any of the other objective measures (movement, posture, spinal loads, muscle activity) could be related to discomfort. It may be that the FO in the present model, which resulted in low and similar pressure gradients across participants, prevented a correlation with LFIS-IF score.

Alternatively, simplifications in the model geometries may not have allowed for distinguishing LFIS-IF score or instances of bursae, erosion and synovial hypertrophy. Any bursae present were not included in the models, nor was detailed anatomy of the MTP joints or inflammation that would result in pain. More complex models including these features may show relationships between the model results and the above parameters. The model simplifications, such as use of a bulk soft tissue group and fused MTP joints, were thought suitable for the purpose of this study and future purpose of the models which centres on comparisons between FO design, for which the absolute values of pressure and strain are not necessary. However, the simplifications may have limited the differences in predictions between the models.

Other model limitations stemmed from the loading conditions, such as the ground reaction forces that were applied to the models. As previously mentioned, a key improvement would be the use of forefoot MR data with the soft tissues and bones in a loaded position, as well as collecting kinetic data for the participants being modelled. In the present study, the GRFs applied to the models were based a set load distribution across the forefoot, albeit scaled to the participant's weight and relative locations of the metatarsal heads. Thus, the pressure and strain predictions may be inaccurate, particularly given that some individuals with RA adapt their gait to off-load painful or affected forefoot regions [33, 44]. To use these models to assess FO design on a personalised level, load distributions based on the individual's gait pattern would be beneficial.

Additionally, using static midstance loads does not encompass the peak pressures experienced by the forefoot during toe-off, or the full sesamoid bone movement as would occur during dynamic gait influencing pressure and strain distributions. However, as conditions were consistent across participants, comparisons were still valid. Another drawback of using static models was that PTI differences between participants could not be examined. Given the importance of sustained loading and how it can relate to pain experienced by those with RA [38], and risk of tissue damage [239], dynamic modelling should also be explored.

5.4 Summary

Through this novel computational assessment of the internal effects of loading on multiple individuals with RA, the research question of whether computational models of the forefoot could distinguish different aspects of RA disease was addressed. The model predictions for those with RA were highly influenced by the participant's BMI and the medial plantar MH1 curvature. Due to limitations of the dataset, it was unclear whether the tissue depth under MH1 and the unloaded lateral offset of the sesamoids bone directly impacted model results. No relation was found between the model's pressure or strain predictions and LFIS-IF score or instances of bursae, erosion and synovial hypertrophy. The wide ranges observed in the model predictions emphasises the importance of modelling interventions across multiple pathological individuals rather than a single healthy case.

The simplified forefoot models produced differing biomechanical predictions between people with RA, with the variation relating to some condition-related factors but not to others. The models also produced differing results for a healthy individual and people with RA. These differences likely stemmed from variations in participant morphology and applied loads. Thus, with the limitations from the present study addressed, the models could provide a suitable basis for comparing FO designs based on individual requirements, particularly as they relate to BMI and alleviating internal tissue strains around bony prominences.

Chapter 6 Evaluation of Foot Orthosis Design through Computational Modelling and Clinical Assessment

In Chapter 5, a set of computational forefoot models were developed for 13 individuals with RA to assess whether the models could differentiate between factors such as participant morphology and pain scores. In particular, BMI and bony anatomy were found to relate well to model predictions indicative of tissue damage risk, suggesting that the models were capable of highlighting individuals more at risk. The purpose was to establish models that could be used for assessing orthosis and footwear choices for individuals with RA. As discussed in Section 1.3.2, no single FO design is currently considered best practice to reduce pain and improve quality of life in RA treatment. Thus, further understanding of the effects of different design parameters on the soft tissue is key. This is particularly true for the effects on deep tissue vulnerability, seen through measures such as soft tissue strain, which is not examined as commonly or as understood as superficial tissue vulnerability, measured through plantar pressures.

The study detailed in this chapter aimed to assess different design parameters – FO material, shape, and shoe type – for individuals with RA. Previous modelling studies of single healthy individuals have shown the impact of FO material and shape on the soft tissue [158, 161, 168, 170], however no previous studies have assessed the effects in people with RA. Additionally, most previous modelling studies have not included the shoe upper, despite evidence that it affects soft tissue loading and footwear choices are important for those with RA [174, 175]. A model which can distinguish between different orthosis configurations would pave the way towards determining optimal orthosis design based on individual requirements.

This chapter addresses research question 3 through the following objectives:

RQ 3: To what extent can computational models provide knowledge to inform the design of safe and effective lower limb orthoses?

1. Develop model sets for a group of individuals with RA to compare clinically-used orthosis design variables:
    a. FO material choice
    b. Shoe configurations
    c. FO shape – flat vs total contact
2. Compare the model outcomes for the different FO and shoe configurations, with consideration to relevant clinical data and morphological measurements identified previously

6.1 Methods

The development of the base models for each participant (RA1-13) was detailed in Section 5.1. This included participant information, MR segmentation methods, material properties, loading and boundary conditions, and mesh parameters. The method section for this chapter will focus on additional methods and input parameters that were part of the orthosis and shoe comparisons.

6.1.1 Foot Orthosis Material and Shoe Type Comparisons

Four different FO material combinations and two different shoe configurations were assessed to form a total of seven models per participant (Table 6.1). The FO materials chosen are commonly used clinically in RA treatment, with an Ethylene-vinyl acetate (EVA) foam compared to as a stiffer control material. The leather shoe had a 3mm upper and 6mm sole, while the training shoe had a 5mm upper and 15mm sole (Figure 6.1). The minimum FO thickness was 3mm, as per the methods detailed in Chapter 5 (Figure 5.1).

Table 6.1: Model configurations for FO and shoe comparisons

Configuration	FO Materials	Shoe Type
L_EVA	EVA – Microcell Puff Regular (min. 3mm)	Leather shoe
L_PC	Poron Cushioning (min. 3mm)	Leather shoe
L_PF	Poron Firm (min. 3mm)	Leather shoe
L_PP	Multi-layer: Poron Firm (3mm) + Plastazote medium (min. 1mm)	Leather shoe
T_PC	Poron Cushioning (min. 3mm)	Training shoe
T_PF	Poron Firm (min. 3mm)	Training shoe
T_PP	Multi-layer: Poron Firm (3mm) + Plastazote medium (min. 1mm)	Training shoe

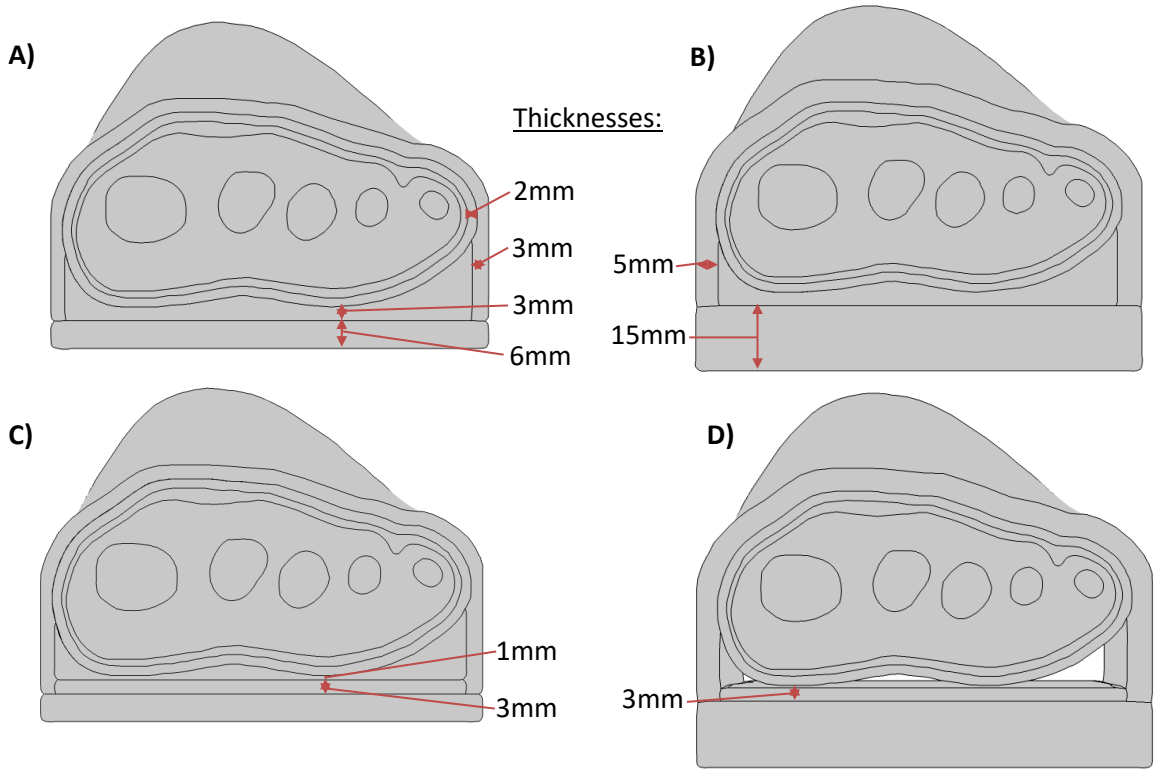

Figure 6.1: Example models for a single individual (RA2) developed for **A)** Leather shoe with total contact 3mm orthosis; **B)** Training shoe with total contact 3mm orthosis; **C)** Leather shoe with multi-layer total contact 3mm + 1mm orthosis; **D)** Training shoe with flat 3mm orthosis

All FO materials were modelled using Storakers hyperelastic model (Eq.4.2) using constitutive property values from literature [195](Table 6.2. Figure 6.2). Similarly to the leather upper, the training shoe upper was assumed to be linear elastic, and was assigned a Young's Modulus of 8.5MPa and Poisson's ratio of 0.061 [219]. All other material properties, including leather upper and shoe sole were as previously described (Table 4.2). For the models containing a multi-layer orthosis, the two layers were bonded together.

Table 6.2: Hyperelastic material properties for FOs

Material	**μ (kPa)**	**α**	**β**
Microcell Puff Regular (EVA)	490	7.24	0.154
Poron Cushioning (Polyurethane foam)	144	4.013	0.057
Poron Firm (Polyurethane foam)	229	4.51	0.01
Plastazote Medium (Polyethylene foam)	198	7.549	0.169

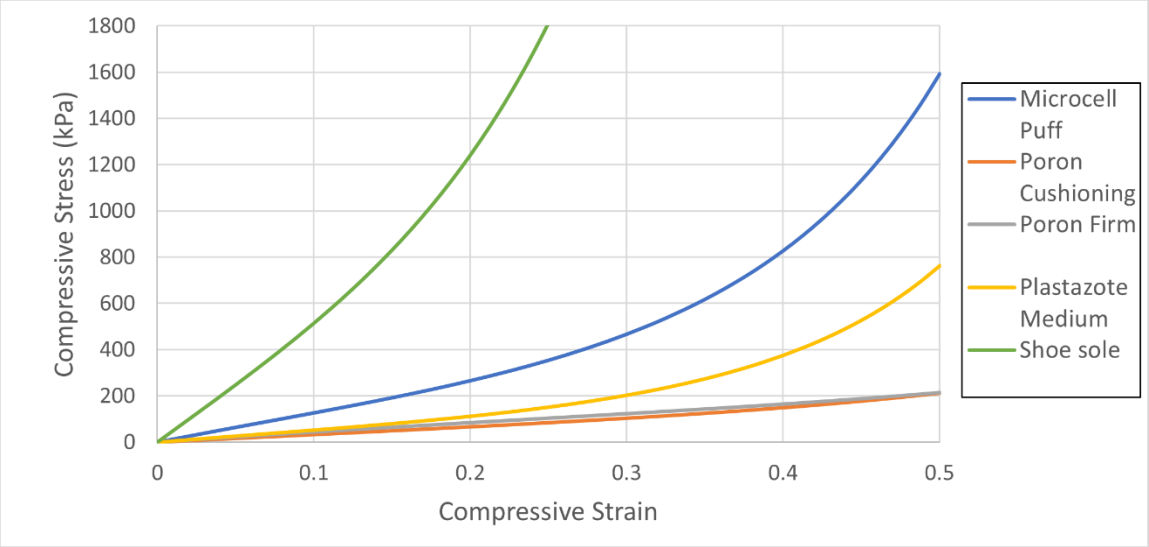

Figure 6.2: Storakers hyperelastic material model curves for the four FO materials, displaying the shoe sole material for comparison. Note: shoe sole material curve extends to 15800kPa at 0.5 strain.

6.1.2 Orthosis Shape

All the previously described models utilised FOs with profiles that perfectly matched the plantar profile of the foot. These have been referred to as total contact FOs, and represented an orthosis either moulded to an individual's foot shape or conformed to the foot shape through use. Case study comparisons were also carried out between these total contact FOs and flat FOs for participants RA1, 2, 6, 11 and 12 (Figure 6.1). The flat FOs were 3mm thick, or 3mm + 1mm for the multi-layer orthosis. Models for all 7 configurations (Table 6.1) were run using the flat orthosis so that any differences in the effects of FO material or shoe type could be compared between flat and total contact FOs.

6.1.3 Data Analysis

Four parameters were used to provide indications of tissue damage risk as per Chapters 4 and 5:

1. 99th percentile shear strain (calculated from Green-Lagrange strain tensor) in the soft tissues,
2. volume of tissue above 10% shear strain,
3. 99th percentile plantar pressure,
4. maximum plantar pressure gradient.

These parameters were calculated in MATLAB from the model output data according to the processes described in Section 4.1.4.

SPSS Statistics (v.27, IBM Corp., Armonk, NY, USA) was used to carry out statistical analyses of the different model configuration results. Shapiro-Wilk normality tests were performed to determine whether parametric or non-parametric tests were appropriate. For the FO material and shoe type comparisons, paired sample t-tests were used to assess the differences for the normally distributed model predictions alongside mean difference and 95th% confidence intervals (CIs). For the volume over 10% shear strain predictions, which were skewed, Wilcoxon signed rank tests were performed. The Hodges-Lehmann estimate was then used to calculate the difference and CIs between groups for the volume metric using the Excel Real Statistics Resource Pack Add-in (Release 7.8). This estimate is a non-parametric calculation of a pseudo-median and CIs. Assessments were made comparing each FO material using the same shoe type (e.g. L_PC vs L_PF) and comparing shoe types using the same FO material (e.g. L_PC vs T_PC) (Table 6.3).

Table 6.3: Model configurations between which statistical comparisons were performed

Configuration 1	**Configuration 2**
L_EVA – *EVA FO, leather shoe*	L_PC – *Poron Cushioning, leather shoe*
L_EVA – *EVA FO, leather shoe*	L_PF – *Poron Firm, leather shoe*
L_EVA – *EVA FO, leather shoe*	L_PP – *Poron Firm + Plastazote, leather shoe*
L_PC – *Poron Cushioning, leather shoe*	L_PF – *Poron Firm, leather shoe*
L_PC – *Poron Cushioning, leather shoe*	L_PP – *Poron Firm + Plastazote, leather shoe*
L_PF – *Poron Firm, leather shoe*	L_PP – *Poron Firm + Plastazote, leather shoe*
T_PC – *Poron Cushioning, training shoe*	T_PF – *Poron Firm, training shoe*
T_PC – *Poron Cushioning, training shoe*	T_PP – *Poron Firm + Plastazote, training shoe*
T_PF – *Poron Firm, training shoe*	T_PP – *Poron Firm + Plastazote, training shoe*
L_PC – *Poron Cushioning, leather shoe*	T_PC – *Poron Cushioning, training shoe*
L_PF – *Poron Firm, leather shoe*	T_PF – *Poron Firm, training shoe*
L_PP – *Poron Firm + Plastazote, leather shoe*	T_PP – *Poron Firm + Plastazote, training shoe*

As FO shape was only assessed for five case study participants, statistical analyses were not performed. Instead, the model predictions were compared directly for each participant and model configuration. Additionally, the differences in values between the flat and total contact models were compared for the different FO materials and shoe types, to assess whether the effects of material or shoe type changed with FO shape.

6.2 Results

6.2.1 FO Material and Shoe Type Comparisons

The model predictions for the different FO materials and shoe types were compared as both absolute values (Figure 6.3) and the average differences (Table 6.4).

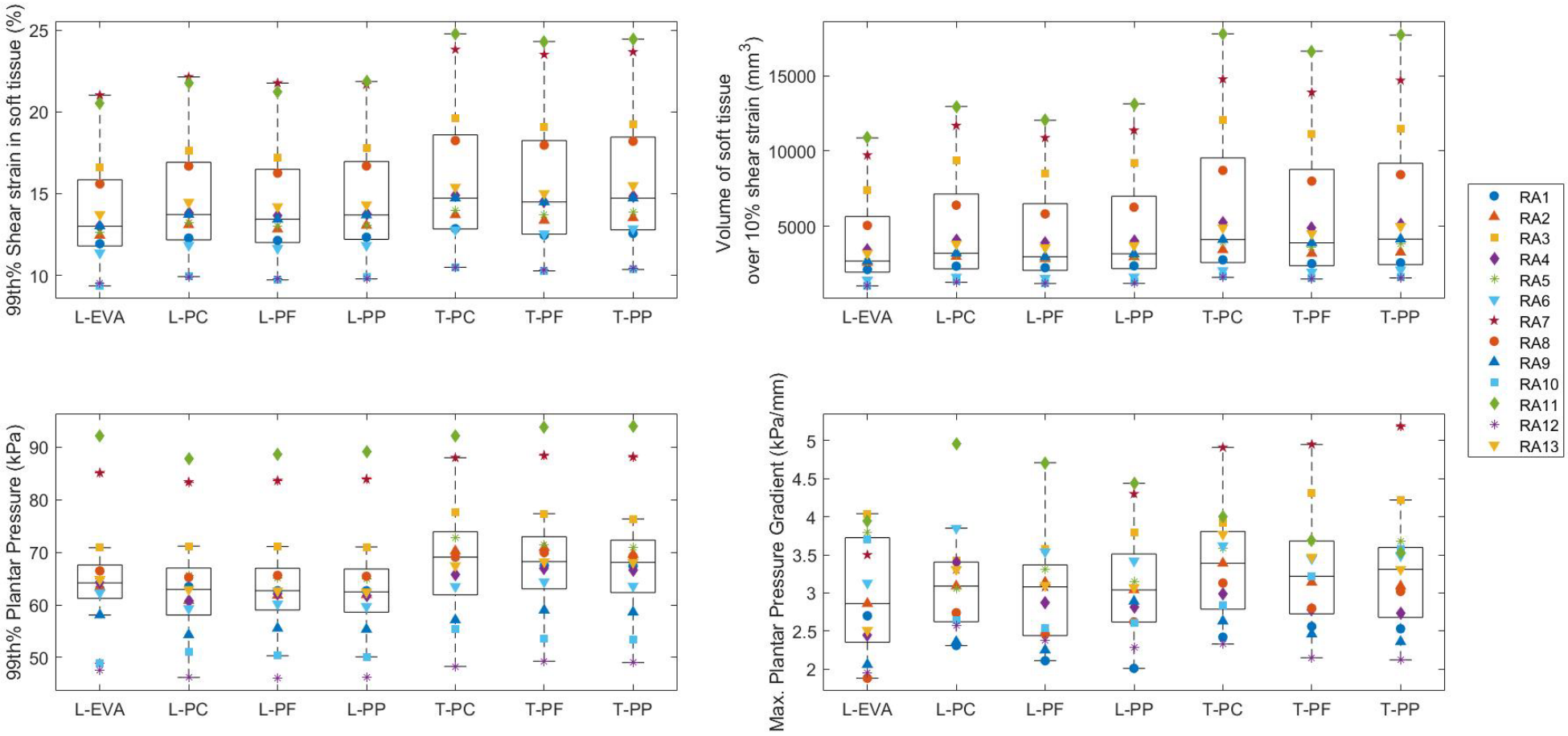

Figure 6.3: Comparison of different FO materials and shoe types for 13 participants with RA. Coding System: L-XX = leather shoe; T-XX = training shoe; X-EVA = EVA FO; X-PC = Poron Cushioning FO; X-PF = Poron Firm FO; X-PP = Poron Firm + Plastazote FO.

Table 6.4: Mean differences, or Hodges-Lehmann estimates for the volume metric, (95% CIs) between FO material and shoe types for the model prediction variables. *Significant at p<0.05; **Significant at p<0.01.

Models Compared	99th% shear strain in soft tissues, %	Volume of tissue of 10% shear strain, mm^3	99th% plantar pressure, kPa	Max. plantar pressure gradient, kPa/mm
L_EVA – L_PC	−0.75 (−0.92, −0.58)**	−744 (−1292, −358)**	1.56 (0.39, 2.73)*	−0.19 (−0.62, 0.24)
L_EVA – L_PF	−0.47 (−0.58, −0.36)**	−449 (−723, −200)**	1.29 (0.50, 2.09)**	−0.04 (−0.40, 0.32)
L_EVA – L_PP	−0.69 (−0.89, −0.50)**	−674 (−1236, −308)**	1.34 (0.58, 2.11)**	−0.15 (−0.52, 0.23)
L_PC – L_PF	0.28 (0.21, 0.35)**	328 (141, 532)**	−0.26 (−0.72, 0.19)	0.15 (0.03, 0.27)*
L_PC – L_PP	0.06 (−0.04, 0.15)	65 (8, 135)*	−0.21 (−0.69, 0.27)	0.05 (−0.23, 0.32)
L_PF – L_PP	−0.22 (−0.35, −0.09)**	−225 (−495, −102)**	0.05 (−0.11, 0.22)	−0.11 (−0.35, 0.14)
T_PC – T_PF	0.33 (0.27, 0.39)**	403 (210, 652)**	−0.33 (−1.05, 0.39)	0.07 (−0.08, 0.22)
T_PC – T_PP	0.12 (0.03, 0.21)*	94 (21, 207)*	0.11 (−0.64, 0.86)	0.05 (−0.15, 0.26)
T_PF – T_PP	−0.21 (−0.27, −0.14)**	−268 (−557, −144)**	0.44 (0.19, 0.69)**	−0.01 (−0.11, 0.08)
L_PC – T_PC	−1.18 (−1.62, −0.74)**	−1315 (−2575, −571)**	−4.96 (−6.10, −3.83)**	−0.19 (−0.56, 0.17)
L_PF – T_PF	−1.13 (−1.60, −0.66)**	−1221 (−2430, −499)**	−5.03 (−6.00, −4.06)**	−0.28 (−0.68, 0.12)
L_PP – T_PP	−1.11 (−1.51, −0.72)**	−1220 (−2287, −560)**	−4.64 (−5.44, −3.84)**	−0.19 (−0.51, 0.13)

The EVA orthosis caused significantly higher plantar pressures (1.29-1.56kPa mean difference) but significantly lower shear strain metrics (0.47-0.75% strain and 449-744mm^3 average differences) than the other material combinations, within the leather shoe results. In the plantar pressure predictions, the only other significant difference between orthosis materials was that Poron Firm produced higher pressures than Poron + Plastazote when combined with the training shoe. However, the magnitude of this difference was minimal at 0.44kPa. The two shear strain metrics produced more significant differences between Poron materials than the pressure predictions. Poron Firm produced the lowest 99th% shear strain and volume of soft tissue over 10% shear strain, followed by Poron Firm + Plastazote, and Poron Cushioning with the highest results. The majority of these differences were significant albeit small (max. average differences of 0.33% strain and 403mm^3). The exceptions were the difference in strain between Poron Cushioning and

Poron Firm + Plastazote, which were at most borderline significant for the four comparisons ($0.012<p<0.208$).

There were greater differences in the results between shoe types than between orthosis materials. The training shoe caused significantly higher 99th% shear strain, volume of tissue over 10% strain and 99th% plantar pressures than the leather shoe (average differences of 1.11-1.18% strain, 1220-1315mm^3, 4.64-5.03kPa respectively).

The average pressure gradient predictions followed similar trends in the differences between orthosis and shoe types to the shear strain metrics (Figure 6.3). However, none of these differences were significant, except for Poron Cushioning producing higher pressure gradients than Poron Firm when combined with the leather shoe.

On an individual basis, most participants tended to follow the overall mean trends described above, particularly where differences were significant. However, in the plantar pressure predictions, four of thirteen participants experienced lower plantar pressures for the EVA compared to Poron materials rather than higher (RA1, 3, 5, 10). Conversely, these same four participants were the only people to show higher pressure gradients for EVA than Poron.

When separating the participants into those with normal BMI (<25; range: 21.7-24.8) or high BMI (≥25; range: 26.7-30.9), there was a greater range of model predictions for those with high BMI (Figure 6.4). Additionally, the average differences were generally greater for the high BMI group compared to normal BMI. This was particularly true for the differences between the EVA and other orthotic materials (99th% shear strain: (-0.52 to -0.85% strain) *vs*. (-0.43 to -0.67% strain), volume over 10% shear strain: (-698 to -1208mm^3) *vs.* (-324 to -533mm^3), 99th% plantar pressures: (1.4 to 1.7kPa) *vs.* (1.1 to 1.4kPa) for the high and normal BMI groups respectively). The average differences between the two shoe types for those three metrics were also greater for the high BMI group than the normal BMI group ((-1.32 to -1.47% strain) *vs.* (-0.90 to -0.93% strain), (-1955 to -2084mm^3) *vs.* (-828 to -897mm^3), (-5.4 to -5.9kPa) *vs.* (-4.0 to -4.2kPa)). The full model predictions for each participant and model configuration can be found in Appendix M (p.191), along with the difference in mean values for the two BMI groups.

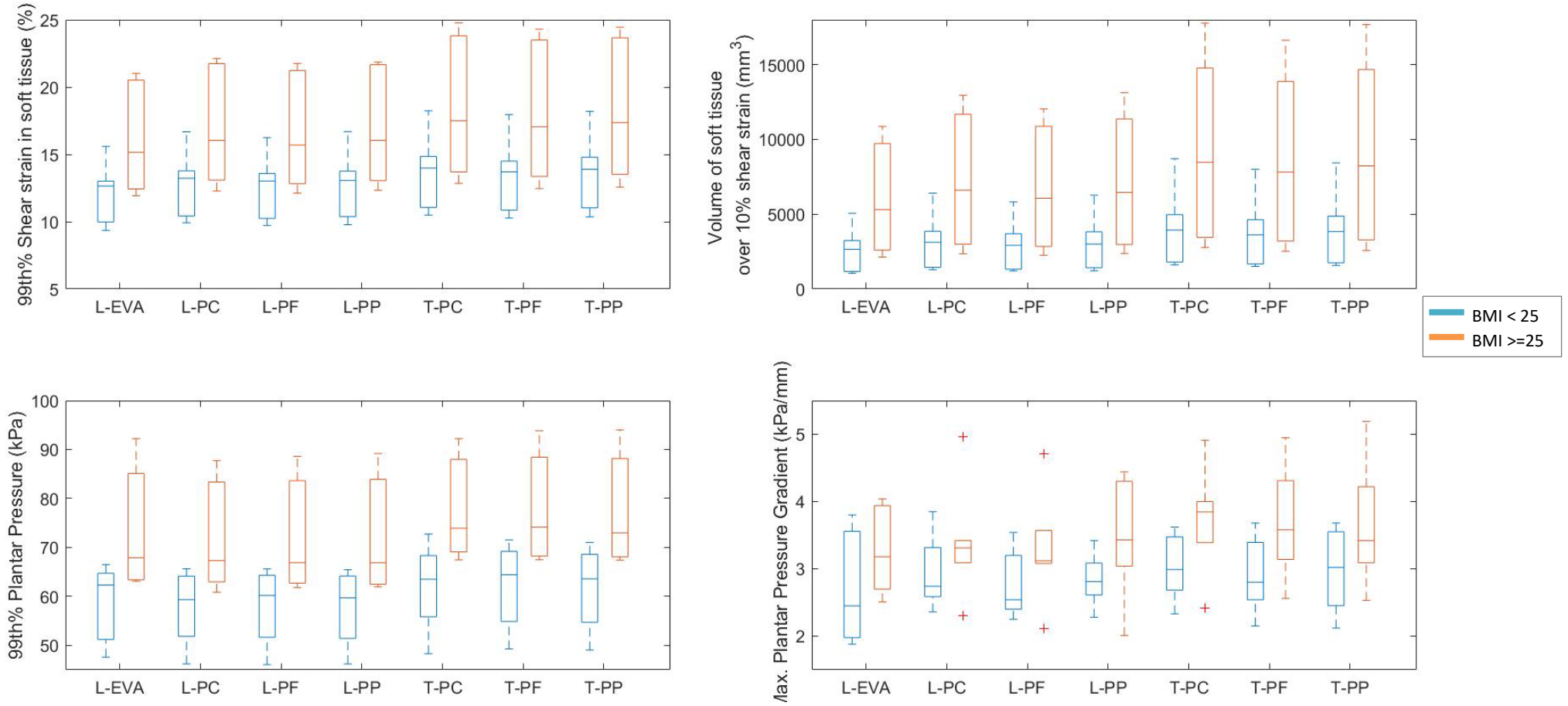

Figure 6.4: Comparison of different FO materials and shoe types separated into 7 participants with BMI<25, and 6 participants with BMI>=25. Coding System: L-XX = leather shoe; T-XX = training shoe; X-EVA = EVA FO; X-PC = Poron Cushioning FO; X-PF = Poron Firm FO; X-PP = Poron Firm + Plastazote FO.

6.2.2 Orthosis Shape

The pressure, pressure gradient and shear strain metrics were higher for the flat FO models than their total contact equivalents for the five participants tested, with the exception of the RA11 trainer models (Figure 6.5. Figure 6.6). The location of the peak pressures remained under MH1 for the flat orthoses, though a secondary peak was also present in the lateral forefoot, which was more distinct than with the total contact orthosis (Figure 6.5A&B). Similarly, while the peak shear strain still surrounded MH1, the regions surrounding the other metatarsal bones were also elevated in the flat FO models (Figure 6.5C&D).

The trends in 99th% plantar pressure across the orthosis and shoe configurations were the same for the flat orthosis as for the total contact, with EVA producing higher pressures than the Poron configurations and the trainer higher than the leather shoe. However, there were greater differences in pressure between FO/shoe types for the flat orthoses than the total contact. This was particularly the case comparing EVA to Poron orthoses, and was accompanied by varying contact area between the orthosis and limb (Table 6.5). Additionally, differences between the flat and total contact FO pressure predictions were greater for EVA compared to Poron with the leather shoe (34.9-49.6kPa *vs.*20.2-37.4kPa differences respectively), (Figure 6.6). The flat orthoses also caused far greater variation in pressure gradient predictions than the total contact orthoses, both between model configurations and between participants (Figure 6.6).

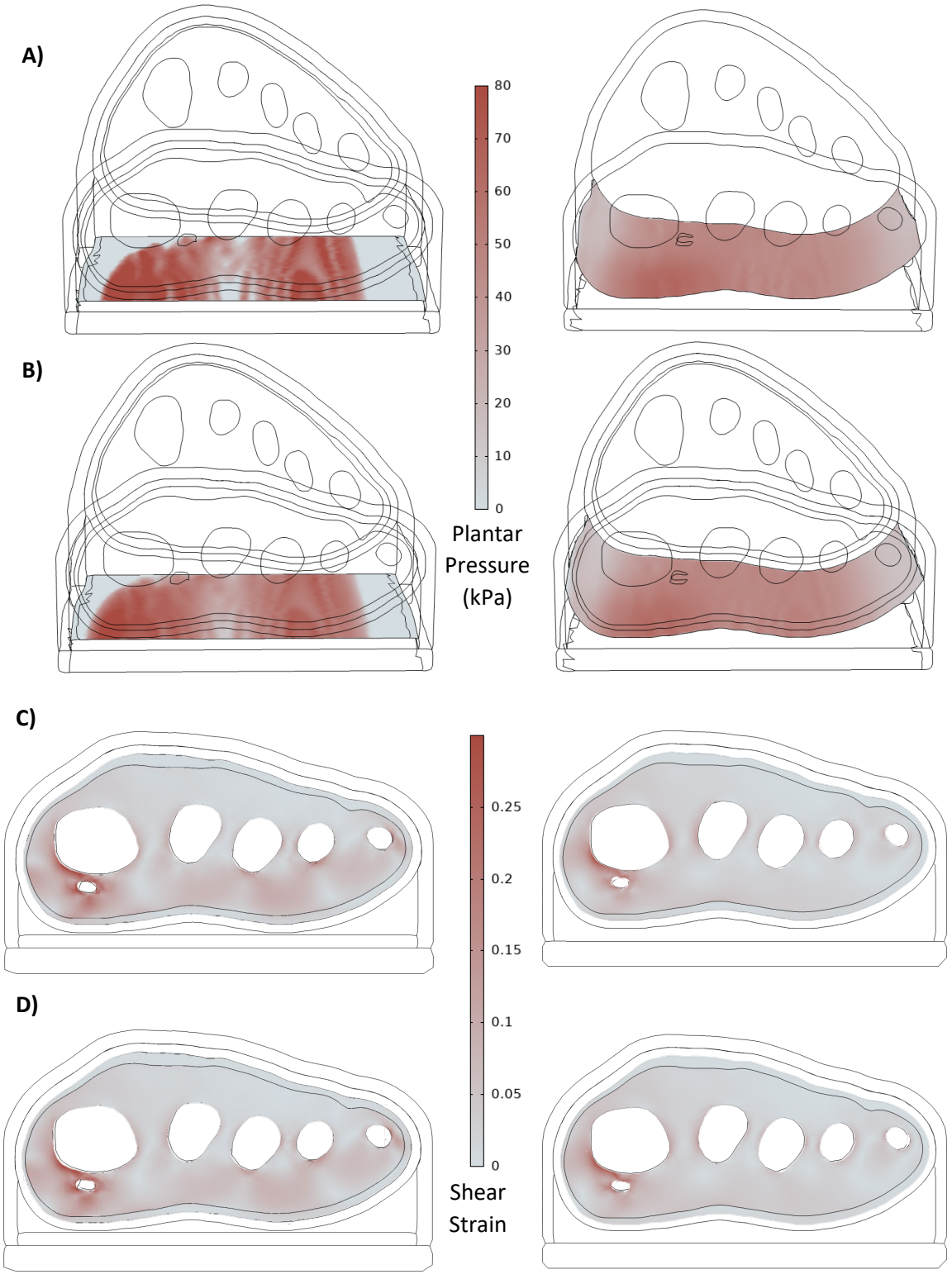

Figure 6.5: Flat vs Total Contact FO model predictions for RA2 for plantar pressures for **A)** EVA FO (L_EVA) and **B)** Poron Cushioning FO (L_PC); and shear strain for **C)** EVA FO (L_EVA) and **D)** Poron Cushioning (L_PC). Note – the lateral sesamoid was not in-plane with the lateral sesamoid so is not present in C&D.

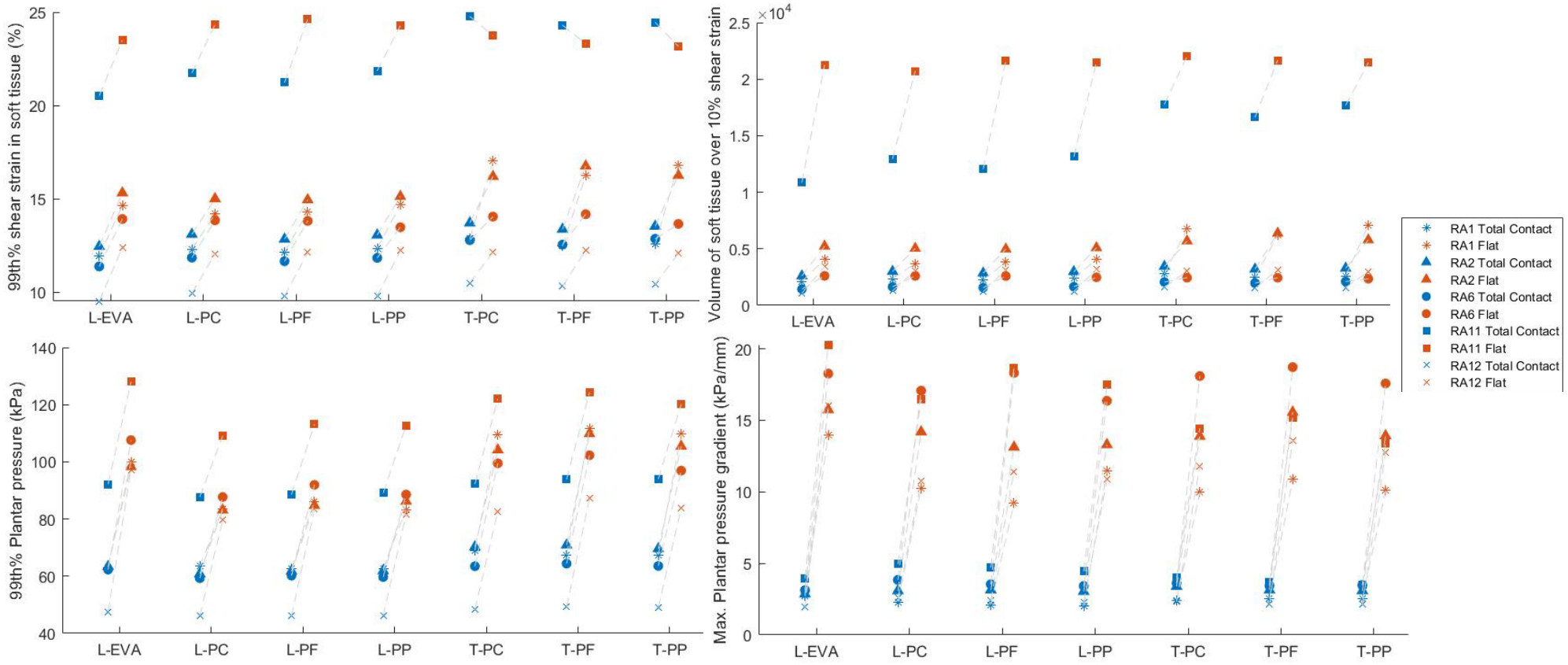

Figure 6.6: Model predictions comparing flat and total contact FOs for RA1, RA2, RA6, RA11, RA12. Coding System: L-XX = leather shoe; T-XX = training shoe; X-EVA = EVA FO; X-PC = Poron Cushioning FO; X-PF = Poron Firm FO; X-PP = Poron Firm + Plastazote FO.

Table 6.5: Differences in pressure and contact area between EVA and Poron Cushioning for the Flat and Total Contact FOs

	99th% Plantar Pressure, kPa	**99th% Plantar Pressure, kPa**	**Contact Area, mm² (proportion of total area)**	**Contact Area, mm² (proportion of total area)**
	L_EVA	**L_PC**	**L_EVA**	**L_PC**
RA1 – Flat FO	100.1	83.6	2299 (73.9%)	2518 (81.0%)
RA1 – Total Contact FO	63.1	63.5	(100%)	(100%)
RA2 – Flat FO	98.3	83.2	3002 (69.9%)	3376 (78.6%)
RA2 – Total Contact FO	63.4	60.8	(100%)	(100%)
RA6 – Flat FO	107.6	87.7	2009 (68.1%)	2267 (76.9%)
RA6 – Total Contact FO	62.3	59.3	(100%)	(100%)
RA11 – Flat FO	128.0	109.1	2524 (76.1%)	2692 (81.1%)
RA11 – Total Contact FO	92.2	87.8	(100%)	(100%)
RA12 – Flat FO	97.1	79.7	2812 (71.0%)	3083 (77.8%)
RA12 – Total Contact FO	47.6	46.2	(100%)	(100%)

The shear strain trends across FO/shoe types were not consistent between the flat and total contact orthosis for these five participants. Where strain produced by the EVA orthosis (L_EVA) was consistently lower than the three Poron orthoses (L_PC/PF/PP) for the total contact FO, it was usually higher for the flat FOs. A similar pattern was observed in the Poron Firm configurations (L_PF and T_PF), which tended to produce lower strains than the other Poron orthoses for the total contact FOs (in 9/10 instances across the five participants and two shoe types). However, for the flat FOs, the strain differences between Poron orthoses were more varied.

Finally, there were differences in how some of the model predictions varied between participants for the flat compared to total contact orthoses, showing how their reactions to orthosis shapes differed. For example, RA6 experienced much smaller differences in tissue volume over 10% strain predictions between flat and total contact results (234 to 1172mm^3 difference) than any of the other four participants (1328 to 10386mm^3 difference). Additionally, RA11 was the only participant to display higher 99th% shear strain with a total-contact FO than a flat FO, which occurred only in the trainer models. The differences were -1.28 to -1.01% strain for RA11 trainer models, and 0.8 to 4.24% strain for the other four participants.

6.3 Discussion

The aim of this study was to address whether computational models of the forefoot could be used to assess FO and footwear design with the view of optimising their effectiveness for individuals with RA. Three design parameters were assessed: FO material, shoe type, and FO shape. Differences in 99th% shear strain, volume of tissue over 10% shear strain, and 99th% plantar pressure predictions were observed for all three design parameters. There were significant differences between the leather and training shoes for both strain variables and plantar pressure. This was also the case when comparing the stiffer EVA orthosis with Poron Cushioning, Poron Firm, or a combination of Poron Firm and Plastazote. The differences between Poron Cushioning and Poron Firm or Poron Firm and Poron+Plastazote were consistently significant for the strain variables but not for the pressure. Poron Cushioning and Poron+Plastazote were only borderline significantly different for the shear variables. Case studies comparing the total contact FOs with flat FOs found that the flat orthosis produced higher shear strain, plantar pressure and pressure gradients.

Previous experimental studies of people with RA [62] and computational modelling studies of single healthy or diabetic individuals [161, 169, 240] have shown greater pressure reductions with softer material orthoses. The present study concurs with those findings, as the softer Poron materials led to significantly lower plantar pressures than the stiffer EVA. The plantar pressure reduction due to increased contact area with a total contact orthosis compared to a flat orthosis also agrees with literature [158, 170]. Goske et al. [158] identified that FO material had less impact on plantar pressure reductions than FO shape, which was also the case in the present study (Figure 6.6).

Goske et al. [158] also found that while Poron Cushioning reduced pressures more than EVA for a flat FO, EVA performed better as a thin (6.3mm) FO of fully conforming shape (similar to the present total contact FO). They attributed this to the softer material bottoming out. In this study, the minimum FO thickness was 3mm, and though the pressures were still generally higher for the total contact EVA orthosis compared to the Poron equivalent, the difference was much reduced compared to the flat equivalents. Though the maximum displacements of the Poron Cushioning total contact FOs were much closer to the minimum FO thickness of 3mm than occurred with the EVA FO, neither FO seemed to completely bottom out (Figure 6.7). This may explain why the present plantar pressure predictions were not quite aligned with Goske et al.'s findings for the thin total contact shape. However, the shear strain trends were similar to those reported by Goske et al.'s, with lower strain predictions for the softer FOs for the flat model but not the total contact. It is possible that the shear strain predictions were more affected by the FO nearly

bottoming out, than the pressure predictions were. The flat FO trends were likely due to the reduced contact area, and thus increased pressures and shear strain, that occur with the flat EVA orthosis compared to the Poron (Figure 6.5). With the total contact orthosis, material stiffness cannot affect contact area and so those variations would not occur. This implies that optimal material choice may vary depending on FO shape and how well it represents the plantar profile of the foot.

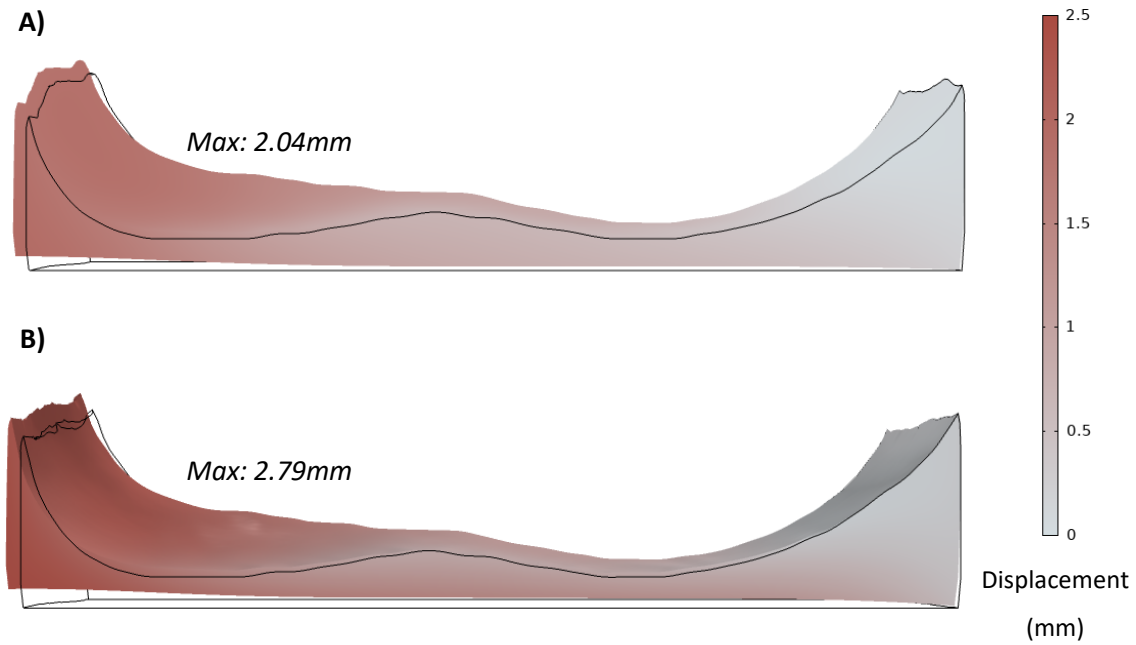

Figure 6.7: Example displacement plots for the FO region of the RA2 models (using scale factor of 1), for **A)** Total contact EVA FO; **B)** Total contact Poron Cushioning FO.

None of the mentioned modelling studies assessing FO material examined strain or shear stresses, but Cheung et al. [161]'s FEA study found lower von Mises stress with softer material orthoses in the forefoot where the FO was flat, which corresponded to their pressure results. The flat FOs in the present study also produced lower shear strain for the softer Poron compared to EVA. However, the pressure and shear strain trends did not correspond for the total contact models, suggesting again the influence of orthosis shape was dominant. Zhang et al. [172] found that a moderate stiffness FO produced lower forefoot von Mises stress than stiffer or softer materials. However, this was potentially confounded by changes in arch height and lateral wedge angle which were being assessed concurrently. They did not report plantar pressure so it is unknown whether their pressure and internal stress trends would be consistent.

The total contact EVA orthosis produced higher plantar pressures but lower shear strains than the Poron orthoses, which may be key to FO design analysis. Currently, FO effectiveness is often tied to plantar pressure reductions as that can be easily determined experimentally, and has been

shown to aid people with diabetes. However, as evidence for FO effectiveness in treating RA is more conflicting, additional parameters must be examined. Shear strain may be more indicative of tissue damage risk than plantar pressures, and if the two parameters do not align then optimal orthosis choice may be affected. Previous modelling studies have often reported von Mises or normal stress in the soft tissues in addition to plantar pressure, if stress/strain has been reported at all. One study did report that both pressure and compressive strain under the MHs decreased with increasing FO thickness [168]. However, the peak strain trends in the neighbouring tissues were more varied, and may not have reflected the peak pressure trends, though direct comparisons for those neighbouring regions were not provided. Further research would be required to corroborate and understand the causes of potential discrepancies between plantar pressure and internal shear strain in these circumstances.

The training shoe unexpectedly caused higher pressure and shear predictions than the leather shoe. It was thought that the higher sole thickness and softer, less restrictive training shoe upper material would lead to lower predictions of pressure and strain. This was based on previous literature which showed the benefits of increased FO thickness, and running shoes compared to both control and orthopaedic footwear [99, 158, 168]. Possible explanations for the present results stem from the models' representation of the shoe. Previously identified benefits of running shoes may have been due to better shoe fit and conformity, as footwear prescribed for RA often features extra depth to accommodate deformity and FOs [241]. In these models, the fit of the shoe types around the foot and orthosis was consistent, so any pinching of a stiff leather shoe on the limb would not have been included. Another possibility is that the models were more representative of a soft compliant leather shoe, as are often prescribed to those with RA. The leather upper material properties may have been sufficiently stiff to provide support but not so stiff as to negatively interact with the foot. Thus, the leather shoe may have taken on a greater share of the applied load, easing the load applied to the foot in a way the training shoe model could not. The material properties applied to each shoe were homogenous, so the training shoe upper did not include any reinforcement structures that are present in reality and may not have provided the expected level of support. However, while the shoe types may not have been truly representative of real-world examples, the significant differences present in the results show that the models can distinguish between simplified representations of different shoe stiffness and geometry. This suggests that the models would be able to compare other, more accurately modelled, footwear types.

The significant differences between the model configurations would imply that the models are suitable for assessing FO and footwear design. However, the differences were generally quite small, and therefore may not be clinically significant. The mean differences in 99^{th}% shear strain

between FO materials were less than 1% strain, which may indicate that material choice would not have an appreciable real-world effect on the internal soft tissues. However, the majority of the strain results were significantly different, stemming from the consistency of the trends between the design parameters. This would suggest that the differences were due to the design parameters rather than any other aspect of the model or method used, and that the models were suitable for purpose.

Regarding the pressure results, a previous experimental study examining pain and pressure during gait found that two different custom-made FOs reduced mean peak pressures by 34% and 46% compared to a flat EVA orthosis [202]. These pressure reductions were accompanied by lower pain scores, though those percentages may not have been the minimum pressure reductions required to reduce pain. If a relationship between pressure and pain reductions is assumed, then it is possible that the pressure differences between FOs in the present study would be too small to affect pain. However, there is much debate over whether plantar pressure and pain are related, with several other studies finding no relationship between the two [38, 106, 149]. As such, it is difficult to draw conclusions over whether the differences between FOs in the present study would be clinically significant, in terms of pain reduction, based on the plantar pressure predictions alone.

Also of note, was that the inter-participant variability in pressure and strain predictions was far greater than the differences between design parameters (Figure 6.3). This was particularly the case for those with BMI>=25, who showed both a greater range of predictions for each model configuration and increased differences between model configurations (Figure 6.4). There is an association between increased BMI and factors such as pain and joint swelling due to RA [175]. Thus, ensuring interventions meet their needs is vitally important, when the design choices may have more impact. It may be that generic prefabricated FOs are suitable for some individuals, such as those with normal BMI, for whom different design parameters have limited impact. However, custom-made FOs may provide far more benefits to other individuals, such as those with high BMI, where there may be greater scope for improving the FO through design choices.

Additionally, the trends between the design parameters were not always consistent across all participants – seen in the pressure and pressure gradient predictions, and the differences between participants for the flat vs total contact FO comparisons. The four participants who displayed lower plantar pressures and higher pressure gradients for EVA compared to Poron covered the full range of clinical and morphological data (Table 6.6), as well as having differing plantar profiles (Figure 5.2). There was also nothing that set these four apart in terms of plantar pressure distribution, with the peaks still concentrated at the medial forefoot. In examining the

maximum displacements in the FOs, there was no indication that the difference in trends for these four participants was due to the softer material Poron FOs bottoming out, as was discussed earlier. It is possible that there were other morphological features, e.g. bone position or size, common to these participants that were not assessed here and resulted in the differing trends.

Table 6.6: Clinical and morphological data (with rank in the full dataset) for the 4 participants with differing pressure trends

	RA1	**RA3**	**RA5**	**RA10**
Weight (kg)	82 (10/13)	85 (11=/13)	69 (6=/13)	66 (5/13)
BMI	26.7 (8/13)	30.9 (13/13)	21.7 (1/13)	24.8 (7/13)
Disease duration (years)	14 (9/13)	1 (1/13)	3 (3/13)	35 (13/13)
LFIS-IF (0-21)	13 (7=/13)	5 (2=/13)	18 (13/13)	4 (1/13)
Instances of bursae (0-9), erosion (0-5), synovial hypertrophy (0-5)	8 (9=/12)	3 (3=/12)	0 (1/12)	1 (2/12)
Depth of tissue under MH1 (mm)	12.9 (10/13)	18.8 (3/13)	14.1 (9/13)	9.9 (13/13)
Unloaded lateral offset of sesamoid from MH1 edge (% of MH1 width)	40.0 (12/13)	14.2 (3/13)	29.0 (9/13)	72.0 (13/13)
Average principal curvature of MH1 (mm^{-1})	0.112 (1/13)	0.168 (11/13)	0.163 (10/13)	0.120 (3/13)

The differences between participants when comparing FO shape may have been due to differences in plantar profile and thus contact areas. Though all five participants had similar proportions of contact area for the flat FO models, there were considerable differences in the absolute contact area. The differing contact areas between participants seemed to correspond somewhat to the pressure predictions but not perfectly. This may have been because pressure predictions were also influenced by participant weight and thus applied load – RA11 with the highest applied load of the five also had the highest pressure predictions despite ranking 3/5 in contact area. The potential relationship between plantar pressures and contact area also did not seem to hold true for the training shoe, potentially due to the limitations mentioned previously in the representation of the shoe types.

The difference in trends between participants when comparing FO shape also lends credence to the thought that shoe fit would affect the model predictions. The total contact FO models had no space within the shoe due to the perfect conformity assumed. With the flat FO models, there was space available in the shoe that the foot could displace into freely. However, the volume of space available was dependent on each of the participants' plantar profile and so varied. This may have caused the difference in trends between shoes for the flat vs total contact models and between

participants for the flat FOs. These differences in trends between participants show the importance of assessing FO design with clinically relevant people, and on an individual basis.

Generally, there were no significant differences in the pressure gradient results between the different FO materials/shoe types. This reflected the previous chapter's findings that pressure gradient had little to no significant correlation with the participants' clinical or morphological data (see Section 5.2.3). It was theorised that this was due to the total contact FO considerably reducing the pressure gradients, limiting differences between cases. This was corroborated here, where the flat orthosis models predicted considerably higher gradients, and increased differences both between orthosis/shoe types and participants. The flat FOs were only modelled as case studies for a limited number of participants and so statistical analyses could not be performed. It is possible that with a larger sample size there would be significant differences in pressure gradients present between the different FO materials and shoe types for the flat FOs. Pressure gradients have been used as predictors of tissue damage risk as an external representation of underlying shear strain, and may be particularly relevant in the forefoot [181]. However, for total contact FOs, pressure gradients may not be as helpful in assessing the effects of different FO designs due to the consistently low magnitudes. Despite that, it may still prove to be a useful parameter to assess FO geometries where the contact area between the limb and orthosis varies.

There were some limitations to the present study. Firstly, though the flat orthosis results provided a strong indicator that the models were differentiating between the two orthosis shapes and highlighted differences between individuals, only five individuals were modelled. This was due to the increased solving time and convergence difficulties that occurred with the flat FO models due to the differing contact conditions between the limb and orthosis. The flat FO models took considerably longer to solve than the total contact equivalent (e.g. RA6 L_EVA: Flat – 28.35h, Total Contact – 8.05h), and many of the participants' models did not converge and so could not be included in the analysis. The participants' characteristics were compared for those whose models did converge with those whose did not (Table 6.7). The participants whose models converged had a range of characteristics, with their clinical and morphological data falling at the lower, middle and higher end of the full participant dataset range. Thus, the lack of convergence for the other participants did not appear to be due to any of the above parameters. As discussed in Chapter 5, the MR data was not originally intended for modelling purposes, so the forefoot was not positioned to represent loading and as such the plantar profiles of the participants varied considerably. In the context of the flat FO model, this resulted in the amount of distance between orthosis and limb, thus contact under any given load, also noticeably different between participants. The participants whose models converged averaged a distance of 2.53mm between the plantar surface of the limb and the orthosis, against an average of 3.35mm for those who

didn't converge. This would suggest that the convergence issues were related to the specific MR data used for this study, and that MR data collected in a stance position with low, nominal loading may allow these models to converge more reliably. To confirm the trends observed in this study regarding FO shape, a larger population would need to be modelled.

Table 6.7: Clinical and morphological data (with rank in the full dataset) for the participants whose flat FO models converged

	RA1	**RA2**	**RA6**	**RA11**	**RA12**
Weight (kg)	85 (10=/13)	69 (6/13)	58 (1/13)	108 (13/13)	60 (2/13)
BMI	26.7 (8/13)	28.3 (9/13)	22.3 (4/13)	30.2 (12/13)	22.9 (5/13)
Disease duration (years)	14 (9/13)	8 (7/13)	30 (12/13)	5 (5/13)	28 (11/13)
LFIS-IF (0-21)	13 (7=/13)	12 (6/13)	5 (2=/13)	17 (12/13)	16 (11/13)
Instances of bursae (0-9), erosion (0-5), synovial hypertrophy (0-5)	8 (9=/13)	4 (5=/12)	3 (3=/12)	4 (5=/13)	NA
Depth of tissue under MH1 (mm)	12.9 (10/13)	10.9 (2/13)	12.5 (3/13)	20.8 (1/13)	15.6 (7/13)
Unloaded lateral offset of sesamoid from MH1 edge (% of MH1 width)	40 (12/13)	17.3 (4/13)	39.8 (12/13)	5.7 (1/13)	32.9 (10/13)
Average principal curvature of MH1 (mm^{-1})	0.112 (1/13)	0.118 (2/13)	0.169 (12/13)	0.156 (9/13)	0.128 (4/13)

Another limitation of the models was in the total contact FO shape and how that interacted with the limb based on the static loading applied. Total contact orthoses provide benefits such as reduced plantar pressure, pain and disability, through the increased contact area [170, 242], as was shown in this study in the pressure and strain reductions. However, built-up regions of an orthosis can also cause adverse effects if improperly positioned relative to the foot [168]. The static loading applied in these models did not allow for relative movement of the foot which could have caused negative interactions with the orthosis. Thus, dynamic modelling could provide huge improvements in being able to examine how the contact points between the orthosis and forefoot would change from midstance through to toe-off, and the subsequent effect on tissue damage risk. The use of dynamic modelling would also allow pressure-time integrals (PTIs) to be assessed, which may relate to pain better than peak pressures [38], and so would aid in determining whether differences between FOs are clinically significant.

For dynamic modelling to be introduced, the bone constraints used may also have to be re-examined. The fixed bone constraints applied to the metatarsal heads were more representative

of a healthy forefoot, where the bones are relatively stable thanks to structures such as the deep transverse metatarsal ligament. However, RA can cause subluxation of the MTP joints, and eversion of the subtalar joint [231]. Thus, the MTP joints are destabilised, resulting in increased relative movement between the joints, particularly rotation of MH1. In the current static loading condition, the fixed constraints were deemed a suitable simplification, as little bone movement would be expected and the constraint improved model stability. With the addition of dynamic loading, a better representation of the relative bone displacement caused by RA may be required to allow more accurate assessments.

6.4 Summary

In this study, it was found that with a total contact FO, stiffer FO materials generally resulted in higher plantar pressures but lower soft tissue shear strains. However, inter-participant geometry and loading differences led to far greater variability in FO pressure and soft tissue strain than materials. A leather shoe produced lower pressures and shear than a training shoe, which may have been due to the representation of the shoe types in the models. Flat FOs caused far greater pressure, pressure gradients and shear strain than total contact FOs. Additionally, in a limited sample size, FO shape seemed to affect the strain trends between orthosis materials. Also of note was that the trends between FO and shoe types were not always consistent between shear strain and plantar pressure, emphasising that considering pressure alone may not benefit FO design.

Though there were some limitations to the models, including model convergence with the flat FO, the models were capable of determining significant differences between the different design parameters, and between participants. Thus, the models have fulfilled the aim of the research question and would be suitable to assess different FO and footwear design for individuals with RA. FO designs have not been previously assessed through computational modelling for multiple individuals with RA, and so this study has provided further understanding of the internal effects of loading and variability experienced by people affected pathologically by the condition.

Chapter 7 Overall Discussion

This research aimed to investigate how different lower limb orthosis designs affect the foot and ankle soft tissues, both in terms of the mechanical interactions and the microclimate conditions they generate. These were evaluated with respect to the relative risk of tissue damage in vulnerable bony prominences on the plantar aspect of the foot. This was assessed through two different scenarios: healthy individuals wearing AFOs, and individuals with RA wearing FOs. Three research questions were posed to fulfil this aim, and the findings that have addressed these questions have been summarised (Figure 7.1) and are discussed further in the next section:

- Research question 1: How does AFO design affect the physical conditions between the device and skin interface? *This was answered through a combination of experimental testing and computational modelling*. *The physical conditions were affected by AFO geometry and material. This was evidenced by differences in the interface pressures and microclimate measured experimentally and predicted plantar pressures at the interface of the computational models.*
- Research question 2: To what extent can computational models of individuals with morphological changes in the forefoot distinguish between different aspects of RA disease? *This was addressed through computational modelling of 13 individuals with RA to determine whether the model predictions would vary depending on condition-related factors and compared to a healthy individual. Through this, it was determined that the simplified forefoot models could distinguish between some aspects of disease severity or vulnerability. As such, the models were suitable to assess orthosis design requirements for individuals with differing presentations of RA.*
- Research question 3: To what extent can computational models provide knowledge to inform the design of safe and effective lower limb orthoses? *This was considered for both AFO and FO design, for which the merits and limitations of the simplified forefoot models in assessing orthosis design were examined. The computational models were able to distinguish between some of the orthosis design parameters, such as interface material, FO shape and shoe type, as seen in the differences in computational biomarkers. However, there were limitations to the simplified models in differentiating between AFO fit, which may have been due to how the parameter was represented in the models.*

Increased understanding of how different orthosis designs may affect soft tissue health, and how that may vary between individuals, will aid in improving device effectiveness and user satisfaction.

There are different aspects to the novelty of this combined experimental and computational work which have improved that understanding:

- Consideration of how AFOs affect soft tissue health, both experimentally and computationally – previous research in this area has been limited, and microclimate has not been assessed before (see Chapter 2). Novel contributions included:
    - Quantitative measurement of the devices' effect on microclimate and interface pressure metrics experimentally (including spatial and temporal aspects), and computational model predicted plantar pressure, gradients and underlying shear strain,
    - Assessment of the influence of static and dynamic loading at the orthotic interface with comparisons between devices,
    - Assessment of the role of sock material in the management of microclimate,
- Computational assessment of orthosis designs through modelling of multiple individuals, and in the case of the FO modelling, pathological individuals with RA – most previous studies have modelled a single healthy individual (see Sections 2.3.2 and 2.3.3),
    - This also included comparison between computational biomarkers and clinical and morphological data for the individuals with RA,
- Representation of both the shoe sole and shoe upper in the modelling – despite their impact on the mechanical interactions of orthoses, and subsequent soft tissue pressures and strains, they have frequently been excluded from previous modelling research.

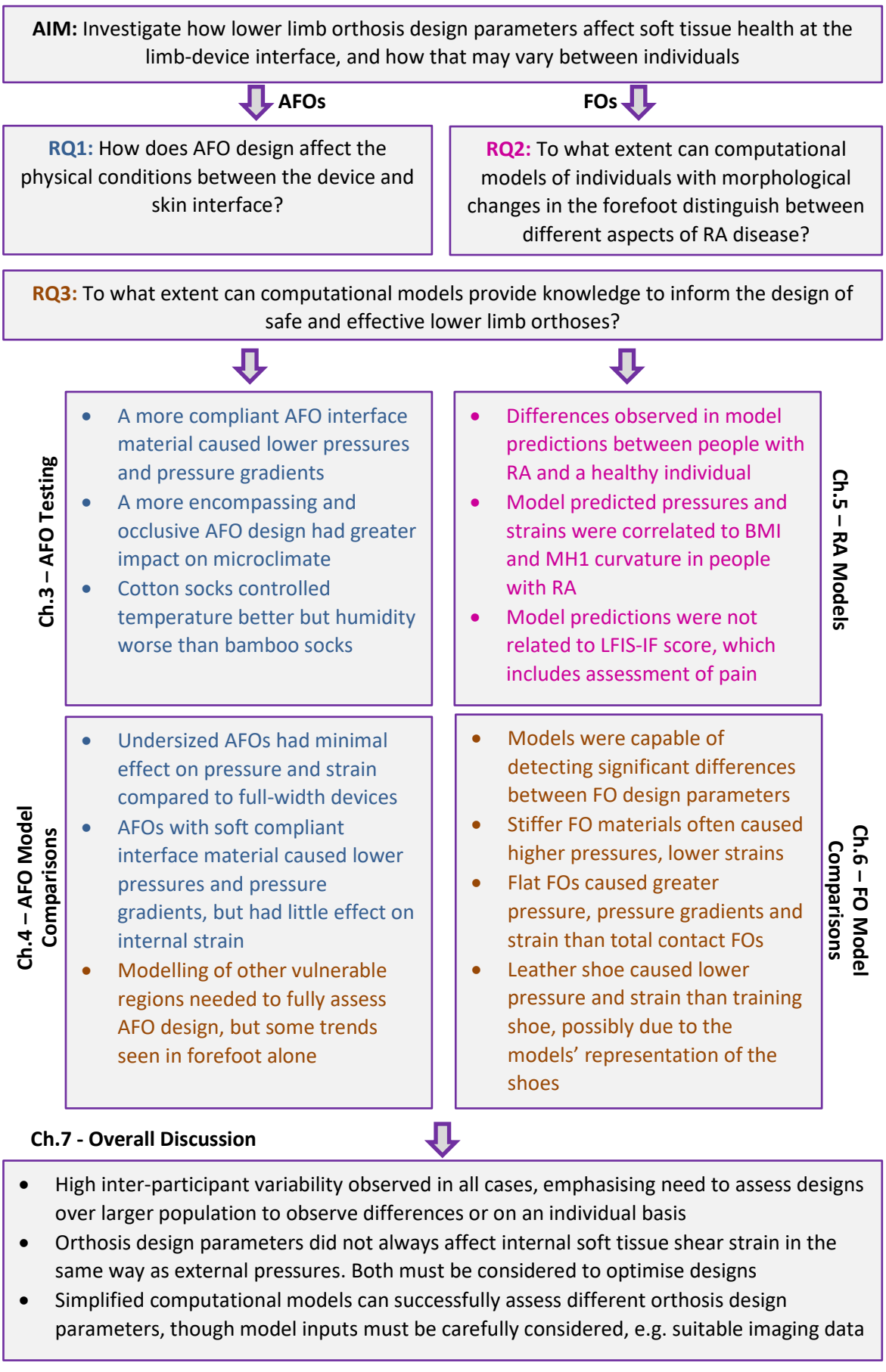

Figure 7.1: Schematic summarising research questions (RQ1-3) and findings. Findings are colour-coded to the relevant research question.

7.1 Summary and Applicability of Findings

Throughout this research, a variety of orthosis design parameters were assessed for their effect on indicators of damage risk to both superficial and deep soft tissues. While the small sample sizes limit the generalisability of the findings and statements of optimal designs, trends were observed which were substantially consistent across the different studies. Orthosis material had a clear impact on plantar pressures both experimentally and computationally, with softer materials – a cushioning layer on an AFO, or the FO material itself – generally resulting in lower interface pressures and pressure gradients. However, the models did not predict a corresponding reduction in shear strains in the soft tissues (particularly in the 99th% shear strain predictions), with the softer materials causing minor differences or sometimes higher tissue strains. On the other hand, FO shape affected plantar pressures, pressure gradients and shear strains, with a flat FO generating higher values of these computational biomarkers than an FO in total contact with the limb. The effect of AFO fit was assessed through computational modelling, but there was little difference in the forefoot pressure and strain results between a normally fitted full-width AFO and an undersized device. This may have been due to lack of contact between the participants' limbs and the undersized device's edges (discussed in Section 6.3).

The experimental testing also allowed observation of the effect of AFO design on microclimate at the AFO/skin interface. Both AFO and sock material affected the interface temperature and humidity, alongside the AFO geometry and how encompassing the devices were at different foot locations.

Collectively, experimental and numerical analysis of these different design parameters provided evidence to build our understanding around research questions 1 and 3. Greater understanding of how the different orthoses affect the interface conditions was gained, and by displaying where design parameters did and did not affect metrics indicative of tissue damage risk, the models were shown to be promising for assessing orthosis design.

One of the common themes identified was the high degree of inter-participant variability, which supports clinical knowledge of patient variability and the differing orthosis requirements between individuals. Previous experimental research examining plantar pressures for individuals with RA has also shown significant inter-participant variability [33, 38]. The present research has revealed that this variation is also predicted for the internal effects of orthoses, in addition to the plantar pressures. In fact, in many cases it was found that differences in the pressure and shear strain results were greater between participants than between design parameter variables. The design parameters, such as FO material and addition of cushioning to an AFO, were chosen based on clinical use so distinction between the variables would be expected. That the inter-participant

differences were often more noticeable than the differences between design parameters emphasises the need for personalised devices. It also indicates that future modelling studies of standardised orthosis design should include multiple participants, rather than just parametric assessments with the same individual. This is particularly necessary as observations for one individual may not apply to others, as shown by the trends between orthosis design parameters sometimes being inconsistent between participants. For example, with the stiffer FO material it was observed that 4/13 of the participants' models predicted lower plantar pressure results rather than the higher results observed in the other nine participants (Chapter 6). Thus, by modelling a larger sample, improvements to orthosis design can be identified both across a population in general, and for subsets of the population who may have different requirements. This would allow people more at risk of tissue damage to be identified, who may need more consideration given to their orthosis design, and could provide a balance between standardised and personalised treatment.

For that reason, the capability of the simplified forefoot models to differentiate between individuals with differing presentations of RA was assessed (see research question 2, Chapter 5). This determined whether clinical factors that could affect orthosis requirements or prescription practices were observable through the simplified model predictions. BMI was shown to have a clear impact on model parameters, which did not appear to be due to differences in participant weight and thus applied load (see Section 5.3). As such, this may be taken forward as something to consider in a clinical setting if individuals with higher BMI are known to be more at risk of tissue damage (see Section 5.3). LFIS-IF score, a measure of pain and discomfort specific to RA [243], was also compared to the model outcome measures, as currently FOs are often prescribed, at least in part, to alleviate pain. However, as there was no correlation between the two, the selected modelling outcome measures may not correspond with predictions of pain, be able to identify higher-risk participants in that regard, or how effective orthosis designs would be at reducing pain. The lack of correlation may have been due to the subjectivity of the pain metric or the model simplifications (see Section 5.3).

Another notable finding of this research was the differences between the results for plantar pressures and shear strains in the soft tissues. For both modelled orthosis types, AFOs and FOs, the plantar pressure and internal strain trends between orthosis designs were not always aligned. This would suggest that interface conditions, and how superficial tissues are affected, may not correspond to the strains occurring in the deeper tissues. This could have significant clinical implications with regards to minimising tissue damage risk through orthosis design. It also reaffirms previous research which has argued that external pressure measurements may not be indicative of risk to the deeper soft tissues [147]. Clinically, there is still a focus on reducing the

external pressures as those are easier to measure than internal strain, and reducing the interface pressure metrics may help protect the superficial tissues. However, as this research has shown, an orthosis optimised for plantar pressure reductions may not be optimal for reducing internal shear strains and so risk of deeper tissue injuries. This may also link to the uncertainty around the effectiveness of FOs in the treatment of RA, as offloading the superficial tissues tends to be targeted to protect them from high plantar pressures. This becomes even more important as the modelling studies showed the peak soft tissue strains were occurring in the deeper tissues surrounding the bones, rather than the superficial tissues. It has been previously shown in pressure injury development, that while applied loads may lead to superficial injuries, often damage starts in the deeper tissues and propagates outward [244]. As such, the effect that different orthoses have on those deeper tissues must be considered. If only the external effects are examined, the internal strains may not reflect this, and so the orthoses may prove less effective than anticipated.

The computational models developed can be used to assess how orthoses affect deeper soft tissues as well as superficial tissues, and so could be used to aid orthosis design. However, it would not necessarily be feasible to perform this in a clinical setting due to availability of imaging and model generation and analysis time, for example. Thus, there is a need for other methods that can assess the deeper tissues. In the treatment of RA, clinicians often use palpation and ultrasound to assess manifestations of RA, and how the tissues have been affected [245-247]. However, this does not provide a full understanding of how at risk the soft tissues would be under loading. Researchers have begun to explore the potential of using ultrasound elastography as a non-invasive technique of assessing soft tissue stiffness, and displaying the strains occurring internally under compressive loading [248-250]. This could be used alongside the computational modelling methods of FO optimisation that were explored here. The models could pre-determine optimal orthosis designs for individuals with certain tissue properties or how orthoses could best aid vulnerable regions indicated by elastography. These relationships between manifestations of RA and optimal orthosis design could form a database which could then be referred to through point-of-care elastography to aid FO prescription. This would provide a clinical method of understanding the how the deeper tissues are being affected on an individual basis, and could be more effective than tailoring orthosis design through pressure measurements. Further research would be required to explore this, and to understand how the methods could be used in the diagnosis and orthosis prescription processes.

Measuring external pressure gradients has also been previously proposed, in areas such as support surface and foot research, as a more reliable method of assessing tissue damage risk than using pressure measurements alone, as they may relate better to internal shear strains but can

still be easily measured experimentally [179, 181, 183]. In the experimental testing (Chapter 3), pressure gradients provided clearer distinction between AFOs than the pressures. However, these could not be compared to the AFOs' effects on internal tissues which were not assessed experimentally, and the computational models, which could compare the utility of different metrics, provided less clarity. In the AFO models, the pressure gradients between orthoses followed the same trends as the pressures, and neither corresponded well to the shear strain predictions. In the FO models, the pressure gradient trends between orthosis materials were far more like the internal strain trends than the pressure trends. However, for the total contact FOs, these differences in pressure gradients were minimal and often not significant. As such, this research has not provided conclusive evidence for the effectiveness of pressure gradients and their relation to how the underlying tissues are affected. With that said, the results from Chapter 5 did show a significant correlation between the curvature of the first metatarsal head (MH1) and the model pressure gradient predictions. This would suggest that to some degree the pressure gradients were related to the underlying bony anatomy. Additionally, the differences in trends observed between the pressure gradients and peak pressure metrics in some of the cases shows the benefit of assessing pressure gradients, through the additional insight they may provide that peak pressures cannot.

It may also be that the full benefits of pressure gradients over peak pressures could not be observed in the specific scenarios that were modelled. Both the AFOs and FOs modelled only contacted the foot in the plantar region, and the pressure metrics were obtained at this interface. Thus, the effect that the metatarsal head bony prominences had where the soft tissue coverage is thinnest, at the medial aspect of MH1, may not have been fully captured in the plantar pressure and pressure gradient predictions presented. For assessing AFO designs, pressure gradients could still prove effective in other regions of the foot and ankle where the device may apply more direct loading to the bony prominences (e.g. the malleoli), as has been seen in support surface and seating literature [179, 251].

The 99th% shear strains predicted by the models ranged from 13-21% in the AFO models and 9-25% in the FO models, which are lower than thresholds for high risk of tissue damage that have been reported in literature. While there is still much unknown about specific injury thresholds, due to the number of influencing factors, previous research has compared muscular damage occurring in rats to shear strains under deformation. Although some tissue damage did occur at lower maximum shear strains, damage was far more likely if the maximum shear strain was above 65% [176]. In modelling of tissue damage risk with spine boards, shear strains of 50-60% were considered as the threshold at which direct deformation damage may occur [109]. Damage

thresholds have also been found to decrease with increasing exposure time to the deformation, particularly if ischaemia occurs [85].

There are several things to note about the relatively low strain values observed in these models. Firstly, midstance loads were applied rather than toe-off peaks, which would likely result in higher shear strains. Secondly, percentile values were examined here rather than maximum strains to eliminate outliers that would affect comparisons between models. In many cases the maximum shear strain values were above 50% (Figure 7.2). However, based on the minimum and average element volumes it may have been only a few isolated elements experiencing those higher strains. By also using a metric for volume of soft tissue at higher strain values, the tissues at strains higher than the 99th% value were accounted for without giving undue attention to outlier strain values that only occurred in a limited number of model elements. Finally, the majority of damage thresholds in literature only account for direct deformation damage, rather than damage due to ischaemia. No clinical studies of FOs or AFOs report direct deformation damage at the forefoot due to the devices, and so model predictions exceeding those damage thresholds would be unexpected. However, both AFOs and FOs are likely to be worn for lengthy periods and so ischaemic damage would be a risk that could occur with the lower shear strain values predicted by the models. Orthosis wearers are also likely to have increased tissue vulnerabilities which may not have been fully reflected in these simplified models, such as impaired tissue structures which would affect tissue properties and perfusion issues. Thus, the previously identified thresholds must be applied with caution, and do not mean that the individuals modelled here would experience no tissue damage if wearing any of these orthosis designs. That aside, the models are still highly applicable for comparing and optimising orthosis designs through the reduction of strains, no matter how the absolute values predicted correspond to damage thresholds.

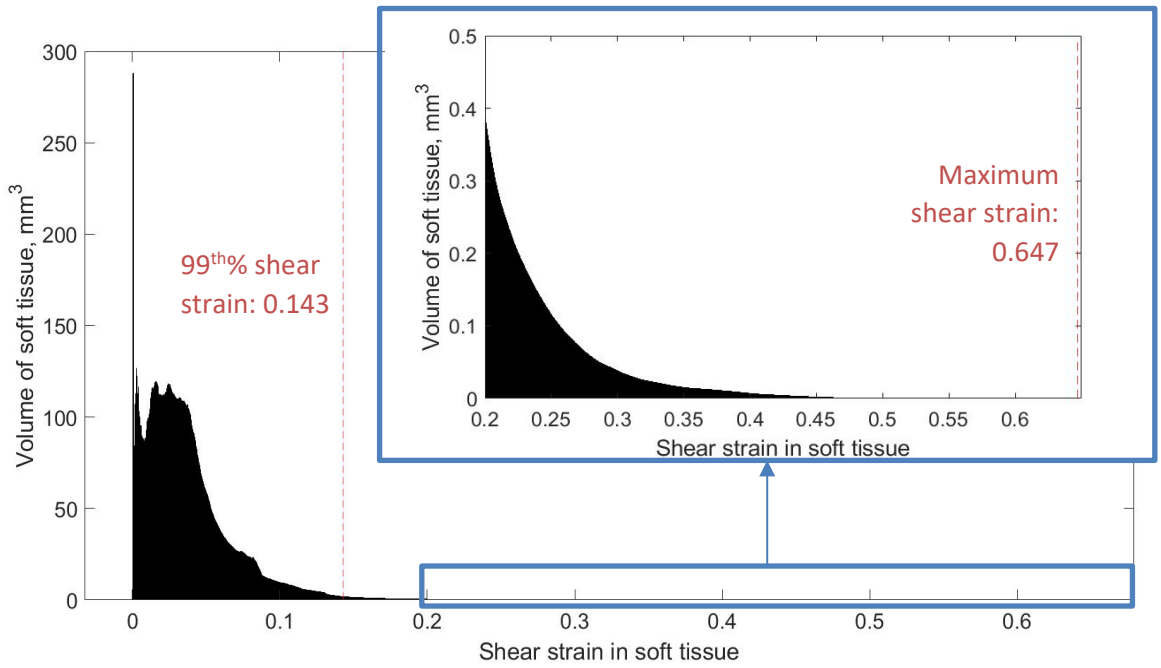

Figure 7.2: Example histogram from N1 Normal_PP AFO model, indicating the 99th% and maximum shear strains. Minimum soft tissue element volume ≈ 0.02mm^3; average element volume in skin ≈ 0.12 mm^3 ; average element volume in underlying soft tissue ≈ 0.42mm^3.

Computational modelling is a valuable tool for assessing the effects of different orthosis designs on deeper soft tissues, and the simplified models developed were found to be suitable for carrying out those evaluations. The use of simplified models meant that the comparative effects of different designs could be assessed for multiple individuals in a more efficient manner. Through the model predictions, differences between individuals and the comparative effects of different orthosis designs, or lack thereof, were observed. By assessing the soft tissue strains associated with device use, orthoses could be optimised to reduce tissue damage risk, potentially reducing pain and improving the comfort of the wearer. However, it should be noted that improvements to tissue damage risk, for example through softer orthosis material, must also be balanced with device functionality and durability in a real-world environment. If this could be achieved, both the effectiveness of the orthoses and the users' adherence could be improved.

The models were largely successful in their intended purpose, but important considerations in the modelling process were also identified that would be key to further assessment of orthosis designs using this methodology. The use of suitable imaging data, accurate representations of design parameters such as shoe type, and assessment of all potential regions of tissue vulnerability were shown to be vital to ensuring the models can properly portray the effects of different orthosis designs. Some of these considerations are discussed further in the following section, alongside other limitations of the studies and areas for future research.

7.2 Limitations and Future Work

The studies detailed in this project all featured a limited number of participants, which in some cases meant inferential statistical analyses were not possible or outcomes were inconclusive due to potential artefacts of the sample. Despite low statistical power, the studies were still more extensive than previous research and so present a step forward in the field. However, the limited sample sizes meant that while the effectiveness of these methods in comparing AFO and FO designs could be assessed, few firm conclusions could be drawn about the effectiveness of the designs in reducing tissue damage risk. This is particularly relevant given the variation between participants in these studies. Further research could build upon the work in this thesis to identify optimal AFO and FO designs across a larger population of individuals.

Imaging data could not be collected during this project and MR data are not routinely collected for these clinical interventions, so the modelling studies were secondary analyses of MR data previously collected for other purposes. As such, the individuals modelled for the AFO study were healthy, and so the results obtained may not reflect all individuals who require the devices. The RA participant MR data used for the FO study also had drawbacks which may have affected the model predictions, as it had not been collected for modelling purposes (as discussed in Section 5.3). If building on the modelling studies presented in this thesis, it would be beneficial to utilise imaging data of individuals with relevant foot pathologies, collected in a suitable configuration for modelling purposes. A suitable configuration could consist of imaging the foot under a nominal load as opposed to unloaded, as the RA dataset was. Experimental data of pressures during gait could also be collected for the modelled individuals to ensure the applied loads would be reflective of each individual's gait pattern and to aid in model validation.

The models developed were simplified to improve efficiency when solving for multiple participants and across multiple design parameters. However, it is unlikely that the models are efficient enough to run in a clinical setting to tailor orthosis designs to individuals, particularly as some orthosis configurations were time-consuming to run. Additionally, MR imaging is expensive and rarely acquired clinically for people going through an orthosis prescription process. Elastography was discussed earlier as a potential method for incorporating the modelling predictions into a clinical setting. However, if the efficiency of the modelling process was improved, the models themselves could be implemented clinically to optimise personalised orthosis design. A potential way of achieving this would be to incorporate statistical shape modelling into the model generation. This has previously been used for applications such as prosthetic socket design [252], and similar processes have also been explored for morphing foot anatomy [253]. This would involve quantifying the variation in morphology between individuals,

and then adjusting a baseline geometry to represent each new participant. Once the statistical shape model has been generated, this would eliminate the need for collecting MR data of every individual to be assessed. Care would need to be taken that the models could still reflect an individual's foot morphology accurately enough to produce effective orthosis designs, but simplified anatomies similar to those utilised in this research could be generated.

Although there was sound reasoning behind the simplified models, particularly as they were being used for comparative purposes, the simplifications do present some limitations. In using static loading conditions representing midstance, the models do not consider how contact between the orthosis and limb would vary throughout gait. The joint movement and relative positioning of the MTP joints and sesamoid bones to the applied load would also vary throughout gait. Incorporating these aspects could improve understanding of tissue damage risks, as there may be increased vulnerability at other time-points during gait than were assessed here. Dynamic modelling could be utilised, but some of the model simplifications would affect the model predictions more in a dynamic model than the present static one. To dynamically load the models, the bones could not be constrained in the way there were here, and the MTP joint would have to be incorporated, rather than fused. This could involve inclusion of a stiffer material around the joint to represent the joint capsule, or addition of ligaments to stabilise the joints. However, it is likely that by making the models more detailed in this regard, the efficiency of the models would be reduced significantly. Nonetheless, another benefit of allowing bone and joint movement would be that differences between individuals in joint stability could be observed, which can impact orthosis requirements. For example, people with RA who have higher levels of instability may be prescribed a stiffer FO to provide the support and stability they require [254].

The inclusion of the separate skin layer in the computational models meant that they would incorporate any skin thinning due to conditions or medication effects (from corticosteroids prescribed for RA, for example), or skin thickening due to callus formation. However, the material properties assigned to the skin were not varied to reflect how its functionality may have differed with those morphological changes. Similarly, the underlying soft tissues were modelled as a bulk group with the same tissue properties assigned to each individual, which limited the models' ability to differentiate between people. This is relevant to conditions like RA where orthotic requirements may be affected by the presence of bursae or previous tissue injuries, or the degree to which the plantar fat pad is affected, for example. This could be addressed by including subject-specific tissue properties determined through ultrasound indentation testing or elastography, or by varying the soft tissue parameters used to reflect the muscle to fat ratio present on the MR data.

During the experimental testing of AFOs in Chapter 3, the effect of different AFO designs and sock materials on the microclimate was shown. However, while it is known that microclimate conditions can affect tissue damage risk, that link was not explored further here due to time constraints. Future experimental testing of AFO designs could include this through measurements of erythema, transepidermal moisture loss, or inflammatory biomarkers for example (see Table 2.1, Section 2.1.1). Assessing the effects of microclimate could also be incorporated into the computational models, through multiphysics modelling, which would also allow the damage risk to deeper tissues to be examined. Preliminary work was carried out to identify relevant thermal properties and coupling equations between thermal and mechanical properties, which could be used for multiphysics modelling. The COMSOL Bioheat Transfer module operates using the Pennes bioheat equation which states that changes in temperature over time are caused by perfusion of blood transferring heat to the tissue, conduction of heat through the tissues, and heat generated by the metabolism [255, 256]:

$$\rho c \frac{\delta T}{\delta t} = \nabla k \nabla T + \omega_b \rho_b c_b (T_b - T) + q_m \quad \text{Eq7.1.}$$

where ρ is the tissue density (kg/m^3), c is the specific heat capacity (J/kg.K), T is the tissue temperature (K), t is the time (s), k is the temperature conductivity (W/m.K), x_b subscript denotes the properties of blood, T_b is the arterial blood temperature (K), ω_b is the rate of perfusion (ml/ml.s), and q_m is the rate of metabolic heat flow (W/m^3/s). Fiala et al. [257] have detailed values that can be used for these parameters for the foot tissues. Countercurrent heat exchange could also be accounted for by setting the arterial blood temperature input to reflect the temperature of peripheral blood rather than core blood.

Coupling between the microclimate and mechanical behaviour could be implemented through equations linking the temperature changes at the skin interface to sweat production and so relative humidity (RH) of the skin. This in turn would affect the CoF between the device and the limb and the skin's shear strength. Fiala et al. [258] provided the following equations to determine sweat production based on core and skin temperature:

$$Sweating, SW \left(\frac{g}{min}\right) = [0.8 \tanh(0.59\Delta T_{skin\,mean} - 0.19) + 1.2]\Delta T_{skin\,mean} + [5.7 \tanh(1.98\Delta T_{core} - 1.03) + 6.3]\Delta T_{core} \quad \text{Eq7.2.}$$

$$Local\ sweat\ rate\ in\ foot \left(\frac{g}{min}\right) = 0.035 \times SW \times 2^{\frac{\Delta T_{skin\,local}}{10}} \quad \text{Eq7.3.}$$

The change in mean skin temperature ($\Delta T_{skin\,mean}$) could be calculated based on the assumption that skin temperature in other regions was unchanged, and using the coefficient for the foot temperature change provided by Fiala et al. of 0.075. Further calculations would then be required

to convert the sweat production rate in g/min to a relative humidity of the skin. From there, the relative humidity can be related to the CoF at the skin interface, for example using equations determined by Klaassen et al. [259] who assessed the static and dynamic CoF between the forearm and a cotton covered polyurethane probe at different RH values (Figure 7.3).

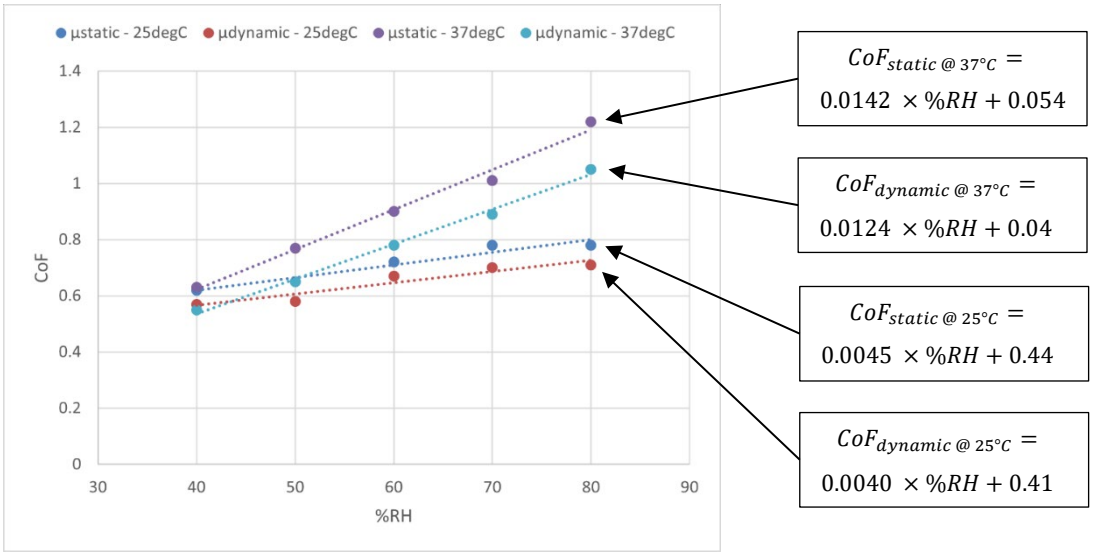

Figure 7.3: Effect of relative humidity (%RH) and temperature on coefficient of friction (CoF), results from Klaassen et al.

Considering candidate tissue injury criteria, the RH could also be related to the skin's shear strength. According to Geerligs et al. [117], the shear strength of the stratum corneum changed from around 12kPa at 25%RH to 4kPa at 98%RH. As the relationship appeared to be relatively linear, this would result in the following equation:

$$Shear\ strength\ (kPa) = -0.1096 \times \%RH + 14.74 \qquad \text{Eq7.4.}$$

These equations could provide the basis for a multiphysics model, which would allow tissue damage risk of different device designs to be assessed, incorporating both the risk from the applied loads and due to the elevated microclimate.

In this research, computational models were used to assess orthosis design parameters such as shape and material. In each case, pre-determined values or configurations were used for the inputs. For example, the AFO and FO material properties were based on existing materials used for those purposes. As such, the parameters assessed were constrained. However, the models could be used to help tailor design requirements by identifying the parameters required to best protect the soft tissues through reduction of pressures and strains. As observed here, those requirements may not be the same for everyone. An optimisation study could be performed, to assess a wider range of design parameters to determine which parameters lead to the best outcomes. Optimised designs could be identified on a personalised level or as broader categories

for people with similar condition presentations or other demographic strata, and thus orthosis requirements. These assessments could incorporate other design parameters that were not explored here, such as CoF, material permeability, FO thickness or geometric features such as metatarsal pads, or other regions of interest, such as the ankle for AFO design.

The studies detailed in this thesis have provided a basis for improved assessment of orthosis design, identifying some key considerations and design parameters that may be more relevant for further evaluation. Through the areas of future work identified here, the impact of different designs on tissue health can be explored further. This would pave the way for more effective orthoses, with improved user comfort and satisfaction.

Appendix A Chapter 3 – CSD-OPUS Questionnaire

This appendix contains the Client Satisfaction with Device subsection of the Orthotics and Prosthetics User Survey that was used during the AFO experimental testing detailed in Chapter 3.

Session Number and Test Condition:	TODAY'S DATE MM / DD / YY	PARTICIPANT ID NUMBER

I. Thinking about your prosthesis or orthosis, how true are the following statements for you?

	Strongly Agree	Agree	Disagree	Strongly Disagree
1. My prosthesis / orthosis fits well.	☐	☐	☐	☐
2. The weight of my prosthesis / orthosis is manageable.	☐	☐	☐	☐
3. My prosthesis / orthosis is comfortable throughout the day.	☐	☐	☐	☐
4. It is easy to put on my prosthesis / orthosis.	☐	☐	☐	☐
5. My prosthesis / orthosis looks good.	☐	☐	☐	☐
6. My prosthesis / orthosis is durable.	☐	☐	☐	☐
7. My clothes are free of wear and tear from my prosthesis / orthosis.	☐	☐	☐	☐
8. My skin is free of abrasions and irritations.	☐	☐	☐	☐
9. My prosthesis / orthosis is pain free to wear.	☐	☐	☐	☐

Any additional comments are welcome:

_____

_____

_____

_____

 Follow-up

Appendix B Pressure Gradient Calculation Code

The following code allows the maximum pressure gradient to be calculated from a matrix of pressure results extracted from a pressure sensor system, in the case the F-scan system.

```
function [Max_PG_per_point] = pressure_gradients(foot_region)
%Pressure gradients. Finds the pressure gradients between sensels for a
%   region of the foot
%   For each value in the matrix, finds the difference between that value
%   and the 8 surrounding values - less if on edge of matrix and accounting
%   for '0' values were there was no sensor. Then returns matrix of the
%   maximum difference at each point in the matrix. Output PG is in kPa/mm
%   by dividing by the distance between sensels.

[no_rows no_columns] = size(foot_region);
Max_PG_per_point = zeros(no_rows, no_columns);
Sensel_distance_vert_hor = 5.1;
Sensel_distance_diag = 7.2;

for r=1:no_rows
    for c = 1:no_columns
        if foot_region(r,c) == 0
            Max_PG_per_point(r,c) = 0;
        else
            if r ==1 %top row of the matrix

                if c==1 %left hand column

                [PG1] = PG_is_it_0(foot_region(r,c), foot_region(r+1,c));
                PG1 = PG1/Sensel_distance_vert_hor;
                [PG2] = PG_is_it_0(foot_region(r,c), foot_region(r,c+1));
                PG2 = PG2/Sensel_distance_vert_hor;
                [PG3] = PG_is_it_0(foot_region(r,c), foot_region(r+1,c+1));
                PG3 = PG3/Sensel_distance_diag;
                max_PG = max([PG1, PG2, PG3]);

                elseif c == no_columns %right hand column
                [PG1] = PG_is_it_0(foot_region(r,c), foot_region(r+1,c));
                PG1 = PG1/Sensel_distance_vert_hor;
                [PG2] = PG_is_it_0(foot_region(r,c), foot_region(r,c-1));
                PG2 = PG2/Sensel_distance_vert_hor;
                [PG3] = PG_is_it_0(foot_region(r,c), foot_region(r+1,c-1));
                PG3 = PG3/Sensel_distance_diag;
                max_PG = max([PG1, PG2, PG3]);

                else %centre of matrix
                [PG1] = PG_is_it_0(foot_region(r,c), foot_region(r+1,c));
                PG1 = PG1/Sensel_distance_vert_hor;
                [PG2] = PG_is_it_0(foot_region(r,c), foot_region(r,c+1));
                PG2 = PG2/Sensel_distance_vert_hor;
                [PG3] = PG_is_it_0(foot_region(r,c), foot_region(r+1,c+1));
                PG3 = PG3/Sensel_distance_diag;
                [PG4] = PG_is_it_0(foot_region(r,c), foot_region(r,c-1));
                PG4 = PG4/Sensel_distance_vert_hor;
                [PG5] = PG_is_it_0(foot_region(r,c), foot_region(r+1,c-1));
                PG5 = PG5/Sensel_distance_diag;
                max_PG = max([PG1, PG2, PG3, PG4, PG5]);
                end
```

```
elseif r ==no_rows % bottom row of matrix

    if c==1 %left hand column
    [PG1] = PG_is_it_0(foot_region(r,c), foot_region(r-1,c));
    PG1 = PG1/Sensel_distance_vert_hor;
    [PG2] = PG_is_it_0(foot_region(r,c), foot_region(r,c+1));
    PG2 = PG2/Sensel_distance_vert_hor;
    [PG3] = PG_is_it_0(foot_region(r,c), foot_region(r-1,c+1));
    PG3 = PG3/Sensel_distance_diag;
    max_PG = max([PG1, PG2, PG3]);

    elseif c == no_columns %right hand column
    [PG1] = PG_is_it_0(foot_region(r,c), foot_region(r-1,c));
    PG1 = PG1/Sensel_distance_vert_hor;
    [PG2] = PG_is_it_0(foot_region(r,c), foot_region(r,c-1));
    PG2 = PG2/Sensel_distance_vert_hor;
    [PG3] = PG_is_it_0(foot_region(r,c), foot_region(r-1,c-1));
    PG3 = PG3/Sensel_distance_diag;
    max_PG = max([PG1, PG2, PG3]);

    else %centre of matrix
    [PG1] = PG_is_it_0(foot_region(r,c), foot_region(r-1,c));
    PG1 = PG1/Sensel_distance_vert_hor;
    [PG2] = PG_is_it_0(foot_region(r,c), foot_region(r,c+1));
    PG2 = PG2/Sensel_distance_vert_hor;
    [PG3] = PG_is_it_0(foot_region(r,c), foot_region(r-1,c+1));
    PG3 = PG3/Sensel_distance_diag;
    [PG4] = PG_is_it_0(foot_region(r,c), foot_region(r,c-1));
    PG4 = PG4/Sensel_distance_vert_hor;
    [PG5] = PG_is_it_0(foot_region(r,c),foot_region(r-1,c-1));
    PG5 = PG5/Sensel_distance_diag;
    max_PG = max([PG1, PG2, PG3, PG4, PG5]);
    end

else % middle of matrix
    if c==1 %left hand column
    [PG1] = PG_is_it_0(foot_region(r,c),foot_region(r-1,c));
    PG1 = PG1/Sensel_distance_vert_hor;
    [PG2] = PG_is_it_0(foot_region(r,c), foot_region(r-1,c+1));
    PG2 = PG2/Sensel_distance_diag;
    [PG3] = PG_is_it_0(foot_region(r,c),foot_region(r,c+1));
    PG3 = PG3/Sensel_distance_vert_hor;
    [PG4] = PG_is_it_0(foot_region(r,c), foot_region(r+1,c+1));
    PG4 = PG4/Sensel_distance_diag;
    [PG5] = PG_is_it_0(foot_region(r,c), foot_region(r+1,c));
    PG5 = PG5/Sensel_distance_vert_hor;
    max_PG = max([PG1, PG2, PG3, PG4, PG5]);
```

```
                elseif c == no_columns %right hand column
                [PG1] = PG_is_it_0(foot_region(r,c), foot_region(r-1,c));
                PG1 = PG1/Sensel_distance_vert_hor;
                [PG2] = PG_is_it_0(foot_region(r,c),foot_region(r-1,c-1));
                PG2 = PG2/Sensel_distance_diag;
                [PG3] = PG_is_it_0(foot_region(r,c), foot_region(r,c-1));
                PG3 = PG3/Sensel_distance_vert_hor;
                [PG4] = PG_is_it_0(foot_region(r,c),foot_region(r+1,c-1));
                PG4 = PG4/Sensel_distance_diag;
                [PG5] = PG_is_it_0(foot_region(r,c), foot_region(r+1,c));
                PG5 = PG5/Sensel_distance_vert_hor;
                max_PG = max([PG1, PG2, PG3, PG4, PG5]);

                else %centre of matrix
                [PG1] = PG_is_it_0(foot_region(r,c), foot_region(r-1,c));
                PG1 = PG1/Sensel_distance_vert_hor;
                [PG2] = PG_is_it_0(foot_region(r,c), foot_region(r-1,c+1));
                PG2 = PG2/Sensel_distance_diag;
                [PG3] = PG_is_it_0(foot_region(r,c),foot_region(r,c+1));
                PG3 = PG3/Sensel_distance_vert_hor;
                [PG4] = PG_is_it_0(foot_region(r,c),foot_region(r+1,c+1));
                PG4 = PG4/Sensel_distance_diag;
                [PG5] = PG_is_it_0(foot_region(r,c), foot_region(r+1,c));
                PG5 = PG5/Sensel_distance_vert_hor;
                [PG6] = PG_is_it_0(foot_region(r,c), foot_region(r+1,c-1));
                PG6 = PG6/Sensel_distance_diag;
                [PG7] = PG_is_it_0(foot_region(r,c), foot_region(r,c-1));
                PG7 = PG7/Sensel_distance_vert_hor;
                [PG8] = PG_is_it_0(foot_region(r,c), foot_region(r-1,c-1));
                PG8 = PG8/Sensel_distance_diag;
                max_PG = max([PG1, PG2, PG3, PG4, PG5, PG6, PG7, PG8]);
                end
            end
        Max_PG_per_point(r,c) = max_PG;
        end
    end
end
end
```

```
function [PG] = PG_is_it_0(centre_p, surrounding_p)
%PG_is_it_0 For the pressure_gradients function - finds if the one of the
%surrounding points is 0 and if so, sets PG between the two points to 0.
%If non-zero, calculates the pressure gradient.
if surrounding_p ==0
    PG = 0;
else
    PG = centre_p - surrounding_p;
end
end
```

Appendix C Chapter 3 – Pressure Results

This Appendix contains further pressure results from the experimental testing of AFOs in Chapter 3, including:

- Median and IQR peak pressure, pressure gradient and PTI (where relevant) data for both gait and standing test conditions, including breakdown into subsections of the foot,
- Individual peak pressure and pressure gradient data for the standing test conditions.

C.1 Plantar peak pressure (PP), pressure gradient (PG), and pressure-time integral (PTI) results during gait, displaying median (IQR)

Foot Region	Test Condition	PP (kPa) AFO foot	PP (kPa) Control foot	PG (kPa/mm) AFO foot	PG (kPa/mm) Control foot	PTI using % gait cycle AFO foot	PTI using % gait cycle Control foot
Forefoot	ES Bamboo	303 (208 – 445)	322 (255 – 471)	34.4 (32.2 – 46.5)	26.5 (24.7 – 67.5)	12972 (11256 – 17804)	12316 (9519 – 16194)
	ES Cotton	352 (212 – 407)	300 (234 – 470)	47.6 (37.5 – 69.4)	25.7 (23.1 – 67.5)	14367 (11776 – 15173)	11212 (9322 – 17300)
	Push Bamboo	233 (211 – 269)	341 (305 – 404)	25.7 (24.3 – 27.5)	28.4 (25.9 – 42.4)	11481 (10340 – 11500)	13323 (12800 – 15908)
	Push Cotton	239 (222 – 279)	327 (295 – 346)	31.0 (29.4 – 32.0)	30.8 (22.4 – 41.4)	11111 (10531 – 11147)	12408 (11989 – 15026)

Foot Region	Test Condition	PP (kPa) AFO foot	PP (kPa) Control foot	PG (kPa/mm) AFO foot	PG (kPa/mm) Control foot	PTI using % gait cycle AFO foot	PTI using % gait cycle Control foot
MH1	ES Bamboo	298 (196 – 402)	236 (214 – 471)	32.2 (17.1 – 46.5)	24.7 (21.3 – 54.3)	8025 (7437 – 14165)	9302 (7117 – 15198)
	ES Cotton	346 (179 – 352)	222 (217 – 470)	47.6 (37.5 – 69.4)	25.5 (17.6 – 62.4)	10480 (6439 – 10709)	7824 (7759 – 16796)
	Push Bamboo	179 (170 – 251)	264 (229 – 275)	22.4 (21.8 – 25.9)	22.5 (21.3 – 29.8)	7505 (7461 – 8401)	8936 (8652 – 9623)
	Push Cotton	181 (176 – 230)	230 (184 – 302)	29.2 (25.7 – 32.0)	25.1 (18.4 – 25.6)	6745 (6120 – 8292)	7843 (7260 – 9580)
MH5	ES Bamboo	206 (167 – 267)	94 (93 – 219)	29.0 (13.3 – 31.6)	16.9 (13.5 – 18.6)	7751 (7016 – 10607)	5150 (4859 – 8632)
	ES Cotton	193 (111 – 265)	88 (72 – 177)	30.8 (14.3 – 32.5)	15.0 (7.84 – 16.9)	7784 (5053 – 9851)	4662 (3982 – 7891)
	Push Bamboo	130 (117 – 154)	128 (118 – 147)	16.4 (12.6 – 17.6)	16.5 (11.8 – 19.4)	6625 (6320 – 6938)	6849 (6038 – 8012)
	Push Cotton	140 (135 – 144)	128 (123 – 135)	17.1 (14.7 – 21.0)	13.3 (12.7 – 13.7)	6696 (5478 – 7225)	6247 (6241 – 6758)
Rearfoot	ES Bamboo	298 (256 – 353)	368 (284 – 426)	43.9 (41.9 – 50.0)	34.7 (26.3 – 41.2)	12237 (12109 – 14332)	15827 (12622 – 18934)
	ES Cotton	316 (223 – 329)	361 (259 – 381)	63.3 (37.4 – 64.5)	34.1 (20.6 – 47.6)	13856 (12635 – 14479)	15410 (11941 – 17227)
	Push Bamboo	224 (223 – 262)	457 (320 – 466)	38.4 (38.2 – 38.4)	33.9 (27.1 – 41.6)	10159 (10071 – 11730)	18853 (12165 – 21031)
	Push Cotton	268 (196 – 275)	408 (261 – 463)	35.1 (30.4 – 36.3)	27.6 (19.6 – 43.1)	12074 (9156 – 13420)	16740 (10316 – 20841)
Lateral Heel	ES Bamboo	158 (127 – 197)	211 (187 – 243)	32.4 (25.7 – 43.9)	23.9 (20.8 – 30.4)	8085 (6157 – 10502)	8906 (7793 – 10768)
	ES Cotton	157 (128 – 169)	197 (180 – 199)	26.5 (21.2 – 64.5)	22.4 (20.6 – 23.8)	7578 (5183 – 9963)	8019 (7012 – 8717)
	Push Bamboo	135 (119 – 168)	250 (217 – 269)	25.1 (18.2 – 28.8)	26.3 (22.5 – 27.1)	7004 (5843 – 7778)	9961 (7386 – 11305)
	Push Cotton	157 (139 – 159)	228 (183 – 259)	24.1 (23.3 – 24.3)	20.4 (19.6 – 21.0)	7618 (7501 – 8515)	8171 (6477 – 11179)
Medial Heel	ES Bamboo	254 (159 – 269)	266 (205 – 271)	35.9 (32.0 – 42.2)	28.9 (26.3 – 35.5)	8981 (6573 – 10635)	9244 (7948 – 11172)
	ES Cotton	238 (142 – 270)	238 (209 – 255)	36.9 (34.3 – 38.6)	28.3 (18.4 – 30.0)	8179 (6051 – 11622)	9990 (8347 – 10201)
	Push Bamboo	183 (145 – 194)	242 (235 – 295)	27.5 (25.9 – 38.4)	26.7 (18.6 – 36.3)	8575 (6235 – 9044)	11063 (8552 – 11808)
	Push Cotton	174 (126 – 193)	252 (198 – 270)	26.1 (21.8 – 31.8)	21.4 (15.5 – 30.6)	9269 (6086 – 9346)	9981 (8708 – 11516)

Foot Region	Test Condition	PP (kPa) AFO foot	PP (kPa) Control foot	PG (kPa/mm) AFO foot	PG (kPa/mm) Control foot	PTI using % gait cycle AFO foot	PTI using % gait cycle Control foot
Posterior Heel	ES Bamboo	192 (146 – 278)	245 (241 – 315)	41.9 (38.8 – 50.0)	34.7 (26.3 – 37.5)	9325 (8166 – 10294)	10164 (9441 – 14145)
	ES Cotton	234 (148 – 257)	243 (213 – 272)	37.4 (24.3 – 49.8)	34.1 (20.6 – 35.7)	9989 (7875 – 10792)	9417 (9192 – 10792)
	Push Bamboo	160 (114 – 161)	195 (194 – 272)	30.0 (27.6 – 38.2)	27.1 (21.0 – 33.9)	6802 (6416 – 7889)	7356 (6586 – 11902)
	Push Cotton	159 (135 – 171)	212 (172 – 316)	30.0 (29.0 – 30.4)	20.4 (18.2 – 31.7)	6876 (6763 – 9873)	8363 (6428 – 12739)

C.2 Plantar peak pressure (PP) and pressure gradient (PG) results during stationary standing, displaying median (IQR)

Foot Region	Test Condition	PP (kPa) AFO foot	PP (kPa) Control foot	PG (kPa/mm) AFO foot	PG (kPa/mm) Control foot
Forefoot	ES Bamboo	97 (74 – 119)	65 (43 – 69)	8.04 (6.47 – 27.8)	7.65 (4.12 – 9.22)
	ES Cotton	77 (45 – 124) *	48 (37 – 53)	10.9 (4.61 – 17.5) *	5.88 (5.88 – 12.9)
	Push Bamboo	43 (39 – 72)	54 (52 – 73)	9.80 (9.41 – 12.4)	8.24 (7.06 – 10.8)
	Push Cotton	59 (53 – 61)	58 (45 – 61)	8.04 (7.25 – 9.80)	8.24 (5.69 – 8.63)
MH1	ES Bamboo	42 (25 – 74)	61 (39 – 65)	5.10 (3.14 – 8.04)	7.65 (4.12 – 9.22)
	ES Cotton	46 (19 – 80) *	47 (33 – 48)	8.04 (2.84 – 14.5) *	5.88 (4.51 – 11.8)
	Push Bamboo	32 (28 – 40)	40 (31 – 52)	6.86 (5.69 – 8.82)	8.24 (6.67 – 8.61)
	Push Cotton	42 (31 – 50)	45 (34 – 48)	5.88 (5.10 – 6.27)	5.69 (5.69 – 7.84)

* ES Cotton AFO foot data did not record correctly for one participant, so median is from four results.

Foot Region	Test Condition	PP (kPa) AFO foot	PP (kPa) Control foot	PG (kPa/mm) AFO foot	PG (kPa/mm) Control foot
MH5	ES Bamboo	37 (26 – 43)	44 (33 – 49)	4.51 (3.14 – 5.69)	5.69 (2.94 – 6.08)
	ES Cotton	43 (21 – 68) *	30 (26 – 38)	4.41 (2.40 – 8.97) *	4.31 (3.92 – 5.29)
	Push Bamboo	38 (24 – 43)	41 (39 – 49)	5.29 (5.10 – 6.47)	6.67 (6.47 – 7.06)
	Push Cotton	33 (28 – 53)	33 (30 – 55)	5.88 (3.33 – 8.24)	4.17 (3.33 – 5.88)
Rearfoot	ES Bamboo	102 (91 – 109)	167 (101 – 171)	16.3 (13.3 – 27.8)	12.0 (8.63 – 14.9)
	ES Cotton	108 (66 – 164) *	140 (71 – 144)	16.7 (14.3 – 23.5) *	14.5 (11.2 – 15.1)
	Push Bamboo	82 (74 – 115)	159 (125 – 159)	21.0 (12.5 – 22.7)	15.3 (14.2 – 18.8)
	Push Cotton	84 (82 – 115)	152 (142 – 181)	15.7 (13.9 – 21.8)	20.0 (11.1 – 20.8)
Lateral Heel	ES Bamboo	71 (55 – 80)	54 (42 – 117)	12.0 (10.2 – 18.6)	9.02 (4.51 – 9.41)
	ES Cotton	67 (39 – 100) *	59 (43 – 90)	14.5 (11.1 – 22.2) *	7.25 (5.49 – 12.0)
	Push Bamboo	70 (67 – 72)	72 (68 – 84)	9.41 (7.65 – 10.0)	9.02 (6.25 – 11.3)
	Push Cotton	77 (74 – 80)	76 (71 – 82)	9.41 (7.84 – 10.8)	9.80 (8.63 – 10.0)
Medial Heel	ES Bamboo	78 (63 – 91)	65 (57 – 120)	16.3 (13.3 – 27.8)	8.24 (7.65 – 11.0)
	ES Cotton	81 (50 – 107) *	62 (62 – 87)	12.8 (10.1 – 18.7) *	10.2 (10.0 – 13.9)
	Push Bamboo	71 (62 – 103)	123 (120 – 132)	14.1 (10.8 – 14.9)	11.8 (11.2 – 14.2)
	Push Cotton	82 (69 – 87)	106 (101 – 120)	15.7 (13.9 – 19.2)	13.3 (10.6 – 17.5)
Posterior Heel	ES Bamboo	91 (70 – 112)	101 (97 – 138)	16.1 (12.9 – 20.0)	11.8 (8.63 – 12.0)
	ES Cotton	93 (64 – 126) *	110 (60 – 124)	13.0 (11.1 – 20.0) *	12.4 (10.0 – 14.5)
	Push Bamboo	63 (57 – 83)	103 (87 – 106)	13.9 (12.5 – 18.4)	14.2 (13.5 – 15.3)
	Push Cotton	73 (60 – 76)	102 (80 – 116)	12.9 (12.0 – 13.1)	11.8 (11.1 – 13.2)

C.3 Comparison of the peak pressures and maximum pressure gradients in the forefoot and rearfoot during stationary standing between the AFO foot and the control foot

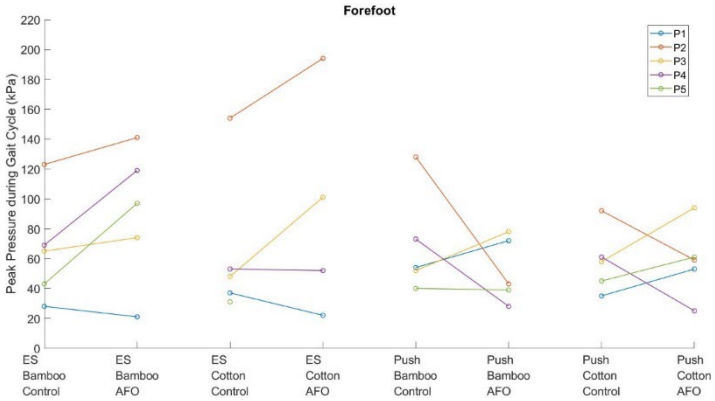

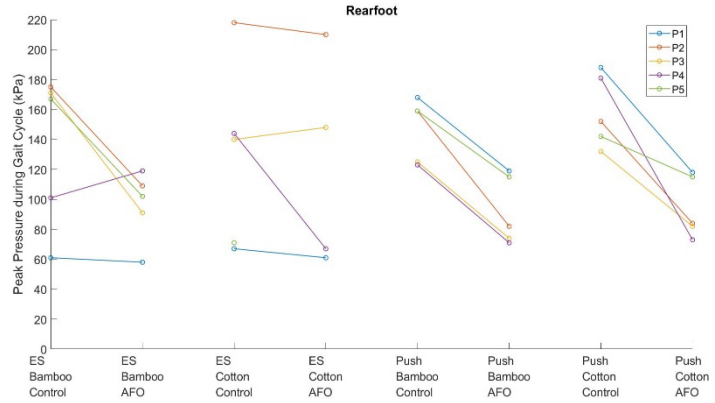

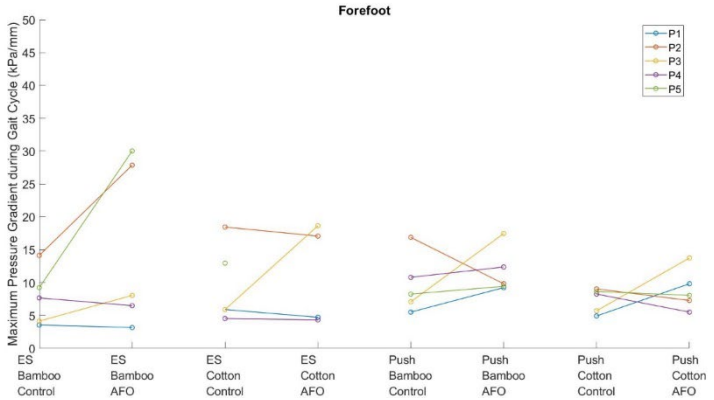

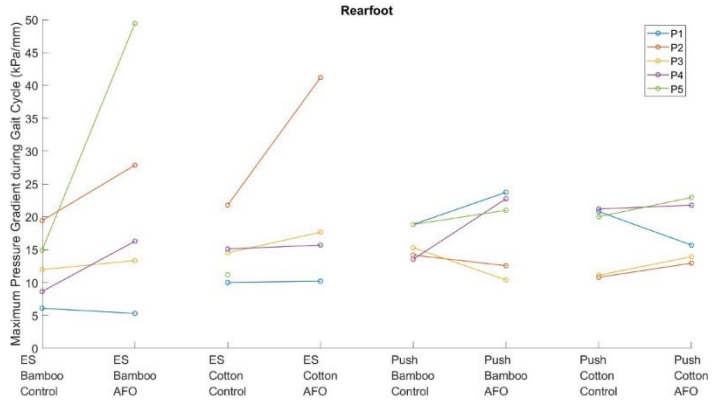

Appendix D Chapter 3 – Microclimate Results for Standing Test Conditions

D.1 Temperature (°C) results for the standing test conditions, showing all participants' individual data. Markers are colour coded to ambient temperature: Blue: <16°C, Yellow: 16-18°C, Red: 18-20°C

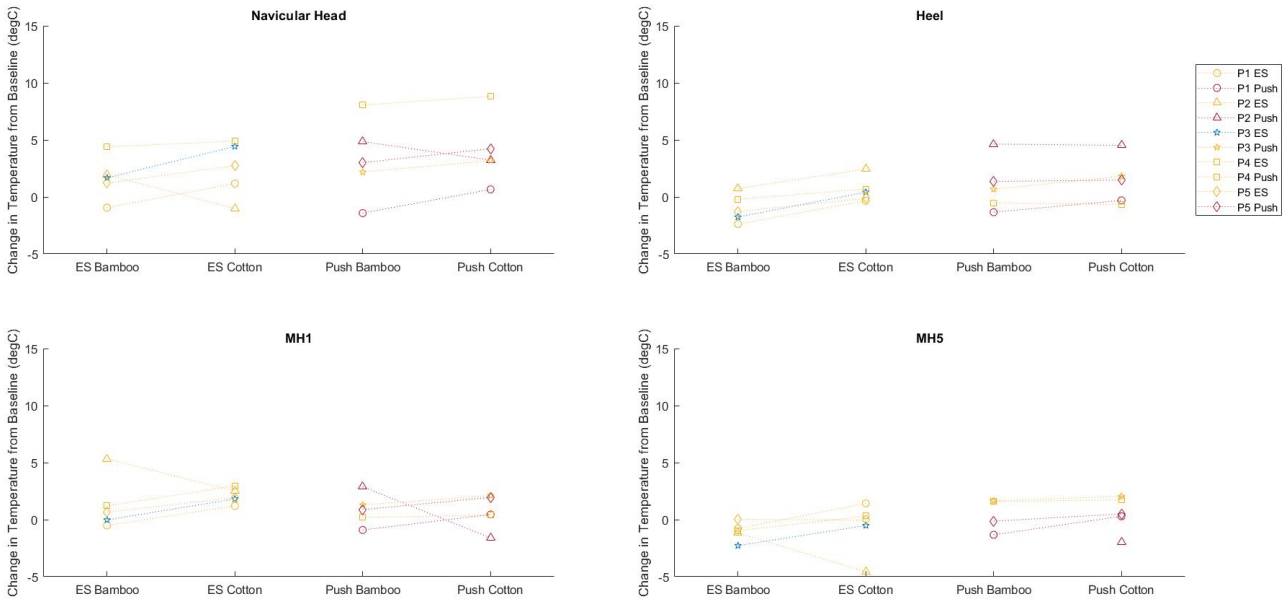

D.2 Relative humidity (%RH) results for the standing test conditions, showing all participants' individual data. Markers are colour coded to ambient humidity: Blue: 30-40%, Yellow: 40-50%, Red: 50-60%.

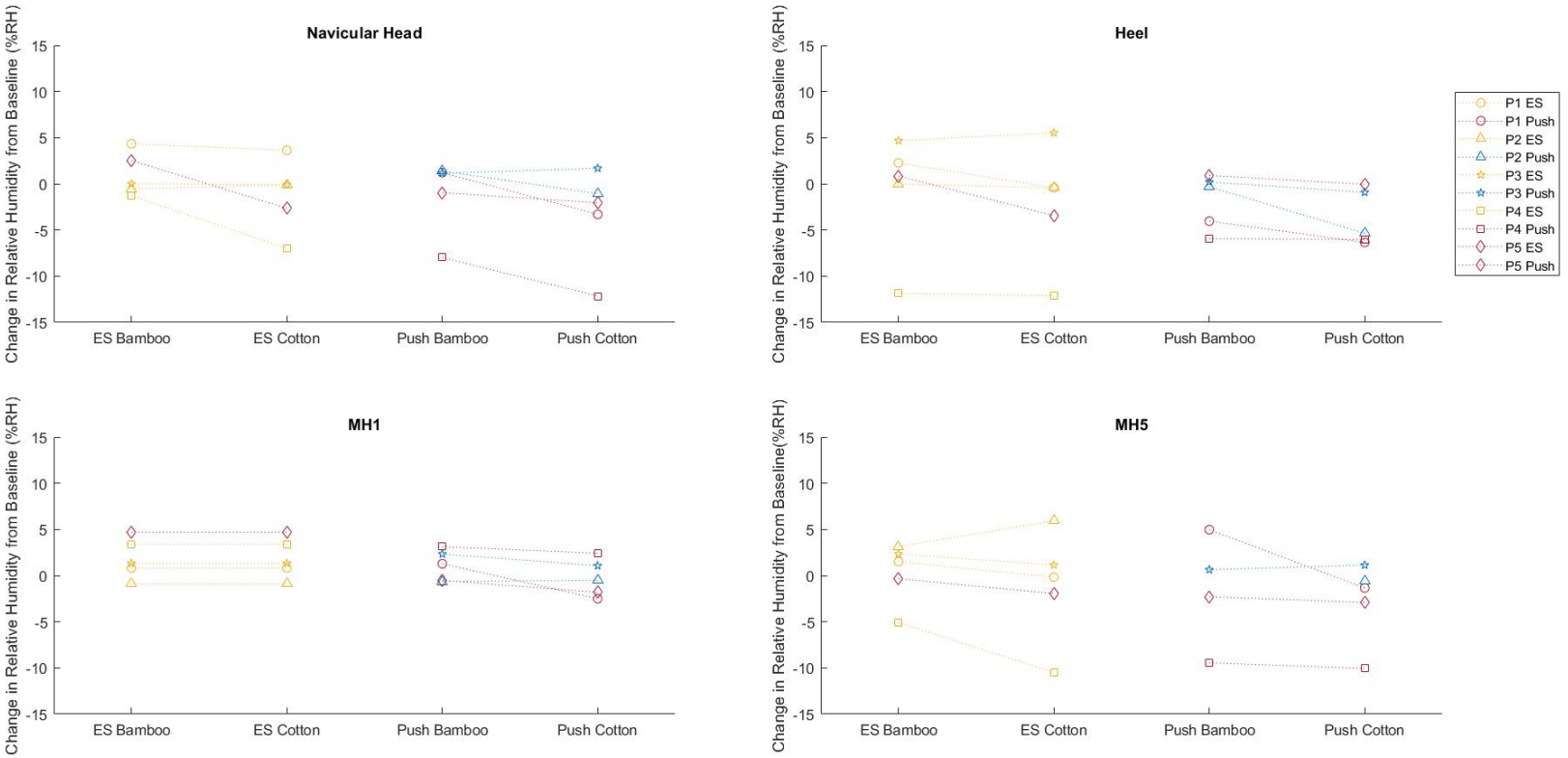

D.3 Change in temperature and relative humidity under AFO from baseline conditions, during stationary standing displaying Median (IQR).

Foot Region	Test Condition	Temperature, change from baseline (°C)	Relative Humidity, change from baseline (%RH)
MH1	ES Bamboo	0.7 (0.0 – 1.2)	1.3 (0.8 – 3.4)
	ES Cotton	1.9 (1.8 – 2.5)	0.2 (-1.3 – 0.5)
	Push Bamboo	0.9 (0.2 – 1.3)	1.3 (-0.5 – 2.3)
	Push Cotton	0.5 (0.4 – 2.0)	-0.5 (-1.8 – 1.1)
MH5	ES Bamboo	-1.0 (-1.2 – -0.8)	1.5 (-0.3 – 2.3)
	ES Cotton	0.0 (-0.5 – 0.3)	-0.2 (-1.9 – 1.2)
	Push Bamboo	0.7 (-0.4 – 1.6) *	-0.8 (-4.1 – 1.7) *
	Push Cotton	0.5 (0.3 – 1.7)	-1.3 (-2.9 – -0.6)
Navicular Head	ES Bamboo	1.7 (1.2 – 1.9) *	0.0 (-0.5 – 2.5) *
	ES Cotton	2.7 (1.2 – 4.4)	-0.1 (-2.6 – -0.1)
	Push Bamboo	3.0 (2.2 – 4.9)	1.2 (-1.0 – 1.2)
	Push Cotton	3.2 (3.2 – 4.2)	-2.1 (-3.3 – -1.1)
Medial Heel	ES Bamboo	-1.3 (-1.8 – -0.2)	0.8 (0.0 – 2.3)
	ES Cotton	0.4 (-0.1 – 0.7)	-0.4 (-3.4 – -0.4)
	Push Bamboo	0.7 (-0.5 – 1.4)	-0.3 (-4.0 – 0.2)
	Push Cotton	1.5 (-0.3 – 1.8)	-5.4 (-6.0 – -0.9)

D.4 Temperature change under AFO vs control foot during stationary standing displaying median (IQR)

Foot Region	Test Condition	Temperature, change from baseline (°C) AFO foot	Temperature, change from baseline (°C) Control foot
MH1	ES Bamboo	0.7 (0.0 – 1.2)	0.8 (-0.8 – 2.5)
	ES Cotton	1.9 (1.8 – 2.5)	2.2 (-0.1 – 2.7)
	Push Bamboo	0.9 (0.2 – 1.3)	2.4 (0.0 – 2.5)
	Push Cotton	0.5 (0.4 – 2.0)	1.8 (1.5 – 2.2)

* Data from one participant failed to record or cut-off prior to end of the test condition.

Foot Region	Test Condition	Temperature, change from baseline (°C) AFO foot	Temperature, change from baseline (°C) Control foot
Lateral Heel	ES Bamboo	2.6 (1.7 – 2.9)	1.8 (1.0 – 2.7)
	ES Cotton	4.2 (3.4 – 4.5)	3.2 (2.6 – 3.4)
	Push Bamboo	3.0 (2.5 – 3.8)	1.9 (0.4 – 2.1)
	Push Cotton	3.7 (1.5 – 4.0)	1.5 (0.9 – 1.8)
Calf	ES Bamboo	6.5 (4.7 – 7.2)	1.3 (0.6 – 1.9)
	ES Cotton	9.1 (5.2 – 9.6)	1.1 (0.4 – 2.8)
	Push Bamboo	4.4 (3.9 – 6.0)	4.0 (0.9 – 4.5)
	Push Cotton	5.7 (4.5 – 6.2)	4.7 (1.5 – 5.0)

D.5 Comparison of temperature changes from baseline between the AFO foot and the control foot during stationary standing. Colour coded to ambient temperature: Blue: <16°C, Yellow: 16-18°C, Red: 18-20°C

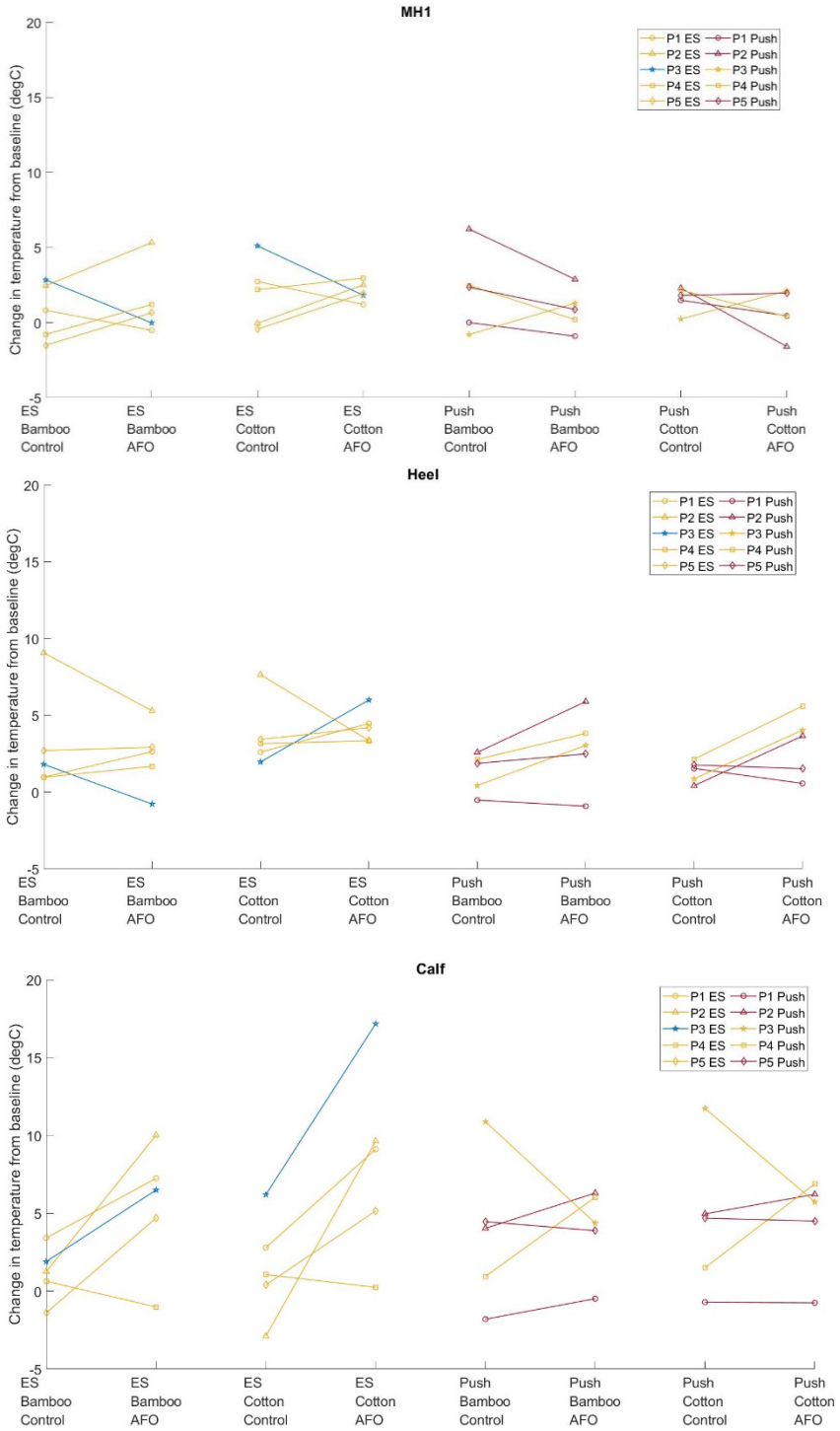

Appendix EChapter 3 – Ambient and Baseline Temperature and Humidity

E.1 Ambient and navicular head baseline temperatures for each participant and test session

Participant	Ambient Temp. – ES AFO (°C)	Ambient Temp. – Push AFO (°C)	Navicular Head Baseline Temp. – ES AFO (°C)	Navicular Head Baseline Temp. – Push AFO (°C)	Heel Baseline Temp. – ES AFO (°C)	Heel Baseline Temp. – Push AFO (°C)	MH1 Baseline Temp. – ES AFO (°C)	MH1 Baseline Temp. – Push AFO (°C)	MH5 Baseline Temp. – ES AFO (°C)	MH5 Baseline Temp. – Push AFO (°C)
1	16.4	19.4	26.9	29.7	28.6	29.0	23.7	26.1	25.7	25.4
2	16.2	18.3	29.6	27.1	29.3	24.6	24.9	29.8	28.3	29.0
3	12.0	16.7	21.5	22.7	25.5	24.5	19.8	19.9	21.4	19.0
4	17.9	17.3	23.1	21.3	26.4	31.6	22.1	25.4	23.9	23.0
5	17.0	19.3	22.2	23.2	25.6	26.8	20.2	23.1	21.3	24.7

E.2 Ambient and navicular head baseline relative humidity (RH) for each participant and test session

Participant	Ambient RH – ES AFO (%RH)	Ambient RH – Push AFO (%RH)	Navicular Head Baseline RH – ES AFO (%RH)	Navicular Head Baseline RH – Push AFO (%RH)	Heel Baseline RH – ES AFO (%RH)	Heel Baseline RH – Push AFO (%RH)	MH1 Baseline RH – ES AFO (%RH)	MH1 Baseline RH – Push AFO (%RH)	MH5 Baseline RH – ES AFO (%RH)	MH5 Baseline RH – Push AFO (%RH)
1	43.8	59.6	37.2	46.2	30.6	52.3	42.3	50.6	32.4	49.7
2	40.8	34.1	31.2	28.8	24.9	28.2	29.2	27.7	28.3	28.1
3	49.9	37.7	35.4	31.8	26.0	26.9	34.0	32.9	39.9	34.6
4	48.0	57.9	46.9	56.5	47.6	40.8	44.3	43.1	51.7	55.3
5	51.9	56.1	47.4	53.5	38.1	42.1	43.6	50.1	44.3	50.5

Appendix F Chapter 3 – Testing of Micropore Tape to hold Sensirion Sensors in Place

Four Sensirion SHT75 sensors were taped to the skin and the temperature and humidity recorded for two minutes for each of three test conditions:

1. No tape – Tape only in contact with the sensor port and not with the sensor itself,
2. Tape over sensors - Tape lightly covering the main body of the sensor,
3. Tape over pins – Tape over the sensor pins but not covering the sensing element.

The average temperature and humidity for each sensor in each condition was calculated and the effect of using the tape examined.

F.1 The combined temperature/humidity sensor, showing where tape was applied in the test conditions

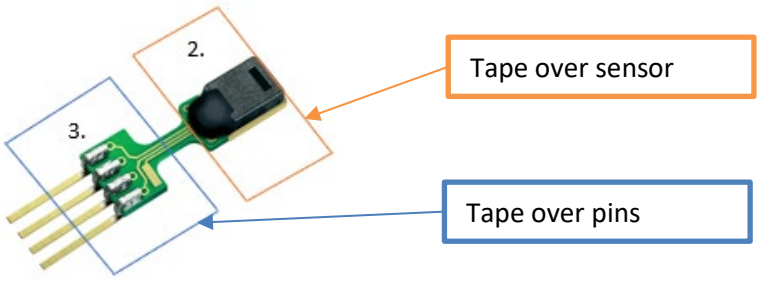

F.2 Temperature and humidity results for testing of micropore tape to hold Sensirion sensors in place

Sensor – Temperature (°C) or Humidity (%RH)	No Tape (1.)	Tape over sensors (2.)	Tape over pins (3.)	% change between Condition 2 and 1	% change between Condition 3 and 1
S1 – RH	31.79	36.76	33.32	15.70	4.81
S2 – RH	30.51	35.81	31.07	17.37	1.82
S3 – RH	29.20	37.94	30.87	29.94	5.72
S4 - RH	30.65	33.38	30.15	8.91	-1.62
S1 - Temperature	32.88	32.18	33.09	-2.11	0.65
S2 - Temperature	31.45	30.92	31.41	-1.70	-0.15
S3 - Temperature	32.57	32.03	32.69	-1.66	0.37
S4 - Temperature	32.47	31.99	32.71	-1.47	0.75

Taping over the sensing element showed a clear difference in the temperature and humidity recorded compared to only taping over the port of the sensor. When only taping over the pins, there was very little difference in the temperature compared to the No Tape Condition. For the humidity, there was a slight increase for two of the four sensors though considerably less than when taping over the sensing element. The other two sensors showed limited difference. It is possible that any difference present was due to a change in the amount of contact with the skin rather than due to the micropore tape.

Appendix G Chapter 4 – Individual Participant Data and Model Predictions

This appendix contains the full participant data for Chapter 4.

G.1 Clinical data for the participants in Chapter 4.

Participant	Gender (M/F)	Age (years)	Weight (kg)	Haglunds?
N1	F	31	57	No
N2	F	42	61	Yes
N3	F	25	80	No
N4	M	50	77	Maybe
N5	F	34	41	No

G.2 Model predictions for the participants in Chapter 4.

Participant	AFO Configuration	99th% shear strain in the soft tissue (%)	Volume of tissue over 10% shear strain (mm^3)	99th% plantar pressure (kPa)	Max. plantar pressure gradients (kPa/mm)
N1	Normal_PP	14.05	2876	161.6	24.8
	Normal_C	13.72	2475	95.4	12.8
	Undersize_PP	15.13	3458	159.1	25.3
	Undersize_C	14.68	2964	97.7	12.6
N2	Normal_PP	12.75	2395	157.3	26.4
	Normal_C	13.30	2675	82.4	12.0
	Undersize_PP	13.22	2708	170.1	25.1
	Undersize_C	13.54	2809	86.1	11.7
N3	Normal_PP	19.54	8275	167.4	27.5
	Normal_C	19.47	7407	117.9	14.4
	Undersize_PP	20.10	8765	171.8	28.3
	Undersize_C	19.76	7623	120.2	17.1
N4	Normal_PP	20.33	13546	157.0	26.2
	Normal_C	19.97	11826	105.1	15.6
	Undersize_PP	20.99	14764	154.2	19.9
	Undersize_C	20.37	12378	104.4	14.4
N5	Normal_PP	18.52	6750	158.5	25.9
	Normal_C	17.71	5221	106.7	12.3
	Undersize_PP	19.32	7149	158.8	25.3
	Undersize_C	18.83	5998	107.5	12.8

Appendix H Chapter 4 – Undersize AFO Measurements

The undersize AFO modelled in Chapter 4 was based on the measurements of the AFO Extra Strong (OrthoEurope) from Chapter 3 (see Section 3.1.1.1). The off-the-shelf device came in four different sizes – small (shoe size <6), medium (shoe size 6.5-9), large (shoe size 7-9.5) and extra large (shoe size >9.5). A surface scan was taken of each size of device, using a structured white light scanner (Creaform Academia 50, Quebec, Canada). Using the acquisition software (VXelements, v8.1.1), linear measurements were taken across the widest point of the forefoot region of the device to reflect the region being modelled. Three measurements were taken for each device and then the mean forefoot width for each device was calculated.

H.1 Surface scan of the AFO Extra Strong, indicating an example forefoot width measurement taken

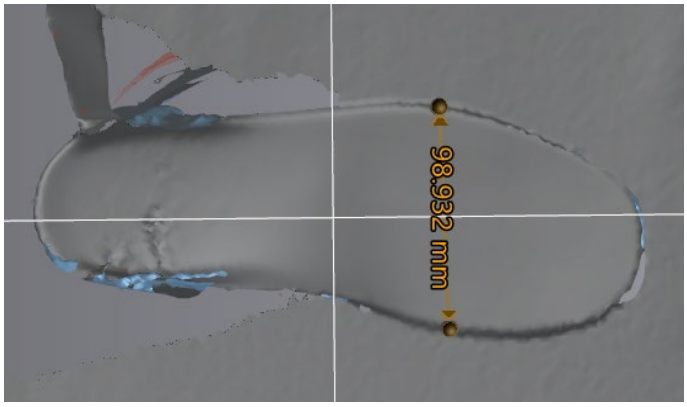

H.2 Forefoot width measurements of the four different AFO Extra Strong sizes

AFO size	Small	Medium	Large	Extra Large
Measurement 1 (mm)	77.58	92.80	98.93	96.22
Measurement 2 (mm)	78.56	95.08	95.11	96.98
Measurement 3 (mm)	77.82	94.47	96.60	97.80
Average forefoot width (mm)	77.99	94.12	96.88	97.00

The biggest difference in forefoot width occurred between the small and medium sizes, with a difference of 16.1mm. Thus, it was assumed that the maximum undersizing would be 8.05mm,

assuming the AFO wearer had a forefoot width exactly half the difference in sizes and was given a small device rather than a medium. This size difference amounted to approximately 10% of the total width, and so for the undersize AFO models, 5% was removed from both sides of the device.

Appendix I Experimental Testing of Forefoot Pressures in Midstance – Normal Gait

In Chapter 3, experimental testing of healthy participants comparing AFO design and sock material was discussed. As part of this testing, the participants also walked normally without an AFO to collect data that could be used for modelling purposes. In the modelling chapters, the data was used to establish plantar pressure distributions between the forefoot and the rest of the foot and across the forefoot. For Chapter 5, peak forefoot pressures during midstance were also compared to the model results. A brief overview of the methods and results is included below.

I.1 Methods

Five healthy participants (2 male, 3 female) were recruited to examine plantar pressures during gait. Ethical approval was granted by the University of Southampton (ERGO ID: 51969). Each participant walked at a self-selected pace on a treadmill for 2 minutes, whilst wearing training shoes of an appropriate size that were provided for them (NDB Lightweight Cross-training running trainers). In-shoe plantar pressures were sampled at 50Hz using F-scan sensors (Tekscan, Massachusetts, USA) throughout the testing.

The F-scan Research Software (v.7.5, Tekscan, USA) was then used to extract the peak pressures experienced by both feet in different foot regions during midstance. The 10th stance was used for the analysis for each participant – this was chosen arbitrarily from the middle of the test condition. Midstance was identified and the peak pressures in the forefoot from that time point were recorded. These peak pressures were then used for comparison to the model results to determine whether the midstance pressures predicted by the models were within the expected range. Additionally, the peak pressures in the toes, forefoot, midfoot and rearfoot, and under each metatarsal head were extracted and the ratios for pressure across the foot and within the forefoot calculated.

I.2 Peak forefoot pressures measured during midstance of gait

Participant	Left foot peak pressure (kPa)	Right foot peak pressure (kPa)
P1	105	85
P2	352	176
P3	133	92

Participant	Left foot peak pressure (kPa)	Right foot peak pressure (kPa)
P4	151	129
P5	151	70

I.3 Ratio of peak pressures between regions of the foot during midstance for both left (LF) and right (RF) feet of each participant

	P1 LF	P1 RF	P2 LF	P2 RF	P3 LF	P3 RF	P4 LF	P4 RF	P5 LF	P5 RF	Avg.
Toes	1.09	0.32	0.21	0.27	0.42	0.33	0.28	0.36	0.45	0.68	0.44
Forefoot	1.09	1.12	2.44	1.68	1.39	1.24	1.05	1.38	1.52	0.85	1.38
Midfoot	0.38	1.19	1.09	1.39	1.03	0.95	0.67	0.87	0.72	1.24	0.95
Rearfoot	1.45	1.37	0.26	0.67	1.16	1.48	2.00	1.38	1.31	1.24	1.23

I.4 Ratio of peak pressures under each metatarsal head (MH1-5) during midstance for both left (LF) and right (RF) feet of each participant

	P1 LF	P1 RF	P2 LF	P2 RF	P3 LF	P3 RF	P4 LF	P4 RF	P5 LF	P5 RF
MH1	0.73	1.17	0.91	1.03	0.90	1.21	1.08	1.10	1.31	1.35
MH2	0.99	1.22	1.41	1.16	1.03	1.18	1.26	1.17	1.08	1.29
MH3	1.10	1.02	1.02	1.04	1.23	1.16	1.14	1.28	1.20	0.96
MH4	1.25	0.86	0.81	0.92	1.05	0.70	0.92	0.99	0.92	0.74
MH5	0.93	0.73	0.84	0.85	0.79	0.76	0.60	0.45	0.49	0.66

The ratios of peak pressures across the forefoot varied considerably between participants, with the location of the maximum forefoot pressure occurring under MH1 three times, MH2 four times, MH3 twice and MH4 once. As MH2 was the location of peak pressure most commonly during the testing, it was decided that the models would use a similar load distribution. As such, the ratios with peaks under MH2 (P1 RF, P2 LF, P2 RF, P4 LF) were averaged to form a viable forefoot load distribution to use for the modelling: 1.05, 1.26, 1.06, 0.88 and 0.75 for MH1 to MH5 respectively.

Appendix J Model Mesh Convergence and Sensitivity Analyses

This Appendix contains the mesh convergence analyses for the models from Chapters 4, 5, and 6 as well as the sensitivity analysis performed to determine the effect of the cut edges of the modelled forefoot section.

J.1 AFO Model Mesh Convergence

A mesh convergence analysis was performed using participant N1's Normal_PP model, a 6mm full-width polypropylene AFO. The element size in the sock, skin, and underlying soft tissue regions was varied, and the 99th% plantar pressure and shear strain model predictions were compared to the finest mesh. Based on the results of the convergence analysis, Mesh 2 was used for the AFO models in Chapter 4 for a balance of accuracy and computational solving time.

J.1.1 AFO model mesh convergence results

	Mesh 1 (finest)	Mesh 2 (used)	Mesh 3	Mesh 4
No. elements	487932	269138	229385	152146
99th% plantar pressure (kPa)	212.6	200.3	187.8	179.7
% difference in pressure from finest mesh	NA	-5.79	-11.67	-15.50
99th% shear strain in soft tissues (%)	13.30	13.65	13.79	14.02
% difference in shear strain from finest mesh	NA	2.63	3.68	5.41

J.2 FO Model Mesh Convergence

A mesh convergence analysis for the RA FO models was performed using the RA1 model with a leather shoe and total contact EVA FO (L_EVA). The element size in the sock, upper boundary of the FO which interfaced with the limb, skin, and underlying soft tissue regions was varied. Based on the results of the mesh convergence, Mesh 3 was used in the FO modelling studies in Chapters 5 and 6 as the 99th% plantar pressure and shear strain were within 2.5% of the finest mesh.

J.2.1 FO model mesh convergence results

	Mesh 1 (finest)	Mesh 2	Mesh 3 (used)	Mesh 4
No. elements	492125	396891	338505	261034
99th% plantar pressure (kPa)	63.62	63.64	63.57	63.51
% difference in pressure from finest mesh	NA	0.03	-0.08	-0.17
99th% shear strain in soft tissues (%)	10.36	10.49	10.60	10.68
% difference in shear strain from finest mesh	NA	1.25	2.32	3.09

J.3 Sensitivity Analysis of Forefoot Section Cut Edges

A sensitivity analysis was performed to ensure that the proximity of the forefoot section's cut edges to the region of interest would not affect the model results. Example models were run, removing a coronal MR slice at a time from both edges of the data. It was determined that as long as there was a slice between the region of interest (e.g. the sesamoid bones) and the section edge, the results were unaffected by the edge proximity (<0.5% difference in percentile strain and pressure). The sensitivity analysis was run using a total contact foot orthosis with leather shoe model (see Chapter 5), and it was assumed that the results would apply to the other orthosis configurations used in Chapters 4 and 6.

J.3.1 Results from sensitivity analysis of removing coronal MR slices from forefoot section model

Model Prediction Parameter	Original Model	Model with 1 slice removed from edges	Model with 2 slices removed from edges
99th% shear strain in soft tissues (%)	12.28	12.33	11.88
Volume of tissue over 10% shear strain (mm^3)	2359	2392	1406
99th% plantar pressure (kPa)	63.47	63.63	62.65

Appendix K Experimental Peak Midstance Pressures with AFO

This appendix contains the peak midstance pressures and pressure gradients measured in the forefoot region during the experimental testing in Chapter 3, which were used to assess the validity of the AFO models in Chapter 4. The results were extracted from the F-scan data of the right feet of the participants, which was the foot which wore the AFO. Note that the volunteers involved in the Chapter 3 testing were not the volunteers modelled in Chapter 4. The four relevant gait conditions examined were as follows:

- ES Bamboo – ES AFO with a bamboo sock
- ES Cotton – ES AFO with a cotton sock
- Push Bamboo – Push AFO with a bamboo sock
- Push Cotton – Push AFO with a cotton sock.

The ranges and medians reported in the discussion of the AFO modelling (Chapter 4) were calculated for the ES and Push AFOs, combining the results from the test conditions with the bamboo and cotton socks for each.

K.1 Peak midstance plantar pressures (kPa) in the forefoot measured experimentally during four test conditions

Participant	ES Bamboo	ES Cotton	Push Bamboo	Push Cotton
P1	77	65	92	121
P2	216	173	103	78
P3	135	120	105	110
P4	109	110	100	115
P5	122	146	112	104

K.2 Maximum midstance pressure gradients (kPa/mm) in the forefoot measured experimentally during four test conditions

Participant	ES Bamboo	ES Cotton	Push Bamboo	Push Cotton
P1	8.8	7.1	16.5	18.6
P2	65.1	44.3	21.6	9.2
P3	15.5	17.8	16.5	13.7
P4	17.8	22.5	15.5	23.1

Participant	ES Bamboo	ES Cotton	Push Bamboo	Push Cotton
P5	12.9	30.0	17.3	20.0

Appendix L Chapter 5 – Individual Participant Data and Results in Full

This appendix contains the full results for the:

- Clinical data for each participant
- Morphological measurements for each participant
- Computational model predictions for each participant
- Relevant correlations between clinical data and morphological measurements

L.1 Clinical data for each participant

	BMI	Disease Duration (years)	LFIS-IF Score	Instances of bursae between and below joints	Instances of erosion at joints	Instances of synovial hypertrophy at joints	Total instances of bursae, erosion, hypertrophy
RA1	26.7	14	13	4	3	1	8
RA2	28.3	8	12	4	0	0	4
RA3	30.9	1	5	1	1	1	3
RA4	23.2	2	9	1	0	5	6
RA5	21.7	3	18	0	0	0	0
RA6	22.3	30	5	0	1	2	3
RA7	29.5	4	13	2	1	5	8
RA8	21.7	22	15	2	4	2	8
RA9	22.1	12	7	1	4	2	7
RA10	24.8	35	4	1	0	0	1
RA11	30.2	5	17	0	3	1	4
RA12	22.9	28	16	NA	NA	NA	NA
RA13	28.4	6	15	4	4	2	10

L.2 Morphological measurements per participant taken from MR data. For participants with RA: green indicates ranking 1-4 and red indicates ranking 10-13

	Sesamoid Position (Normal/Displaced)	Unloaded lateral offset of sesamoid from MH1 edge (as % of MH1 width)	Depth of Tissue under MH1 (mm)	Average Principal Curvature of MH1 (mm^{-1})
RA1	Displaced	40.0	12.9	0.112
RA2	Normal	17.3	10.9	0.118
RA3	Normal	14.2	18.8	0.168
RA4	Normal	17.8	16.2	0.152
RA5	Normal	29.0	14.1	0.163
RA6	Displaced	39.8	12.5	0.169
RA7	Normal	20.2	15.1	0.170
RA8	Normal	23.4	19.8	0.144
RA9	Normal	22.1	17.6	0.149
RA10	Displaced	72.0	9.9	0.120
RA11	Normal	5.7	20.8	0.156
RA12	Displaced	32.9	15.6	0.128
RA13	Normal	14.0	18.1	0.144
Healthy	Normal	14.4	16.7	0.079

L.3 Results from computational models per participant. For participants with RA: green indicates ranking 1-4 and red indicates ranking 10-13

	99^{th}% Shear strain in soft tissues (%)	Volume of tissue over 10% shear strain (mm^3)	99^{th}% Plantar pressure (kPa)	Max. plantar pressure gradient (kPa/mm)
RA1	12.28	2359	63.47	2.31
RA2	13.09	2999	60.84	3.09
RA3	17.60	9377	71.18	3.42
RA4	13.80	4078	60.76	3.40
RA5	13.23	3124	65.62	3.06

	99th% Shear strain in soft tissues (%)	Volume of tissue over 10% shear strain (mm^3)	99th% Plantar pressure (kPa)	Max. plantar pressure gradient (kPa/mm)
RA6	11.84	1641	59.31	3.85
RA7	22.13	11686	83.37	3.31
RA8	16.68	6407	65.24	2.74
RA9	13.72	3214	54.30	2.36
RA10	9.96	1386	51.01	2.64
RA11	21.74	12955	87.76	4.96
RA12	9.92	1285	46.19	2.57
RA13	14.47	3833	62.94	3.31
Healthy	12.33	1418	55.57	3.37

L.4 Correlations for clinical data and morphological measurements. Moderate to strong correlations (>0.4) are bolded. * indicates significant (p<0.05) correlation.

Variable 1	Variable 2	Correlation (p value)
Disease duration	Unloaded lateral offset of sesamoid	**0.698 (0.008)***
Disease duration	Tissue Depth under MH1	**-0.428 (0.145)**
Disease duration	LFIS-IF	-0.309 (0.304)
Disease duration	Instances of bursae, erosion, synovial hypertrophy	-0.198 (0.537)
Disease duration	Average principal curvature of MH1	**-0.401 (0.174)**
LFIS-IF Score	Unloaded lateral offset of sesamoid	**-0.425 (0.148)**
LFIS-IF Score	Tissue Depth under MH1	0.332 (0.267)
LFIS-IF Score	Instances of bursae, erosion, synovial hypertrophy	0.259 (0.417)
LFIS-IF Score	Average principal curvature of MH1	-0.069 (0.823)
Instances of bursae, erosion, synovial hypertrophy	Tissue Depth under MH1	**0.406 (0.190)**
Instances of bursae, erosion, synovial hypertrophy	Average principal curvature of MH1	-0.124 (0.701)
Tissue Depth under MH1	Unloaded lateral offset of sesamoid	**-0.721 (0.005)***

Appendix M Chapter 6 – FO/shoe type comparisons

M.1 Full results for each participant

The following tables include the model predictions for each participant and each model configuration:

- L_EVA = leather shoe with EVA orthosis
- L_PC = leather shoe with Poron Cushioning orthosis
- L_PF = leather shoe with Poron Firm orthosis
- L_PP = leather shoe with Poron Firm + Plastazote orthosis
- T_PC = training shoe with Poron Cushioning orthosis
- T_PF = training shoe with Poron Firm orthosis
- T_PP = training shoe with Poron Firm + Plastazote orthosis

M.1.1 99th% shear strain in the soft tissue predictions (%) for each participant

Participant	L_EVA	L_PC	L_PF	L_PP	T_PC	T_PF	T_PP
RA1	11.93	12.28	12.13	12.33	12.85	12.46	12.57
RA2	12.44	13.09	12.83	13.05	13.70	13.36	13.52
RA3	16.58	17.60	17.19	17.77	19.63	19.09	19.22
RA4	13.00	13.80	13.64	13.78	14.89	14.51	14.82
RA5	12.65	13.23	13.02	13.06	13.99	13.70	13.89
RA6	11.37	11.84	11.65	11.83	12.78	12.54	12.85
RA7	21.02	22.13	21.76	21.67	23.81	23.50	23.66
RA8	15.59	16.68	16.25	16.69	18.24	17.96	18.20
RA9	13.02	13.72	13.43	13.69	14.72	14.49	14.72
RA10	9.35	9.96	9.72	9.90	10.49	10.27	10.36
RA11	20.52	21.74	21.23	21.85	24.77	24.30	24.45
RA12	9.51	9.92	9.78	9.78	10.49	10.30	10.42
RA13	13.72	14.47	14.20	14.31	15.39	15.00	15.49

M.1.2 Volume of the soft tissue over 10% shear strain predictions (mm^3) for each participant

Participant	L_EVA	L_PC	L_PF	L_PP	T_PC	T_PF	T_PP
RA1	2136	2359	2257	2378	2775	2523	2579
RA2	2604	2999	2850	2976	3446	3203	3284
RA3	7424	9377	8536	9198	12038	11122	11464

Participant	L_EVA	L_PC	L_PF	L_PP	T_PC	T_PF	T_PP
RA4	3421	4078	3931	4038	5250	4882	5116
RA5	2657	3124	2922	3002	3938	3624	3841
RA6	1438	1641	1561	1647	2065	1969	2114
RA7	9728	11686	10877	11372	14771	13885	14683
RA8	5063	6407	5827	6272	8712	8002	8431
RA9	2701	3214	2979	3178	4124	3908	4154
RA10	1045	1386	1242	1351	1715	1577	1632
RA11	10869	12955	12037	13133	17779	16631	17689
RA12	1076	1285	1209	1214	1611	1506	1578
RA13	3203	3833	3592	3735	4906	4517	4999

M.1.3 99th% plantar pressure predictions (kPa) for each participant

Participant	L_EVA	L_PC	L_PF	L_PP	T_PC	T_PF	T_PP
RA1	63.07	63.47	62.69	62.70	69.09	67.47	67.41
RA2	63.39	60.84	61.81	61.92	70.26	70.89	69.61
RA3	70.89	71.18	71.09	71.02	77.57	77.36	76.34
RA4	64.19	60.76	62.13	61.84	65.78	66.99	66.60
RA5	64.89	65.62	65.03	64.92	72.71	71.51	70.99
RA6	62.30	59.31	60.19	59.70	63.50	64.40	63.58
RA7	85.12	83.37	83.64	83.91	88.00	88.42	88.17
RA8	66.47	65.24	65.61	65.44	69.16	69.93	69.24
RA9	58.07	54.30	55.56	55.35	57.13	58.98	58.62
RA10	48.91	51.01	50.33	50.11	55.36	53.51	53.39
RA11	92.21	87.76	88.61	89.18	92.22	93.84	94.01
RA12	47.57	46.19	46.04	46.19	48.29	49.27	49.03
RA13	64.86	62.94	62.69	62.47	67.46	68.22	68.09

M.1.4 Maximum plantar pressure gradient predictions (kPa/mm) for each participant

Participant	L_EVA	L_PC	L_PF	L_PP	T_PC	T_PF	T_PP
RA1	2.70	2.31	2.11	2.01	2.42	2.56	2.53
RA2	2.86	3.09	3.14	3.04	3.39	3.14	3.09
RA3	4.04	3.42	3.57	3.79	3.92	4.31	4.22
RA4	2.45	3.40	2.87	2.81	2.99	2.78	2.73
RA5	3.80	3.06	3.31	3.15	3.59	3.68	3.68
RA6	3.13	3.85	3.54	3.42	3.62	3.45	3.49
RA7	3.50	3.31	3.08	4.30	4.91	4.95	5.19
RA8	1.88	2.74	2.46	2.62	3.13	2.80	3.02

Participant	L_EVA	L_PC	L_PF	L_PP	T_PC	T_PF	T_PP
RA9	2.06	2.36	2.25	2.89	2.63	2.46	2.36
RA10	3.70	2.64	2.54	2.61	2.84	3.22	3.57
RA11	3.94	4.96	4.71	4.44	4.00	3.69	3.53
RA12	1.95	2.57	2.38	2.28	2.33	2.15	2.12
RA13	2.51	3.31	3.10	3.07	3.77	3.47	3.31

M.2 High vs. normal BMI comparisons

The following tables contain the mean differences between the FO/shoe types separated into two normal and high BMI groups. The normal BMI group (BMI<25) consisted of RA4, RA5, RA6, RA8, RA9, RA10, RA12, and the high BMI group (BMI>=25) consisted of RA1, RA2, RA3, RA7, RA11, RA13.

M.2.1 Mean differences in 99th% shear strain in the soft tissues (%) for the high and normal BMI groups

Model 1	Model 2	High BMI group	Normal BMI group
L_EVA	L_PC	-0.85	-0.67
L_EVA	L_PF	-0.52	-0.43
L_EVA	L_PP	-0.80	-0.61
L_PC	L_PF	0.33	0.24
L_PC	L_PP	0.06	0.06
L_PF	L_PP	-0.27	-0.18
T_PC	T_PF	0.41	0.26
T_PC	T_PP	0.21	0.05
T_PF	T_PP	-0.20	-0.21
L_PC	T_PC	-1.47	-0.92
L_PF	T_PF	-1.40	-0.90
L_PP	T_PP	-1.32	-0.93

M.2.2 Median differences in volume of the soft tissue over 10% shear strain (mm^3) for the high and normal BMI groups

Model 1	Model 2	High BMI group	Normal BMI group
L_EVA	L_PC	-1208	-533
L_EVA	L_PF	-698	-324
L_EVA	L_PP	-1138	-472
L_PC	L_PF	510	209
L_PC	L_PP	70	62
L_PF	L_PP	-440	-147

Model 1	Model 2	High BMI group	Normal BMI group
T_PC	T_PF	639	278
T_PC	T_PP	170	78
T_PF	T_PP	-470	-200
L_PC	T_PC	-2084	-897
L_PF	T_PF	-1955	-828
L_PP	T_PP	-1984	-881

M.2.3 Mean differences in 99th% plantar pressure (kPa) for the high and normal BMI groups

Model 1	Model 2	High BMI group	Normal BMI group
L_EVA	L_PC	1.66	1.42
L_EVA	L_PF	1.50	1.07
L_EVA	L_PP	1.39	1.26
L_PC	L_PF	-0.16	-0.35
L_PC	L_PP	-0.27	-0.16
L_PF	L_PP	-0.11	0.19
T_PC	T_PF	-0.27	-0.38
T_PC	T_PP	0.16	0.07
T_PF	T_PP	0.43	0.45
L_PC	T_PC	-5.84	-4.21
L_PF	T_PF	-5.95	-4.24
L_PP	T_PP	-5.41	-3.99

M.2.4 Mean differences in maximum plantar pressure gradients (kPa/mm) for the high and normal BMI groups

Model 1	Model 2	High BMI group	Normal BMI group
L_EVA	L_PC	-0.14	-0.24
L_EVA	L_PF	-0.03	-0.05
L_EVA	L_PP	-0.18	-0.12
L_PC	L_PF	0.12	0.18
L_PC	L_PP	-0.04	0.12
L_PF	L_PP	-0.16	-0.06
T_PC	T_PF	0.05	0.08
T_PC	T_PP	0.09	0.02
T_PF	T_PP	0.04	-0.06
L_PC	T_PC	-0.34	-0.07
L_PF	T_PF	-0.40	-0.17
L_PP	T_PP	-0.20	-0.17

List of References

1. Kelly, E.S., Dickinson, A.S., Worsley, P.R., *Effects of Ankle-Foot Orthosis Design on the Pressure and Microclimate Between the Device and Limb*, in *International Society for Prosthetics and Orthotics (ISPO) 18th World Congress 2021*. 2021, Prosthetics and Orthotics International. p. 148.

2. Kelly, E.S., et al., *Predicting Forefoot-Orthosis Interactions in Rheumatoid Arthritis Using Computational Modelling.* Frontiers in Bioengineering & Biotechnology, 2021. **9**: 803725.

3. Healy, A., et al., *A scoping literature review of studies assessing effectiveness and cost-effectiveness of prosthetic and orthotic interventions.* Disability and Rehabilitation: Assistive Technology, 2020. **15**(1): p. 60-66.

4. World Health Organisation (WHO), *Standards for prosthetics and orthotics*. 2017.

5. International Committee of the Red Cross (ICRC), *Physical Rehabilation Programme 2018 Annual Report*. 2018.

6. LeBlanc, M.A., *Patient Population And Other Estimates Of Prosthetics And Orthotics In The U.S.A.* Orthotics and Prosthetics Library, 1973. **27**(3): p. 38-44.

7. NHS, *Improving the Quality of Orthotic Services in England*. 2015, NHS England.

8. Ikeda, A.J., et al., *A scoping literature review of the provision of orthoses and prostheses in resource-limited environments 2000–2010. Part one: Considerations for success.* Prosthetics and Orthotics International, 2014. **38**(4): p. 269-286.

9. NHS, *Scottish Orthotic Services Review*. 2005, NHS Scotland.

10. American Board for Certification in Orthotics, P.P., Inc., *Practice Analysis of Certified Practitioners in the Disciplines of Orthotics and Prosthetics*. 2019, American Board for Certification in Orthotics, Prosthetics & Pedorthics, Inc.

11. Chockalingam, N., N. Eddison, and A. Healy, *Cross-sectional survey of orthotic service provision in the UK: does where you live affect the service you receive?* BMJ Open, 2019. **9**(10): e028186.

12. Dobson, A., et al., *Economic value of orthotic and prosthetic services among medicare beneficiaries: a claims-based retrospective cohort study, 2011-2014.* Journal of neuroengineering and rehabilitation, 2018. **15**(Suppl 1): p. 55.

13. Ramstrand, N. and Brodtkorb, T.H., *Considerations for developing an evidenced-based practice in orthotics and prosthetics.* Prosthetics and Orthotics International, 2008. **32**(1): p. 93-102.

14. Brockett, C.L. and G.J. Chapman, *Biomechanics of the ankle.* Orthopaedics and Trauma, 2016. **30**(3): p. 232-238.

15. Drake, R.L., Vogel, A.W., and Mitchell, A.W.M., *Gray's Anatomy for Students, 3rd edition*. Philadelphia: Churchill Livingstone, Elsevier.

16. Chan, C.W. and A. Rudins, *Foot biomechanics during walking and running.* Mayo Clinic proceedings, 1994. **69**(5): p. 448-461.

17. Riegger, C.L., *Anatomy of the ankle and foot.* Physical therapy, 1988. **68**(12): p. 1802-1814.

18. Sims, A.L. and Kurup, H.V., *Painful sesamoid of the great toe.* World journal of orthopedics, 2014. **5**(2): p. 146-150.

19. Bader, D.L., Worsley, P.R., and Gefen, A., *Bioengineering considerations in the prevention of medical device-related pressure ulcers.* Clinical Biomechanics, 2019. **67**: p. 70-77.

20. Wang, Y.N. and Sanders, J.E., *How does skin adapt to repetitive mechanical stress to become load tolerant?* Medical Hypotheses, 2003. **61**(1): p. 29-35.

21. Cherry, L., et al., *The reliability of a novel magnetic resonance imaging-based tool for the evaluation of forefoot bursae in patients with rheumatoid arthritis: the FFB score.* Rheumatology (Oxford), 2014. **53**(11): p. 2014-2017.

22. McMinn, R.M.H., Logan, B.M., and Bowden, D.J., *McMinn's color atlas of lower limb anatomy*. 5th ed. 2018, [S.l.]: Elsevier.

23. Malas, B.S., *What variables influence the ability of an AFO to improve function and when are they indicated?* Clinical orthopaedics and related research, 2011. **469**(5): p. 1308-1314.

24. Chisholm, A.E. and Perry, S.D., *Ankle-foot orthotic management in neuromuscular disorders: recommendations for future research.* Disability and rehabilitation. Assistive technology, 2012. **7**(6): p. 437-449.

25. Cakar, E., et al., *The ankle-foot orthosis improves balance and reduces fall risk of chronic spastic hemiparetic patients.* European journal of physical and rehabilitation medicine, 2010. **46**(3): p. 363-368.

26. Gonzalez, H., Olsson, T., and Borg, K., *Management of postpolio syndrome.* The Lancet Neurology, 2010. **9**(6): p. 634-642.

27. Polliack, A.A., et al., *Lower Extremity Orthoses for Children with Myelomeningocele: User and Orthotist Perspectives.* JPO: Journal of Prosthetics and Orthotics, 2001. **13**(4): p. 123-129.

28. Cans, C., *Surveillance of cerebral palsy in Europe: a collaboration of cerebral palsy surveys and registers.* Developmental Medicine & Child Neurology, 2000. **42**(12): p. 816-824.

29. Sankar, C. and Mundkur, N., *Cerebral palsy-definition, classification, etiology and early diagnosis.* Indian journal of pediatrics, 2005. **72**(10): p. 865-868.

30. Bulley, C., et al., *Experiences of functional electrical stimulation (FES) and ankle foot orthoses (AFOs) for foot-drop in people with multiple sclerosis.* Disability and rehabilitation. Assistive technology, 2014. **10**(6): p. 458-467.

31. Phillips, M., Radford, K., and Wills, A., *Ankle foot orthoses for people with Charcot Marie Tooth disease--views of users and orthotists on important aspects of use.* Disability and Rehabilitation. Assistive Technology, 2011. **6**(6): p. 491-499.

32. Uhlig, T., Moe, R.H., and Kvien, T.K., *The burden of disease in rheumatoid arthritis.* Pharmacoeconomics, 2014. **32**(9): p. 841-851.

33. Bowen, C.J., et al., *Forefoot pathology in rheumatoid arthritis identified with ultrasound may not localise to areas of highest pressure: cohort observations at baseline and twelve months.* Journal of foot and ankle research, 2011. **4**: 25.

34. Nix, S.E., et al., *Characteristics of foot structure and footwear associated with hallux valgus: a systematic review.* Osteoarthritis and Cartilage, 2012. **20**(10): p. 1059-1074.

35. Jaakkola, J.I. and Mann, R.A., *A Review of Rheumatoid Arthritis Affecting the Foot and Ankle.* Foot & Ankle International, 2004. **25**(12): p. 866-874.

36. Bowen, C.J., et al., *Assessment of the natural history of forefoot bursae using ultrasonography in patients with rheumatoid arthritis: a twelve-month investigation.* Arthritis Care & Research, 2010. **62**(12): p. 1756-1762.

37. Van Hul, E., et al., *Pseudotumoural soft tissue lesions of the foot and ankle: a pictorial review.* Insights into Imaging, 2011. **2**(4): p. 439-452.

38. van der Leeden, M., et al., *Forefoot joint damage, pain and disability in rheumatoid arthritis patients with foot complaints: the role of plantar pressure and gait characteristics.* Rheumatology (Oxford), 2006. **45**(4): p. 465-469.

39. Firth, J., et al., *The prevalence of foot ulceration in patients with rheumatoid arthritis.* Arthritis Care & Research, 2008. **59**(2): p. 200-205.

40. Chua-Aguilera, C.J., Möller, B., and Yawalkar, N., *Skin Manifestations of Rheumatoid Arthritis, Juvenile Idiopathic Arthritis, and Spondyloarthritides.* Clinical Reviews in Allergy & Immunology, 2017. **53**(3): p. 371-393.

41. Poetker, D.M. and Reh, D.D., *A comprehensive review of the adverse effects of systemic corticosteroids.* Otolaryngologic Clinics of North America, 2010. **43**(4): p. 753-768.

42. Baan, H., et al., *Gait analysis of the lower limb in patients with rheumatoid arthritis: a systematic review.* Seminars in Arthritis and Rheumatism, 2012. **41**(6): p. 768-788 e8.

43. Louwerens, J.W.K. and Schrier, J.C.M., *Rheumatoid forefoot deformity: pathophysiology, evaluation and operative treatment options.* International orthopaedics, 2013. **37**(9): p. 1719-1729.

44. Carroll, M., et al., *Gait characteristics associated with the foot and ankle in inflammatory arthritis: a systematic review and meta-analysis.* BMC Musculoskeletal Disorders, 2015. **16**(1): 134.

45. Reina-Bueno, M., et al., *Effectiveness of custom-made foot orthoses in patients with rheumatoid arthritis: a randomized controlled trial.* Clinical Rehabilation, 2019. **33**(4): p. 661-669.

46. Dorset Orthopaedics. *SAFO: Silicone Ankle Foot Orthosis*. [Accessed: June 2019]; Available from: https://www.dorset-ortho.com/en/patient-services/safo/.

47. International Committee of the Red Cross (ICRC), *Manufacturing Guidelines: Ankle-foot orthosis*. 2007.

48. Pratt, D.J. and Sanner, W.H., *Paediatric foot orthoses.* The Foot, 1996. **6**(3): p. 99-111.

49. Brown, R., Byers-Hinkley, K., and Logan, L., *The Talus Control Ankle Foot Orthosis.* Orthotics and Prosthetics Library, 1987. **41**(3): p. 22-31.

50. Arizona AFO. *Supra Malleolar Orthosis (SMO)*. 2019 [Accessed: March 2020]; Available from: https://www.arizonaafo.com/products/thermoplastic/supra-malleolar-orthosis-smo.html.

51. Beckerman, H., et al., *Walking ability of stroke patients: efficacy of tibial nerve blocking and a polypropylene ankle-foot orthosis.* Archives of Physical Medicine and Rehabilitation, 1996. **77**(11): p. 1144-1151.

52. Bill, M., McIntosh, R., and Myers, P., *A series of case studies on the effect of a midfoot control ankle foot orthosis in the prevention of unresolved pressure areas in children with cerebral palsy.* Prosthetics and Orthotics International, 2001. **25**(3): p. 246-250.

53. Swinnen, E., et al., *Neurological patients and their lower limb orthotics: An observational pilot study about acceptance and satisfaction.* Prosthetics and Orthotics International, 2017. **41**(1): p. 41-50.

54. Holtkamp F.C., et al., *Use of and Satisfaction with Ankle Foot Orthoses.* Clinical Research on Foot & Ankle, 2015. **3**: 167.

55. Supan, T.J. and Hovorka, C.F., *A Review of Thermoplastic Ankle-Foot Orthoses Adjustments/Replacements in Young Cerebral Palsy and Spina Bifida Patients.* JPO: Journal of Prosthetics and Orthotics, 1995. **7**(1): p. 15-22.

56. Eddison, N., Healy, A., and Chockalingam, N., *Does user perception affect adherence when wearing biomechanically optimised ankle foot orthosis - footwear combinations: A pilot study.* The Foot, 2019. **43**: 101655.

57. Sugawara, A.T., et al., *Abandonment of assistive products: assessing abandonment levels and factors that impact on it.* Disability and rehabilitation. Assistive technology, 2018. **13**(7): p. 716-723.

58. Frasuńska, J., et al., *Compliance with prescriptions for wheelchairs, walking aids, orthotics, and pressure-relieving devices in patients with traumatic spinal cord injury.* European journal of physical and rehabilitation medicine, 2019. **56**(2): p. 160-168.

59. Kern, V., et al., *Ankle bracing practices in ambulatory, corticosteroid-naive boys with Duchenne muscular dystrophy.* Muscle & nerve, 2020. **61**(1): p. 52-57.

60. Kluding, P.M., et al., *Foot Drop Stimulation Versus Ankle Foot Orthosis After Stroke.* Stroke, 2013. **44**(6): p. 1660-1669.

61. Chapman, L.S., et al., *Foot orthoses for people with rheumatoid arthritis: a survey of prescription habits among podiatrists.* Journal of foot and ankle research, 2019. **12**: 7.

62. Tenten-Diepenmaat, M., et al., *Systematic review on the comparative effectiveness of foot orthoses in patients with rheumatoid arthritis.* Journal of foot and ankle research, 2019. **12**: 32.

63. Riskowski, J., Dufour, A.B.,, and Hannan, M.T., *Arthritis, foot pain and shoe wear: current musculoskeletal research on feet.* Current opinion in rheumatology, 2011. **23**(2): p. 148-155.

64. Hennessy, K., Woodburn, J., and Steultjens, M.P.M., *Custom foot orthoses for rheumatoid arthritis: A systematic review.* Arthritis Care & Research, 2012. **64**(3): p. 311-320.

65. Redmond, A.C., Landorf, K.B., and Keenan, A.M., *Contoured, prefabricated foot orthoses demonstrate comparable mechanical properties to contoured, customised foot orthoses: a plantar pressure study.* Journal of foot and ankle research, 2009. **2**: 20.

66. Tan, J.M., et al., *The efficacy of foot orthoses in individuals with patellofemoral osteoarthritis: a randomised feasibility trial.* Pilot and Feasibility Studies, 2019. **5**: 90.

67. Hsieh, R.L. and W.C. Lee, *Immediate and medium-term effects of custom-moulded insoles on pain, physical function, physical activity, and balance control in patients with knee osteoarthritis.* Journal of Rehabilitation Medicine, 2014. **46**(2): p. 159-165.

68. Hähni, M., Hirschmüller, A., and Baur, H., *The effect of foot orthoses with forefoot cushioning or metatarsal pad on forefoot peak plantar pressure in running.* Journal of Foot and Ankle Research, 2016. **9**: 44.

69. Bouten, C.V., et al., *The etiology of pressure ulcers: skin deep or muscle bound?* Archives of Physical Medicine and Rehabilitation, 2003. **84**(4): p. 616-619.

70. de Wert, L.A., et al., *A new method to evaluate the effects of shear on the skin.* Wound repair and regeneration, 2015. **23**(6): p. 885-890.

71. Peirce, S.M., Skalak, T.C., and Rodeheaver, G.T., *Ischemia-reperfusion injury in chronic pressure ulcer formation: A skin model in the rat.* Wound Repair and Regeneration, 2000. **8**(1): p. 68-76.

72. Kalogeris, T., et al., *Cell biology of ischemia/reperfusion injury.* International review of cell and molecular biology, 2012. **298**: p. 229-317.

73. Kayser, S.A., et al., *Prevalence and Analysis of Medical Device-Related Pressure Injuries: Results from the International Pressure Ulcer Prevalence Survey.* Advances in skin & wound care, 2018. **31**(6): p. 276-285.

74. Dealey, C., et al., *Challenges in pressure ulcer prevention.* International Wound Journal, 2015. **12**(3): p. 309-312.

75. Edsberg, L.E., et al., *Revised National Pressure Ulcer Advisory Panel Pressure Injury Staging System: Revised Pressure Injury Staging System.* Journal of wound, ostomy, and continence nursing : official publication of The Wound, Ostomy and Continence Nurses Society, 2016. **43**(6): p. 585-597.

76. Mirtaheri, P., et al., *A review of the role of the partial pressure of carbon dioxide in mechanically loaded tissues: the canary in the cage singing in tune with the pressure ulcer mantra.* Annals of biomedical engineering, 2015. **43**(2): p. 336-347.

77. Bader, D.L. and P.R. Worsley, *Technologies to monitor the health of loaded skin tissues.* Biomedical engineering online, 2018. **17**(1): 40.

78. Kottner, J., et al., *Skin response to sustained loading: A clinical explorative study.* Journal of Tissue Viability, 2015. **24**(3): p. 114-122.

79. Schario, M., et al., *Effects of two different fabrics on skin barrier function under real pressure conditions.* Journal of Tissue Viability, 2017. **26**(2): p. 150-155.

80. Bronneberg, D., et al., *Cytokine and chemokine release upon prolonged mechanical loading of the epidermis.* Experimental dermatology, 2007. **16**(7): p. 567-573.

81. Bramley, J.L., et al., *Establishing a measurement array to assess tissue tolerance during loading representative of prosthetic use.* Medical engineering & physics, 2020. **78**: p. 39-47.

82. Worsley, P.R., et al., *Investigating the effects of strap tension during non-invasive ventilation mask application: a combined biomechanical and biomarker approach.* Medical Devices (Auckland, NZ), 2016. **9**: p. 409-417.

83. Mee, J.B., et al., *Counter-Regulation of Interleukin-1α (IL-1α) and IL-1 Receptor Antagonist in Murine Keratinocytes.* Journal of Investigative Dermatology, 2005. **124**(6): p. 1267-1274.

84. Terui, T., et al., *An increased ratio of interleukin-1 receptor antagonist to interleukin-1α in inflammatory skin diseases.* Experimental Dermatology, 1998. **7**(6): p. 327-334.

85. Loerakker, S., et al., *The effects of deformation, ischemia, and reperfusion on the development of muscle damage during prolonged loading.* Journal of Applied Physiology, 2011. **111**(4): p. 1168-1177.

86. Stekelenburg, A., et al., *Role of ischemia and deformation in the onset of compression-induced deep tissue injury: MRI-based studies in a rat model.* Journal of applied physiology, 2007. **102**(5): p. 2002-2011.

87. Lilja, M., Hoffmann, P., and Oberg, T., *Morphological changes during early trans-tibial prosthetic fitting.* Prosthetics and Orthotics International, 1998. **22**(2): p. 115-122.

88. Brienza, D., et al., *An MRI investigation of the effects of user anatomy and wheelchair cushion type on tissue deformation.* Journal of Tissue Viability, 2018. **27**(1): p. 42-53.

89. Call, E., et al., *Off loading wheelchair cushion provides best case reduction in tissue deformation as indicated by MRI.* Journal of Tissue Viability, 2017. **26**(3): p. 172-179.

90. Petre, M., Erdemir, A., and Cavanagh, P.R., *An MRI-compatible foot-loading device for assessment of internal tissue deformation.* Journal of biomechanics, 2008. **41**(2): p. 470-474.

91. Bogie, K.M., Nuseibeh, I., and Bader, D.L., *Early progressive changes in tissue viability in the seated spinal cord injured subject.* Paraplegia, 1995. **33**(3): p. 141-147.

92. Bates-Jensen, B.M., et al., *Subepidermal moisture differentiates erythema and stage I pressure ulcers in nursing home residents.* Wound repair and regeneration, 2008. **16**(2): p. 189-197.

93. Hsiao, H., Guan, J., and Weatherly, M., *Accuracy and precision of two in-shoe pressure measurement systems.* Ergonomics, 2002. **45**(8): p. 537-555.

94. Woodburn, J. and Helliwell, P.S., *Observations on the F-Scan in-shoe pressure measuring system.* Clinical Biomechanics, 1996. **11**(5): p. 301-304.

95. Novel Electronics. *pedar Systems*. [Accessed: November 2022]; Available from: http://www.novelelectronics.de/novelcontent/systems-hardware/pedar-hardware-systems.

96. Martinez-Santos, A., Preece, S., and Nester, C.J., *Evaluation of orthotic insoles for people with diabetes who are at-risk of first ulceration.* Journal of foot and ankle research, 2019. **12**: 35.

97. Hellstrand Tang, U., et al., *Comparison of plantar pressure in three types of insole given to patients with diabetes at risk of developing foot ulcers - A two-year, randomized trial.* Journal of clinical & translational endocrinology, 2014. **1**(4): p. 121-132.

98. Stewart, S., et al., *The effect of good and poor walking shoe characteristics on plantar pressure and gait in people with gout.* Clinical Biomechanics, 2014. **29**(10): p. 1158-1163.

99. Hennessy, K., Burns, J., and Penkala, S., *Reducing plantar pressure in rheumatoid arthritis: A comparison of running versus off-the-shelf orthopaedic footwear.* Clinical Biomechanics, 2007. **22**(8): p. 917-923.

100. Chung, C., et al., *Biomechanical Comparison of a New Dynamic Ankle Orthosis to a Standard Ankle-Foot Orthosis During Walking.* Journal of biomechanical engineering, 2020. **142**(5): 051003.

101. Chang, J.S., Lee, H.Y., and Kim, M.K., *Effects of the ankle angle of an ankle foot orthosis on foot pressure during the gait in healthy adults.* Journal of physical therapy science, 2015. **27**(4): p. 1033-1035.

102. Kearney, R.S., et al., *In-shoe plantar pressures within ankle-foot orthoses: implications for the management of achilles tendon ruptures.* The American journal of sports medicine, 2011. **39**(12): p. 2679-2685.

103. Laing, S., et al., *An Investigation of Pressure Profiles and Wearer Comfort During Walking With a Transtibial Hydrocast Socket.* American Journal of Physical Medicine & Rehabilation, 2019. **98**(3): p. 199-206.

104. Gerhardt, L.C., et al., *Study of skin–fabric interactions of relevance to decubitus: friction and contact-pressure measurements.* Skin Research and Technology, 2008. **14**(1): p. 77-88.

105. Rosenbaum, D., et al., *Plantar sensitivity, foot loading and walking pain in rheumatoid arthritis.* Rheumatology, 2006. **45**(2): p. 212-214.

106. Konings-Pijnappels, A.P.M., et al., *Forefoot pathology in relation to plantar pressure distribution in patients with rheumatoid arthritis: A cross-sectional study in the Amsterdam Foot cohort.* Gait & Posture, 2019. **68**: p. 317-322.

107. Hodge, M.C., Nathan, D., and Bach, T.M., *Plantar Pressure Pain Thresholds and Touch Sensitivity in Rheumatoid Arthritis.* Foot & Ankle International, 2009. **30**(1): p. 1-9.

108. Gefen, A., *Reswick and Rogers pressure-time curve for pressure ulcer risk. Part 2.* Nursing standard 2009. **23**(46): p. 40-44.

109. Oomens, C.W.J., et al., *A numerical study to analyse the risk for pressure ulcer development on a spine board.* Clinical Biomechanics, 2013. **28**(7): p. 736-742.

110. Traa, W.A., et al., *There is an individual tolerance to mechanical loading in compression induced deep tissue injury.* Clinical Biomechanics, 2019. **63**: p. 153-160.

111. Sanders, J.E., Goldstein, B.S., and Leotta, D.F., *Skin response to mechanical stress: adaptation rather than breakdown--a review of the literature.* Journal of Rehabilitation Research & Development, 1995. **32**(3): p. 214-226.

112. Freeman, D.B., *Corns and calluses resulting from mechanical hyperkeratosis.* American family physician, 2002. **65**(11): p. 2277-2280.

113. Coleman, S., et al., *A new pressure ulcer conceptual framework.* Journal of Advanced Nursing, 2014. **70**(10): p. 2222-2234.

114. Kottner, J., et al., *Microclimate: A critical review in the context of pressure ulcer prevention.* Clinical Biomechanics, 2018. **59**: p. 62-70.

115. Alderden, J., et al., *Risk factors for pressure injuries among critical care patients: A systematic review.* International Journal of Nursing Studies, 2017. **71**: p. 97-114.

116. Gefen, A., et al., *Device-related pressure ulcers: SECURE prevention.* Journal of Wound Care, 2020. **29**(Sup2a): p. S1-S52.

117. Geerligs, M., et al., *Linear shear response of the upper skin layers.* Biorheology, 2011. **48**(3-4): p. 229-245.

118. Lboutounne, Y., et al., *Microclimate next to the skin: influence on percutaneous absorption of caffeine (ex-vivo study).* Skin Research and Technology, 2014. **20**(3): p. 293-298.

119. Cravello, B. and Ferri, A., *Relationships between skin properties and environmental parameters.* Skin Research and Technology, 2008. **14**(2): p. 180-186.

120. Gerhardt, L.C., et al., *Influence of epidermal hydration on the friction of human skin against textiles.* Journal of The Royal Society Interface, 2008. **5**(28): p. 1317-1328.

121. Schwartz, D., et al., *Effects of humidity on skin friction against medical textiles as related to prevention of pressure injuries.* International Wound Journal, 2018. **15**(6): p. 866-874.

122. Clark, M., *Microclimate: Rediscovering an Old Concept in the Aetiology of Pressure Ulcers*, in *Science and Practice of Pressure Ulcer Management*, C.M. Romanelli M., Gefen A., Ciprandi G., 2018, Editor: Springer, London. p. 103-110.

123. Ramirez, J.F., Pavon, J.J., and Toro, A., *Experimental assessment of friction coefficient between polypropylene and human skin using instrumented sclerometer.* Proceedings of the Institution of Mechanical Engineers Part J-Journal of Engineering Tribology, 2015. **229**(3): p. 259-265.

124. Taylor, N.A.S. and Machado-Moreira, C.A., *Regional variations in transepidermal water loss, eccrine sweat gland density, sweat secretion rates and electrolyte composition in resting and exercising humans.* Extreme Physiology & Medicine, 2013. **2**: 4.

125. Korpelainen, J.T., Sotaniemi, K.A., and Myllyla, V.V, *Asymmetric sweating in stroke: a prospective quantitative study of patients with hemispheral brain infarction.* Neurology, 1993. **43**(6): p. 1211-1214.

126. Yang, T.F., et al., *Power spectrum analysis of heart rate variability for cerebral palsy patients.* American Journal of Physical Medicine and Rehabilitation, 2002. **81**(5): p. 350-354.

127. Maltais, D., et al., *Responses of children with cerebral palsy to treadmill walking exercise in the heat.* Medicine and Science in Sports and Exercise, 2004. **36**(10): p. 1674-1681.

128. Bogerd, C.P., Brühwiler, P.A., and Rossi, R.M., *Heat loss and moisture retention variations of boot membranes and sock fabrics: A foot manikin study.* International Journal of Industrial Ergonomics, 2012. **42**(2): p. 212-218.

129. Kaplan, S. and Aslan, S., *Subjective wear trials to evaluate thermal comfort of the foot clothing system including a sweat pad.* The Journal of The Textile Institute, 2017. **108**(8): p. 1340-1349.

130. West, A.M., et al., *Shoe microclimate: An objective characterisation and subjective evaluation.* Applied Ergonomics, 2019. **78**: p. 1-12.

131. Irzmańska, E., *Case study of the impact of toecap type on the microclimate in protective footwear.* International Journal of Industrial Ergonomics, 2014. **44**(5): p. 706-714.

132. Irzmańska, E., *Evaluating the comfort of use of protective footwear: Validation of a method based on microclimate parameters and peripheral blood flow.* Measurement, 2016. **77**: p. 34-39.

133. Stewart, S.F., Palmieri, V., and Cochran, G.V., *Wheelchair cushion effect on skin temperature, heat flux, and relative humidity.* Archives of Physical Medicine and Rehabilitation, 1980. **61**(5): p. 229-233.

134. Fisher, S.V., et al., *Wheelchair cushion effect on skin temperature.* Archives of Physical Medicine & Rehabilitation, 1978. **59**(2): p. 68-72.

135. Ferguson-Pell, M., et al., *Thermodynamic rigid cushion loading indenter: a buttock-shaped temperature and humidity measurement system for cushioning surfaces under anatomical compression conditions.* Journal of Rehabilitation Research and Development, 2009. **46**(7): p. 945-956.

136. Hodges, G.J., et al., *Comparison of different wheelchair seating on thermoregulation and perceptual responses in thermoneutral and hot conditions in children.* Journal of tissue viability, 2019. **28**(3): p. 144-151.

137. Tomova-Simitchieva, T., et al., *Comparing the effects of 3 different pressure ulcer prevention support surfaces on the structure and function of heel and sacral skin: An exploratory cross-over trial.* International Wound Journal, 2018. **15**(3): p. 429-437.

138. Worsley, P.R. and Bader, D.L., *A modified evaluation of spacer fabric and airflow technologies for controlling the microclimate at the loaded support interface.* Textile Research Journal, 2019. **89**(11): p. 2154-2162.

139. Denzinger, M., et al., *A quantitative study of hydration level of the skin surface and erythema on conventional and microclimate management capable mattresses and hospital beds.* Journal of tissue viability, 2020. **29**(1): p. 2-6.

140. Visscher, M.O., et al., *Face Masks for Noninvasive Ventilation: Fit, Excess Skin Hydration, and Pressure Ulcers.* Respiratory Care, 2015. **60**(11): p. 1536-1547.

141. Ielapi, A., Forward, M., and De Beule, M., *Computational and experimental evaluation of the mechanical properties of ankle foot orthoses: A literature review.* Prosthetics and orthotics international, 2019. **43**(3): p. 339-348.

142. Yamamoto, S., et al., *Comparative Study of Mechanical Characteristics of Plastic AFOs.* JPO: Journal of Prosthetics and Orthotics, 1993. **5**(2): p. 59/47-52/64.

143. Kobayashi, T., Leung, A.K., and Hutchins, S.W., *Design of a manual device to measure ankle joint stiffness and range of motion.* Prosthetics and Orthotics International, 2011. **35**(4): p. 478-481.

144. Ishak, N.Z., et al. *Experimental Analysis of Ankle Foot Orthosis Using Pneumatic Artificial Muscle*. in *11th Asian-Pacific Conference on Medical and Biological Engineering*. 2021. Cham: Springer International Publishing.

145. Russell Esposito, E., Schmidtbauer, K.A., and Wilken, J.M., *Experimental comparisons of passive and powered ankle-foot orthoses in individuals with limb reconstruction.* Journal of NeuroEngineering and Rehabilitation, 2018. **15**: 111.

146. Nowak, M.D., Abu-Hasaballah, K.S., and Cooper, P.S., *Design enhancement of a solid ankle-foot orthosis: Real-time contact pressures evaluation.* Journal of Rehabilitation Research and Development, 2000. **37**(3): p. 273-281.

147. Oomens, C.W.J., Loerakker, S., and Bader, D.L., *The importance of internal strain as opposed to interface pressure in the prevention of pressure related deep tissue injury.* Journal of Tissue Viability, 2010. **19**(2): p. 35-42.

148. Simonsen, M.B., et al., *Different types of foot orthoses effect on gait mechanics in patients with rheumatoid arthritis.* Journal of Biomechanics, 2022. **139**: 110496.

149. Tenten-Diepenmaat, M., et al., *Outcomes and potential mechanism of a protocol to optimize foot orthoses in patients with rheumatoid arthritis.* BMC Musculoskeletal Disorders, 2020. **21**: 348.

150. Actis, R.L., et al., *Numerical simulation of the plantar pressure distribution in the diabetic foot during the push-off stance.* Medical and Biological Engineering and Computing, 2006. **44**(8): p. 653-663.

151. Cheung, J.T., Zhang, M., and An, K.N., *Effects of plantar fascia stiffness on the biomechanical responses of the ankle-foot complex.* Clinical Biomechanics, 2004. **19**(8): p. 839-846.

152. He, K., et al., *Comparisons in finite element analysis of minimally invasive, locking, and non-locking plates systems used in treating calcaneal fractures of Sanders type II and type III.* Chinese medical journal, 2014. **127**(22): p. 3894-3901.

153. Zhang, M.Y., Xu, C., and Li, K.H., *Finite element analysis of nonanatomic tenodesis reconstruction methods of combined anterior talofibular ligament and calcaneofibular ligament deficiency.* Foot & ankle international, 2011. **32**(10): p. 1000-1008.

154. Wang, Y., Wong, D.W.C., and Zhang, M., *Computational Models of the Foot and Ankle for Pathomechanics and Clinical Applications: A Review.* Annals of Biomedical Engineering, 2016. **44**(1): p. 213-221.

155. Chu, T.M., Reddy, N.P., and Padovan, J., *Three-dimensional finite element stress analysis of the polypropylene, ankle-foot orthosis: static analysis.* Medical Engineering & Physics, 1995. **17**(5): p. 372-379.

156. Chen, W.M., et al., *Effects of internal stress concentrations in plantar soft-tissue--A preliminary three-dimensional finite element analysis.* Medical engineering & physics, 2010. **32**(4): p. 324-331.

157. Jamshidi, N., et al., *Modelling the interaction of ankle-foot orthosis and foot by finite element methods to design an optimized sole in steppage gait.* Journal of Medical Engineering & Technology, 2010. **34**(2): p. 116-123.

158. Goske, S., et al., *Reduction of plantar heel pressures: Insole design using finite element analysis.* Journal of Biomechanics, 2006. **39**(13): p. 2363-2370.

159. Zheng, Y.P., et al., *Biomechanical assessment of plantar foot tissue in diabetic patients using an ultrasound indentation system.* Ultrasound in Medicine & Biology, 2000. **26**(3): p. 451-456.

160. Chen, W.M. and Lee, P.V., *Explicit finite element modelling of heel pad mechanics in running: inclusion of body dynamics and application of physiological impact loads.* Computer methods in biomechanics and biomedical engineering, 2015. **18**(14): p. 1582-1595.

161. Cheung, J.T.M. and Zhang, M., *A 3-dimensional finite element model of the human foot and ankle for insole design.* Archives of Physical Medicine and Rehabilitation, 2005. **86**(2): p. 353-358.

162. Uning, R., Abu Osman, N.A., and Abdul Rahim, R.B., *3D Finite Element Analysis of Ankle-Foot Orthosis on Patients with Unilateral Foot Drop: A Preliminary Study*. In *4th Kuala Lumpur International Conference on Biomedical Engineering 2008*. 2008. Berlin, Heidelberg: Springer Berlin Heidelberg.

163. Darwich, A., et al., *Ankle-foot orthosis design between the tradition and the computerized perspectives.* The International journal of artificial organs, 2019. **43**(5): p. 354-361.

164. Maruyama, N., et al., *Deformation Analysis of an Ankle Foot Orthosis during Stance Phase by the Dynamic Finite Element Method using a Human Lower Leg Model.* Transactions of Japanese Society for Medical and Biological Engineering, 2009. **47**(5): p. 450-456.

165. Jena, S., Arunachalam, T., and Panda, S.K., *Experimental and numerical investigation of a polypropylene orthotic device for assistance in level ground walking.* Proceedings of the Institution of Mechanical Engineers. Part H, Journal of engineering in medicine, 2020. **234**(4): p. 356-369.

166. Fontanella, C.G., et al., *Analysis of heel pad tissues mechanics at the heel strike in bare and shod conditions.* Medical engineering & physics, 2013. **35**(4): p. 441-447.

167. Spears, I.R., et al., *The potential influence of the heel counter on internal stress during static standing: A combined finite element and positional MRI investigation.* Journal of Biomechanics, 2007. **40**(12): p. 2774-2780.

168. Chen, W.M., Lee, S.J., and Lee, P.V., *Plantar pressure relief under the metatarsal heads: therapeutic insole design using three-dimensional finite element model of the foot.* Journal of biomechanics, 2015. **48**(4): p. 659-665.

169. Cheung, J.T.-M. and Zhang, M., *Parametric design of pressure-relieving foot orthosis using statistics-based finite element method.* Medical Engineering & Physics, 2008. **30**(3): p. 269-277.

170. Chen, W.-P., Ju, C.W., and Tang, F.T., *Effects of total contact insoles on the plantar stress redistribution: a finite element analysis.* Clinical Biomechanics, 2003. **18**(6): p. S17-S24.

171. Telfer, S., et al., *Virtually optimized insoles for offloading the diabetic foot: A randomized crossover study.* Journal of Biomechanics, 2017. **60**: p. 157-161.

172. Zhang, H.W., et al., *Computational modelling of foot orthosis for midfoot arthritis: a Taguchi approach for design optimization.* Acta of Bioengineering and Biomechanics, 2020. **22**(4): p. 75-83.

173. Jafarzadeh, E., Soheilifard, R., and Ehsani-Seresht, A., *Design optimization procedure for an orthopedic insole having a continuously variable stiffness/shape to reduce the plantar pressure in the foot of a diabetic patient.* Medical Engineering & Physics, 2021. **98**: p. 44-49

174. Woodburn, J. and Helliwell, P.S., *Relation between heel position and the distribution of forefoot plantar pressures and skin callosities in rheumatoid arthritis.* Annals of the Rheumatic Diseases, 1996. **55**(11): p. 806-810.

175. Dahmen, R., et al., *Higher body mass index is associated with lower foot health in patients with rheumatoid arthritis: baseline results of the Amsterdam-Foot cohort.* Scandinavian Journal of Rheumatology, 2020. **49**(3): p. 186-194.

176. Ceelen, K.K., et al., *Compression-induced damage and internal tissue strains are related.* Journal of Biomechanics, 2008. **41**(16): p. 3399-3404.

177. Steer, J.W., et al., *Key considerations for finite element modelling of the residuum–prosthetic socket interface.* Prosthetics and Orthotics International, 2021. **45**(2): p. 138-146.

178. Traa, W.A., et al., *MRI based 3D finite element modelling to investigate deep tissue injury* Computer Methods in Biomechanics and Biomedical Engineering, 2018. **21**(14): p. 760-769.

179. Lung, C.-W., et al., *Dynamic changes in seating pressure gradient in wheelchair users with spinal cord injury.* Assistive Technology, 2020. **32**(5): p. 277-286.

180. Aissaoui, R., Lacoste, M., and Dansereau, J., *Analysis of sliding and pressure distribution during a repositioning of persons in a simulator chair.* IEEE transactions on neural systems and rehabilitation engineering, 2001. **9**(2): p. 215-224.

181. Mueller, M.J., Zou, D., and Lott, D.J., *"Pressure gradient" as an indicator of plantar skin injury.* Diabetes Care, 2005. **28**(12): p. 2908-2912.

182. Mueller, M.J., et al., *Plantar stresses on the neuropathic foot during barefoot walking.* Physical therapy, 2008. **88**(11): p. 1375-1384.

183. Zou, D., Mueller, M.J., and Lott, D.J., *Effect of peak pressure and pressure gradient on subsurface shear stresses in the neuropathic foot.* Journal of Biomechanics, 2007. **40**(4): p. 883-890.

184. Rohan, P.Y., et al., *Prediction of the biomechanical effects of compression therapy on deep veins using finite element modelling.* Annals of biomedical engineering, 2015. **43**(2): p. 314-324.

185. Yamada, H., et al., *Skin stiffness determined from occlusion of a horizontally running microvessel in response to skin surface pressure: a finite element study of sacral pressure ulcers.* Medical & biological engineering & computing, 2017. **55**(1): p. 79-88.

186. Shariatmadari, M.R., English, R., and Rothwell, G., *Finite Element Study into the Effect of Footwear Temperature on the Forces Transmitted to the Foot during Quasi-Static Compression Loading*. In *9th World Congress on Computational Mechanics and 4th Asian Pacific Congress on Computational Mechanics*. 2010. Sydney, Australia. **10:** 012126

187. Quenneville, C.E. and Dunning, C.E., *Development of a finite element model of the tibia for short-duration high-force axial impact loading.* Computer methods in biomechanics and biomedical engineering, 2011. **14**(2): p. 205-212.

188. Ahanchian, N., et al., *Estimating the material properties of heel pad sub-layers using inverse Finite Element Analysis.* Medical Engineering & Physics, 2017. **40**: p. 11-19.

189. Gu, Y., et al., *Heel skin stiffness effect on the hind foot biomechanics during heel strike.* Skin research and technology, 2010. **16**(3): p. 291-296.

190. Nakamura, S., Crowninshield, R.D., and Cooper, R.R., *An analysis of soft tissue loading in the foot--a preliminary report.* Bulletin of prosthetics research, 1981. **10-35**: p. 27-34.

191. Fontanella, C.G., et al., *Investigation of the mechanical behaviour of the plantar soft tissue during gait cycle: Experimental and numerical activities.* Proceedings of the Institution of Mechanical Engineers. Part H, Journal of engineering in medicine, 2015. **229**(10): p. 713-720.

192. Schrank, E.S., et al., *Assessment of a virtual functional prototyping process for the rapid manufacture of passive-dynamic ankle-foot orthoses.* Journal of Biomechanical Engineering, 2013. **135**(10): 101011.

193. Zou, D., et al., *Experimental and computational analysis of composite ankle-foot orthosis.* Journal of Rehabilitation Research and Development, 2014. **51**(10): p. 1525-1536.

194. Syngellakis, S., Arnold, M.A., and Rassoulian, H., *Assessment of the non-linear behaviour of plastic ankle foot orthoses by the finite element method.* Proceedings of the Institution of Mechanical Engineers. Part H, Journal of engineering in medicine, 2000. **214**(5): p. 527-539.

195. Petre, M.T., Erdemir, A., and Cavanagh, P.R., *Determination of elastomeric foam parameters for simulations of complex loading.* Computer Methods in Biomechanics and Biomedical Engineering, 2006. **9**(4): p. 231-242.

196. Erdemir, A., et al., *Local plantar pressure relief in therapeutic footwear: design guidelines from finite element models.* Journal of biomechanics, 2005. **38**(9): p. 1798-1806.

197. Sanders, J.E., et al., *Material properties of commonly-used interface materials and their static coefficients of friction with skin and socks.* Journal of rehabilitation research and development, 1998. **35**(2): p. 161-176.

198. Carlson, J.M., *Functional Limitations From Pain Caused by Repetitive Loading on the Skin: A Review and Discussion for Practitioners, With New Data for Limiting Friction Loads.* JPO: Journal of Prosthetics and Orthotics, 2006. **18**(4): p. 93-103.

199. Stewart, S., et al., *Region-specific foot pain and plantar pressure in people with rheumatoid arthritis: A cross-sectional study.* Clinical Biomechanics, 2018. **55**: p. 14-17.

200. Tuna, H., et al., *Pedobarography and its relation to radiologic erosion scores in rheumatoid arthritis.* Rheumatology International, 2005. **26**: p. 42-47.

201. Mulcahy, D., et al., *Rheumatoid forefoot deformity: a comparison study of 2 functional methods of reconstruction.* Journal of Rheumatology, 2003. **30**(7): p. 1440-1450.

202. Chang, B.-C., et al., *Dynamic impression insole in rheumatoid foot with metatarsal pain.* Clinical Biomechanics, 2012. **27**(2): p. 196-201.

203. Shimoda, H., et al., *Effects of forefoot arthroplasty on plantar pressure, pain, gait and disability in rheumatoid arthritis.* Modern Rheumatology, 2020. **30**(2): p. 301-304.

204. Schmiegel, A., et al., *Pedography and radiographic imaging for the detection of foot deformities in rheumatoid arthritis.* Clinical Biomechanics, 2008. **23**(5): p. 648-652.

205. Hodge, M.C., Bach, T.M., and Carter, G.M., *Orthotic management of plantar pressure and pain in rheumatoid arthritis.* Clinical Biomechanics, 1999. **14**(8): p. 567-575.

206. Jackson, L., Binning, J., and Potter, J., *Plantar pressures in rheumatoid arthritis using prefabricated metatarsal padding.* Journal of the American Podiatric Medical Association, 2004. **94**(3): p. 239-245.

207. Stick, C., Hiedl, U., and Witzleb, E., *Volume changes in the lower leg during quiet standing and cycling exercise at different ambient temperatures.* European journal of applied physiology and occupational physiology, 1993. **66**(5): p. 427-433.

208. Krijnen, R.M.A., et al., *Diurnal volume changes of the lower legs in healthy males with a profession that requires standing.* Skin Research and Technology, 1998. **4**(1): p. 18-23.

209. Solorio-Ferrales, K., et al., *Comparison of regenerated bamboo and cotton performance in warm environment.* Journal of Applied Research and Technology, 2017. **15**(3): p. 205-210.

210. Atasağun, H.G., et al., *Determination of the effect of fabric properties on the coupled heat and moisture transport of underwear–shirt fabric combinations.* Textile Research Journal, 2018. **88**(11): p. 1319-1331.

211. Antonsson, E.K. and Mann, R.W., *The frequency content of gait.* Journal of Biomechanics, 1985. **18**(1): p. 39-47.

212. Tekscan. *F-scan System*. 2018. [Accessed: May 2019]; Available from: https://www.tekscan.com/products-solutions/systems/f-scan-system.

213. Sensirion. *Digital Humidity Sensor SHT7x (RH/T)*. 2017. [Accessed: May 2019]; Available from: https://www.sensirion.com/en/environmental-sensors/humidity-sensors/pintype-digital-humidity-sensors/.

214. Heinemann, A.W., Bode, R.K., and O'Reilly, C., *Development and measurement properties of the Orthotics and Prosthetics Users' Survey (OPUS): A comprehensive set of clinical outcome instruments.* Prosthetics and Orthotics International, 2003. **27**(3): p. 191-206.

215. Lung, C.W., et al., *Quantifying Dynamic Changes in Plantar Pressure Gradient in Diabetics with Peripheral Neuropathy.* Frontiers in bioengineering and biotechnology, 2016. **4**: 54.

216. West, A.M., et al., *Sweat distribution and perceived wetness across the human foot: the effect of shoes and exercise intensity.* Ergonomics, 2019. **62**(11): p. 1450-1461.

217. Gil-Calvo, M., et al., *Effects of prefabricated and custom-made foot orthoses on skin temperature of the foot soles after running.* Physiological measurement, 2019. **40**(5): 054004.

218. Shimazaki, Y., Matsutani, T., and Satsumoto, Y., *Evaluation of thermal formation and air ventilation inside footwear during gait: The role of gait and fitting.* Applied ergonomics, 2016. **55**: p. 234-240.

219. Rupérez, M.J., Monserrat, C., and Alcañiz, M., *Simulation of the deformation of materials in shoe uppers in gait. Force distribution using finite elements.* International Journal on Interactive Design and Manufacturing (IJIDeM), 2008. **2**(2): p. 59-68.

220. Tian, H., et al., *Study of knitted fabrics with ultra-low modulus based on geometrical deformation mechanism.* Textile Research Journal, 2019. **89**(5): p. 891-899.

221. Zhou, J.Y., et al., *The Poisson Ratio and Modulus of Elastic Knitted Fabrics.* Textile Research Journal, 2010. **80**(18): p. 1965-1969.

222. Jung, Y., et al., *Dynamically adjustable foot-ground contact model to estimate ground reaction force during walking and running.* Gait & Posture, 2016. **45**: p. 62-68.

223. Oomens, C.W., et al., *A numerical study to analyse the risk for pressure ulcer development on a spine board.* Clinical Biomechanics, 2013. **28**(7): p. 736-742.

224. Steer, J., et al., *Key considerations for finite element modelling of the residuum–prosthetic socket interface.* Prosthetics and Orthotics International, 2021. **45**(2): p. 138-146.

225. Shahar, F.S., et al., *A review on the orthotics and prosthetics and the potential of kenaf composites as alternative materials for ankle-foot orthosis.* Journal of the Mechanical Behaviour of Biomedical Materials, 2019. **99**: p. 169-185.

226. Cheung, J.T.-M., et al., *Three-dimensional finite element analysis of the foot during standing—a material sensitivity study.* Journal of Biomechanics, 2005. **38**(5): p. 1045-1054.

227. Akrami, M., et al., *Subject-specific finite element modelling of the human foot complex during walking: sensitivity analysis of material properties, boundary and loading conditions.* Biomechanics and Modeling in Mechanobiology, 2018. **17**(2): p. 559-576.

228. Helliwell, P., et al., *Development of a foot impact scale for rheumatoid arthritis.* Arthritis Care & Research, 2005. **53**(3): p. 418-422.

229. Ben Shabat, Y. and Fischer, A., *Design of Porous Micro-Structures Using Curvature Analysis for Additive-Manufacturing.* Procedia CIRP, 2015. **36**: p. 279-284.

230. Rusinkiewicz, S. *Estimating curvatures and their derivatives on triangle meshes*. in *Proceedings. 2nd International Symposium on 3D Data Processing, Visualization and Transmission, 2004. 3DPVT 2004.* 2004.

231. Turner, D.E., et al., *The impact of rheumatoid arthritis on foot function in the early stages of disease: a clinical case series.* BMC Musculoskeletal Disorders, 2006. **7**: 102.

232. Symmons, D., et al., *The prevalence of rheumatoid arthritis in the United Kingdom: new estimates for a new century.* Rheumatology, 2002. **41**(7): p. 793-800.

233. Kato, H., et al., *The reduction and redistribution of plantar pressures using foot orthoses in diabetic patients.* Diabetes Research and Clinical Practice, 1996. **31**(1): p. 115-118.

234. Aliberti, S., et al., *Influence of patellofemoral pain syndrome on plantar pressure in the foot rollover process during gait.* Clinics (Sao Paulo), 2011. **66**(3): p. 367-372.

235. Kanatli, U., et al., *[Pressure distribution patterns under the metatarsal heads in healthy individuals].* Acta Orthopaedica et Traumatologica Turcica, 2008. **42**(1): p. 26-30.

236. Luboz, V., et al., *Foot ulcer prevention using biomechanical modelling.* Computer Methods in Biomechanics and Biomedical Engineering: Imaging & Visualization, 2014. **2**(4): p. 189-196.

237. Mickle, K.J. and Steele, J.R., *Obese older adults suffer foot pain and foot-related functional limitation.* Gait & Posture, 2015. **42**(4): p. 442-447.

238. de Looze, M.P., Kuijt-Evers, L.F., and van Dieën, J., *Sitting comfort and discomfort and the relationships with objective measures.* Ergonomics, 2003. **46**(10): p. 985-997.

239. Gefen, A., *Reswick and Rogers pressure-time curve for pressure ulcer risk. Part 1.* Nursing standard, 2009. **23**(45): p. 64-74.

240. Spirka, T.A., et al., *Simple finite element models for use in the design of therapeutic footwear.* Journal of biomechanics, 2014. **47**(12): p. 2948-2955.

241. Frecklington, M., et al., *Footwear interventions for foot pain, function, impairment and disability for people with foot and ankle arthritis: A literature review.* Seminars in Arthritis and Rheumatism, 2018. **47**(6): p. 814-824.

242. Rome, K., et al., *Clinical effectiveness and cost-effectiveness of foot orthoses for people with established rheumatoid arthritis: an exploratory clinical trial.* Scandinavian Journal of Rheumatology, 2017. **46**(3): p. 187-193.

243. Helliwell, P., et al., *Development of a foot impact scale for rheumatoid arthritis.* Arthritis & Rheumatology, 2005. **53**(3): p. 418-422.

244. Kottner, J., Dassen, T., and Lahmann, N., *Prevalence of deep tissue injuries in hospitals and nursing homes: two cross-sectional studies.* International Journal of Nursing Studies, 2010. **47**(6): p. 665-670.

245. Siddle, H.J., et al., *Survey of ultrasound practice amongst podiatrists in the UK.* Journal of Foot and Ankle Research, 2018. **11**: 18.

246. Huijbrechts, E.J., et al., *Clinical guidance for podiatrists in the management of foot problems in rheumatic disorders: evaluation of an educational programme for podiatrists using a mixed methods design.* Journal of Foot and Ankle Research, 2021. **14**: 15.

247. Grassi, W., et al., *The clinical features of rheumatoid arthritis.* European Journal of Radiology, 1998. **27**(Suppl1): p. S18-S24.

248. Bowen, C.J., et al., *Using ultrasound to image the foot in rheumatoid arthritis: current understanding, challenges and future scope.* Imaging in Medicine, 2013. **5**(4): p. 347-356.

249. Kang, T., et al., *The evolution of ultrasound in rheumatology.* Therapeutic advances in musculoskeletal disease, 2012. **4**(6): p. 399-411.

250. Drakonaki, E.E., Allen, G.M., and Wilson, D.J., *Ultrasound elastography for musculoskeletal applications.* The British Journal of Radiology, 2012. **85**(1019): p. 1435-1445.

251. Supriadi, et al., *Interface pressure, pressure gradient with pressure ulcer development in Intensive Care Units.* Journal of Nursing Education and Practice, 2014. **4**(9): p. 146-154.

252. Steer, J.W., et al., *Predictive prosthetic socket design: part 1-population-based evaluation of transtibial prosthetic sockets by FEA-driven surrogate modelling.* Biomechanics and modeling in mechanobiology, 2019. **19**(4): p. 1331-1346.

253. Lochner, S.J., Huissoon, J.P., and Bedi, S.S., *Development of a patient-specific anatomical foot model from structured light scan data.* Computational Methods in Biomechanics and Biomedical Engineering, 2014. **17**(11): p. 1198-1205.

254. Chapman, L.S., et al., *Foot orthoses for people with rheumatoid arthritis: a survey of prescription habits among podiatrists.* Journal of Foot and Ankle Research, 2019. **12**: 7.

255. Pennes, H.H., *Analysis of tissue and arterial blood temperatures in the resting human forearm.* Journal of applied physiology, 1948. **1**(2): p. 93-122.

256. Peery, J.T., et al., *A three-dimensional finite element model of the transibial residual limb and prosthetic socket to predict skin temperatures.* IEEE transactions on neural systems and rehabilitation engineering, 2006. **14**(3): p. 336-343.

257. Fiala, D., Lomas, K.J., and Stohrer, M., *A computer model of human thermoregulation for a wide range of environmental conditions: the passive system.* Journal of applied physiology, 1999. **87**(5): p. 1957-1972.

258. Fiala, D., et al., *UTCI-Fiala multi-node model of human heat transfer and temperature regulation.* International Journal of Biometeorology, 2012. **56**(3): p. 429-441.

259. Klaassen, M., Schipper, D.J., and Masen, M.A., *Influence of the relative humidity and the temperature on the in-vivo friction behaviour of human skin.* Biotribology, 2016. **6**: p. 21-28.